## The University of Sheffield

Faculty of Engineering

Department of Electronic & Electrical Engineering

---

# Application of Flywheel Energy Storage Systems

---

*A thesis submitted in fulfilment of the requirements for the degree of Doctor of Philosophy*

Andrew James HUTCHINSON

April 2023

## Abstract

Energy Storage is an increasingly prevalent part of the modern electricity system. With rapid development and innovation, energy storage is being deployed across an ever-increasing range of applications.

The limitations of mature energy storage technologies such as Li-Ion Batteries are now more widely understood, and with use-based degradation becoming a dominant factor in selecting the appropriate energy storage medium for a given application other technologies may hold an advantage. To this end, specialist energy storage systems focusing on very short-duration storage, such as Flywheels, are becoming a more viable option for certain applications, both as standalone and hybrid systems.

This study looks in detail at the role that Flywheel Energy Storage Systems (FESSs) can play within the electricity generation and distribution system from both a technical and economic standpoint, giving a detailed assessment of the configurations and pricing that would need to be achieved in order for FESSs to be viable for deployment, whilst also opening up further avenues for the research and development of FESSs.

A detailed modelling framework is presented for both a Battery Energy Storage System (BESS) and a FESS, offering a fast and modular method for simulating new energy storage applications. The BESS model is verified against a real-world installation, and the degradation element is also verified against experimental results. The work demonstrates a novel and reliable model that can be used as a tool for rapid complex assessments of ESS deployment.

The novel application of energy storage in locally driven export-limited distributed generation is introduced for the first time. A high-level investigation exploring the theory of implementing a system utilising a FESS is performed showing significant potential techno-economic benefit, which is then followed up with a specific site case study that verifies these findings and shows the economic impact can be even higher in a real-world scenario. A comparison between BESSs and FESSs for this application is presented, showing that excessive cycling limits the effectiveness of a BESS but makes a FESS more suitable.

The work then moves to an investigation into the feasibility of FESSs for performing frequency response services. Initially, this is done by assessing standalone FESSs performing Dynamic Frequency Response (DFR), where it is shown that low energy capacity storage is unsuitable for this application and that hybridising with a high energy ESS does not necessarily improve the performance of the site. The effect of introducing a FESS into an existing BESS installation for this application is then explored, with multiple novel control strategies for hybrid control introduced and analysed. It is shown that significant economic benefits can be achieved through

hybridisation, with FESSs able to provide a positive impact up to a total capital cost of £5,855/kW depending on configuration and control strategy.

Finally, the study looks towards the future of frequency response services and the role that flywheels may be able to play. Firstly, this is done by conducting a novel analysis of FESSs performing the new suite of National Grid Electricity System Operator (NGESO) frequency response services. This study shows that whilst some configurations of FESS may be technically capable of delivery, the state of energy requirements makes their deployment prohibitive. This leads to the final investigation of the work, where a bespoke service is designed specifically for delivery by a FESS, showing that a 20C FESS could provide 95% availability whilst performing the service 24/7. The subsequent economic analysis shows that if this response envelope were implemented a FESS could compete with and in some cases economically outperform BESSs.

# List of Publications

Parts of the work presented in this thesis have been reported in the following internationally-respected publications:

## Journal Publications

1. **A. J. Hutchinson**, D. T. Gladwin, "Optimisation of a wind power site through utilisation of flywheel energy storage technology,", *Energy Reports*, vol. 6, pp. 259–265, 2020. *(Chapter 4)*

2. **A. J. Hutchinson**, D. T. Gladwin, "Verification and analysis of a Battery Energy Storage System model,", *Energy Reports*, vol. 8, pp. 41–47, 2022. *(Chapter 3)*

3. **A. J. Hutchinson**, D. T. Gladwin, " Techno-Economic Assessment of Novel Hybrid Energy Storage Control Strategies for Dynamic Frequency Response,", *Journal of Energy Storage*, vol. 55, Part D, 2022. *(Chapter 6)*

4. **A. J. Hutchinson**, D. T. Gladwin, "Capacity factor enhancement for an export limited wind generation site utilising a novel Flywheel Energy Storage strategy,", *Accepted for publication in Journal of Energy Storage* *(Chapter 4)*

## Conference Proceedings

1. **A. J. Hutchinson**, D. T. Gladwin, "Sensitivity analysis of a wind farm with integrated flywheel energy storage," in *2020 IEEE International Conference on Industrial Technology (ICIT)*, pp. 549–553, 2020. *(Chapter 4)*

2. **A. J. Hutchinson**, D. T. Gladwin, "Modeling and Simulation framework for hybrid Energy Storage Systems including degradation mitigation analysis under varying control schemes," in *2021 International Conference on Electrical, Computer and Energy Technologies (ICECET)*, pp. 1–6, 2021. *(Chapter 3)*

3. **A. J. Hutchinson**, D. T. Gladwin, "Techno-Economic Analysis of a Flywheel Energy Storage System performing a Dynamic Frequency Response Service," in *2021 IEEE 30th International Symposium on Industrial Electronics (ISIE)*, pp. 1–6, 2021. *(Chapter 5)*

4. **A. J. Hutchinson**, D. T. Gladwin, "Genetic Algorithm Optimisation of Hybrid Energy Storage System providing Dynamic Frequency Response," in *2022 IEEE 31st International Symposium on Industrial Electronics (ISIE)*, pp. 98–103, 2020. *(Chapter 6)*

5. **A. J. Hutchinson**, D. T. Gladwin, "A Bespoke Frequency Response Service suitable for delivery by Flywheel Energy Storage Systems" in *2022 IEEE International Conference on Smart Grid Technologies Europe (ISGT-Europe)*, pp. 1–5, 2022. ***(Chapter 7)***

6. **A. J. Hutchinson**, D. T. Gladwin, "Suitability Assessment of Flywheel Energy Storage Systems for providing new Frequency Response Services in the UK" in *2022 IEEE International Conference on Smart Grid Technologies Asia (ISGT-Asia)*, pp. 495–499, 2022. ***(Chapter 7)***

7. **A. J. Hutchinson**, D. T. Gladwin, "Flywheel Energy Storage for Export Limitation Mitigation in GB: A Case Study,", *Accepted to International Conference on Compatibility, Power Electronics and Power Engineering 2023* ***(Chapter 4)***

# Acknowledgements

Firstly, I would like to express my heartfelt thanks to my supervisor Professor Dan Gladwin for not only being a brilliant source of technical expertise and guidance but for being a great friend and mentor, especially when my own self-doubt threatened to get the best of me. His unwavering faith in my ability is humbling, and I hope to repay that faith over the years on many more international trips! I also want to mention Professor Martin Foster who brought me back into the Sheffield fold, I truly appreciate you reaching out to me 5 years ago.

I am grateful to the Energy Storage and Its Applications Centre for Doctoral Training (ESA CDT) for giving me the chance to realise my long-held ambition of undertaking a PhD. Particular thanks to Tracey McNeilly, who was never short of help when seeking to attend conferences and events.

The Cohort 5 group, both in Sheffield and Southampton, have all been brilliant and great teammates to work through the many challenges we have faced. Charlie, Tom, Jethro and Flora, you guys have been great fun to work with and I can't wait to see what you do next. George, the celebration in the Red Deer will live long in the memory!

To all of my friends, thank you for supporting me and bearing with me disappearing onto Flywheel tangents during pub chats. Alex, Brett and Steve, you guys have been so important to my ability to get this over the line, and I truly appreciate it. Tom and Fork, who have always been like family to me and supported me all the way. To the Skipsea guys, thank you for being my emotional sounding board and stress relief! And finally, the Lawrencefield boys, who I would never have reached this stage without, thank you.

My Mum, Dad, Sister and the rest of my family, and Hannah's Mum and Dad as well, have supported me every step of the way, and I couldn't have done it without you all. There aren't words available to describe my thanks for your unwavering support.

Finally, to Hannah. Words can't express my appreciation for you not only being OK with me abandoning my previous career to pursue the one I wanted but actively encouraging it. No one could have envisioned how hard it would be when we made the decision, but we got through it together just like we always will. I can't wait for the next Chapter now that this thesis is finally submitted! My son Rory, who lights up every room he enters, has kept me sane in the past few very difficult years, I can't wait until you are old enough to be bored of me telling you to read this little one!

# Contents

# List of Figures

# List of Tables

# List of Acronyms

**BESS**      Battery Energy Storage System.
**DC**      Dynamic Containment.
**DFR**      Dynamic Frequency Response.
**DG**      Distributed Generation.
**DM**      Dynamic Moderation.
**DR**      Dynamic Regulation.
**ELS**      Export Limitation Scheme.
**ESS**      Energy Storage System.
**FESS**      Flywheel Energy Storage System.
**GA**      Genetic Algorithm.
**GBP**      Great British Pound (£).
**HESS**      Hybrid Energy Storage System.
**Li-ion**      Lithium Ion.
**NGESO**      National Grid Electricity System Operator.
**NPV**      Net Present Value.
**NPVC**      Net Present Value Change.
**RMSE**      Root Mean Squared Error.
**SOC**      State of Charge.
**TCC**      Total Capital Cost (£/kW).
**UK**      United Kingdom.

# Nomenclature

| | |
|---|---|
| $A_h$ | Energy throughput over time period $t$. |
| $A_{vail}$ | Availability of a frequency response site. |
| $C_{inst}$ | Instantaneous C-Rate of a given ESS over a 1 second period. |
| $C_{investment}$ | Initial investment. |
| $C_{rated}$ | Rated C-Rate of an Energy Storage System. |
| $C_{revenue}$ | Yearly income. |
| $X_r$ | Crossover rate of genetic algorithm. |
| $\rho$ | Density of flywheel rim. |
| $d$ | Discount rate. |
| $E_{deliv}$ | Total energy delivered by a service. |
| $E_{ESS}$ | Energy capacity of an Energy Storage System. |
| $E$ | Energy. |
| $E_{actual}$ | Actual energy generated over one year. |
| $E_{req}$ | Total energy requested by a service. |
| $E_t$ | Energy stored in an Energy Storage System at time $t$. |
| $\sigma$ | Hoop stress. |
| $I_{rate}$ | C-rate over time period $t$. |
| $I$ | Moment of inertia. |
| $k$ | Shape factor of flywheel. |
| $m_f$ | Mass of flywheel. |
| $M_r$ | Mutation rate of genetic algorithm. |
| $N$ | System lifetime. |
| $N_{Gen}$ | Maximum generations for genetic algorithm. |
| $N_{Pop}$ | Population size for genetic algorithm. |
| $NPV_{Expenditure}$ | NPV of total lifetime cost. |
| $NPV_{Income}$ | NPV of total lifetime income. |
| $f_1$ | Positive maximum power point. |
| $f_{-1}$ | Negative maximum power point. |
| $P_{base}$ | Base export power of wind generation site at current time step. |
| $P_{cha}$ | Power charged by ESS. |
| $P_{DFR}$ | Power requested by frequency response service. |
| $P_{dis}$ | Power discharged by ESS. |
| $P_{ESS}$ | Power rating of an Energy Storage System. |
| $P_{ESS}$ | Power delivered by ESS. |
| $f_k$ | Positive knee point. |
| $f_{-k}$ | Negative knee point. |
| $P_{limit}$ | Limit of allowed export power at a wind generation site. |
| $P_{rated}$ | Rated power of wind generation site. |

| | |
|---|---|
| $Q^{cycleloss}$ | Degredation of a battery due to cycling. |
| $r$ | Outer radius of flywheel. |
| $SOC_{ESS}$ | ESS SOC at current time step. |
| $SOC_{high}$ | Upper limit of ESS SOC. |
| $SOC_{low}$ | Lower limit of ESS SOC. |
| $t_{Av}$ | Duration over which the average power request is calculated. |
| $T$ | Temperature. |
| $\omega$ | Angular velocity. |
| $V$ | Volume. |

# Chapter 1

# Introduction

## 1.1 Background & Motivation

The ever-increasing proportion of renewable energy present in the generation mix is driving unprecedented challenges for the generation and distribution industry within the United Kingdom (UK) and the wider world. Beyond this, the current geopolitical situation introduces further instability into the future electricity network with ongoing uncertainty over the continued dependence on imported gas as one of the main forms of electricity generation worldwide.

The widely acknowledged evidence that climate change represents a severe threat has led to both legislation and international agreements regularly being introduced over the past 30 years [3] [4] [5]. These commitments all highlight the main objective of increasing renewable generation to take the place of conventional fossil fuel generation. It is readily apparent from Figure 1.1 that the share of renewable generation in the U.K. is steadily increasing along with a rapid reduction in coal-based generation. At the same time, the demand for and the way in which electricity is used in the U.K. is undergoing rapid transformation due to the electrification of heat and transport [6].

National Grid Electricity System Operator (NGESO) predicts in its 'Future Energy Scenarios' report that by 2050 annual demand for electricity will have increased from 294 TWh in 2020 to a minimum of 459 TWh, whilst the worst-case scenario puts this figure at 702 TWh. The peak electricity demand is also predicted to increase from 58 GW in 2020 to a minimum of 92GW and a maximum of 113GW by 2050 [7]. NGESO are the electricity system operator for the Great Britain grid, with the Northern Ireland electricity system being operated by the system operator for Northern Ireland (SONI). Some key statistics that illustrate these changes are shown in Table 1.1, where it is important to note the significant predicted increase in reliance on electricity to power transportation and residential by 2050, lending
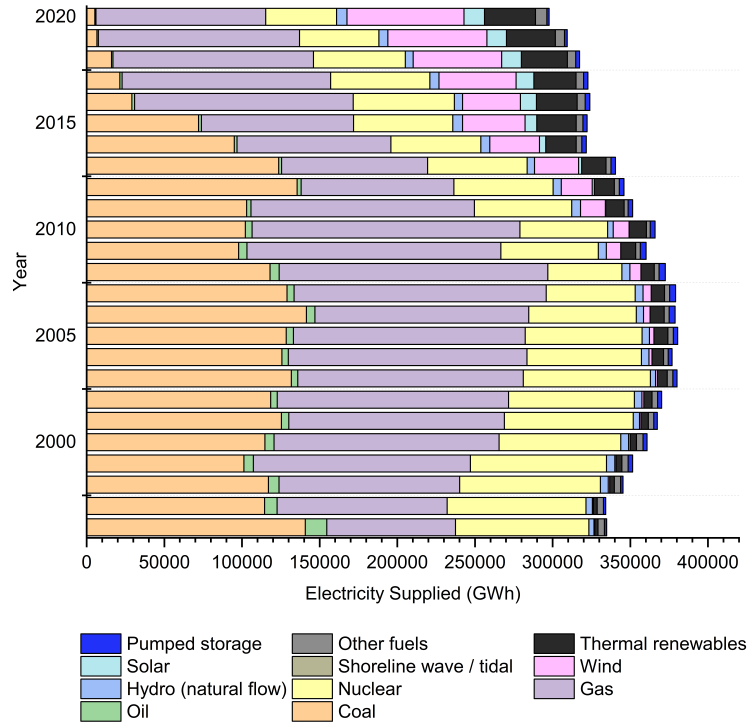
Figure 1.1: U.K. Electricity supply statistics from 1996 to 2020 [8]

further unpredictability to the generation and distribution balance.

The work contained in this thesis seeks to address some of the most important challenges presented to the electricity generation, distribution and consumption network. Two specific areas of interest are that of frequency response services and the economics that allow different energy storage mediums to participate in these markets, and the rapid rise of distributed generation (DG) putting increasing strain on local distribution networks.

Distributed generation is defined as an electricity generating plant that is connected to the distribution network, rather than to the higher voltage transmission network. It has recently been shown that DG constitutes 35% of the total generation capacity within Great Britain, all of which cannot be used for controlling the operation of the system as a whole and thus causing significant challenges in balancing the system [9].

Table 1.1: Selected statistics from the 'Future Energy Scenarios' report (2021) by NGESO [7]

| Category | Subcategory | 2020 Supply/Demand (TWh) | 2050 Scenario Supply/Demand (TWh) | | | |
|---|---|---|---|---|---|---|
| | | | Consumer Transformation | System Transformation | Leading the Way | Steady Progression |
| **Demand** | | | | | | |
| End User Demand | Road Transport (Electricity) | 1 | 102 | 94 | 95 | 101 |
| | Residential (Electricity) | 94 | 146 | 120 | 119 | 130 |
| | Industrial & Commercial (Electricity) | 174 | 275 | 212 | 230 | 191 |
| Transformation Demand | Electrolysis (Electricity Demand) | 0 | 145 | 110 | 212 | 2 |
| | Electricity storage (Annual energy stored) | 2 | 16 | 15 | 10 | 15 |
| **Supply** | | | | | | |
| Generation | Solar | 12 | 68 | 49 | 81 | 28 |
| | Nuclear | 47 | 73 | 49 | 33 | 53 |
| | Wind | 89 | 645 | 514 | 526 | 393 |
| Trading | Import | 27 | 23 | 18 | 78 | 40 |
| | Export | 7 | 164 | 126 | 84 | 79 |
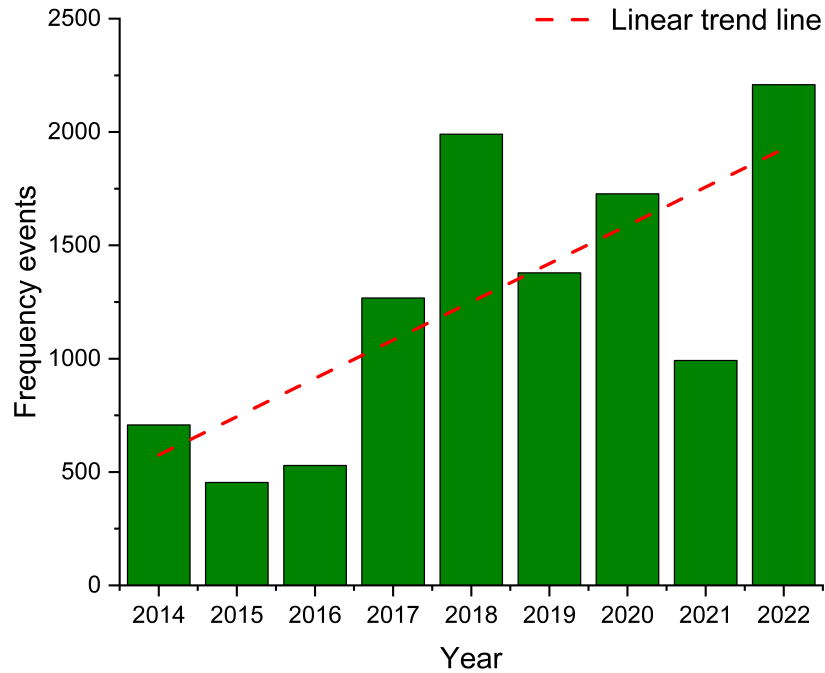
Figure 1.2: Deviations outside of operational frequency limits (+/-0.2Hz) each year from 2014-2022 [10]

One of the key areas of the electricity distribution system that is being affected by these rapid changes is the obligation for NGESO to maintain the frequency of the national grid within statutory (49.5Hz - 50.5Hz) and operational (49.8Hz - 50.2Hz) limits at all times [11]. It has been shown that the regularity of high or low-frequency events (when the frequency goes above 50.2Hz or below 49.8Hz respectively) has been increasing rapidly in recent years with [12] discussing the fact that between 2016 and 2018 the frequency of these events occurring increased by almost four times. Using frequency data from NGESO, the number of times that the frequency deviated outside of the normal operation limits (+/-0.2Hz from 50Hz) for each year from 2014 to 2022 was plotted in Figure 1.2, showing an increasing trend in these occurrences. These events can cause tripping of generators, disconnection of demand, or in the most severe cases damage to equipment and danger to life.

Within the current electricity system, many mechanisms exist that are designed to balance supply and demand in order to maintain the correct operation of the grid and keep it within these limits. One branch of such mechanisms falls under the terminology of 'frequency response services' with Fig. 1.3 showing the various services that are currently either active or recently decommissioned. The new suite of services shown did not exist at the outset of the work contained in this thesis. These services operate by providing a framework for operators to bid to provide a
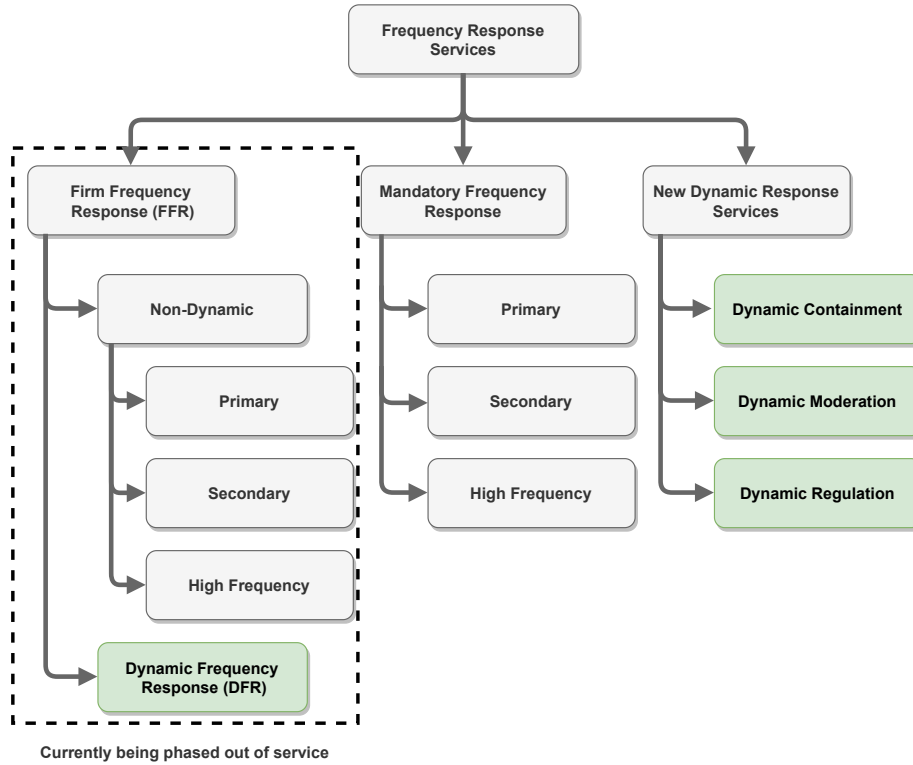
Figure 1.3: Frequency Response Services in Great Britain [13], with the specific areas of interest for this thesis highlighted

service for varying durations and power outputs, with each service having its own bespoke response profile that determines how the operator needs to either provide or take energy from the grid according to the level of deviation away from 50Hz. At the time of writing, NGESO is in the process of replacing firm frequency response with a new suite of dynamic response services consisting of dynamic containment (DC), dynamic moderation (DM) and dynamic regulation (DR). The dynamic arm of the firm frequency response branch (referred to as dynamic frequency response (DFR)) has extensive performance and payment data available and hence represents an excellent tool to benchmark different solutions against when considering the viability of providing these services. The mechanisms for payment and terms of operation for both the existing and proposed services are detailed within Chapter 5 and 7. As the new suite of services is still relatively new, the terms of operation are still being refined through continuous feedback between NGESO and the industry.

Another important area that is both a present and future challenge is the distribution network infrastructure within Great Britain. A 2016 report from the UK Government highlighted that new connection requests continued to rise rapidly along with concerns for geographical variations in costs for these connections [14]. The drive towards DG is putting an increasing strain upon the ability of Distribution Network Operators to connect new DG sites. Within Great Britain, there are 6 ma-
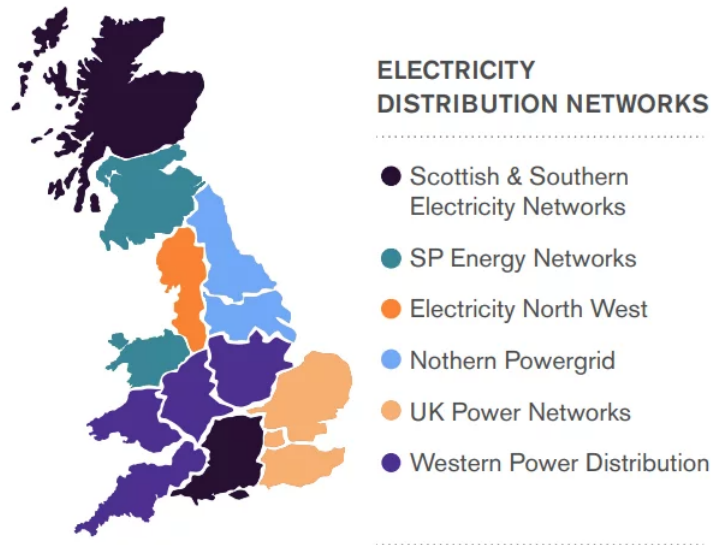
Figure 1.4: Map of the Distribution Network Operators in Great Britain [15] (Note that Western Power Distribution is now operated as National Grid Electricity Distribution)

jor distribution network operators covering a total of 14 geographical areas, as shown in Figure 1.4. They are responsible for operating and maintaining the distribution infrastructure within their geographical area such as substations, transmission lines, and new connections.

To illustrate the difficulties faced by many distribution network operators, Figure 1.5 shows all of the substations owned by the largest Distribution Network Operators in the UK (National Grid Electricity Distribution, previously known as Western Power Distribution) that do not have the capacity for generation in excess of 1MW to be connected. The 1MW criterion is linked to the requirements for the 'Embedded Capacity Register', which requires all distribution network operators to provide information on generation and storage resources which are connected or accepted to connect to the National Grid's distribution network. In total, 56.4% of the substations operated by National Grid Electricity Distribution are rated 'red' in their online capacity map, meaning a connection is unlikely to be achieved without significant investment. The impact of this can be seen primarily in the increasing prevalence of 'Export Limitation Schemes' (ELSs) agreed by local distribution network operators to limit the export of a DG site below an agreed value. This could be driven by equipment limitations such as substation, transformer or distribution cable capacities [16]. Conditions under which an ELS would be considered for implementation include:

- A DG site wishes to install more generation in order to offset their imported electricity costs, but the extra generation would exceed the local distribution network capacity. An ELS may be proposed to allow the generation to be
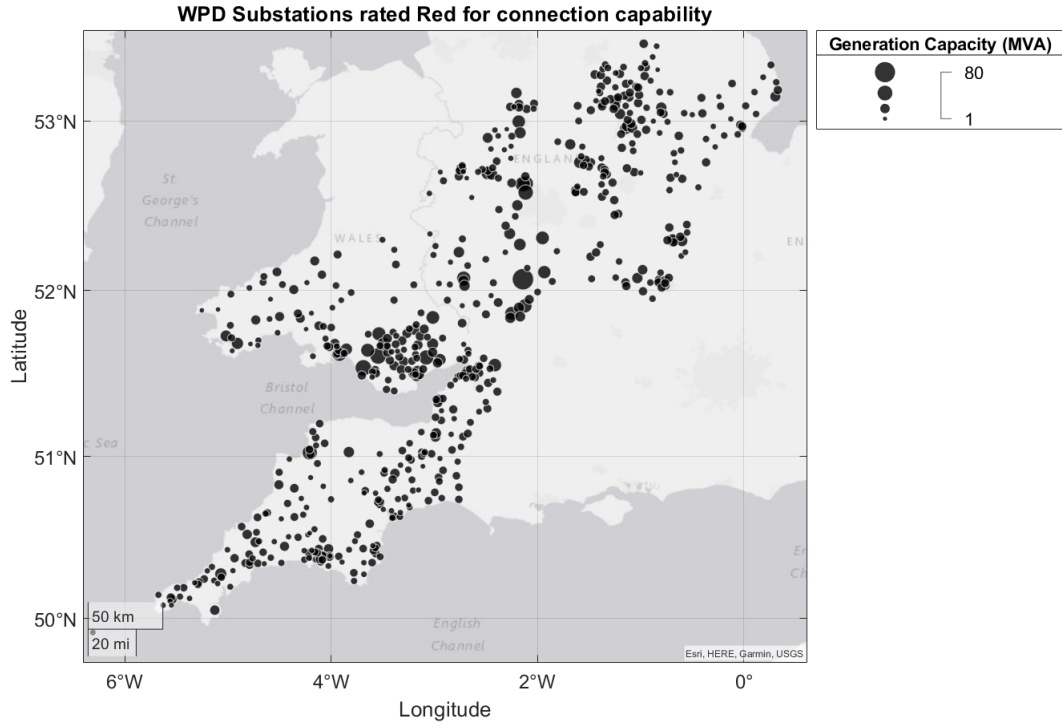
Figure 1.5: National Grid Electricity Distribution Network Capacity Map showing the sites currently rated as 'Red' [17]

connected without adding to the local distribution network.

- A new DG site is proposed but there is insufficient local capacity to connect to the local distribution network. In this instance, an ELS could be sought to allow the project to go ahead without the need for immediate reinforcement works.

Often, a major driving factor in applying for an ELS is the avoidance of the requirement to contribute to upstream network reinforcement, or the need to wait for the potentially lengthy reinforcement works to be completed [18]. Both of these factors play a significant role in the viability of both DG and ESS sites and so an ELS can allow them to be implemented whilst remaining technically and economically viable. As the rapid deployment of DG continues and more parts of the network reach capacity, these local distribution network limitations will become more prevalent impacting both the feasibility of DG projects and the wider national electricity system picture.

When considering solutions to the issues faced by the electricity network in the U.K. and across the world, one of the key areas that receives extensive research and development is energy storage systems (ESSs). In this thesis, the two energy storage technologies primarily focused on are flywheel energy storage systems (FESSs) and Battery energy storage systems (BESSs). A detailed assessment of the strengths and

Table 1.2: High-level FESS and BESS characteristics [1]

| Characteristics | FESS | BESS (Li-Ion) |
|---|---|---|
| Energy Density | 5-200 Wh/kg | 30-300 Wh/kg |
| Application duration | Seconds to minutes | Hours to days |
| Self discharge rate | 20-100% per day | 1-10% per day |
| Cycle life | 100,000+ | 2,000-10,000 |
| Calendar life | 20 years+ | 10-20 years |

weaknesses of both of these energy storage mediums is contained within Chapter 2. During the course of this work, the BESS technology being considered is Li-ion unless stated otherwise.

Lithium-ion has been selected as the technology of choice as it is the most widely deployed and commercially mature BESS technology used for grid-scale ESSs [19] [20]. An overview of the high-level characteristics of the two mediums is shown in Table 1.2 and shows that the two types of ESS have significantly different attributes, which this thesis will seek to exploit.

Within this thesis, FESSs are defined as very short duration energy storage, referring to the fact that generally they are considered best at dispatching power in the region of seconds to minutes. BESSs are generally considered to be short to medium duration ESSs. They mostly operate in the region of hours to days of storage.

The research contained within this thesis was initially sponsored by the company OXTO Ltd [21]. This sponsorship resulted in access to technical specifications of the FESS being developed as well as an introduction to third parties who were interested in developing case studies for grid-based applications such as renewable integration and frequency response services.

### 1.1.1 Study Period

Unless otherwise stated, the frequency data utilised throughout this thesis is from the period between November 2020 and October 2021. This was the most up-to-date data available at the start of the majority of the studies contained in this thesis, and in order to maintain consistency the same data was used throughout subsequent studies.

To provide context for this time period, Figures 1.6 and 1.7 show the operational frequency data from January 2014 to December 2022 for Great Britain. From Figure 1.6 it is clear that the average frequency for each month stays in a very narrow range, from a high of 50.00078Hz in February 2014 to a low of 49.99828Hz in January 2018. In Figure 1.7 the same trend can be observed, with the maximum and minimum
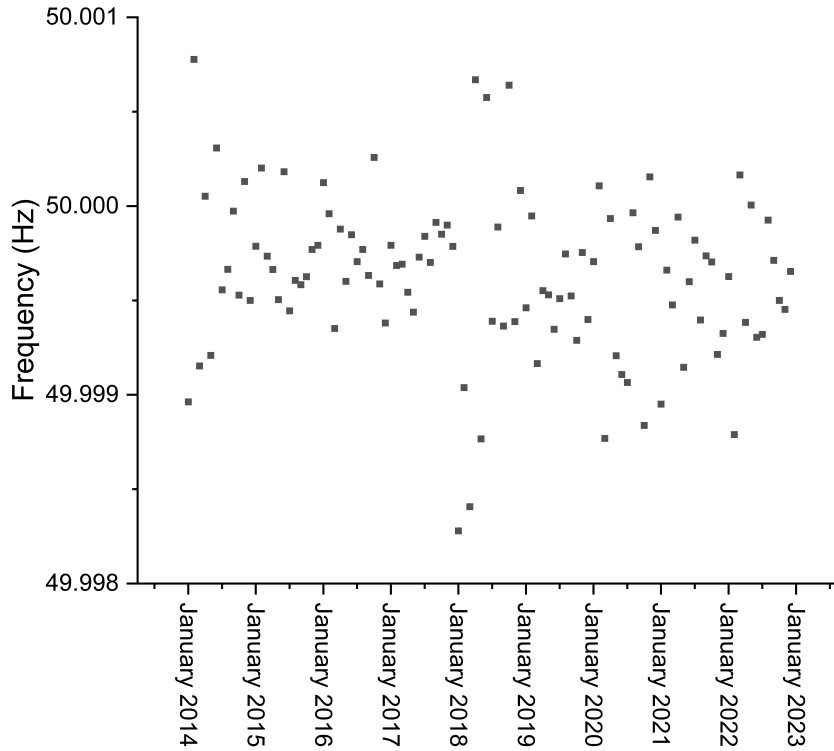
Figure 1.6: Mean frequency of the Great Britain electricity network from January 2014 to December 2022

frequencies staying in a narrow range. The only outlier is August 2019 when a minimum frequency of 48.787Hz was observed due to an event occurring on 9th August 2019 which included a simultaneous loss of generation across the network [22].

Figure 1.8 shows the duration of time that the frequency went outside of the operational (+/-0.2Hz) or regulatory (+/-0.5Hz) limits from January 2014 to December 2022. It can be seen that from January 2018 onwards the time spent outside of these limits becomes more prominent, suggesting that the grid frequency is becoming more unstable.

Overall, it can be determined the grid frequency maintains a similar pattern across the past 8 years of operation, and hence the study period selected is likely to be representative of typical grid conditions.

For the wind generation-based studies, the period chosen for the study was dictated by the data made available by the industrial sponsor for this project, and the effects of changing the studied time period for this application are discussed in Chapter 4.
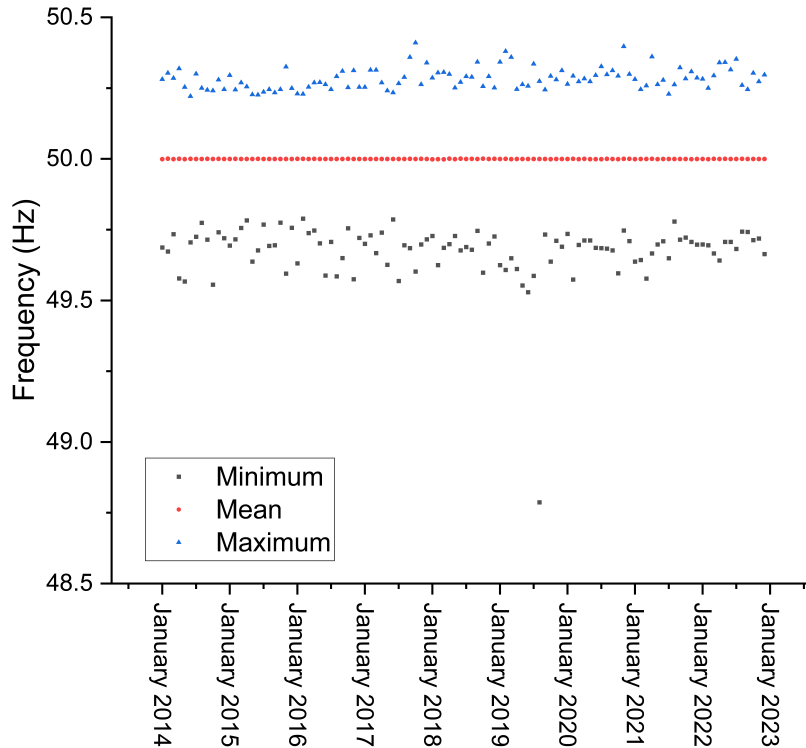
Figure 1.7: Maximum, minimum and mean frequency of the Great Britain electricity network from January 2014 to December 2022

## 1.1.2 Thesis Objectives

The main aim of this research is to explore in detail ways of exploiting the unique characteristics of a FESS to provide a standalone solution to grid stability and distribution network issues, or by using the advantages of both FESS and BESS units to attempt to counter the disadvantages of each individual system by introducing a hybrid energy storage system (HESS), creating a better techno-economic solution. The research has been conducted with an underlying theme of viability considering not just the technical performance of these systems but also the economic performance. The key overarching objectives are detailed below, with more specific objectives detailed at the start of each technical chapter:

1. Develop a model that can rapidly and accurately simulate both flywheel and battery energy storage systems that are also easily configurable to different applications. (Chapter 3)

2. Explore the potential for energy storage systems to provide support to DG sites that are export limited, exploring the techno-economic benefits of different types of ESS (Chapter 4)

3. Produce a detailed exploration of the suitability of FESSs for the provision of
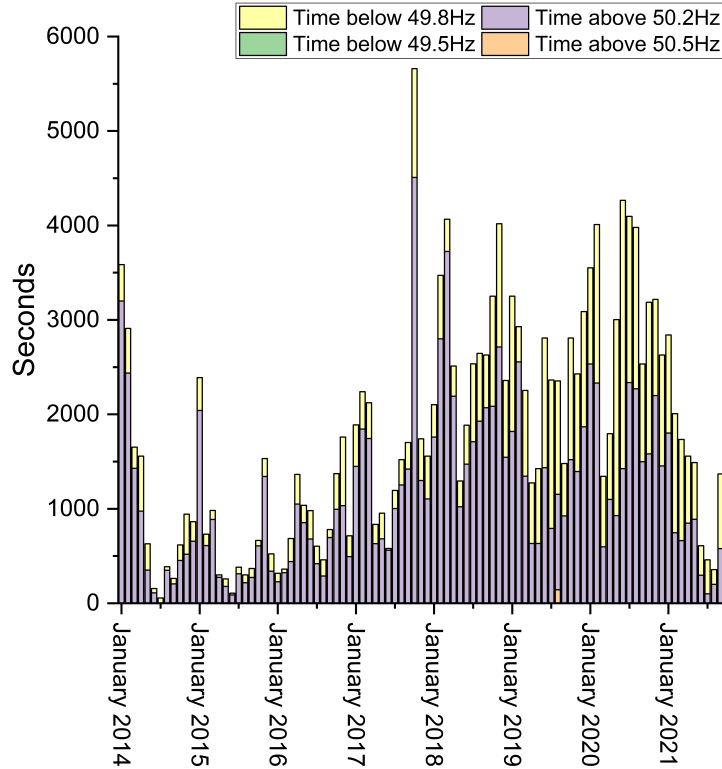
Figure 1.8: Duration of time frequency was outside of regulatory and operational limits from January 2014 to December 2022

traditional frequency response services, both as standalone and hybrid units. (Chapter 5, 6)

4. Explore the possibilities of designing frequency response services specifically for delivery by FESSs, and what technical and economic parameters would be required for this to be feasible. (Chapter 7)

5. Provide an expansive investigation into the required economic parameters that need to be met in order to allow FESSs to be deployed as competitive energy storage units in different applications. (Chapter 4, 5, 6 and 7)

### 1.1.3 Thesis Contributions

In four novel chapters, this work looks at past, present and future scenarios to investigate the ability of a FESS to play a meaningful role in providing solutions to the mounting challenges faced by electricity networks.

A detailed modular FESS and BESS model is developed for fast and accurate modelling which allows for easy re-configuration between different applications. This model is then used as the basis for investigations into grid services and local distribution network applications, firstly looking at how FESS, BESS and HESS technology can be implemented to mitigate export limited DG sites including a specific site case

study. This study illustrates the potential for providing greater techno-economic performance at such sites and allowing further deployment of DG that is important if the electricity grid is to reach the required capacity levels in coming years.

A detailed analysis is also conducted into the feasibility of using a FESS for the provision of frequency response services. Initially, this is done by assessing both FESS and HESS configurations under the operational characteristics of DFR. A techno-economic analysis is conducted across a range of different scenarios, with the well-defined parameters of DFR providing a framework that gives insight into the potential performance across other frequency response services. By exploring HESS configurations both in terms of sizing and control, it is possible to create additional value for such installations and allow a wider range of technologies to be deployed, as well as potentially decreasing the environmental impact of such systems by ensuring they operate over a longer duration of time.

Finally, a novel bespoke frequency response service is designed for provision by FESSs, showing for the first time how such very short duration storage can be effectively deployed as a continuous provider of response services. The economic analysis conducted shows that flywheels could compete with or even surpass the performance of BESSs when their relative strengths are utilised as a key part of the design process.

The novel works produced by this research and contained within this thesis have been presented in four journal articles and seven conference proceedings papers, a list of which is contained at the start of the thesis.

## Rapid application-based modelling and simulation of energy storage systems

Modelling of ESSs is an essential part of the research and development of new solutions to the challenges discussed in this work. Across the literature, many forms of modelling are utilised such as mathematical or electrical models, across a wide range of different programs. In terms of application-based research, it is often difficult to rapidly model and simulate new applications due to the range of detailed input information required for such models. The resources that do exist within the MATLAB/Simulink environment also call for detailed knowledge of the technical characteristics of the system being modelled.

In Chapter 3, a novel set of modular simulation subsystems is introduced, simplifying and speeding up the process of modelling FESS, BESS and HESS systems and providing a basis for similar components to be created for other energy storage mediums. The BESS model is verified against a University of Sheffield-operated 2MW/1MWh lithium titanate battery known as the Willenhall ESS where the model is shown to be an accurate representation of the operation of the real-world ESS.

The work also implements a degradation algorithm for the BESS model, spinning losses for the FESS model, cycle counting based upon instantaneous micro-cycles, and a suite of easily modifiable efficiencies, metrics and control mechanisms.

A second verification exercise is then performed on the degradation aspect of the BESS model, comparing a set of Li-ion cells that have been subjected to cycling tests with the simulated levels of degradation for varying load profiles. These results show a high degree of accuracy between the achieved and simulated levels, illustrating the model's importance as an energy storage application assessment tool.

**Export Limitation: Unlocking the potential of distributed generation using energy storage**

Chapter 4 looks in detail at the export limitation issue facing DG sites in Great Britain. A novel study into the alleviation of export limitation is conducted, showing for the first time how a FESS can be used as an effective method of extracting the full potential from a wind generation site subjected to export limitation. A sensitivity analysis shows that significant capacity factor (CF) increases can be achieved across a range of different scenarios, whilst a novel economic sensitivity analysis shows the total capital cost (TCC) in £/kW that must be achieved to provide a positive economic impact to the site for a variety of different scenarios and FESS specifications. This is important to the continued commercial development of FESSs, with the research providing realistic targets for researchers and manufacturers to aim for in order to develop FESSs that are economically viable for this application.

Subsequently, a novel site-specific case study is undertaken utilising a real-world scenario of an export-limited wind generation site. For this case study, a comparison between FESS and BESS solutions is presented, highlighting the difficulties with using cycle sensitive ESSs for highly cyclic applications such as these, and performing economic analysis to illustrate the scenarios in which either a FESS or BESS may perform better. It is shown that due to the degradation suffered by a BESS for this application, a FESS is a much more suitable candidate, showing real-world applicability to the results produced in this novel application.

**Flywheels as standalone providers of Frequency Response services**

Moving on from the local distribution level discussion of Chapter 4 to a system-level approach, Chapter 5 initially considers the effectiveness of a FESS to provide a DFR service as a standalone storage system. From this, it is shown that for most commercially available FESS configurations, the provision of a 24/7 frequency response service is too energy-intensive to be viable at the commonly found existing

TCC values.

However, the research does identify for the first time the threshold at which various configurations of FESS would become economically viable to provide this service, once again providing key insight for technology developers to aim for specific cost and specification targets. From this study, hybridisation with a BESS is then introduced. An initial sensitivity analysis is conducted on introducing small amounts of BESS to the standalone FESS to determine the techno-economic impact. It is shown that there is a fine balance between the cost of the individual systems and the proportion of each storage medium present in the HESS.

**Hybridisation of flywheels for frequency response service delivery**

Following on from the previous chapter, this work builds upon this initial assessment, firstly by presenting a suite of novel HESS control schemes. These control schemes are introduced and detailed, all representing different ways of attempting to lessen the strain on the BESS whilst increasing or maintaining an acceptable level of technical performance.

Following this, the analysis of hybrid systems is split into two subsections. The first concerns the use of a genetic algorithm to determine the optimum FESS configuration that will provide the greatest increase to the economic performance of the site, showcasing that a wide range of different configurations can have a positive impact on the net present value of the installation.

The approach is then shifted to an iterative one, through various sensitivity analysis both the economic performance and the required level of total capital cost to provide a positive impact is explored. This provides important information for FESS researchers and manufacturers, as a guideline for the cost that different configurations will be required to achieve to perform this service.

**Assessment of flywheel energy storage for participation in future frequency response markets**

The final chapter looks to the future of providing frequency response services for the Great Britain grid. In Chapter 7, the suitability of FESSs for providing the new suite of frequency response services is assessed for the first time in a novel sensitivity analysis study. It is shown that whilst a wide range of FESS configurations can provide the required level of availability for DC, the current rules around the minimum duration and energy capacity rule FESSs out of delivering it. Looking at the remaining two new services, it is shown that no configuration of FESS analysed can provide the requisite level of performance for DR and only a narrow window of configurations can provide DM. These results are key in continuing the dialogue

with NGESO to encourage revisions that allow a wider range of ESS mediums to participate, often stated as an original goal of the new suite of services.

To fully explore this issue, Chapter 7 closes with the development of a novel frequency response service designed specifically for delivery by a FESS. A response envelope is developed through an iterative design process incorporating similar features to the currently marketed services, followed by a sensitivity analysis on how varying configurations of FESS perform when attempting to deliver the service 24/7. It is shown that under this novel response envelope, a significant range of different FESS sizes can achieve the required performance levels delivering a constant service over the course of a year, with increasing levels of performance as the energy capacity of the FESS is increased. This is a significant advancement in the field of FESS research, as it shows that services previously dominated by BESS technology and where a FESS is considered unsuitable, can in fact be provided competitively by a FESS.

Finally, an economic analysis is conducted, outlining the profitability of varying FESS configurations providing such a service. It shows that there would be a significant economic benefit in using the bespoke response profile to provide a similar service to those that are existing or proposed by NGESO. This conclusion can help shape the narrative of grid-scale frequency control, and allow a wider range of storage devices to be utilised in this market.

# Chapter 2

# Energy Storage Systems - Characteristics, Applications and Economics

This chapter concentrates on an overview of ESSs, before specifically focusing on the areas of concern for this thesis. In lieu of a traditional literature review section, the relevant literature is explored within the chapter in which it is most suited as shown in Figure 2.1, and listed below;

- Chapter 3 - Modelling of ESSs, economic analysis methods, modelling of degradation within Li-ion batteries, genetic algorithms

- Chapter 4 - ESSs for curtailment avoidance and mitigation

- Chapter 5 - ESSs for frequency response services

- Chapter 7 - New frequency response services

In the following sections, reference will be made to the specification and operation of different types of ESS. A common set of terminology exists between all ESSs to enable easy comparison between them. The following list sets out the key terms of reference for an ESS;

- State of charge (SOC) - Defined as the total amount of available energy within an ESS at time $t$ as a proportion of the total energy capacity as shown in Equation 2.1 where $E_t$ is the energy currently stored within the ESS at time $t$. For example, a 10kWh ESS with 5kWh of energy currently available would be at 50% SOC.

- Depth of discharge - The most common definition of this is the total energy discharged within one discharge event as a percentage of the total energy

capacity. For example, an ESS at 50% SOC that discharges to 40% SOC would have experienced a 10% depth of discharge. However, in some applications where microcycling is present, this is difficult to extract due to rapid changes in SOC in both directions and this aspect will be discussed in further detail in Chapter 3.

- Energy capacity - The total amount of energy available to be stored within the ESS at 100% SOC, given in kWh throughout this thesis unless otherwise stated.

- Power rating - The maximum power that the ESS can either charge or discharge at, given in kW throughout this thesis unless otherwise stated.

- C-Rate - The C-Rate provides an immediately recognisable metric that can be produced and compared between all ESS mediums. It represents the speed at which an ESS can be fully charged or discharged. For instance, a 1kWh ESS rated at 10C will fully discharge at 10kW in 6 minutes, whilst a 1kWh ESS rated at 1C will fully discharge at 1kW in 60 minutes. Equation 2.2 can be used to calculate the rated C-Rate for a given ESS using energy capacity ($E_{\text{ESS}}$) in kWh and rated power ($P_{\text{ESS}}$) in kW. The units are not relevant within Equation 2.2, as it is purely a ratio between the two values, and no conversion is required between the kWh value and kW value. It is important to note that this is the maximum rated C-Rate for a given ESS, and the instantaneous C-Rate can be lower than this value, i.e. the ESS can be charged or discharged slower than its maximum capability [23]. It can also be described on a basic level as the Power/Energy ratio of the system. In this thesis, all BESSs are considered as 1C unless stated otherwise.

- Cycle life - The most basic indicator of the potential serviceable lifetime of an ESS, the cycle life represents the total number of complete charge/discharge cycles that an ESS can perform before reaching end-of-life. In this thesis, 1 cycle is defined as the energy required to transition an ESS from 0-100% SOC or vice versa.

$$SOC(t) = \frac{E_t}{E_{ESS}} \tag{2.1}$$

$$C_{rated} = \frac{P_{ESS}}{E_{ESS}} \tag{2.2}$$
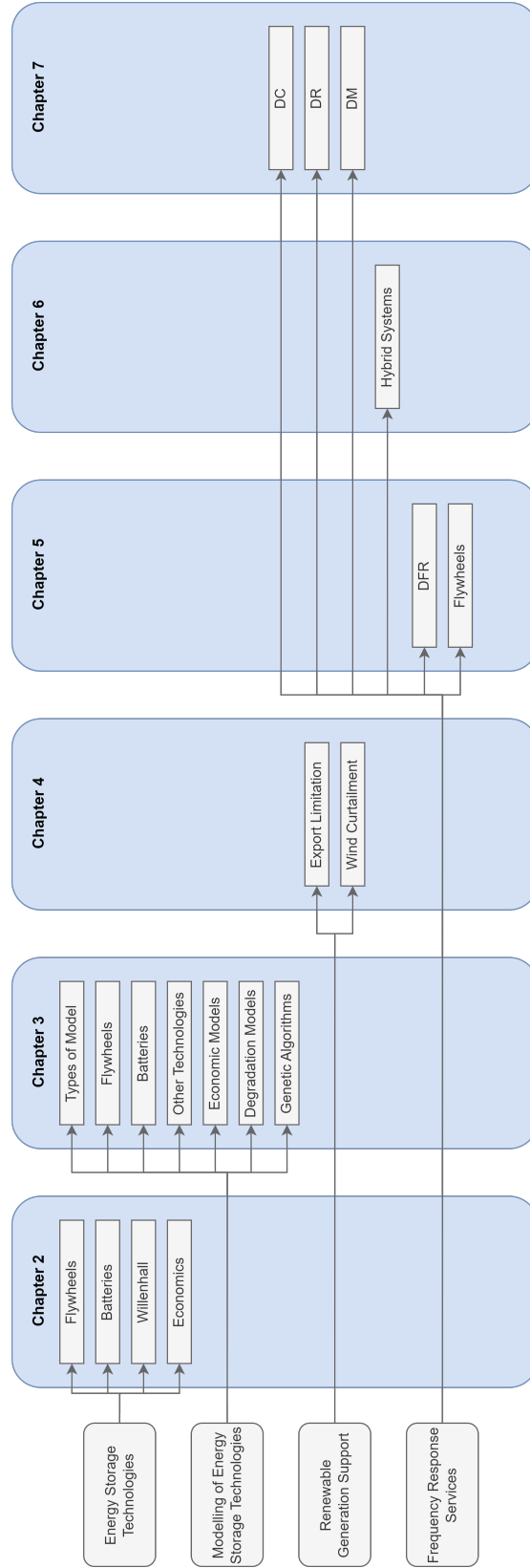
Figure 2.1: Division of Literature Review

ESSs have been a prevalent part of the electricity distribution system since the early 1900s in the form of pumped hydro storage which still dominates the worldwide deployed level of ES capacity [20]. As the electricity system has evolved the requirement for a wide variety of different energy storage mediums has increased, leading to a vast range of different types of storage as seen in Fig. 2.2. In fact, energy storage is now becoming so prevalent that in June 2022, the electricity mix in the U.K. consisted of 1.0% from energy storage, higher than the 0.4% generated from coal [24]. It is also highly likely that the landscape for energy storage technologies will change significantly in the coming decades, as emerging technologies such as hydrogen energy storage, compressed air energy storage and alternative chemistries of BESS reach commercial maturity.

Beyond economic considerations, some of the key characteristics that define ESSs are power density (W/kg), energy density (Wh/kg) and C-Rate. Figure 2.3. shows a diagram of various ESS mediums, the scale of power at which they are typically deployed, the duration they take to discharge fully and typical applications. It is immediately apparent that Li-ion batteries are one of the most versatile ESS mediums currently available, occupying a significant range of both discharge time and power ratings. Looking at other ESS mediums that occupy unique spaces, compressed air energy storage (CAES) and pumped hydro storage both traditionally deliver power at the highest levels and store their energy over significant durations. However, they generally require vast amounts of space or intrusive environmental impacts meaning they are unsuitable for smaller scale and local level systems [26]. Emerging technologies such as thermal energy storage are also being developed to store energy for long durations as well as being able to discharge this energy in multiple forms (either as heat or power).

Of particular interest to the work presented in this thesis are FESSs which offer shorter duration energy storage than other mediums, whilst retaining an excellent power range. FESSs and BESSs constituted the highest proportion of installed capacity (excluding pumped hydro storage) as of 2016 accounting for 28% and 41% respectively [20]. Supercapacitors are the main type of ESS that challenges in a similar region of operation. It is these contrasting areas of operation that will be investigated in detail within this project, looking at how the longer and shorter term ESSs can operate together to create a stronger techno-economic solution for various applications.

The main ESS medium that competes in a similar space to FESSs is supercapacitors, also sometimes referred to as Ultracapacitors. They generally consist of two metal plates with a thin separator between them but differ from traditional capacitors in the fact that the plates are contained within an electrolyte which allows them to create a small 'double layer' of charge between the two plates, thus allowing
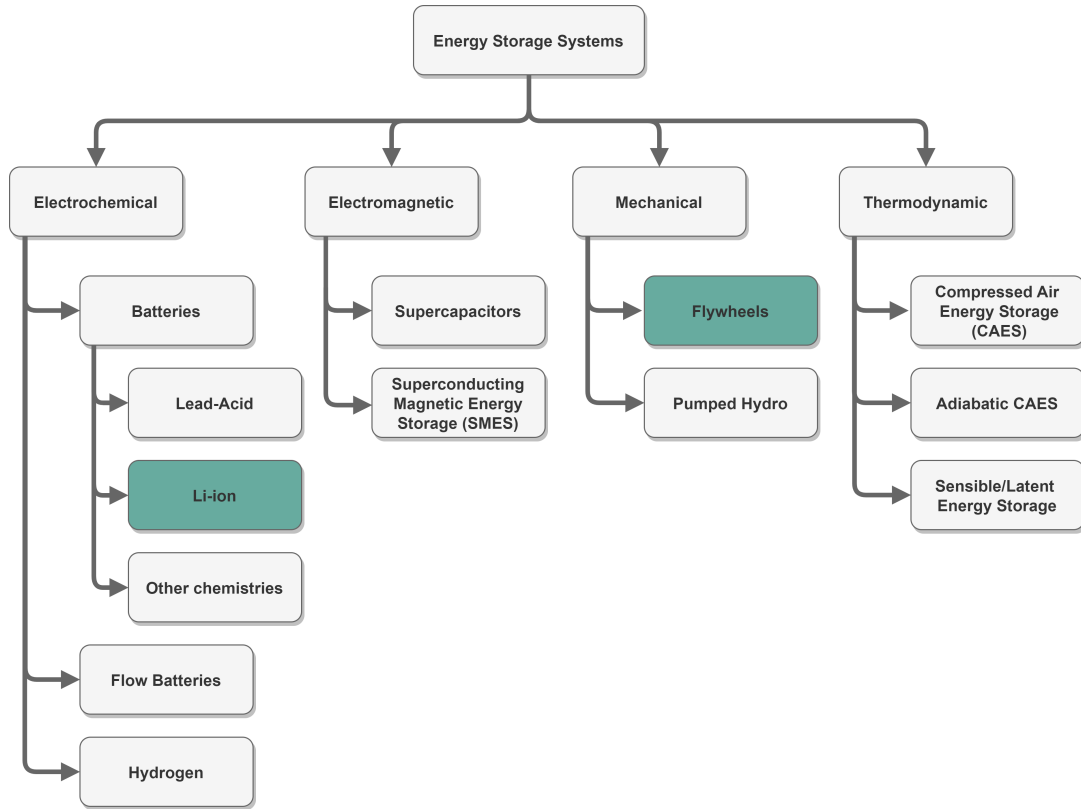
Figure 2.2: Classification of Energy Storage technologies with the areas of interest of this thesis highlighted

them to store more energy due to increased surface area.

## 2.1 Flywheel Energy Storage Systems (FESSs)

FESSs fall under the category of 'mechanical energy storage'. At their base level, they primarily consist of a rotating mass that can be sped up (charged) or slowed down (discharged). This is achieved by using a bi-directional electrical machine connected to the rotor that can be used as a motor to spin the flywheel faster, or that can be driven by the flywheel rotor as a generator when discharging. Figure 2.4 shows a diagrammatic representation of a flywheel, with the key elements consisting of the rotor, the housing (or containment), the electrical machine and the bearings. The representation in Fig. 2.4 is of a horizontal axis FESS which is more common than vertical axis FESSs.

Figure 2.5 shows some examples of different FESS internal design and structure where 'A' shows one of the most common set ups, with the rotor consisting of a disc shape with the electromagnetic machine being connected in line either inside or outside of the containment housing. 'B' illustrates the barrel type where the flywheel rotor is 'hollow', whilst 'C' shows the integrated design type where the electromagnetic machine is integrated directly into the rotor construction.
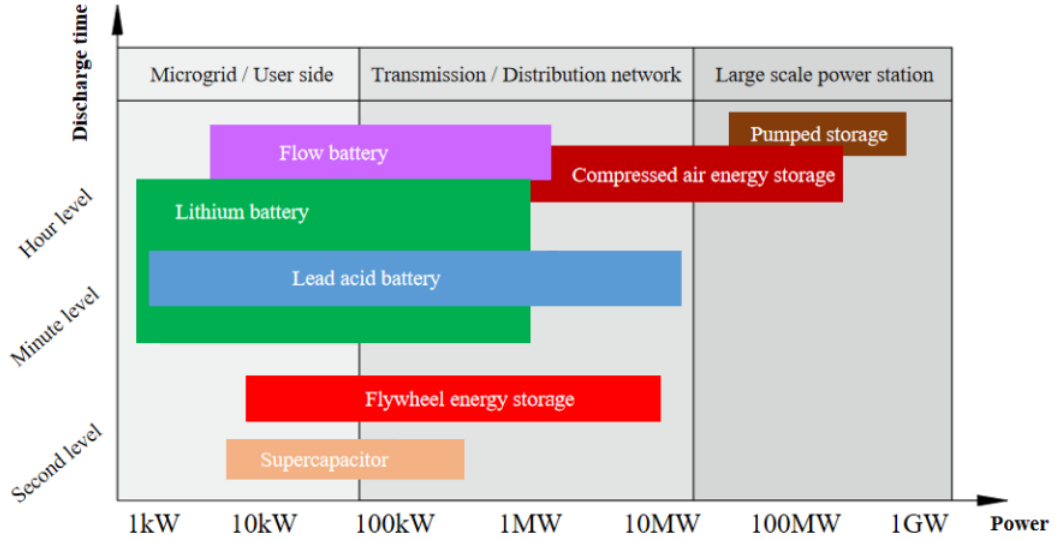
Figure 2.3: Schematic diagram of various ESSs and their associated power and energy capacities adapted from [25]

Figure 2.6 shows three examples of FESS installations. Flywheel systems can vary significantly in size and orientation, with the example in Figure 2.6c showing an installation where the flywheel is submerged below ground as part of the containment. Figure 2.6a and 2.6b show containerised systems consisting of multiple individual units. The FESS in 2.6b is the system being considered within this project as part of the work done by industrial sponsor OXTO Energy.

On a fundamental level, the operation of a flywheel is governed by a set of equations. In Equation 2.3, the energy density of the flywheel is determined where $E$ is energy in joules, $V$ is the volume of the flywheel, $K$ is the shape factor of the flywheel and $\sigma_{max}$ is the maximum hoop stress in megapascals. Some examples of different flywheel forms and their associated shape factors are shown in Figure 2.7. In this thesis, a solid disc flywheel is utilised in the models as this was the chosen shape of the industrial sponsor of this work.

$$\frac{E}{V} = K\sigma_{max} \tag{2.3}$$

Following on from this, equations 2.4, 2.5 and 2.6 show further detail on the various factors that influence a flywheel's operation, where $I$ is the moment of inertia in $kg/m^2$, $m_f$ is the mass of the flywheel in kg, $\omega$ is the angular velocity in radians per second, $\rho$ is the density of the rim in $kg/m^3$ and $r$ is the outer radius of the flywheel.

$$E = \frac{1}{2}I\omega^2 \tag{2.4}$$
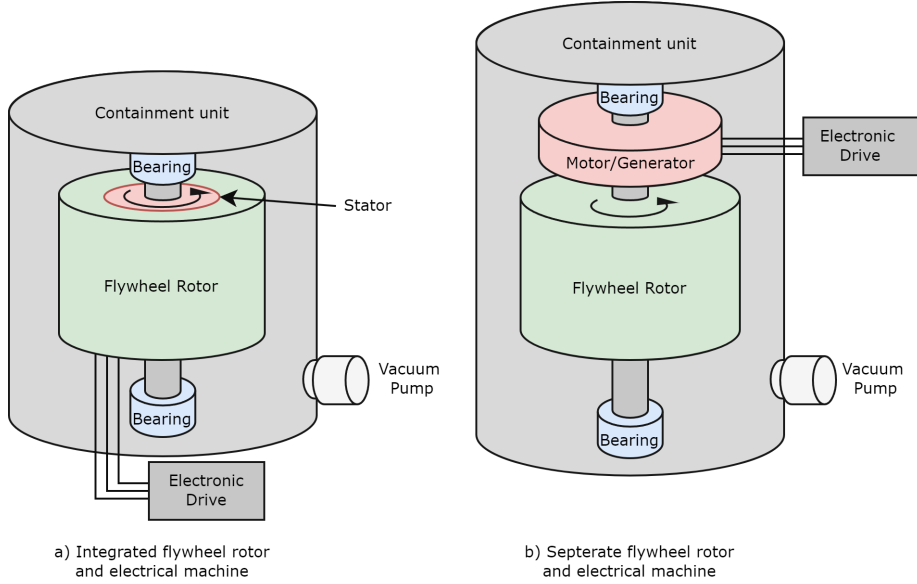
Figure 2.4: Structure of a Flywheel Energy Storage System [27]

$$I = \frac{1}{2}m_f r^2 \tag{2.5}$$

$$\sigma_{max} = \rho r^2 \omega^2 \tag{2.6}$$

The important thing to note from these equations in relation to the work presented in this thesis is that the energy stored within the flywheel is mostly dependent on angular velocity, mass, density of the material, and radius of the flywheel. The angular velocity is one of the main categories where different types of FESS become distinct, being divided into two primary sub-categories consisting of low-speed flywheels (typically 1,000-10,000 rotations per minute) and high-speed flywheels (up to and sometimes beyond 100,000 rotations per minute). Table 2.1 shows a selection of key characteristics from low-speed and high-speed flywheels.

For the purposes of the work presented in this thesis, all of the FESSs that are discussed are low-speed flywheels, specifically due to their low cost, commercial maturity and technical suitability for the applications being discussed. High-speed flywheels are more applicable in very high-power and low-energy applications, such as motor racing or space exploration [33].

The primary characteristic that makes a FESS suitable for this set of research is its excellent resistance to cycle-based degradation. Much of the literature quotes the cycle lifetime of flywheels to be anywhere between 10,000 to 1,000,000 full charge-discharge cycles before failure [35] [36] [37]. The main method of degradation within a FESS is the wear on mechanical bearings (where present) although this is reversible with regular, inexpensive maintenance [27] [38]. Another key method of degradation
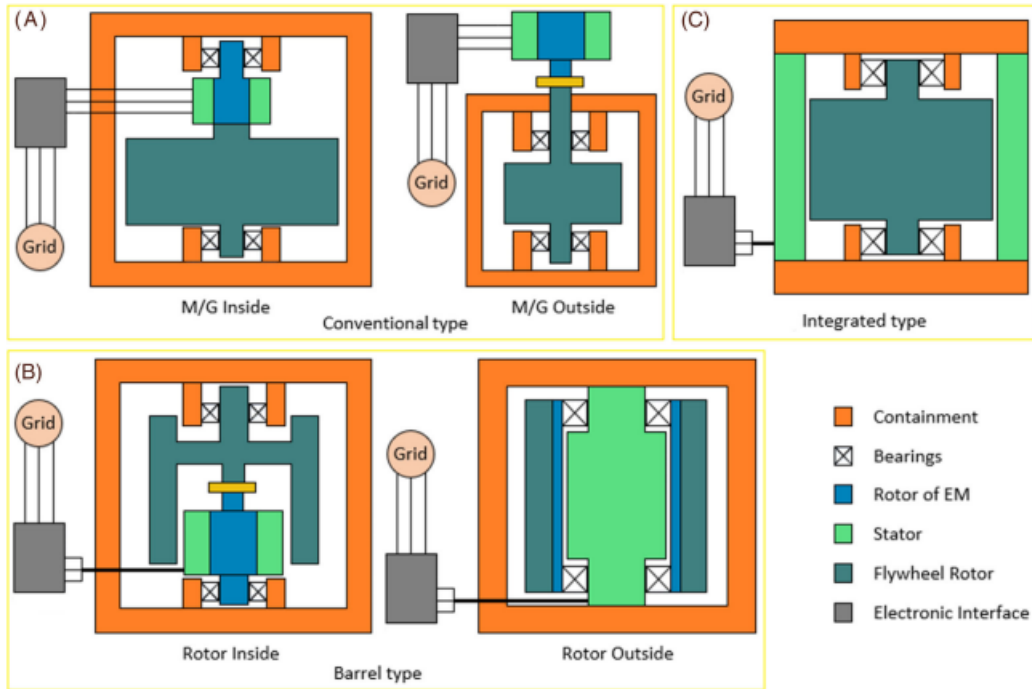
Figure 2.5: Examples of different types of FESS structure [28]

Table 2.1: Table illustrating differences between low and high-speed flywheels adapted from [27] [31] [32] [33] [34]

|  | Low Speed Flywheels | High Speed Flywheels |
|---|---|---|
| Typical Rotor Material | Steel | Composite such as glass or carbon fibre, sometimes steel |
| Typical Material Energy Density (MJ/kg) | 0.15-0.3 | 0.05-2.5 |
| Specific Energy | ~5Wh/kG | ~100Wh/kG |
| Bearing | Mechanical or magnetic | Magnetic |
| Rotations per minute | 1,000-10,000 | 10,000-100,000+ |
| Containment method | Partial vacuum, light gas | Full vacuum |
| Enclosure weight | 2 times weight of flywheel | 0.5 times weight of flywheel |
| Maturity | Commercialised | Early commercialisation |
| Typical applications | Short/Medium term power applications | High power, short duration applications such as traction and aerospace |
| Integration of electrical machine | None or partial integration | Full or partial integration |
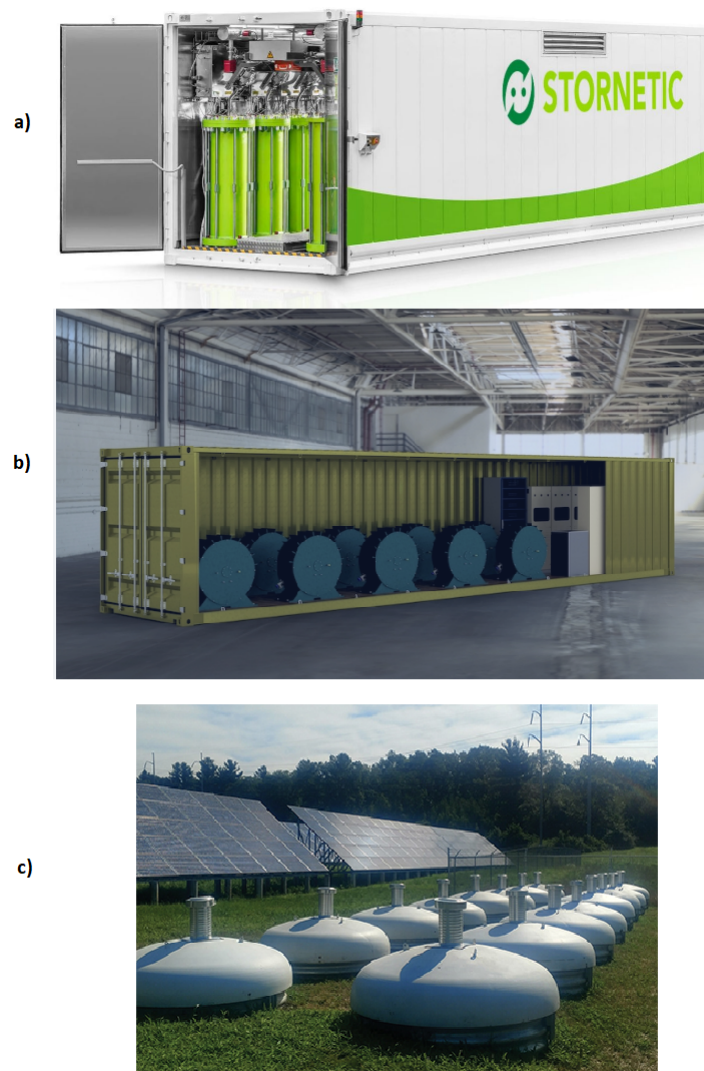
Figure 2.6: Examples of flywheel installations - a) Stornetic b) OXTO c) Amber Kinetics [29] [21] [30]

occurs within the Motor/Generator, with increased heat causing the windings to degrade. A figure of 20 years is the most often quoted statistic for calendar-based lifetime but this can vary based on manufacturers' specifications and warranties.

Magnetic bearings represented a significant advancement in the viability of flywheels for an increased range of applications. Whilst they offer a much-decreased level of self-discharge along with increased lifetime and higher speeds, they also represent a significant increase in the costs of the overall system primarily due to the complexity of design and control [33] [27]. They are mainly utilised for high-speed flywheels and hence are not generally applicable to the class of flywheel that will be studied in depth within this thesis.

Another commonly discussed feature of FESSs is their high levels of self-discharge, often referred to as spinning losses. A flywheel will typically lose between 20-100%
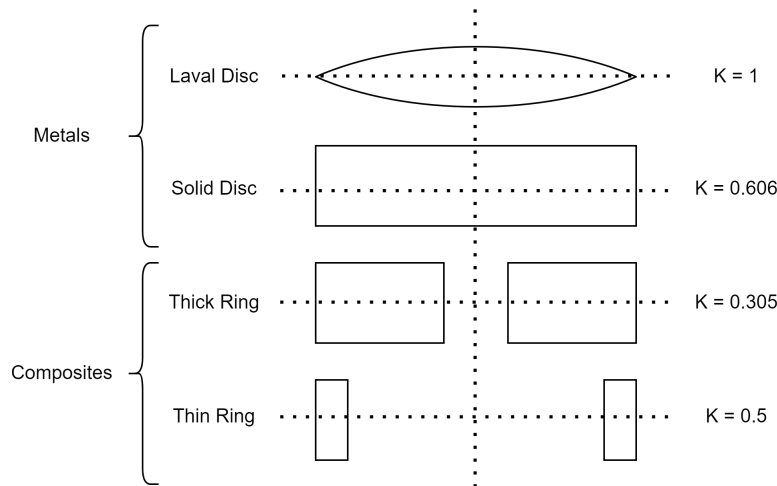
Figure 2.7: Shape factors for different Flywheel forms [28]

of its stored energy over the course of a day [39] [40]. It is for this reason that flywheels are generally most suited to applications where there will be frequent charge/discharge operations enabling them to minimise time spent in an idle state.

Where an ESS is required to charge and discharge frequently the efficiency of the system is an important aspect. Throughout the literature a range of different values for efficiency is quoted spanning from 80% to over 95%, once again indicating a dependence on manufacturer-specific information to be sure of the capabilities of a system. However, it is generally agreed within the literature that flywheels do have a high efficiency compared with other mediums [26] [41] [42]. These efficiency values take into account the total system efficiency, including aspects such as motor/generator efficiency as well as ancillary loads such as the vacuum pump and control systems.

In terms of commercial maturity, there is a wide range of companies operating within the FESS market. Contained in Table 2.2 are details of a range of such manufacturers including information on technical specifications and commercial considerations wherever this information is available. Across the industry, there is increasing variety between both energy-centric and power-centric flywheels giving a good foundation for the investigation of a wide range of applications. Even within the suite of available manufacturers the specified round-trip efficiency ranges between 85% and 99.4%. Several manufacturers claim to have developed flywheels capable of very low rates of self-discharge (0.2-0.3% per hour) which would remove one of the major drawbacks of the technology. The quoted cycle life for many manufacturers is unlimited, whilst all that have the information publicly available specified a minimum of a 100,000 cycle lifetime as well as a minimum calendar lifespan of 20 years.

Table 2.2: Specifications of FESSs either in development or commercially available. Note that blanks represent information not publicly available

| Manufacturer | Energy Capacity per Unit (kWh) | Power Capacity per Unit (kW) | Self Discharge (SOC loss per hour %) | Max Speed (RPM) | Marketed efficiency | Marketed lifespan (years) | Marketed cycle limit | Rotor material | Ref |
|---|---|---|---|---|---|---|---|---|---|
| Active Power | 1.5-3.5 | 300-650 | - | 10,000 | 96-98% | 20 | - | Steel | [43] |
| Adaptive | - | - | - | 16,000 | - | 25 | Unlimited | - | [44] |
| Amber | 32 | 8 | - | 9,000 | >86% | 30 | Unlimited | Steel | [30] |
| Beacon | 25-36 | 50-360 | - | 16,000 | 85% | 20 | 100,000+ | Composite | [45] |
| Energiestro | 10-1,000 | 10-200 | - | - | - | 30 | Unlimited | Concrete | [46] |
| KinetiCore | 50 | 25-250 | - | - | - | 20+ | 200,000 | Composite | [47] |
| Levisys | 10 | 10-40 | 0.20% | - | >97% | 20+ | 500,000 | Carbon fibre | [48] |
| OXTO | 7.5 | 65 | 0.60% | 11,500 | >90% | 25 | Unlimited | Steel | [21] |
| Revterra | - | - | 0.20% | - | 90% | 25 | - | - | [49] |
| Spin | 30 | 6 | 0.30% | 21,000 | >90% | 30 | Unlimited | Carbon fibre | [50] |
| Stornetic | 4 | 60-130 | - | 45,000 | 90% | 20+ | 100,000+ | Carbon fibre | [29] |
| Teraloop | 5-25 | 100-1,000 | 1-10% | - | 95% | 25+ | Unlimited | Carbon fibre | [51] |
| Vycon | 1.3 | 300 | - | 36,750 | 99.40% | 20 | - | Steel | [52] |

Table 2.3: Characteristics of different BESS technology [40] [39] [42] [53] [54] [1] [55]

| BESS Type | Lifetime (years) | Cycle life (cycles x $10^3$) | Estimated cost (£/kWh) | Round trip efficiency (%) | Volumetric energy density (kWh/m$^3$) |
|---|---|---|---|---|---|
| Lead-Acid | 3-20 | 0.3-4.5 | 300-600 | 65-90 | 25-90 |
| Nickel Cadmium | 10-20 | 2-10 | 500-1,500 | 60-90 | 10-80 |
| Sodium Nickel Chloride | 10-15 | 1-4.5 | 150-1,800 | 85-90 | 100-200 |
| Lithium Ion | 2-20 | 0.5-10 | 1,200-4,000 | 75-98 | 90-750 |
| Vanadium Redox/Flow | 2-20 | 0.8-20 | 600-1,500 | 60-90 | 10-70 |
| Sodium Sulphide | 10-15 | 2.5-4.5 | 1,000-3,000 | 65-90 | 150-350 |

## 2.2 Battery Energy Storage Systems (BESSs)

By far the most utilised form of energy storage after pumped hydro storage, the International Energy Agency stated that Li-ion systems consisted of 93% of the total annual installed capacity of storage in 2018, excluding pumped hydro storage [19]. Whilst Li-ion systems are the dominant technology, there are significant numbers of alternative types of BESS either being actively developed or already deployed. In Table 2.3 an overview of the most widely researched different types of BESS is shown.

Across the literature, there is a vast difference in specified characteristics for the various technologies resulting in wide ranges of values for most categories. The key takeaway however is that whilst Li-ion is currently the dominant type of BESS, there are many alternatives that are either in development or commercially available seeking to occupy the same space or to remove some of the drawbacks faced by Li-ion batteries. One area where it is clear that the majority of the systems trying to challenge Li-ion batteries fall short however is round trip efficiency, with none of the other technologies quoted above 90%. The costs included in Table 2.3 represent the whole system cost, including the balance of plant, power electronics and other ancillaries.

For the purposes of this research, the focus will be specifically on Li-ion as the most technically and commercially mature technology that is already operating in many of the areas investigated across this thesis. Due to its maturity, there are widely available statistics on many major metrics such as cost, performance, degradation and sustainability enabling benchmarks to be effectively created when comparing with FESSs.
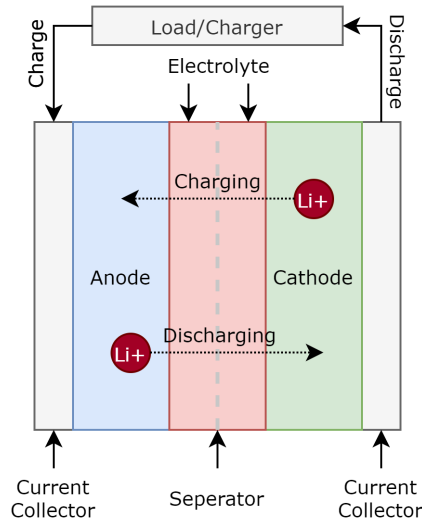
Figure 2.8: Structure of a Li-ion Battery [53]

Throughout this thesis, the BESS configurations used in the investigations are specified as 1C to provide a baseline for comparison with the typically higher C-Rate FESSs being studied. This also represents a 'typical' BESS system, with 1C being the most commonly specified C-Rate for a BESS [23].

Figure 2.8 shows a diagram of a typical Li-ion battery. The basic configuration consists of a positive and negative electrode within a liquid electrolyte with a porous separator in between. The anode will typically be made of a carbon-based metal such as graphite, whilst the cathode will be constructed from a metal such as cobalt, nickel or manganese. During charging, ions are transferred from the cathode to the anode through the application of a potential difference across the terminals, and the discharging process is this reaction in reverse [53].

In terms of advantages, Li-ion batteries offer an excellent level of energy density along with a good power density. These two factors combined, result in a highly versatile energy storage device able to be utilised in a wide range of applications when compared to other ESSs that trade off one of these factors for a benefit in the other, such as a FESS with a high power density but low energy density. They are also commonly characterised as having low self-discharge rates, with most systems generally suffering a loss of state of charge (SOC) in the region of 0.2-5% of per day depending on the specific design of the system. Table 2.4 gives an overview of the most prominent types of Li-ion battery cells as well as their typical characteristics. The Willenhall energy storage system used as a baseline for the models in this thesis is a lithium titanate battery.

Conversely, the major downside of Li-ion batteries is their susceptibility to cycle-based degradation. In Table 2.5 some of the main mechanisms for Li-ion battery degradation are listed where it can be clearly seen that factors such as temperature,

Table 2.4: Types of Lithium-ion battery cells [2]

| | Typical Cell Voltage (V) | Specific Energy Capacity (Wh/kg) | Maximum C-Rate | Cycle Life |
|---|---|---|---|---|
| Lithium Cobalt Oxide | 3.0-4.2 | 150-200 | 1C | 500-1000 |
| Lithium Manganese Oxide | 3.0-4.2 | 100-150 | 10C | 300-700 |
| Lithium Nickel Manganese Cobalt Oxide | 3.0-4.2 | 150-220 | 2C | 1000-2000 |
| Lithium Iron Phosphate | 2.5-3.65 | 90-120 | 25C | 2000+ |
| Lithium Nickel Cobalt Aluminium Oxide | 3.0-4.2 | 200-260 | 1C | 500 |
| Lithium Titanate | 1.8-2.85 | 50-80 | 10C | 3000-7000 |

current and state of charge are all key components of the degradation of a Li-ion battery. It is for this reason that Li-ion systems are often specified with narrow tolerances for operational regions where operating the system outside of these zones will result in a rapidly decreasing lifetime of the BESS. Factors such as C-Rate, temperature, energy throughput, depth of discharge, and SOC have all been shown in the literature to have negative impacts on battery lifetime [56] [57]. BESSs are generally considered to reach the end of life when their capacity falls to 80% of the original capacity. This will be covered in depth within Chapter 3 where a literature review of modelling of BESS degradation is discussed in detail. This thesis explores in depth how this disadvantage can be mitigated through hybridisation and control to extract greater techno-economic performance from a Li-ion BESS.

Table 2.5: Degradation mechanisms for Li-ion batteries

| Degradation Mechanism | Description | Aggravating Factors | Result |
|---|---|---|---|
| | During the first set of charge/discharge cycles, the electroylte reacts with the electrodes and decomposes into compounds that form a layer upon the surface of | | |
| Solid Electrolye Interphase (SEI) growth | the electrode. A small degree of SEI formation is important to the correct operation of a Li-ion battery as it is used to stop further reaction of the electrolyte with the electrodes. However, as the battery ages the thickness of this layer increases. | High temperature, high current | Irreversible capacity loss, increased impedance, power fade |
| Lithium plating | Instead of intercolating with the electrode, metallic Li-ion atoms form on the surface. | Low temperature, high SOC, high current | Contributes to further SEI formation, lithium depletion, reduced conductivity |
| Electrolyte oxidation | When the cell electropotential is beyond the electrolyte oxidative stability limit, the electrolyte will oxidise | Overcharging | Reduced conductive surface area, increased resistance, potential catastrophic failure |

Figure 2.9: Willenhall Energy Storage System

## 2.3 Willenhall Energy Storage System

Willenhall ESS is a Lithium titanate 2MW/1MWh battery system owned by The University of Sheffield [58]. It has been operational since 2016 participating in a range of different markets and services, and for this reason, represents an excellent benchmark for operational data collection and verification.

Figure 2.9 shows the Willenhall installation, with the battery cells situated within the left-hand container, and the power electronics situated within the right-hand container. The electrical connections at the site are shown in Figure 2.10.

This installation is used as the basis for model verification works detailed in Section 3.8. Willenhall has been used due to the extensive access to operational data allowing for a robust verification process. The battery model presented in this thesis is intended to be generic in nature, therefore it is not considered that the specific battery chemistry will have an impact on the validity of the results. This is discussed in further detail within Section 3.9.1.

### 2.3.1 Energy Storage Installations in the United Kingdom

The Renewable Energy Planning Database tracks the progress of renewable energy projects across the U.K [59]. Using the July 2023 database, Figure 2.11 shows the amount of operational Battery ESSs in the U.K. The majority of systems fall in the 0-5MW range, followed by 20-25MW and 45-50MW systems. The work in this thesis concentrates on projects in the 0-5MW range.
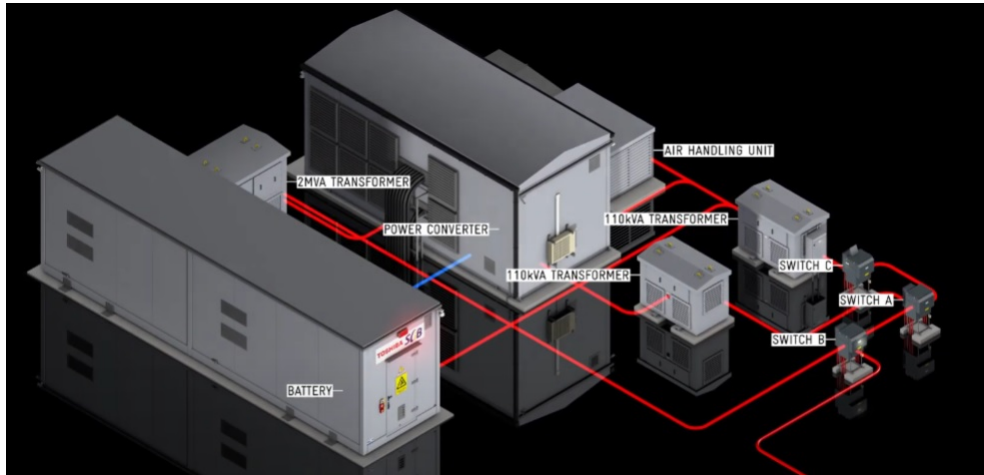
Figure 2.10: Willenhall Energy Storage System Electrical Connections Overview

## 2.4   Electrical System Topology

Whilst this thesis focuses on system-level studies and applications without emphasis on the electrical circuit configuration of the systems being investigated, it is still important to explore the options available for the structure of the electrical systems in question.

A key difference between the operation of flywheels and that of batteries or supercapacitors is that the immediate output from a flywheel via a drive system will most commonly be alternating current whilst from a battery or supercapacitor it will be a direct current. DC output from a flywheel is also possible in certain scenarios, granting it a degree of flexibility when designing the electrical topology. This means that generally, the approach to electrical system design is slightly different between the different ESS mediums. Figure 2.12 shows the two main options for configuring a FESS co-located with distributed generation.

The AC current generated by the FESS will always be passed through a rectifier/inverter combination in order to ensure the outgoing electrical signal synchronizes with the load (whether that be a local microgrid or the main national grid). The point at which the configuration can be varied is where the two separate systems connect together. The topology to be chosen is highly dependant on the application being considered, as the separate DC links can offer greater control over the operation of the FESS, whilst the combined DC link reduces the power electronics costs significantly [36] [60] [61].

For BESSs, the approach is very similar to the BESS operating on DC but with options to convert and connect at either the DC or AC points of the system. This allows for a variety of implementations of electrical system design, with the work in [62] discussing the difference between passive, semi-active and active topologies of a hybrid battery/supercapacitor system. Whilst the passive and semi-active topolo-
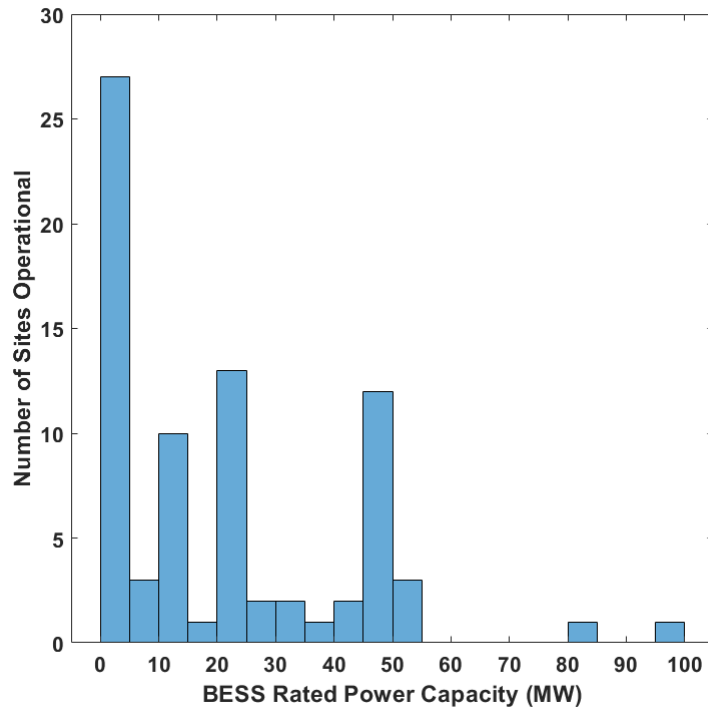
Figure 2.11: Histogram of Operational UK Battery Energy Storage Systems (As of September 2023)

gies are more cost-effective due to a lack of power electronics, they lose significant amounts of control over individual components and can cause excessive strain to be placed on the battery.

Throughout this body of work, HESSs combining FESSs and BESSs are discussed for a variety of applications. Again, the detailed topology of these systems is not covered within the scope of these works, however, three examples of how the topology for such a system would work in practice are shown in Figure 2.13. The work in [63] discusses topologies of such hybrid systems in depth, reviewing various storage technologies, their relative strengths and weaknesses and the control of hybrid systems.

For the purposes of the work contained within this thesis, there will not be a need to discuss the detailed electrical architecture of the systems being considered. It is important that the architecture is designed in order to allow sufficient independent control of various parts of the system and for that reason, the topology assumed will be the separate DC link topology.
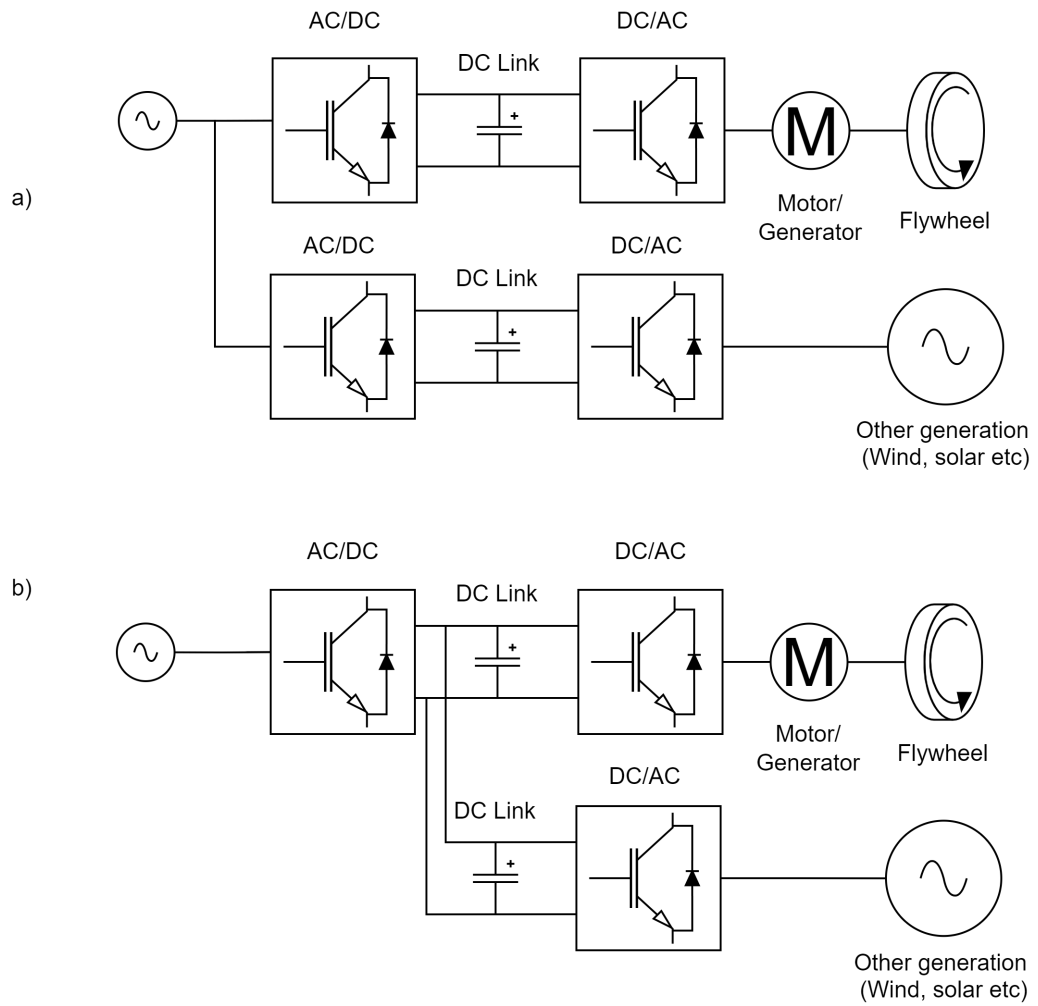
Figure 2.12: Electrical connection options for FESS co-located with distributed generation showing a) separate DC links b) combined DC link
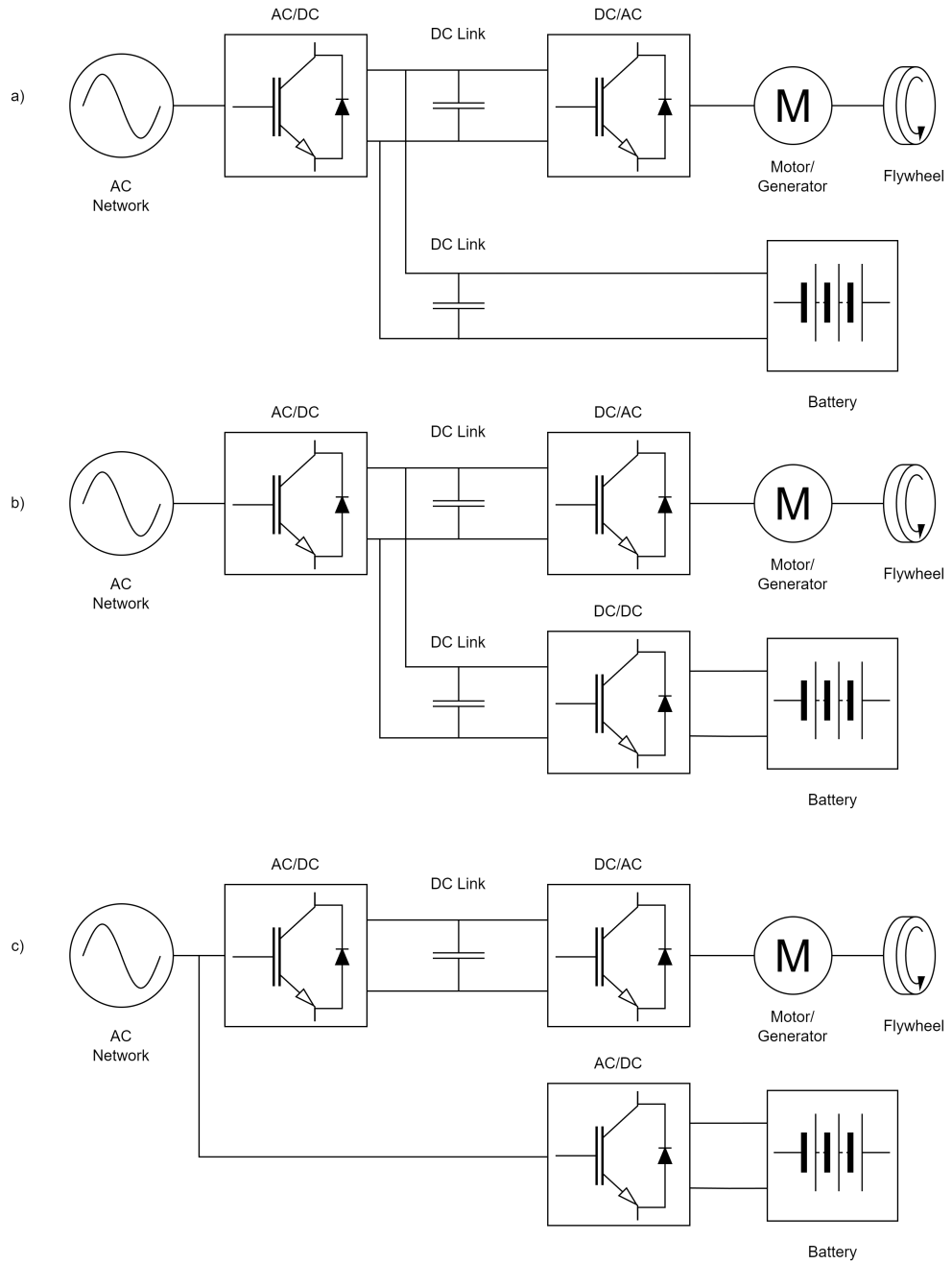
Figure 2.13: Electrical connection options for HESS showing a) passive BESS b) active BESS with DC link c) active BESS with AC link

Table 2.6: Total Capital Costs for Li-Ion BESSs in £/kWh from two selected reports

|      | IRENA | | US DoE | |
| --- | --- | --- | --- | --- |
|      | Best | Worst | Best | Worst |
| 2016 | 150 | 630 | - | - |
| 2018 | - | - | 295 | 436 |
| 2025 | - | - | 231 | 314 |
| 2030 | 59 | 251 | - | - |

## 2.5   Economic Outlook

An economic analysis will factor significantly into the work undertaken within this thesis. It is therefore important that the costs associated with the relevant ESSs are understood in order to correctly carry out any economic studies. The most widespread method of stating the cost of an individual ESS is to use total capital cost (TCC). This can be expressed either in terms of cost per kW (power-based) or cost per kWh (energy-based).

In 2018 the International Renewable Energy Agency produced its 'Electricity Storage and Renewables: Costs and Markets to 2030' report, whilst in 2019 the United States Department of Energy produced the 'Energy Storage Technology and Cost Characterization Report'. Both of these reports looked at the present-day and future costs of ESSs. The costing information in £/kWh for Li-Ion BESS systems produced by these reports is shown in Table 2.6, with the original values in dollars converted to pounds using the average exchange rate for 2018 of (£0.7501/$1) to reflect the time at which the figures were produced. These prices represent the whole system's cost.

It should be noted that with the current global economic struggle with inflation, the actual values are likely to have increased in the time since publication, especially as battery prices have stagnated and even begun to rise in recent years [64]. This is in contrast with the previously predicted trend of a constant reduction in price.

Based on this information from two highly detailed and respected reports and the literature review shown in Table 2.8, the cost of a BESS in the work contained in this thesis has been set as £400/kWh wherever a cost is required to be fixed. It is acknowledged that this cost could vary either higher or lower depending on the system in question and outside market forces, however, this cost represents a strong middle ground between previously documented prices and current energy storage cost trends. Table 2.7 shows a selection of installed or upcoming battery projects along with their estimated costs from reported figures. The average of the values for estimated cost is £463/kW which gives confidence to the value of £400/kWh used in this thesis.

Table 2.7: Grid scale battery projects along with estimated costs based on report values

| Site | Energy Capacity (MWh) | Power Capacity (MW) | Reported Project Cost (£m) | Estimated Cost in £/kWh | Year | Ref |
|---|---|---|---|---|---|---|
| Zenobe Storage Portfolio | 2000 | 1000 | 750 | 375 | 2022 | [65] |
| Tag Energy Luton | 99 | 49.5 | 30 | 303 | 2022 | [66] |
| Normanton Energy Reserve | 1000 | 500 | 350 | 350 | 2023 | [67] |
| RWE Germany | 235 | 220 | 125 | 532 | 2023 | [68] |
| Iberdola | 25 | 50 | 24 | 960 | 2022 | [69] |
| Trafford Low Carbon Energy Park | 2080 | 1040 | 750 | 361 | 2023 | [70] |
| Harmony Pillswood | 196 | 98 | 75 | 383 | 2023 | [71] |

With flywheels being a less commercially developed energy storage medium, the approach to setting a cost differs slightly. For this cost, a wide-ranging literature review has been undertaken with the results shown in Table 2.8 and Figure 2.14, also including a review of literature for BESS costings in order to verify the previous assumption. Figure 2.14 has been produced by converting the costs listed as using other currencies in Table 2.8 into Great British pounds using the relevant exchange rates of the given year.

There is significant variation across the literature in terms of specifying an exact TCC for the two different ESSs. It is evident that from the literature analysed, there is more disagreement over assigning an energy-based cost when compared to power-based costs.

Firstly looking at energy-based costs, the FESS clearly has a significant degree of uncertainty within the literature, which can likely be attributed to its status as a still evolving industry for manufacturers to develop products form with a mean value across the literature of £2468/kWh. Additionally, because FESSs are specified over a much wider range of C-Rates, there is a significant degree of variability in their system costs. For BESSs on the other hand, which are generally specified over a much smaller range of C-Rates, the mean value for the BESS is calculated as £812/kW. This value is significantly higher than the value determined from the two studies discussed above in Table 2.6. Additionally, the median of the values

Table 2.8: Total Capital Costs for Li-ion BESSs and FESSs in literature (values in US Dollars)

| Ref | Li-Ion | | FESS | | |
|-----|--------|------|------|------|------|
|     | kWh | kW | kW | kWh | Year |
| [72] | 2500 | 4000 | 350 | 5000 | 2014 |
| [73] | - | 300-2500 | 130-500 | - | 2014 |
| [74] | 1272 | - | - | - | 2014 |
| [39] | - | 1228 | 918 | - | 2015 |
| [42] | 600-2500 | 1200-4000 | 250-350 | 1000-5000 | 2016 |
| [75] | 440 | - | - | - | 2016 |
| [76] | 400 | - | - | 1600 | 2017 |
| [77] | 325-450 | - | 600-2400 | - | 2017 |
| [78] | 469 | - | 2880 | - | 2018 |
| [79] | 901 | 1859 | - | - | 2018 |
| [80] | 100-2500 | - | 300-1000 | 100-2500 | 2019 |
| [40] | 200-1260 | - | - | 1500-6000 | 2020 |
| [81] | 262 | - | - | - | 2021 |
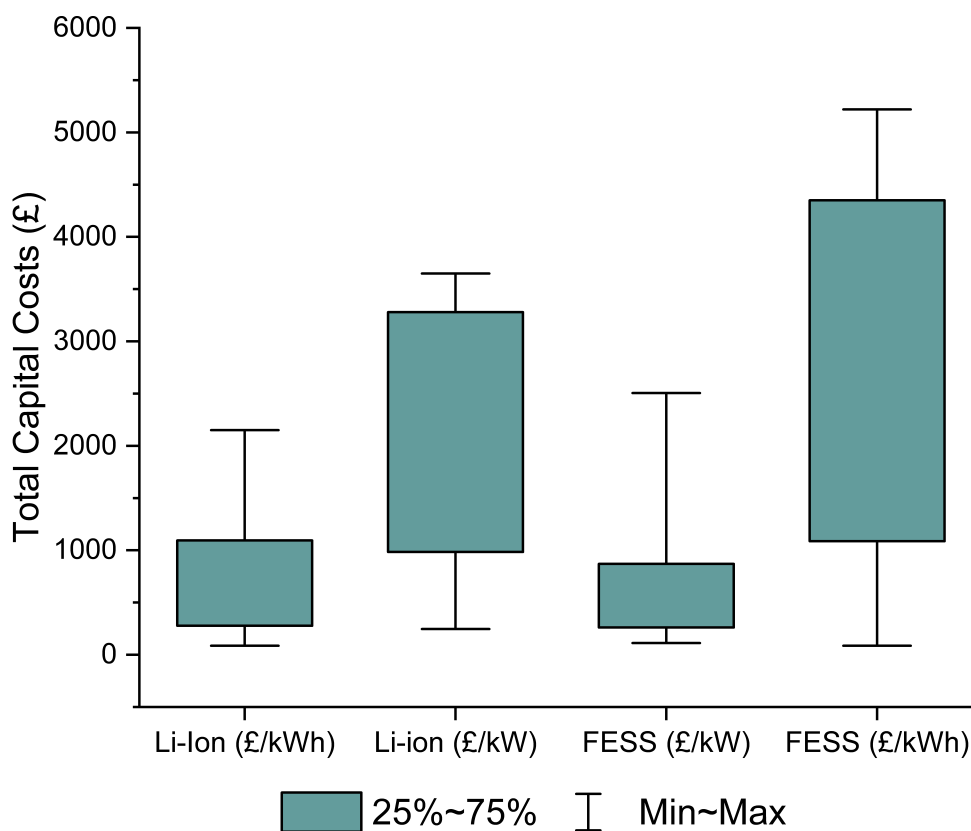


Figure 2.14: Ranges of Total Capital Costs for BESSs and FESSs in literature

presented in Table 2.8 is £402/kWh, suggesting that the BESS systems are quoted more commonly at the lower end of the scale.

When considering power-based costs, the literature categorises the FESS TCC over a much smaller range suggesting greater agreement across different studies. For these costs, FESSs have a mean of £780/kW. This is the value that will be used as the starting point in any studies where the cost is required to be fixed, and will then be varied across the range of values where relevant.

Considering the disagreement between different studies when considering TCC in terms of energy-based costs, power-based TCC costs will be used in this thesis due to the narrower range of values available within the literature. Wherever relevant, TCC sensitivity analysis is conducted to illustrate a range of values.

## 2.6 State-of-the-art

This section presents the current 'state-of-the-art' for the three distinct strands of work considered in this thesis, namely the modelling of energy storage devices, export limitation support, and frequency response services.

### 2.6.1 Modelling of Energy Storage Devices

There are many different approaches to modelling FESSs and BESSs, however, this thesis focuses on the bucket modelling approach. Bucket modelling has been prominent in energy storage studies for many years. It is used extensively in studies where the operation of the energy storage system is not the primary objective. However, the bucket models present in literature today are implemented as generic representations with minimal application-specific complexities. They are mostly used in optimisation studies rather than in techno-economic analysis of applications.

This thesis exploits this gap to produce a more detailed and modular version of a bucket model, that can be applied generically to a wide range of operations but also enables specific ESS characteristics to be implemented creating a more representative model.

### 2.6.2 Export Limitation Support

Export limitation is an emerging and sparsely researched area of energy storage deployment. There are very few studies that consider this issue, and this thesis in itself is state-of-the-art in that regard. The closest comparable area of research is in the field of wind curtailment mitigation, but this is conducted at a much larger operational scale rather than on a more site-specific basis as is investigated in this thesis.

### 2.6.3 Frequency Response Services

This thesis concentrates on frequency response provision by FESSs, and a literature review of this area is provided in Chapter 5. The state-of-the-art in this field is the existing wide-spread deployment of BESSs that are currently active in providing this service. FESSs providing such services as standalone units have received little to no research as they have been widely dismissed as being unsuitable.

In terms of the new frequency response services being deployed by NGESO, there was no prior research conducted in this area before the commencement of the work in this thesis, as they were introduced during the development of the work contained here. The state-of-the-art is generally accepted to be the further deployment of BESSs for these services, but even this has not been extensively researched. This thesis looks to provide the first exploration of this area of frequency response provision.

## 2.7 Conclusions

In this section, the two key types of ESS that are studied in this thesis have been introduced and discussed along with an explanation of the relevant terms of reference that will be used throughout the thesis. The overview contained within this chapter provides the key groundwork upon which the remaining sections of this thesis are built, most specifically the relative strengths and weaknesses of FESSs and BESSs.

Key amongst the discussions within this chapter is that concerning the economic outlook of the respective ESSs. It is clear that the two main storage mediums have differing economic outlooks, with a FESS generally costing less on a power basis, and a BESS generally costing less on an energy basis. This will be key to exploiting the strengths and weaknesses of each technology in order to generate significant techno-economic improvements.

In the coming chapters, application-specific literature is explored in greater depth wherever it is most appropriate as outlined at the beginning of this chapter.

# Chapter 3

# Rapid Application Based Modelling and Simulation of Energy Storage Systems

## 3.1  Introduction

Computer-based modelling and simulation of energy storage systems is an integral part of what is still very much an emerging field. There is a wide range of different techniques used, all suitable for different types of energy storage technologies and areas of interest. Beyond the purely technical modelling of different energy storage mediums, there are other aspects equally as important that inform the decisions that both researchers and industry take.

Key amongst these is economic modelling of the benefits that an ESS can bring, along with techniques for optimisation of a given system. Within the field of BESSs the process of modelling the degradation of a battery according to different use cases is key in understanding how to extract maximum value from an installation, and to determine whether an economic case can be made for an ESS being deployed in certain scenarios.

In this chapter, a detailed review of the available literature on energy storage modelling is undertaken with a particular focus on the reasoning why different approaches are taken along with a discussion of the most appropriate method to be utilised within this thesis. Other energy storage technologies are also discussed, including supercapacitors, compressed air energy storage, and hydrogen energy storage, in order to provide a range of comparisons with the state of the art in the field.

Other aspects covered within the literature review include the different methods for modelling BESS degradation and an overview of the use of genetics algorithms

(GAs) to optimise a given installation. A literature review of the different metrics used for economic analysis in the field of energy storage is presented along with the reasoning behind using specific methods.

The second section of this chapter details the development of two novel models within MATLAB/Simulink, one of a FESS and one of a BESS. A detailed breakdown of the major components along with the benefits of the modular framework is presented, followed by a verification of the BESS model against a physical 2MW/1MWh Lithium-Titanate BESS (referred to within this thesis as the Willenhall ESS) [58]. A degradation algorithm is implemented and then verified against lab-based cell cycling experimental work to replicate real-world operation.

## 3.2 Modelling of Energy Storage Systems

When considering which method of energy storage modelling is most appropriate for the study being conducted, there are a number of different aspects to consider in order to choose the most suitable method. This section considers both BESS and FESS approaches to modelling, as well as providing additional context for these approaches by also looking into alternative energy storage technologies.

Firstly, the purpose of the study is paramount when choosing a modelling approach. Within this review, the two main purposes for modelling ESSs have been divided into two categories; 'Technology Modeling' (TM) and 'Application Modeling' (AM). The first of these, TM, covers all studies where analysis of the ESS technology itself is the goal of the study, such as when modelling a new method of modelling a FESS [82] or representing the degradation rates of certain Li-BESS chemistries [83].

The second of these purposes, AM, covers the studies where the ESS is being deployed for a specific application and the objective is to assess its technical, economic, or techno-economic performance. This could cover aspects such as assessing a supercapacitor/BESS hybrid for electric vehicle applications [84], or the feasibility of deployed compressed air energy storage for wind generation support [85].

The other main consideration when determining a modelling approach is to ensure it is appropriate for the intended duration of the simulation. In this thesis, the durations of simulation are categorised as follows;

- Short Duration - 0 to 60s

- Medium Duration - 60s to 1 day

- Long Duration - Longer than 1 day
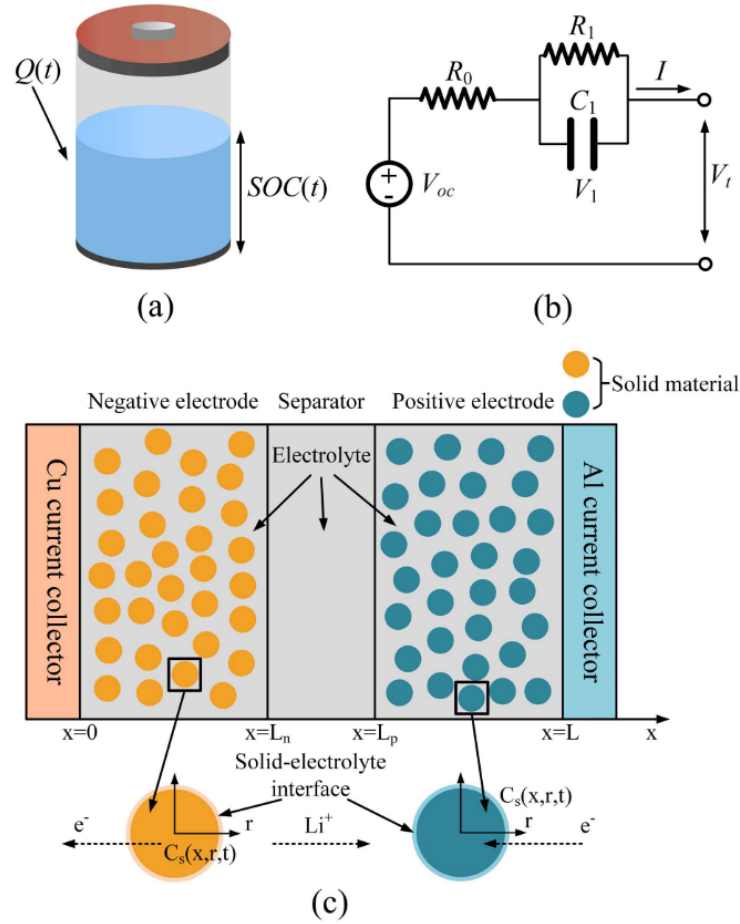
Figure 3.1: Different modelling approaches for BESSs a) Bucket Model, b) Equivalent Circuit Model and c) Electrochemical Model [88]

The simulation duration is important in choosing the correct modelling approach, as using a computationally intensive approach to simulate a long-duration application may result in prohibitively long simulation times. For this reason, there are trade-offs between advantages and disadvantages for each modelling approach [86] [87]. In this section, each approach will be introduced in detail, with examples of existing literature discussed and commentary provided on what scenarios may suit the approach best.

## 3.2.1 Types of Energy Storage Modeling

The field of energy storage modelling and simulation can be categorised into three distinct types of approaches, as detailed in the following sections. In Table 3.1, an overview is given showing examples of what Electrical or Physical modelling would represent for a selection of different ESS technologies. Examples of these approaches for a BESS are shown in Figure 3.1

Table 3.1: Different methods of modelling and simulation of ESSs

| Type | Description | Use Case | Advantages | Disadvantages | Ref |
|---|---|---|---|---|---|
| Bucket (Power / Energy) (Energy Reservoir) | This method represents the ESS as a 'black box' where the bucket is either filled or emptied (charged or discharged) according to set limits. | Long-duration studies where the physical operation of the ESS is not studied. This method is most effective when considering larger-scale applications and where the ESS in question is a known quantity with easily identifiable parameters. | Simplicity, Fast computational speed, Easy parameter control, Ability to introduce additional complexities as required, Fast adaptation to different applications | Is not technology specific in base form, Minimal data on the response of ESSs to instantaneous events | [89] [90] [91] [92] [93] [94] [95] |
| Electrical (Equivalent Circuit) | This method seeks to represent a given ESS as an electrical circuit, modelling the system overall in terms of voltages and current to and from the ESS and a given application. | Investigations, where the electrical operation of the system is of interest, such as for fault, ride through, voltage drop, transient harmonic distortion and short-duration frequency response analysis. | Increased complexity, Ability to analyse response to instantaneous events, Required for certain types of study | Longer computational times, More specific parameter identification is required, Slower to switch between different applications due to need for specific electrical system information | [96] [94] [97] [98] [99] [100] |
| Physical (Electrochemical) (Concentration Based) | When discussing a BESS, this method is referred to as an 'Electrochemical model'. For a BESS, this would represent modelling the specific chemical reactions that take place within the battery. For a FESS, this method would consist of modelling the mechanical kinetic operation of the flywheel. | Investigations where the specific operation or degradation of the ESS itself is of interest. This could consist of studies into the ageing of different battery chemistries or in the design of different flywheel form factors. | Very high accuracy, Degradation and other mechanisms are more easily modelled, required in scenarios where analysis is needed at the pre-fabrication stage | Significantly longer computational times, Parameter identification required to be extensive, Will often need to be combined with other methods if application specific information is required | [96] [101] [102] |

**Bucket Model**

The first of these is referred to in this work as the 'Bucket Model' approach, although it is also commonly referred to as an 'Energy Reservoir Model' and the 'Power-Energy Model'.

The basic approach to this method is to model the ESS as an ideal unit, where the energy currently stored within the ESS is based upon either adding or subtracting energy from that which was stored at the previous time step. This method of modelling can be made more complex by introducing other aspects such as efficiencies, degradation and self-discharge rates [89] [90].

The main benefit of this method is when seeking to perform system-level studies that will be performed over significant periods of time. As it removes the requirement for more complex calculations, the computational requirements are lower and hence long periods of time can be simulated rapidly. This method also lends itself to studies where the performance of storage in regard to specific applications is being assessed, rather than the technical response of the storage itself.

It also benefits from not requiring detailed knowledge of the parameters of the ESS being studied and therefore can be utilised as a generic representation of all types of ESS. This model also provides an easier base from which to easily modify the study for different applications.

However, the drawback remains that the method as a whole is the least technically detailed of the three methods presented in this thesis. Whilst complexities can be added to the model to create a more representative system, the lack of modelling of the mechanisms of the ESS means that certain studies are not possible, or inadvisable from a technical standpoint, to be undertaken using this model. For example, whilst voltage and current can be implemented in the bucket model approach through appropriate conversions, it is less accurate than modelling these characteristics from the start in an Electrical Model.

**Electrical Model**

The second category of ESS modelling is referred to in this work as the 'Electrical Model' although it is also commonly referred to as an 'Equivalent Circuit Model'.

This approach consists of representing the ESS from an electrical point of view, where the electrical characteristics of both the system as a whole and the ESS are modelled, usually with the main variables being studied within the application being Voltage and Current. There are many different levels of electrical models, from a basic simplified model to complex electrical representations.

The main advantage of utilising this method is the ability to study transient events from an electrical perspective in applications such as power quality and in-

stantaneous frequency response.

This method offers greater detail than the bucket model, although that comes with the requirement for more detailed knowledge of the parameters of the ESS being modelled. The electrical characteristics are required to provide an accurate model, and in some cases, further information will be required. The electrical distribution characteristics of the system being modelled are also required, which can make switching between different applications from the same base model more difficult.

It should also be noted that the individual short-term electrical behaviour of the ESS being modelled is 'hidden' behind the power converter, and hence from the viewpoint of the electrical interface with the ESS, the majority of different technologies will operate identically through the power converter.

**Physical Model**

The final category of ESS modelling discussed in this work is referred to as the 'Physical Model'. In the context of BESSs, these are often referred to as an 'Electrochemical Model' or 'Concentration Based Model'.

For this approach, the physical or chemical characteristics of the ESS are modelled. They are primarily used when the objective of the study is to simulate the inherent properties of specific ESS types, such as a particular Li-Ion cell or a new type of steel for a FESS. It also encompasses scenarios where the degradation of an ESS is being modelled, and where the application is of limited impact on the study.

The key advantage of this model is its high degree of accuracy and very detailed level of output. It is critical when attempting to understand the design and operation of the ESS itself. It also enables new materials to be simulated prior to fabrication, and can also be used to characterise different types of ESS.

These models require extensive knowledge of the specific ESS being modelled, such as material type, cell chemistry or other proprietary knowledge. They also often require significant simulation durations. They should only be utilised when the ESS being used is well-defined with detailed information on its construction.

## 3.3 Modelling Applications

This section explores the literature available for different ESS technologies including the simulation duration, the modelling objective, the model utilised and the software used to carry out the simulation.

First, some statistics from the literature review are analysed. In Figure 3.2 the proportion of times that each model type is used in literature for each technology is presented. Note that in some studies multiple approaches are used.
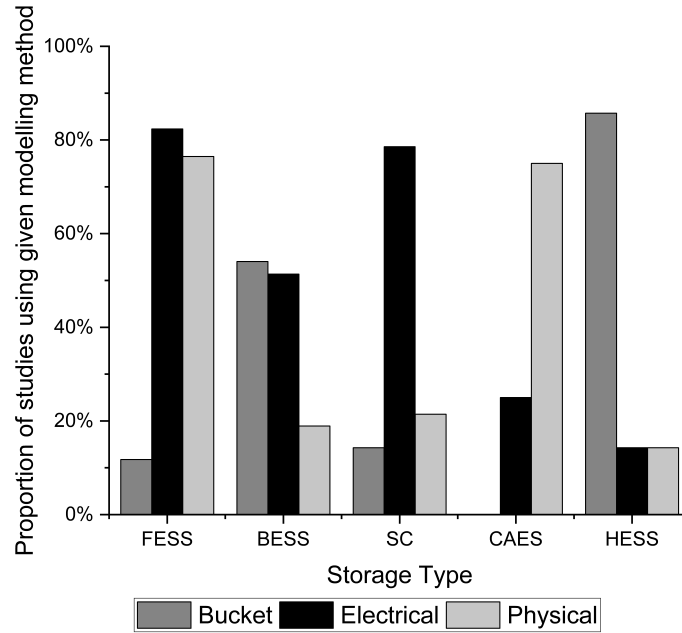
Figure 3.2: Number of times in reviewed literature that a given modelling approach is used as a proportion of total literature studied for that ESS technology

From this data, it can be seen that the approach utilised is highly dependent on the storage technology being researched. For example, a FESS is modelled using the bucket model method in only 11.8% of the literature surveyed whilst it is utilised in 54.1% of BESS studies reviewed. Another key aspect to note is that modelling of a supercapacitor is most commonly conducted using the electrical model approach with 78.6% of literature utilising an electrical model.

The duration of the simulations within the literature, according to the ESS technology being studied, is shown in Figure 3.3. Again there are some immediate conclusions to be drawn from this figure, notably that for compressed air energy storage and hydrogen ESS the general trend is for mostly long-duration simulations with some medium-duration simulations. Short-duration simulation is most prominent for supercapacitors and FESSs which is to be expected considering their position as limited energy capacity assets. The versatility of the BESS is illustrated in the fact that the duration of the simulation is spread fairly evenly across all three durations.

Finally, the software that has been utilised for each study is shown in Figure 3.4. MATLAB/Simulink dominates the software distribution with 42 out of 68 studies analysed utilising this software. Other than MATLAB/Simulink, the software HOMER and DigiSELENT Power Factory are both used in several studies whilst an algorithmic modelling approach is used in 6 studies. Some other packages such as Python and Aspen Plus are used occasionally, but it is apparent that MATLAB/Simulink dominates the software approach to energy storage modelling.
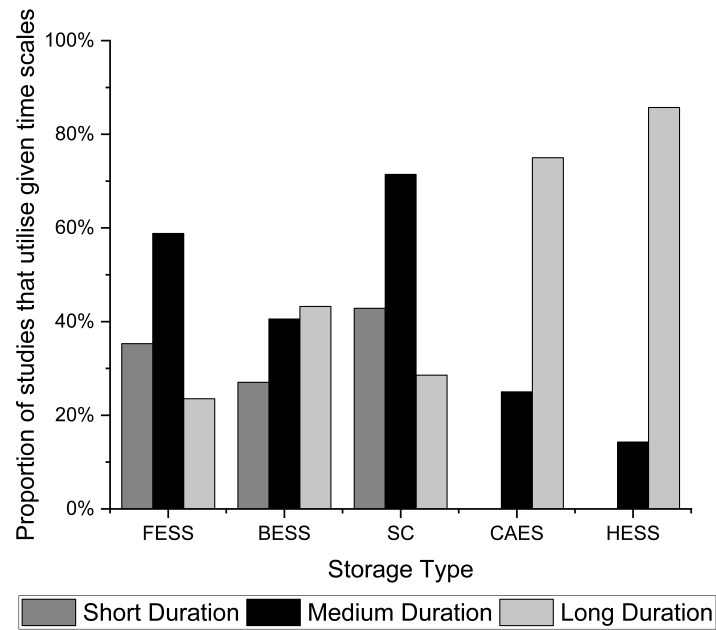
Figure 3.3: Number of times in reviewed literature that a given simulation duration is used as a proportion of total literature studied for that ESS technology
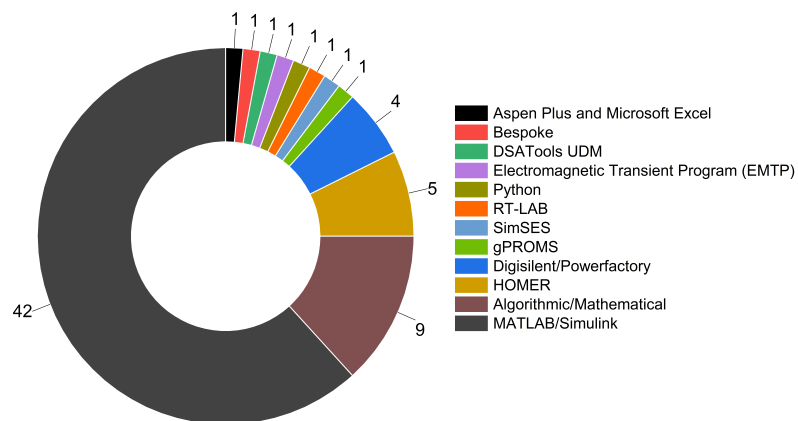


Figure 3.4: Number of times in reviewed literature that a given software package is used for energy storage modelling

### 3.3.1 Battery Energy Storage Systems

The application of BESS models spans many different purposes and approaches. Multiple different models have been proposed and utilised for modelling the physical mechanisms of BESSs, with a wide range of models discussed in literature concentrating on modelling the degradation of a BESS. This is a key aspect of BESS operation; therefore, it is important that the models utilised are accurate, which often leads to significant complexity.

In [99] a complex life cycle model which utilises a combination of equations and electrical modelling to expand a BESS model to include a cycle-life calculator. This model also incorporates thermal aspects and power loss and utilises equivalent cycle counting to predict the maximum number of cycles that a BESS can withstand at different depths of discharge. This work is an example of developing and applying a BESS model with a specific application-neutral approach where the focus is on modelling the technology itself.

A similar approach is taken in [103] which includes an assessment of the single particle method of modelling. In this work, the degradation of a BESS is modelled for different ageing parameters, with the effectiveness of the three model types (physical model, electrical model and bucket model) compared for this application. The single particle model is claimed to be the most accurate, with accuracy decreasing with decreasing model complexity. This further illustrates the need for detailed physical modelling when attempting to simulate the technical characteristics.

A combination of the electrical model and physical model is utilised in [83] where the outputs of an equivalent circuit model are used as an input to the battery degradation model that uses experimental data, literature models, and datasheets to estimate battery lifetime. The authors suggest that this combined approach is effective in accurately modelling the degradation of the BESS and shows the ability of different models to be used together to provide a more effective result.

An electrical model is utilised in a significant number of studies within the literature, with many varied approaches for model development and deployment. In [104] two different approaches to modelling BESSs, a detailed and average electrical model. Small modifications are made to the detailed model to reduce computational demand and the two models are then used to simulate the same frequency response events. Whilst the paper presents that in many cases the two models are equivalent, there are certain scenarios in which the two models diverge, suggesting that it is important to utilise the correct model for the application being simulated to avoid erroneous results.

Elsewhere in [105] a complex electrical model is proposed for grid fault analysis, including detailed converter models and control strategy. The model is then utilised

in a case study, again comparing an average value model with a detailed model showing the average model is accurate for usage in this application with only minimal differences between the two.

Many studies utilise an electrical model with a generic BESS element that has been previously developed and included as a pre-installed unit within software such as MATLAB/Simulink or DigiSILENT PowerFactory. An example of this is seen in [106] which uses the DigiSILENT PowerFactory BESS model within a larger electrical islanded microgrid model. This approach is often utilised in optimisation studies like this one where the operation of the BESS itself is not critical to the objectives of the analysis.

The bucket model method is also used extensively throughout the literature representing an effective method for fast application-specific studies. In [107] this approach is used to simulate capacity degradation in an arbitrage study, an example of introducing additional complexity to a bucket model to achieve the objectives required whilst avoiding over-complication of the model.

A range of different techniques are used when implementing a bucket model, such as in [108] where a memory block within MATLAB/Simulink is used to represent the BESS current state of energy. An alternative approach is shown in [109] where an integrator block, again in MATLAB/Simulink, is used to track the current state of energy. Both studies show effective implementation of these approaches without additional complexities.

## 3.3.2 Flywheel Energy Storage Systems

Referring back to Figure 3.2, it is clear that the majority of FESS models reviewed here are of electrical model or physical model types with limited usage of the bucket model method. However, there are some instances of bucket model usage such as in [110] which concentrates on primary frequency support in an algorithmic model, representing the FESS using simple state of energy equations. As with BESSs, this approach focuses on the deployment of a FESS rather than its operation.

The bucket model approach is also utilised in [111] where the flywheel is modelled using the generic library model within the HOMER library, with the focus of this study being on designing a microgrid for the highest renewable penetration.

Far more common for FESSs is the electrical model approach seen in a significant number of studies within the literature. Often, this comes in the form of representing the FESS using a permanent magnet synchronous motor block in MATLAB/Simulink such as in [82]. This study aims to accurately model the FESS motor speed and current for usage in future microgrid simulations. Additionally in [112] the same approach is used within MATLAB/Simulink as part of a wind-diesel power

system, to control excess active power.

The work in [113] combines the physical model and electrical model approaches, modelling the FESS in terms of aspects such as rotor speed, electromagnetic torque and stator currents and linking this with a larger electrical microgrid model for power quality applications. This approach is also taken in [114] where the FESS is modelled as an equation for rotating mass linked to a permanent magnet synchronous motor and subsequently implemented in an electric rail transport system and [115] where the FESS is modelled with a series of equations within a wind turbine system for power smoothing.

When modelling the physical operation of a flywheel the approach most commonly taken is to develop a series of equations to represent the technical characteristics of the system. This approach is taken in both [116] and [117]. Firstly, in [116], the model is developed in a step-by-step process taking into account torque, mechanical power, rotational frequency and inertia before being implemented in a combined heat and power plant model. The model is also validated with field tests showing a good correlation between the model and real-world tests. In [117] the model is also validated with an experimental set-up as part of a study looking to optimally size the FESS for a frequency regulation application.

### 3.3.3   Supercapacitors

Electrical modelling is the most prevalent type of supercapacitor modelling within the literature presented in this thesis. Despite this, there are some instances of the use of the physical model and bucket model techniques. In [118] the supercapacitor is represented using a set of equations governed solely by the energy contained within the supercapacitor, the SOC limits, and the available power, showing an equation-based representation of the bucket model. As has been the case for other storage technologies, this approach is used in an optimisation study of the size and control of a hybrid system.

In terms of a physical model, the work in [119] combines an electrical model with a thermal model that approximates the physical state of the supercapacitor's thermal characteristics during operation. The thermal model is split into a heat generation and heat transfer model, which feeds back into the electrical model. It also gives an overview of the varying complexities of different types of electro-thermal models for supercapacitors.

Numerical approaches are also used in literature, such as in [120] which concentrates on modelling for electric vehicles. The model includes a thermal element, and tests are undertaken to simulate a hybrid BESS/supercapacitor system for different driving profiles.

An extensive review of the different equivalent circuit models available for representing supercapacitors is conducted in [121]. This study looks at 7 different types of electrical model and analyses their effectiveness for modelling energy storage applications, concluding that of the techniques with a reported accuracy level, the 'Classical Equivalent Circuit II' is the most accurate.

Another study that looks at a range of different supercapacitor electrical model models is [122]. This work was conducted to reduce the complexity of the model to a point that the requirements were readily available from datasheets, whilst retaining the required accuracy. This results in scenario-based recommendations where the effectiveness of different models varies based on the application being modelled.

[123] proposes a new electrical model for supercapacitors utilising MATLAB/ Simulink using a simplified equivalent circuit approach. The supercapacitor is modelled by performing simple charge/discharge cycles and follows this with an experimental set-up to verify the model claiming good agreement between the datasheets, model and experimental test system.

### 3.3.4   Compressed Air Energy Storage

Due to the nature of its operation, compressed air energy storage often requires the modelling of both physical (air flow, recuperator, expander etc) and electrical elements. Referring back to Figure 3.2 none of the studied literature utilised the bucket model method, with a majority of modelling using the physical model method.

A common approach to modelling compressed air energy storage is mathematical, where a significant number of operational equations can be linked together to form a complex model of the physics behind the operation of the system. This approach is taken in [124], [125] and [126]. In [124] a mathematical model is presented for analysing the charging and discharging characteristics, with verification undertaken against literature and experimental results.

The work in [126] presents another mathematical model including operation strategy, this time to design a hybrid compressed air energy storage and wind turbine system for managing power fluctuations. Finally, [125] uses the same approach to develop a micro compressed air energy storage which is verified through extensive experimental tests. The range of different mathematical models available for this technology shows that they are an effective method for modelling compressed air energy storage, and can be deployed for a range of different applications.

In [85], the model is implemented using a combination of Aspen Plus for the compressor and turbines, whilst Microsoft Excel is used to model the cavern itself. This study once again looks at the implementation of compressed air energy storage for wind power support and shows a different approach to the mathematical model

for the same application.

Finally, [127] provides another mathematical that is executed in MATLAB/Simulink. It develops separate control algorithms for charging and discharging modes and follows this up with a simplified model which is implemented in a case study of the model following different step change profiles. The study shows the extensive knowledge of the system characteristics required to model the system accurately with a significant number of parameters stated to inform the case study from both a control and a system perspective. It highlights that when considering the modelling of a compressed air energy storage system, the complexity of the system often requires a more detailed level of the model than other technologies discussed in this thesis.

### 3.3.5   Hydrogen Energy Storage Systems

The software package HOMER is used throughout the literature for hydrogen ESS studies, including in [128], [129], [130] and [131]. The HOMER package has pre-designed blocks for use in power studies that enable the hydrogen ESS to be effectively studied without the requirement for comprehensive system knowledge and is primarily used in economic studies.

In [128] this approach is utilised to demonstrate the potential of $H_2$ESSs as long-term storage for high renewable penetration. The hydrogen ESS presented consists of an electrolyser, fuel cell and hydrogen tank, with the study concentrating on calculating economic benefits from the deployment of a hybrid BESS/hydrogen ESS system.

Another use of HOMER for a hydrogen ESS economic analysis is presented in [131] where a techno-economic analysis is performed for a rural electrification study using a hybrid BESS/hydrogen ESS system. Again, this approach to application modelling for $H_2$ESSs is focused on exploring economic benefits for different scenarios and providing insight on the optimum configurations under varying operating conditions. The fact that this approach is found commonly in the literature suggests it is a robust method of hydrogen ESS modelling for this type of study.

Equation-based modelling of a hydrogen ESS system is presented in [132] where the development of a seasonal storage system using hydrogen storage within salt caverns is discussed. In this case, the modelling of the hydrogen ESS in this way is driven by the complexity of modelling the dynamics of the salt cavern and the long durational nature of the simulation. Through this approach, the significant complexities can be accurately modelled for the given application.

A simulation framework (SimSES), which also includes models for Li-BESSs and RFBs, is presented in [133]. This framework involves interconnected electrical and thermal models, with an integrated techno-economic analysis model. The hydrogen

package is split into four modules, a management system, a fuel cell model, an electrolyser model, and a storage model. The input to the model is power, with a range of analytical outputs available. This package represents a good example of a fully self-contained modelling suite enabling different applications to be studied easily and effectively.

## 3.4   Degradation Models

A significant characteristic of BESSs is the degradation that they experience under different operating conditions, something that will be integral throughout the work presented in this thesis.

One significant piece of work when considering battery degradation modelling is [90] which compares the three main methods of modelling a BESS (Bucket, Electrical and Physical) and assesses their accuracy in predicting degradation compared to empirical results. Whilst the work concludes that the Physical method of modelling produces the most accurate results along with the Bucket method being the least accurate, there are areas where refinement could provide a more accurate result. The bucket model does not consider any other variable than energy throughput which leads to an underestimation of degradation, whilst the temperature is not set equally between the model and experimental works. There is also no mention within the study of the comparative simulation time between the different methods, a key aspect when considering the usability of a modelling system.

There are many approaches to modelling the degradation of batteries taken throughout literature, ranging from estimations based upon numbers of cycles completed to derived equations from known quantities such as SEI formation. There is also a subset of literature that derives equations from empirical testing, matching known degradation curves from laboratory-based experiments to exponential-based curves.

### 3.4.1   Equation-based Degradation Modelling

There are many different options available for the modelling of the degradation of batteries based on equations developed from the mechanical and chemical processes that cause degradation. Some of the most prominent techniques are listed below. The specific workings and equations that these techniques utilise are not within the scope of this research, and therefore will not be covered here.

- 1D+1D+1D multi-scale - This method utilises an electrochemical model that combines different ageing mechanisms such as SEI formation, mechanical cracking of the SEI layer and loss of active material. It uses time-upscaling to sim-

ulate the required timeframes and the main variables that affect the outcome of the calculation are temperature, cycle depth and average SOC. The results in [134], which first presented this method, claim a high prediction accuracy, but overall this approach would be far too complex for integration with the work in this thesis.

- Psuedo-2D - This method, originally developed in [135], uses complex governing models to simulate lithium transport and diffusion. It has often been stated in literature that this method is too complex for real-time applications and hence it is not suitable for this thesis, despite some recent works attempting to simplify the model. An example of this is seen in [136] which concludes that there are still many shortcomings to this approach for such applications.

- Single particle method - A simplification of the 1D model discussed above, this method treats concentration gradients as a lumped solution resistance term and accounts for the solid diffusion in electrode particles and intercalation reaction kinetics [137]. Whilst simplified, this method is still computationally intensive and requires a complex range of known characteristics of individual cells, which does not align with the generic nature of the intended battery model.

- Double exponential - This method represents the battery capacity fade in the form of Equation 3.1 where $Q$ is the capacity of the battery, $k$ is the cycle number, $a$ and $b$ are related to internal impedance and $c$ and $d$ refer to the ageing rate. This is a commonly used approach where the objective is focused purely on analysing the degradation rate of a given battery, but still requires extensive parameterization and machine learning to be implemented, rendering it too computationally intensive for this work [138].

$$Q = a.\exp(b.k) + c.\exp(d.k) \tag{3.1}$$

The work in [139] gives an overview of the different mechanical-chemical degradation modelling approaches for lithium-ion batteries. It implements multiple different physical degradation models under an overarching single-particle model framework. The risks of combining different degradation models are highlighted, and significant differences between models' effectiveness are claimed. The importance of selecting the correct model for a given cycle regime is also emphasised.

The double exponential is discussed in depth in [140] in which it is implemented in tandem with an adaptive filter and genetic algorithm in an attempt to increase the accuracy of the prediction. The authors present that the solution increases

the prediction accuracy for remaining useful life, but this comes at the expense of increased complexity of implementation.

The problem of introducing additional complexity for minor improvements in results is seen again in [141] which proposes a single exponential model with an integrated neural network as an improvement to the double exponential model.

The conclusion from reviewing these studies is that the additional requirements for parameterization and computational impact far outweigh the benefits in the context of this thesis. Whilst this approach may well provide a more accurate method of estimating battery degradation, it does not provide a significant enough advantage to warrant being utilised in these works. For the studies being conducted, this approach would be significantly over the top, especially when the majority of estimations of lifetime contained in this thesis could be conducted using simple cycle life estimation. The inclusion of a degradation equation within the model in this thesis is intended to be a comparison to cycle-based calculations and does not therefore warrant the additional complexity.

### 3.4.2   Data Driven Methods

This thesis will implement a degradation model developed using data-driven methods due to ease of implementation within the Simulink model and faster computational speed. Additionally, this implementation is intended to be an estimate that works in tandem with the cycle counting to give a useful approximation of battery lifetime for use in economic calculations, rather than an exact detailed analysis.

An example of an empirically derived equation is seen in [142] which presents a complex sequence of equations designed to model the mechanical degradation that a Li-ion battery experiences according to cycling, an approach also seen within [143]. Modelling such as this provides a foundation for extracting key equations to be utilised in more streamlined models but would be unsuitable for implementation within larger system models due to the computational drain of the calculations required. An effective implementation of these equations without the computational strain is shown to good effect within [144] which takes an equation developed empirically within [56] and uses the outputs of an electrical system model to inform an ongoing degradation co-efficient.

In [145] and [146] a derived equation from [147] is utilised to perform analysis on the lifetime of batteries providing frequency services. This method of modelling battery degradation can be effectively used within any model where metrics such as instantaneous C-Rate, SOC, depth of discharge and energy throughput can be monitored. There is a risk with utilising these models as the basis for further work that the equations being referenced and utilised are not theoretically sound, and

hence caution should be exercised when adapting them for alternative purposes. The empirical derivation contained within [56] is a thorough and detailed exploration of the subject matter. The testing performed is an extensive study across a range of different temperature coefficients and depths of discharge which lend credibility to the results produced.

[148] attempts to compare the double exponential model with a polynomial model similar to that proposed in these studies. Whilst the article claims that the double exponential model is more accurate, the results show a very minor difference between the two approaches in terms of fitting the curve of battery degradation, suggesting a minimal difference between the two. It subsequently attempts to meld the two approaches together, but this produces limited improvements for significant additional complexity.

This approach has been used as the basis for a significant number of further studies across the subject area and whilst the chemistry does not align with that installed at the Willenhall ESS, it presents a robust analytical derivation that can be adapted to use as a benchmark in tandem with the cycle counting contained in the model presented in this thesis. This element of the model is not intended to be a definitive answer, but rather to work in tandem with cycle counting to provide additional context to the calculations performed. These equations are discussed in more detail later in this chapter.

### 3.4.3   Cycle Counting

As discussed previously and shown in Table 2.3, most Li-ion systems are specified with a recommended maximum number of charge/discharge cycles in the region of 500-10,000 cycles before they reach the end of life. Cycle counting can therefore provide a rudimentary method of estimating the working lifetime of a BESS, and give a useful benchmark to compare with when generating rates of degradation from empirical equations.

To understand the complexities of cycle counting within energy storage for electrical power applications, it is important to be aware of the non-linear nature of the SOC profile commonly found in ESSs participating in electrical systems. An example of a 'basic' charge/discharge profile along with a typical profile showing microcycling from an ESS providing a frequency response service is shown in Figure 3.5. Note the smaller charge/discharge events within the microcycle profile, as opposed to the simple linear typical profile. Microcyles are defined as frequent and rapid changes in the direction of charge, usually referring to durations of seconds rather than minutes or hours [149].

Because of these microcyling events, and the effect that different levels of depth
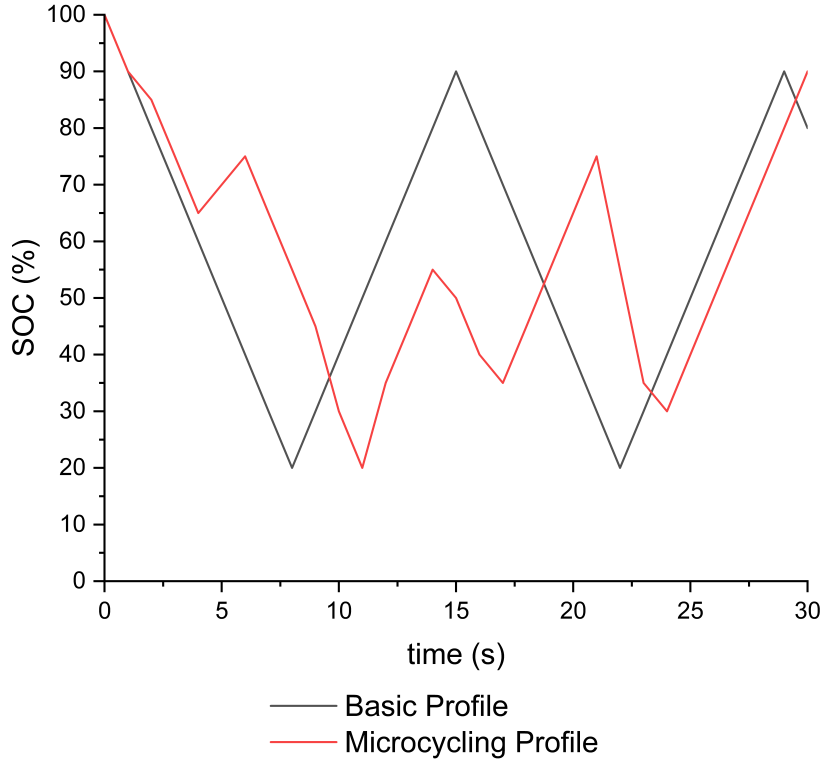
Figure 3.5: Example of different types of ESScycling

of discharge, SOC and C-Rate have on the lifetime of a battery, cycle counting is not as simple as counting the occasions where the ESS moves to and from 0-100% SOC. Instead, the individual peaks and troughs need to be extracted and summed to create an equivalent cycle number.

One of the main methods for microcycle counting is known as the rainflow algorithm, a method that has been most commonly used in the field of semiconductor fatigue analysis [150] [151] and is now being used more extensively in battery cycle life estimation [152] [153]. The basic principle of this method of cycle counting is to identify extreme points within a varying load/SOC profile and convert these into partial cycles through different levels of filtering to remove smaller microcycles, followed by a process of assigning amplitude, mean and quantity of cycles between different SOCs. An example of how this is conducted is shown in Figure 3.6 However, there are some key deficiencies present within the rainflow counting method that render it unsuitable for use within this thesis.

Firstly, as discussed within [155], some microcycles will be removed as part of the hysteresis filtering. When considering a system operating over multiple years this can subsequently add up to significant degradation that is not considered via this method. Additionally, the method only increments the cycles in steps of 0.5, losing a degree of granularity in the data. As mentioned within [149] and [156], this method is traditionally only viable as an offline tool once any simulations are completed, as it
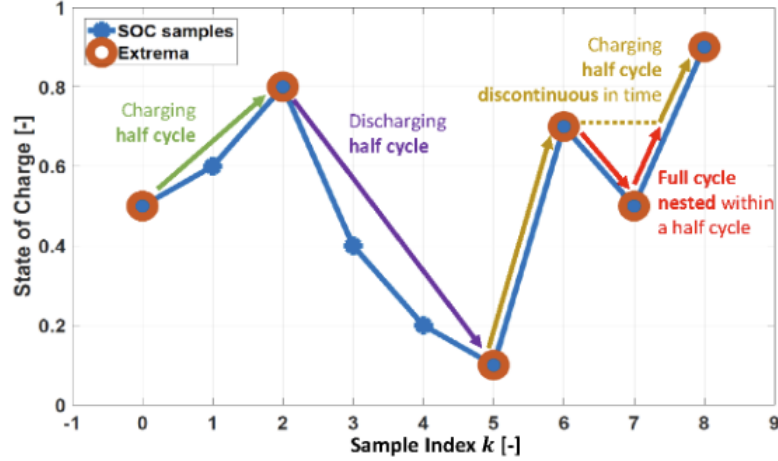
Figure 3.6: Rainflow algorithm cycle counting [154]

relies on a complete data set to be conducted. In applications such as those discussed in this thesis, both the degradation and cycle count must be monitored as the simulation progresses hence rendering the rainflow method insufficient. Whilst [151] presents a real-time implementation of the rainflow counting method, it still requires complex implementation and does not completely solve the issue of memory space, especially when considering long simulations. The other disadvantages of rainflow counting also remain despite the real-time implementation.

Beyond rainflow counting, there have been multiple studies conducted on alternative methods for cycle counting for ESS applications. One such study is shown in [99], which takes a similar approach to the rainflow counting algorithm without the post-processing requirements or loss of resolution in the number of cycles. The method presented is also tied intrinsically to a battery degradation model and rather than necessarily counting the number of cycles experienced, it assigns degradation values to the cycles and counts these instead. It is an efficient and accurate form of degradation calculation and effects from SOC, depth of discharge and average C-Rate are all contained within the work presented in this thesis albeit with alternatively derived equations.

In [149], the author implements a novel method of cycle counting whereby the change in SOC over each time step of the simulation is recorded and assigned to an 'Up index' and a 'Down index', counting the individual directions of travel for each instantaneous SOC change. Once the up and down directions reach a count of either 100% or -100% respectively they are recorded as a half cycle and the index is reset. Figure 3.7 shows how this works in practice. This presents several benefits over other cycle counting methods, such as the ability to count every variation in SOC no matter how small. Additionally, it requires minimal computational power and can be executed over the course of a continuous simulation. However, a slight
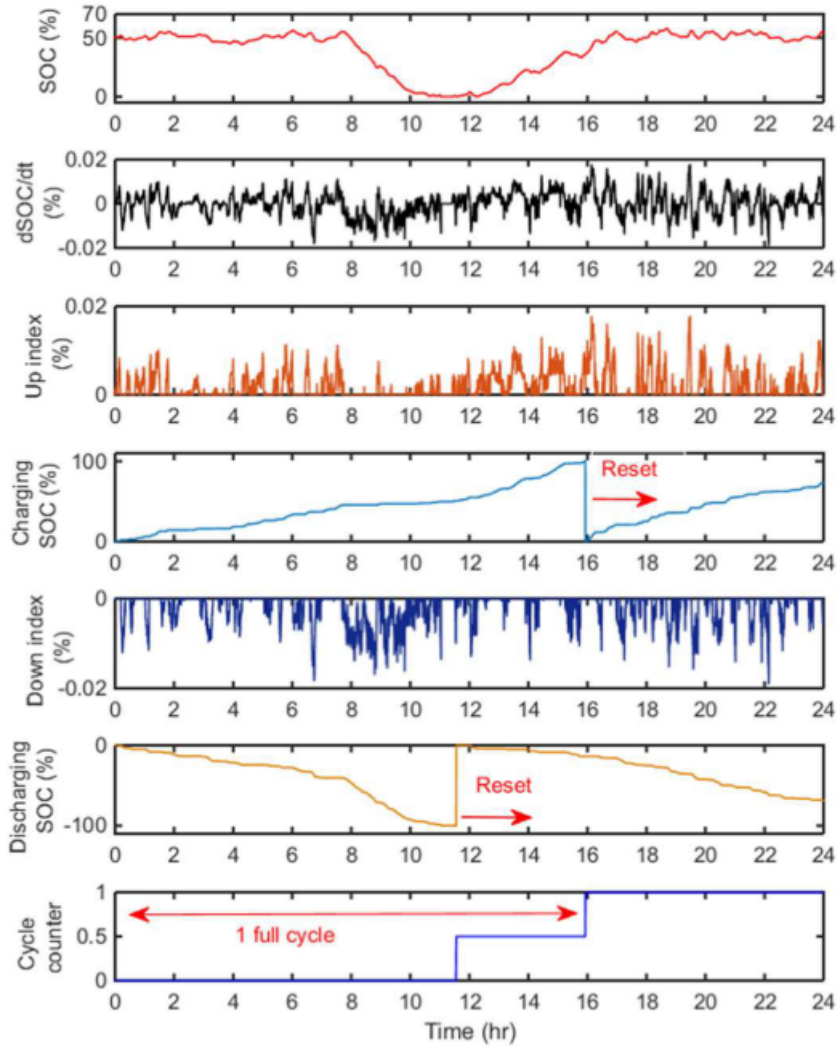
Figure 3.7: Up-Down index cycle counting method [149]

drawback appears to be that splitting the charging and discharging events into separate counters does not achieve any significant benefit whilst introducing unnecessary complexity. Overall this method presents a foundation for development within this thesis to further develop and refine the method.

### 3.4.4 Discussion

It is clear from the literature review conducted that there is a gap in the current field of modelling of ESS systems for a framework that offers a rapid simulation of new applications whilst retaining the complexities associated with more technical models.

When choosing an approach to modelling the ESSs detailed in this thesis, it is important to fully understand the aims and objectives of the projects being undertaken. The general approach taken throughout the works presented here is that the investigations are not looking into how the specific energy storage medium is

operating, rather instead it is assumed that the ESS acts as intended and purely the application is being assessed. For this reason, a physical representation of either a FESS or BESS would provide no benefit to the studies being conducted.

Secondly, a large majority of the systems being investigated are being simulated over significant periods of time, in the region of months and years. It is therefore important that computational time is a significant consideration in the modelling approach taken, which is most effectively provided by the Bucket model.

In terms of modelling the degradation of a BESS, it is clear from the literature that there has been extensive work undertaken to define the degradation experienced based upon key operational criteria. These equations can effectively be used to include degradation elements that do not significantly increase computational time, even in system-level simulations and more simplistic models. This approach of introducing complexity into the more simplistic bucket model approach is one that has been utilised throughout the modelling performed within this thesis.

## 3.5 Economic Analysis of Energy Storage Systems

Whenever an ESS is studied with regards to specific applications, an integral aspect of any study is the consideration of both the technical performance and the economic benefits (or negative impacts) that introducing an ESS can provide. Techno-economic studies are prevalent throughout the literature, and this section will discuss the relative merits of some of the key methods for economic analysis, focusing mainly on net present value (NPV) and levelized cost of electricity.

### 3.5.1 Net Present Value

NPV is a metric that seeks to represent the value of an investment by comparing the current value of cash inflow with the present value of cash outflow where a positive NPV represents all costs being met with the required return on investment provided [157]. NPV is calculated using a generic formula (Equation 3.2) where $C_{investment}$ is the initial investment in the system, $C_{costs}$ is the yearly operational costs such as operation and maintenance, ancillaries and part replacement, $C_{revenue}$ is the yearly income (£), N is system lifetime in years and d is the discount rate. Electricity cost is not included in this thesis as the impact from this when comparing different ESSs would be minimal and would introduce unwarranted complexity to the calculations.

$$NPV = \sum_{n-1}^{N} \frac{C_{revenue} - C_{costs}}{(1+d)^n} - C_{investment} \qquad (3.2)$$

NPV offers an easily comparable value for how economically viable an installation will be under set conditions [158] [159] [160]. One of the main advantages of using NPV is that it can be applied across any application where there are associated costs and income, whether that be generation sites where revenue is generated from exported energy or applications where revenue is generated from providing a given service such as DFR.

In this thesis, where BESS replacement costs are present, they are set as 75% of the original Total Capital Cost and included within the $C_{costs}$ calculation.

[157] explores the potential for residential investment in photovoltaics and batteries, with NPV being the main metric utilised for the analysis. Interestingly, it compares the baseline NPV of no investment with the predicted change to NPV provided by different levels of investment. This is a very useful tool especially when considering the introduction of energy storage into existing systems, with the conclusion of the study showing that for several scenarios there is actually a negative impact on the NPV of the system, showing how important such studies can be to prevent incorrect utilisation of ESSs. This potential negative is also shown in [161] where introducing an ESS to a DC rail system produces a negative NPV under certain conditions as well as in [162] which claims a negative NPV for supercapacitors used in tandem with solar road lighting systems.

A key aspect of the NPV equations is the discount rate $d$. The discount rate accounts for the fact that due to a myriad of factors, discussed below, the value of money in the present day is worth more than its future value. Using a given discount rate, if the resulting NPV is positive it means that the projected earnings for the project will exceed the costs, whilst a negative NPV means that the reverse is true. The discount rate chosen for a given study is impacted by many factors, with the primary influences being as follows [163];

- Inflation - The rate at which goods and services increase in price from year to year. In the UK, during the period 2000-2021, the rate of inflation peaked at 3.86%, with the average inflation in this time being 1.98% [164]. In the final year of this thesis after the completion of the studies included in this work, inflation in the UK increased rapidly, with the value for 2022 standing at 7.92%, the highest level for 32 years. The Bank of England's target for inflation is 2%, so this value is considered an outlier due to temporary market conditions. However, it should be noted that if inflation continues to stay high then the discount rates used throughout this thesis would need to be raised in order to reflect current trends.

- Cost of Energy - Whilst this variable will partially impact the value of inflation, it will have its own specific impact on the calculations involving the storage of energy. In the UK, the cost of electricity varied in the range of £24.13/MWh to £67.69/MWh between 2013-2021. However, in 2020 the market experienced considerable variability, peaking at £576.67/MWh in September 2022. After starting 2023 at a price of £201.89/MWh, the average up to and including September 2023 has fallen to £91.86/MWh, more in line with historical prices [165].

- Cost of Debt - This is generally taken as the interest rate applied to any loan required to finance the construction of a project. In the UK, during the period of 2009-2021, historically low interest rates were applied by the Bank of England, with the value not rising above 1.5% during this time. As with the rate of inflation, interest rates are continuing to rise and in August 2023 reached their latest peak of 5.25%. The studies conducted in this thesis were completed before these increases were implemented, but it is worth noting again that continued higher levels of interest rates would require larger discount rates in order to accurately reflect the value of the time in which the project is implemented [166].

With these variables in mind, selecting a discount rate presents many challenges. It is therefore important to consider the literature from a range of time prior to the studies conducted in this thesis. An overview of different discount rates used throughout the literature and the applications they are used to assess is shown in Table 3.2. It is immediately apparent that there is significant variation from study to study and that NPV is utilised as a reliable metric across a wide range of different applications. The average discount rate from Table 3.2 is 5.3%, providing a good indication of a common starting point for discount rates in energy storage-related studies. This is also shown in Figure 3.8, where it can be seen that the majority of discount rates used in this time period are in the range of 2-5%, whilst there are some studies that consider discount rates as high as 13%.

Not included within the table is [185] which performs a sensitivity analysis varying the required discount rate between 0-12%. This produces interesting results as it claims the threshold at which the installation can provide positive NPV under different scenarios of operation, as well as once again highlighting the risk of reducing the value of a site by introducing incorrectly specified ESS technology. Both of these aspects will be utilised at various points throughout this thesis.
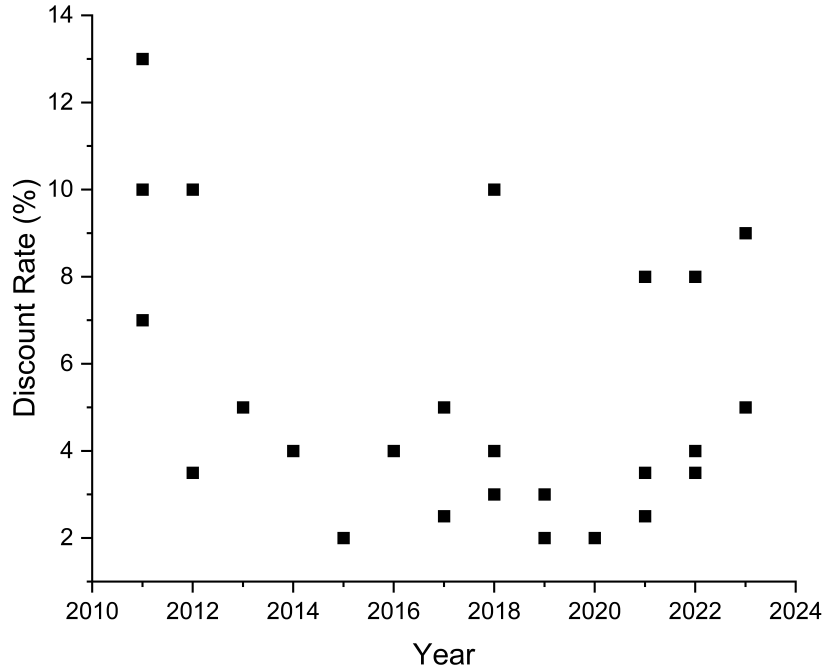
Figure 3.8: Discount rates in literature from 2011-2021

### 3.5.2   Levelized Cost of Electricity

Levelized Cost of Electricity is a similar metric to NPV that is primarily related to electricity generation, broadly defined as the total capital cost per unit of electricity generated for a given installation. It is intrinsically linked to the NPV calculation, but now with a focus on energy generation and income. It is represented by Equation 3.3 where it is shown as the NPV of the total lifetime costs over the NPV of the total lifetime income from energy production.

$$LCOE = \frac{NPV_{Expenditure}}{NPV_{Income}} \qquad (3.3)$$

Generally, this metric is utilised when considering the economic implications of generation installations such as new wind farms or solar generation sites [186]. In [187], which discusses the relative Levelized Cost of Electricity for various generation types in China under different subsidy approaches, it is shown to be a powerful tool for analysing the effectiveness of different types of generation. This method is most commonly utilised for generation sites, and therefore in order to keep consistency throughout the thesis, it is considered that this metric would not be as suitable for the work in this thesis as NPV, which will provide a more consistent account to use the same metric for all applications assessed.

Levelised Cost of Storage is an alternative to Levelized Cost of Electricity, which

Table 3.2: Discount Rates used within previous NPV studies

| Description | Discount Rate | Year | Ref |
|---|---|---|---|
| Different implementations of ESS on a grid-scale | 7,10,13 | 2011 | [167] |
| Optimising the operation of an ESS within a wind curtailment scheme | 3.5,10 | 2012 | [168] |
| Study into the optimal approach for integrating distributed ESSs in energy grids | 5 | 2013 | [169] |
| Different scenarios for Hydrogen storage at a wind farm | 4 | 2014 | [170] |
| Introduces a novel method for economic studies of ESSs in energy and ancillary markets | 2 | 2015 | [171] |
| Energy arbitrage applications for Battery ESSs | 6 | 2016 | [172] |
| Comparing network improvements and electrolysis investment as options to reduce wind curtailment | 2.5 | 2017 | [173] |
| Wayside energy storage for a DC rail system | 5 | 2017 | [161] |
| Analysing the effectiveness of combining wind generation with compressed air energy storage and Biomass Gasification Energy Storage | 10 | 2018 | [174] |
| Residential investment in solar panels and BESSs | 4 | 2018 | [157] |
| BESS viability for frequency regulation in European markets | 3 | 2018 | [175] |
| Solar energy integration within a microbrewery | 3 | 2019 | [176] |
| Study into supercapacitors and batteries for integration with solar road lighting systems | 2 | 2019 | [162] |
| Evaluating PV and ESSs for domestic energy systems in the UK | 2 | 2020 | [177] |
| Strategies for combining wind farm and BESS | 8 | 2021 | [178] |
| Financial analysis of a hybrid battery, wind and solar renewable system | 3.5 | 2021 | [179] |
| Grid-connected BESS providing frequency regulation in different markets | 2.5 | 2021 | [180] |
| Combining a thermal power plant with liquid air energy storage | 4 | 2022 | [181] |
| Analysing the payback time for deploying used electric vehicle batteries for residential energy storage | 3.5 | 2022 | [182] |
| Integration of compressed air energy storage with an industrial plant | 9 | 2023 | [183] |
| Optimising the size of a hybrid hydrogen and battery system for seasonal storage | 5 | 2023 | [184] |

discounts the electricity cost of charging the asset within $NPV_{\text{Expenditure}}$ in Equation 3.3 [188]. This metric was considered for use in this thesis, but the more easily comparable nature of NPV when considering different applications was chosen as a greater benefit.

### 3.5.3    Conclusions

The techno-economic analysis will be a key part of the work presented in this thesis, and it is, therefore, important to understand the correct use of different tools for determining the positive or negative economic impact that introducing ESSs can have. The key metric that has been discussed is NPV which represents a reliable and widely used method of determining the economic impact that can be used consistently across all of the studies presented in this body of work. Levelized Cost of Electricity has also been discussed, and whilst it provides a solid and also widely used metric, it is deemed to be less applicable to this body of work as a whole and hence has been discounted. Discount rates utilised across a range of studies have also been introduced, giving context for the decisions that will be made throughout the following chapters.

## 3.6    Genetic Algorithms in Energy Storage Research

An important tool for the research and design of energy storage systems, especially HESSs, is the Genetic Algorithm (GA). A GA is a process commonly used for the optimisation of a set of variables when given a specific criterion to minimise. An initial population of variables is randomly created within a set of bounds (Generation 1), with each set of variables tested to produce a specific reward value. The GA then creates a second generation by taking the best-performing individuals from generation 1 and creating a new set of individuals through a range of different methods. An overview of how a GA operates within the MATLAB/Simulink environment is shown in Figure 3.9.

The key variables when implementing a GA consist of the following;

- Population Size ($N_{\mathrm{P}}$) - The number of individuals within each iteration of the algorithm. For instance, for a population size of 20, the simulation will be conducted for 20 different sets of variables at each iteration.

- Number of Generations ($N_{\mathrm{G}}$) - The total maximum number of iterations that the algorithm loops through before reaching its conclusion. This, combined with the population size, determines the total number of individuals that are assessed as part of the algorithm.

- Crossover Rate ($X_{\mathrm{R}}$) - This is the probability that any two individuals will swap their characteristics to create a new individual at the end of each generation
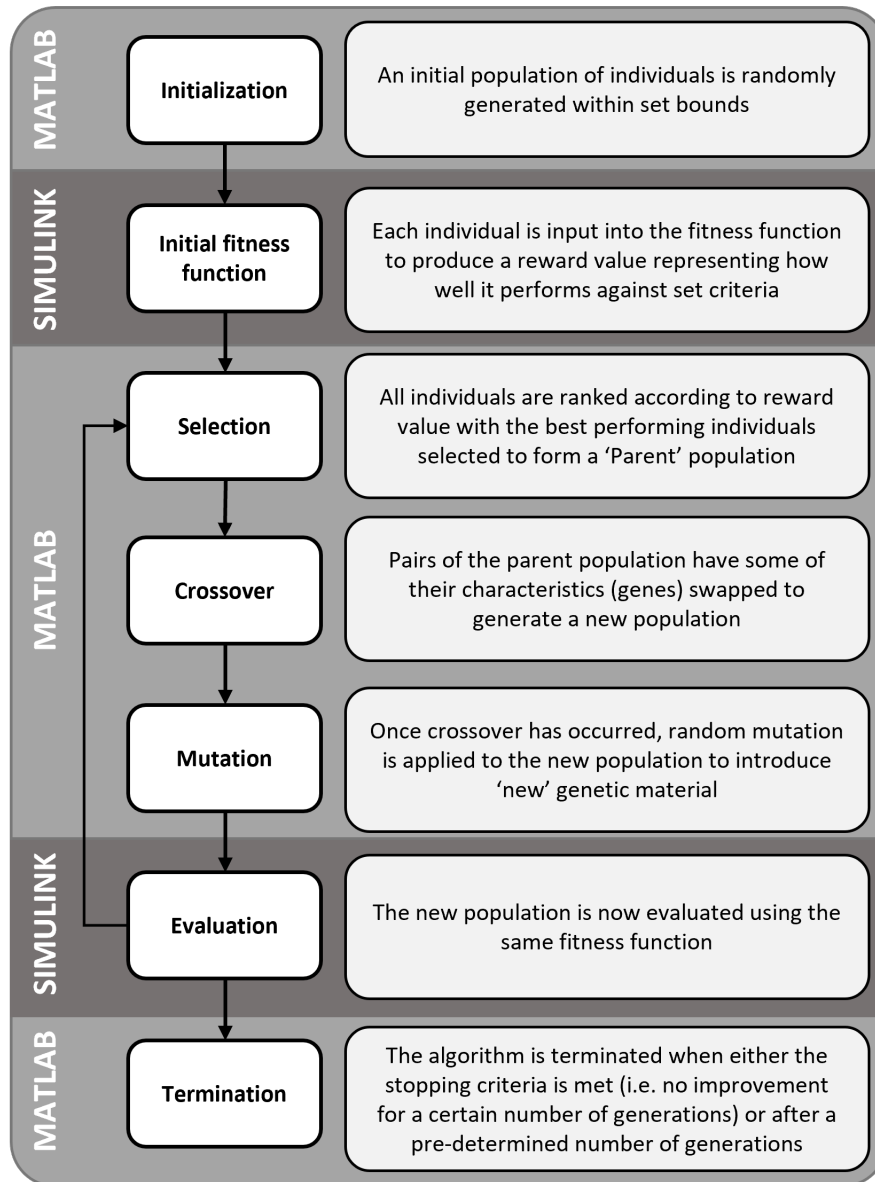
Figure 3.9: Operation of a genetic algorithm

- Mutation Rate ($M_{\mathrm{R}}$) - This is the probability that an individual will have a characteristic randomly altered at the end of each generation

An overview of selected literature where GAs have been utilised for energy storage research is shown in Table 3.3 along with the variable settings for each study. Where a cell is left blank this indicates that the information was not made available in the published study. The key aspect to highlight from this is that the crossover rate is generally several orders of magnitude higher than the mutation rate. The mutation rate is commonly set at 0.05, which is the default setting in the MATLAB/Simulink Genetic Algorithm toolbox. Population and Generation sizes are highly variable, which is to be expected as they will need to be tailored specifically to the range of values to be tested for each specific application.

In [189], a genetic algorithm is utilised to reduce the unit cost of electricity by optimising the parameters of the site. This study highlights a commonly found effect when using GAs, whereby the algorithm very quickly reaches a 'good' solution, and plateaus early as minimal improvements are made into late generations. Of a 100-generation algorithm, both examples presented experienced little further improvement after the 20th generation.

Another relevant piece of work is contained in [190] where the study consists of optimal sizing and siting of a BESS to reduce the effect of renewable energy generation on distribution networks. The GA reaches a plateau quite early on in the process, this time at around the 300th generation of a 1000 generation set up. This is the result that is sought after when running genetic algorithms, as it gives a degree of certainty that the algorithm has found the optimal solution.

The works in [191], [192] and [193] all discuss different implementations of the genetic algorithm toolbox within MATLAB/Simulink. This offers a user-friendly and reliable method for implementing a GA and is widely used throughout the literature. All 3 studies claim to show strong results from using this method, and it allows any associated Simulink model to be integrated directly into the GA process. This is the method for implementing a GA used within this thesis, with the results of this exercise discussed in more detail in Chapter 5.

Table 3.3: Overview of energy storage research utilising genetic algorithms

| Ref | $N_P$ | $N_G$ | $X_R$ | $M_R$ | Description |
|---|---|---|---|---|---|
| [189] | 50 | 100 | 0.6 | 0.05 | Minimisation of the unit discounted cost of electricity generation in a wind generation site with integrated FESS |
| [191] | 800 | 25 | 0.8 | 0.2 | Optimization of capacity and power of a supercapacitor in a hybrid system with a battery to extend the lifetime of the BESS |
| [194] | 500 | 10 | 0.4 | - | Location and sizing of energy storage within LV networks to counter voltage regulation issues |
| [195] | 30 | 300 | 0.95 | 0.05 | Optimal sizing of a wind/PV power system with integrated battery/supercapacitor HESS to increase economic performance |
| [196] | 400 | 200 | 0.5 | 0.05 | Selecting the location and rated power of a BESS within a distribution network to maximise power quality improvement |
| [197] | 40 | 100 | 0.8 | 0.02 | Minimisation of the annual total cost for an educational building by optimally sizing an integrated photovoltaic wind battery |
| [198] | 40 | 100 | 0.7 | 0.15 | Optimal location and size of a supercapacitor in a metro system to maximise economic and technical performance |
| [199] | 50 | 200 | - | - | Sizing of a hybrid energy storage system (supercapacitor and battery) for an electric vehicle to minimize costs whilst extending the lifetime of the battery |
| [192] | 40 | 20 | 0.8 | 0.01 | Improving the frequency stability and efficiency of a shipboard power system by optimising the control and power allocation between an ESS and a diesel generator |
| [200] | 50 | 50 | - | - | Optimised sizing and placement of supercapacitors to minimise energy demand from electric mains from a metro train operation |
| [190] | 60 | 1000 | 0.5 | 0.02 | Minimizing total costs incurred by the distribution network due to power quality factors by optimising the siting and sizing of a BESS |

# 3.7 Overview of ESS Model

In this section, a detailed overview of the MATLAB/Simulink model that has been developed is presented. The most important element of the model and one of its key advantages is the modular subsystems with which it can be built. This enables it to be easily switched from one scenario to another with minimal overall adjustments, thus representing a significantly improved timescale from the conceptualisation of a scenario to producing accurate results. Whilst the core components of the model are built from simple blocks from the main Simulink library, they have been brought together in a way that adds further complexity without sacrificing computational speed.

A high-level overview of the model is shown in Figure 3.10 whilst the model set up with both the FESS and BESS active in a hybrid scenario is shown in Figure 3.11. This is a simplified diagram illustrating the variables required for each block, with the Simulink extracts for each block detailed in the following sections.

As it is the focus of the majority of the work contained in this thesis, the model presented in this section is set up to perform analysis on a DFR service. The main modular components are detailed below;

**Application Block**

This block is modified according to what application is to be simulated. It will consist of whatever components are necessary to generate a power-request signal to the ESS. For delivery of DFR for example, this would consist of input of second-by-second frequency data that can then be converted into a power request using a lookup table populated to provide the required response envelope. This response envelope is set in terms of the proportional power requested and therefore needs to be multiplied by the service block to provide the required output power in kW. Grid services are typically contracted for a given power rating. For example, if the service being provided was 1MW, the value of service would be set to 1000 (to represent 1000kW). The output of this block is the requested power in kW which is the input to the inverter block. The application block as used in a DFR simulation is shown in Figure 3.12.
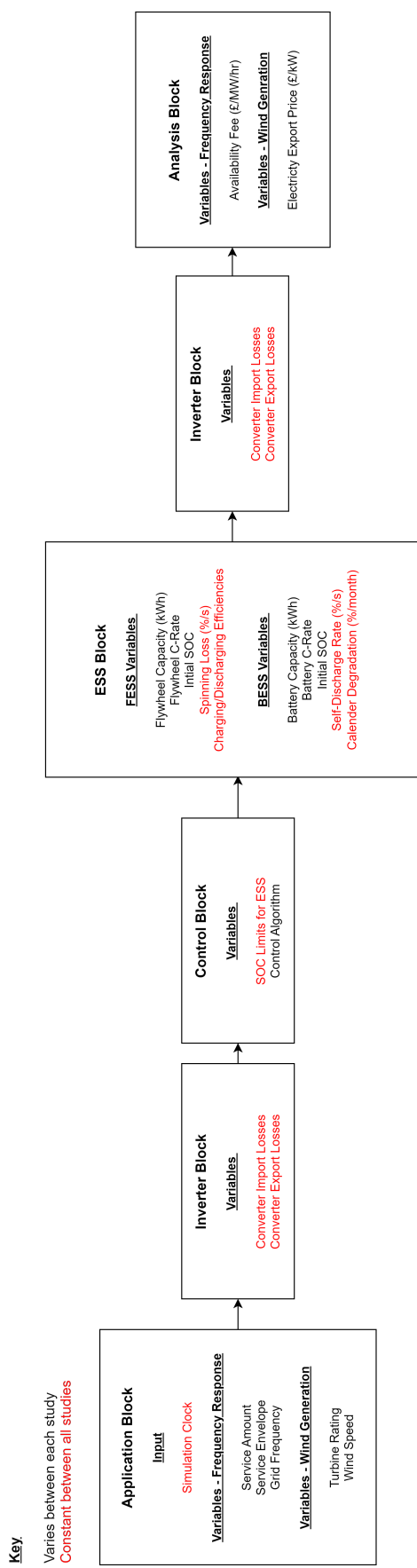
Figure 3.10: High level model diagram
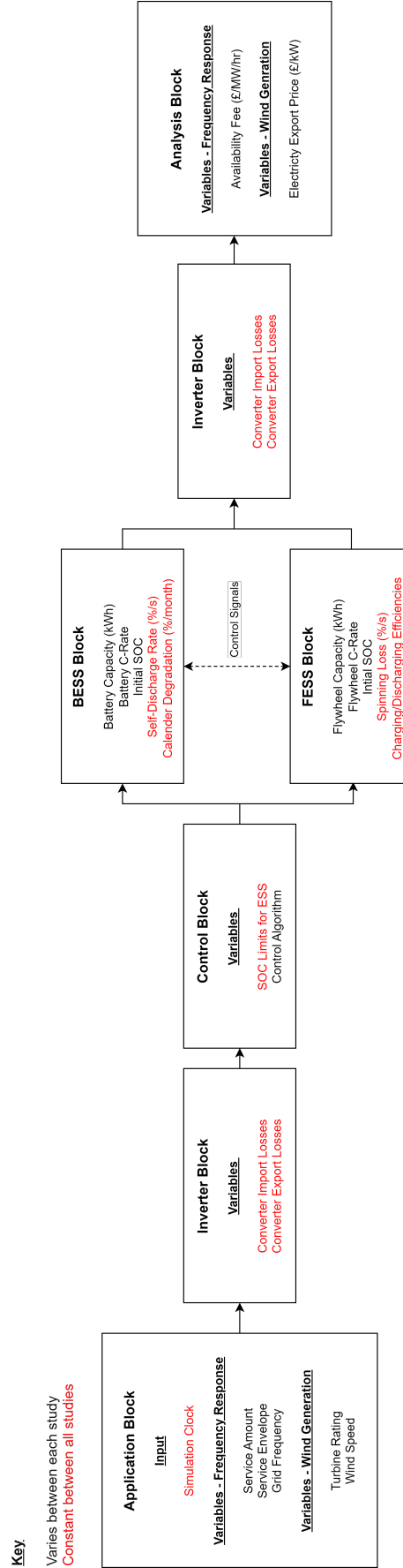


Figure 3.11: High level hybrid model diagram
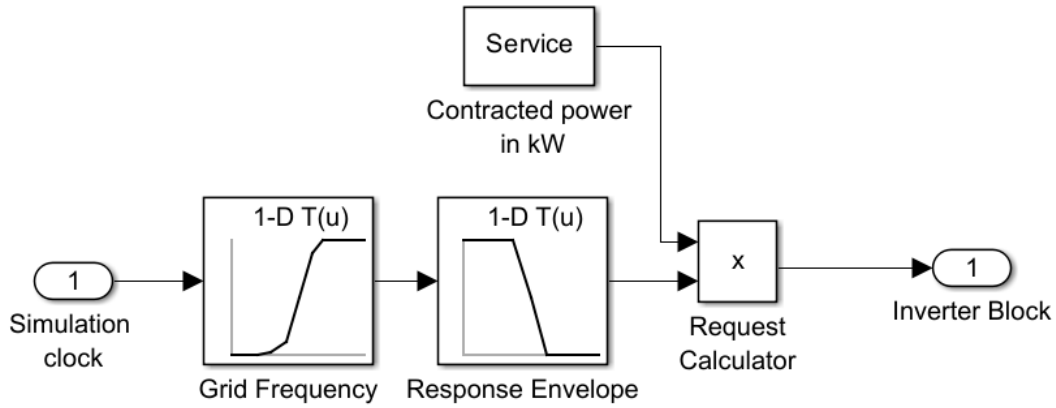
Figure 3.12: Application block from Simulink model
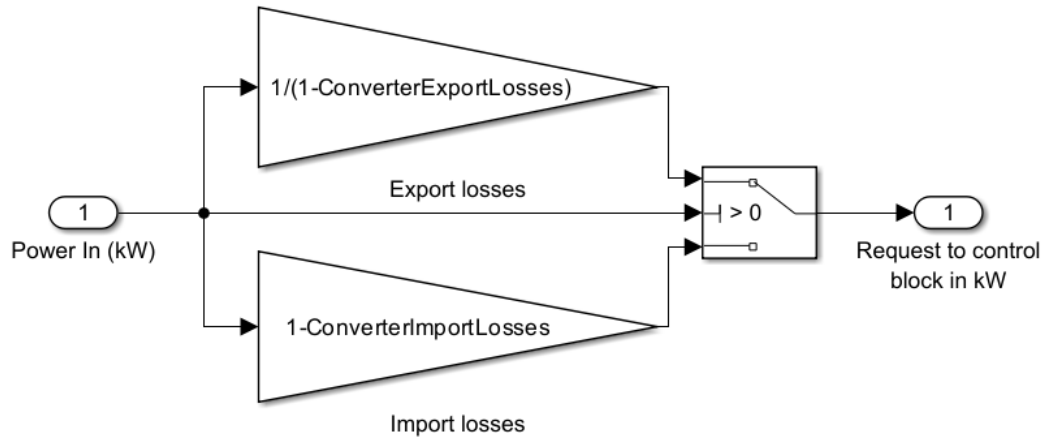


Figure 3.13: Inverter block from Simulink model

**Inverter Block**

This block represents the inverter, calculating the losses experienced by the power electronics present in the system, accounting for these losses by either increasing the request in a discharging scenario or decreasing the request in a charging scenario so that the input/output that the ESS sees is accurate. The output of this block is the requested power in kW, adjusted to represent losses in the power electronics. The model performs this adjustment at this stage to ensure that the ESS experiences the correct change in SOC accounting for the losses. Figure 3.13 shows this block.

**Control Block**

This block consists of a MATLAB function block that controls how and when the ESS charges or discharges. The inputs are power request, current SOC and any required ESS specifications such as capacity, C-Rate and SOC limits which can either be specified as inputs taken from the rest of the model, or within the MATLAB
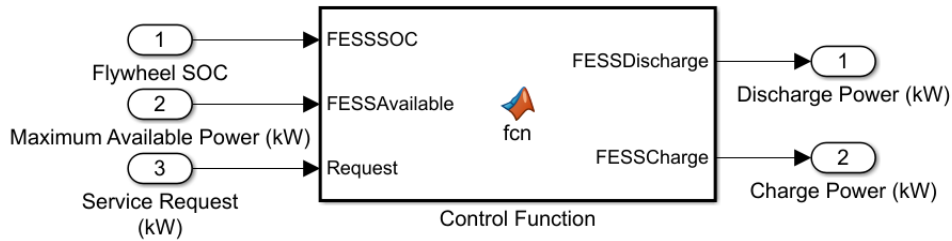
Figure 3.14: Control block from Simulink model

function. The outputs will be charging power and discharging power in kW. Figure A1 within the Appendix shows the control function code for a DFR service, with the Simulink extract shown in Figure 3.14. In a hybrid scenario, the control block will have information from both ESS blocks and make decisions on which to request power from based on control strategy.

**FESS Block**

The block representing the FESS forms a closed loop with the control block, receiving its input from the control block before feeding its output back to it for the next second of simulation. It mainly consists of an integrator block representing the SOC of the flywheel, along with several other sub-systems representing efficiencies, spinning losses and cycle counting. An overview of this block is shown in Figure 3.15. Spinning losses are calculated as a percentage of SOC lost per second. The main parameters of the model have been taken from the manufacturer data sheet provided by OXTO Ltd with parameters such as capacity, C-Rate, and initial SOC able to be specified depending on the system being modelled.

**Cycle Counting Block**

The details cycle counting block seen in Figure 3.15 are shown in Figure 3.16. This block compares the current SOC with that of the previous simulation step and converts the difference in SOC into an equivalent cycle as a proportion of the FESS energy capacity based upon Equation 3.7. This block is identical for both the FESS and BESS models.
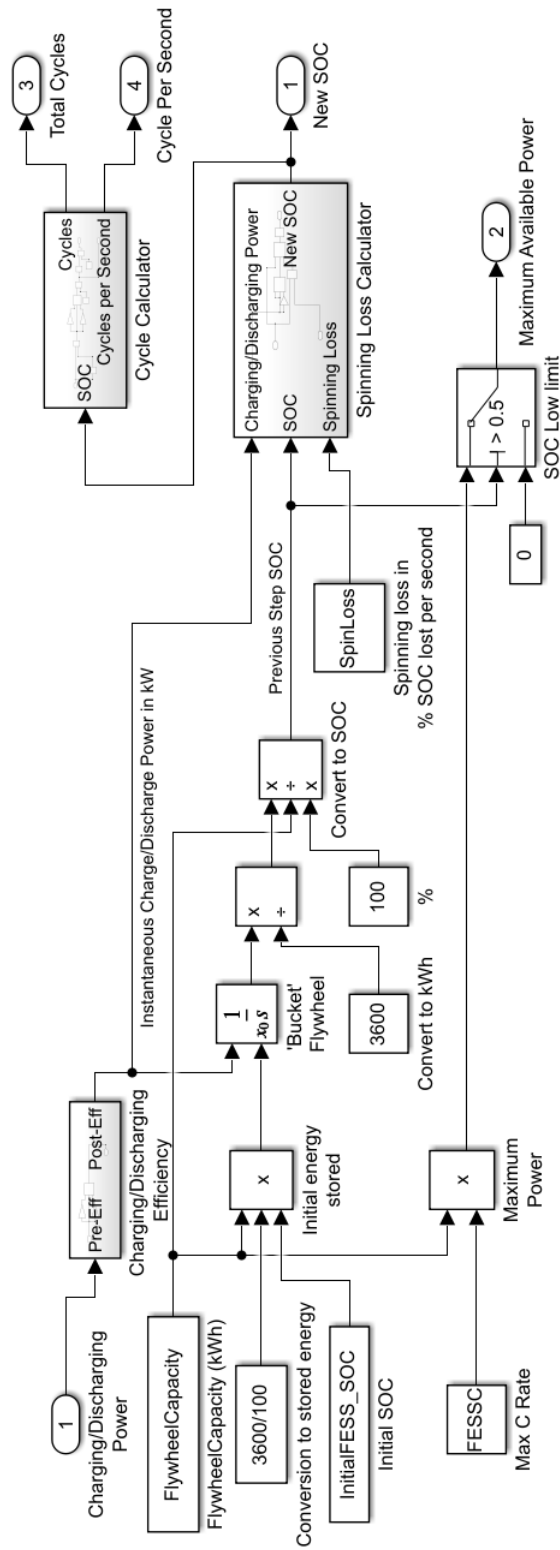
Figure 3.15: FESS block from Simulink model
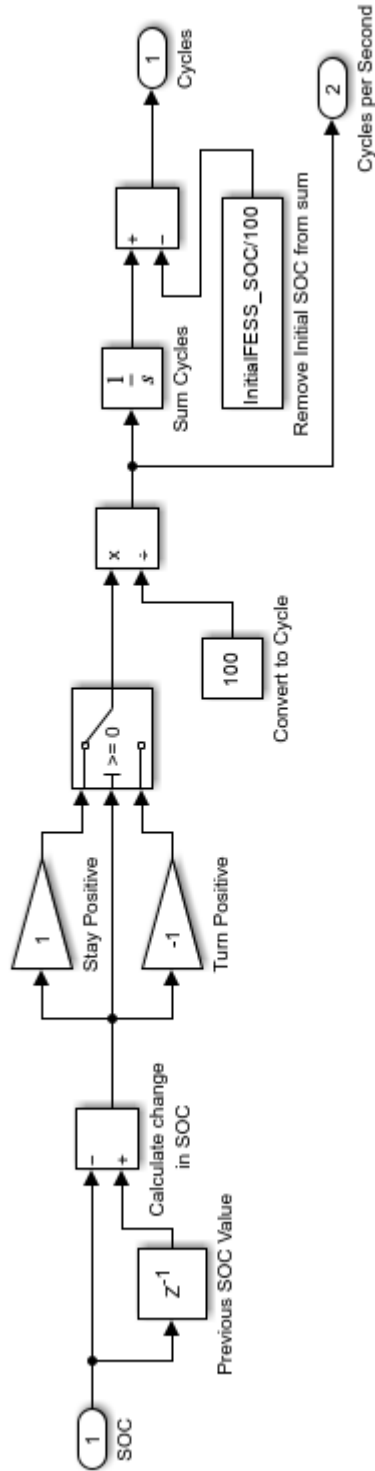
Figure 3.16: Cycle counting block from Simulink model
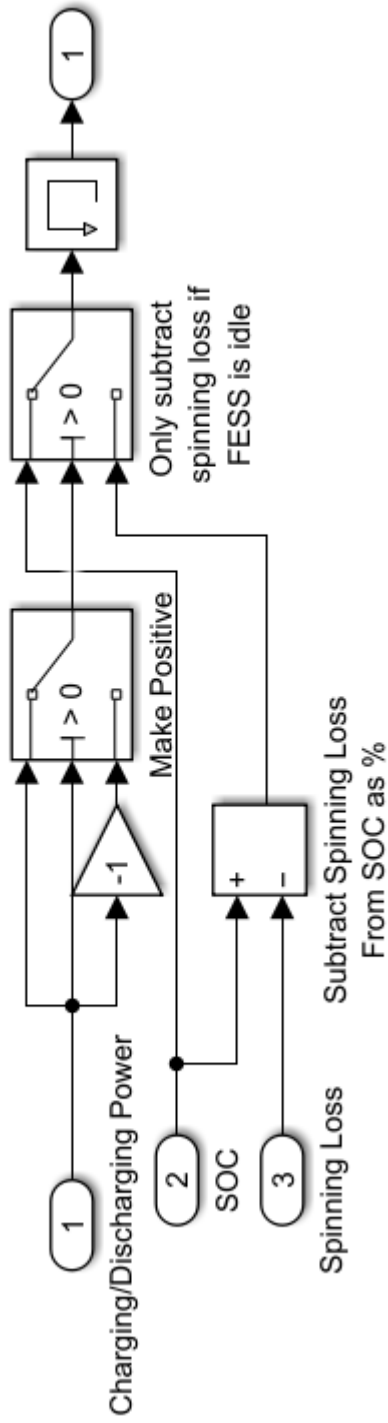
Figure 3.17: Spinning loss block from Simulink model
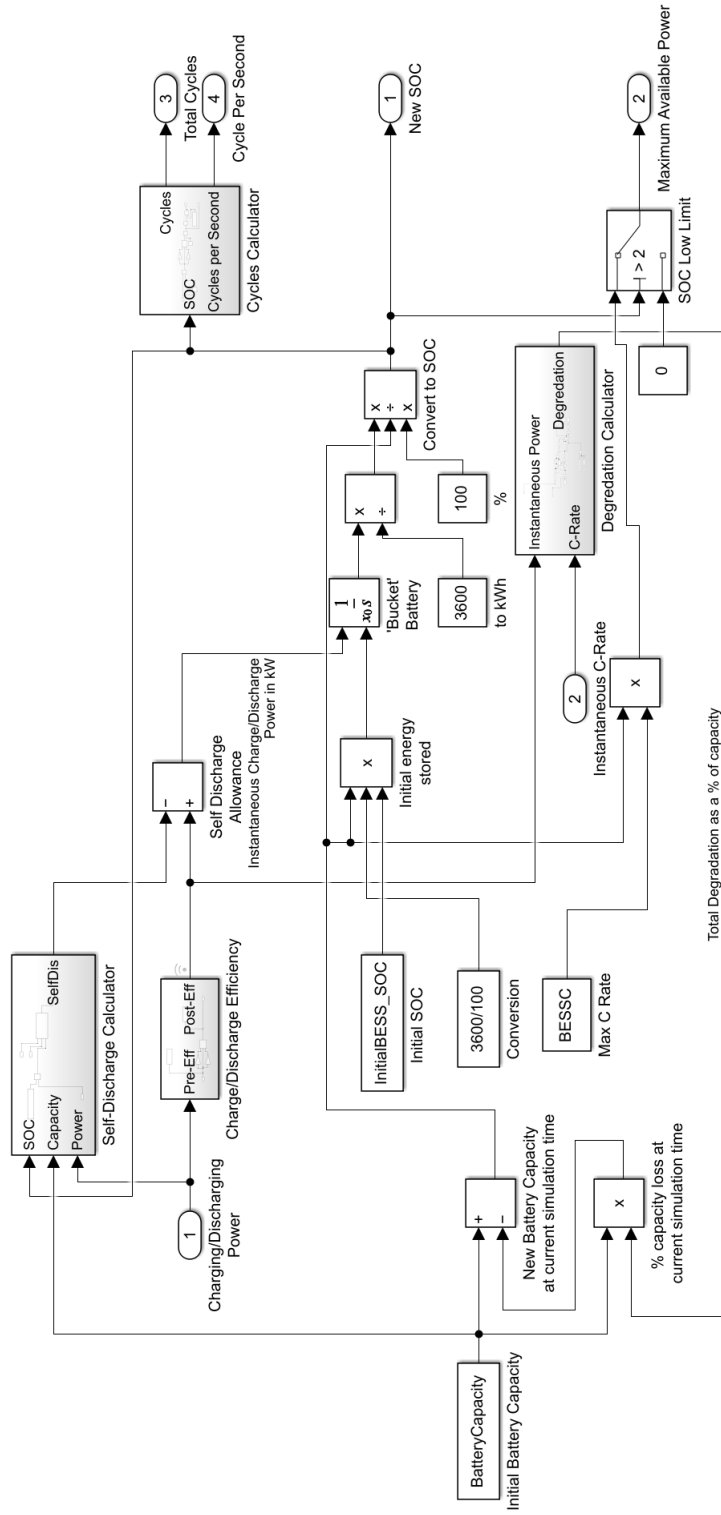
Figure 3.18: BESS block from Simulink model
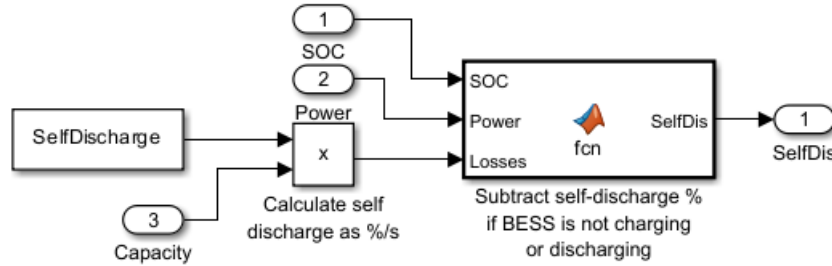
Figure 3.19: Self-discharge block from Simulink model

**Spinning Loss Block**

The spinning loss block specific for the FESS model is shown in Figure 3.17. This block subtracts the spinning loss as a % per second loss for every second that the flywheel is idle. Spinning losses are not applied when the flywheel is charging or discharging.

**BESS Block**

The block representing the BESS contains the same basic structure as the FESS block. The key feature is once again an integrator block representing the SOC of the battery, along with several other sub-systems representing efficiencies, degradation, self-discharge, and cycle counting. The cycle counting block is the same as that discussed for the FESS model. An overview of this block is shown in Figure 3.18.

**Self Discharge Block**

The self-discharge block in Figure 3.19 operates in a similar way to the previously discussed spinning losses block. It applies a reduction in the SOC of the battery at any time step where the BESS is neither charging nor discharging.

**Degradation Block**

In terms of degradation, The equation presented in [56] is used to calculate the incremental degradation for a period $\Delta t$ as shown in Equations 3.4, 3.5 and 3.6. This is represented in Simulink as shown in Figure 3.20. It is primarily based on instantaneous C-Rate and energy throughput, with temperature treated as a constant. This decision has been made in the knowledge that any of the systems proposed within this thesis would be deployed within temperature-controlled units. The general temperature range experienced by the cells at the Willenhall ESS installation is 18-30°C and experiences the largest temperature during constant high C-Rate charging and discharging events. Considering the applications this work is being applied to, these

Table 3.4: BESS degradation equation coefficient values [56]

| Coefficient values and units | |
| --- | --- |
| a | 8.61E-6 |
| b | -5.13E-3 |
| c | 7.63E-1 |
| d | -6.7E-3 |
| e | 2.35 |

events are rare and hence it is a fair assumption to keep the temperature constant. The main parameters of the model have been taken from the manufacturer data sheet for the Willenhall installation with parameters such as capacity, C-Rate, and initial SOC able to be specified depending on the system being modelled.

The chemistry utilised to derive the equations in [56] is Lithium Nickel Manganese Cobalt, and as part of works contained in this thesis the modelling implementation has been verified against a different chemistry, the Willenhall ESS (Lithium Titanate) which was discussed in Section 2.3. This gives confidence that the formula is appropriate to be utilised as representative of BESS degradation for a generic model such as that presented here. Whilst it is acknowledged that different chemistries will have different degradation rates, for the models contained in this thesis, which are intended to be generic fast operating models, it is considered that this approach will provide robust results that are backed up by cycle counting estimation.

$$\Delta Q^{cycleloss}(t) = B_1.e^{B_2.I_{rate}}.A_h\Delta t \tag{3.4}$$

$$B_1 = a.T^2 + b.T + c \tag{3.5}$$

$$B_2 = d.T + e \tag{3.6}$$
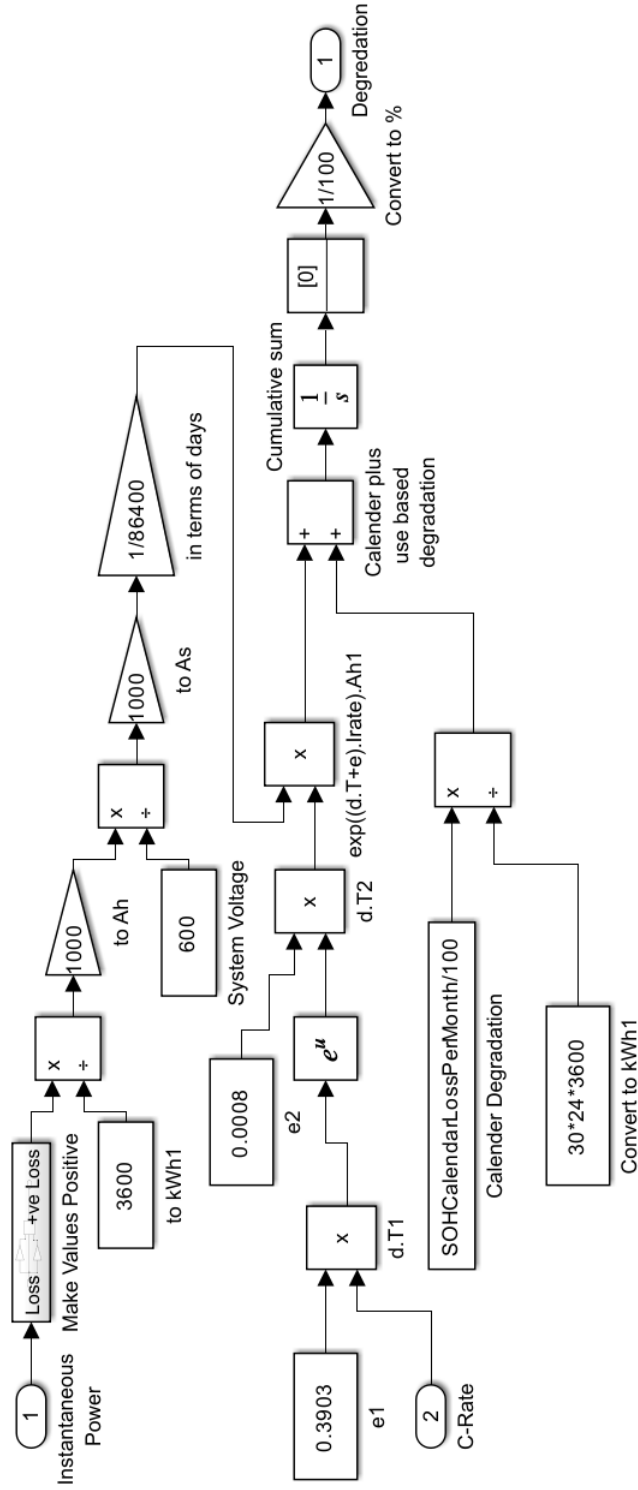
Figure 3.20: Degradation block from Simulink model

Table 3.5: Simulation time in minutes for different models and applications for one year of simulation *PC specifications - Intel Core i7-6700k CPU @ 4GHz*

| Application | BESS Model | FESS Model | HESS Model |
|---|---|---|---|
| Frequency response | 4.2 | 2.5 | 4.9 |
| Wind generation support | 7.6 | 5.8 | - |
| Solar generation support | 4.9 | 3.4 | 4.5 |
| Electric vehicle charging | 3.2 | 2.8 | - |

Where $\Delta Q^{\text{cycleloss}}(t)$ is the % degradation experienced over a given time period t due to cycling, the values of *a*, *b*, *c*, *d*, and *e* are constants as given in Table 3.4, $I_{\text{rate}}$ is the C-Rate for that period, $A_h$ is the energy throughput over that period and T is the temperature. For the purposes of this thesis, it has been assumed that the energy storage is kept in a temperature-controlled housing unit maintaining 20°C (293K). In this model, all instances of $\Delta t$ are 1 second, with the C-Rate calculated as the rate at which the BESS is asked to charge/discharge over that 1 second and the energy throughput calculated over the same period.

Figure 3.21 shows an example simulation in operation, with degradation increasing incrementally with each partial cycle. Higher C-Rates and energy throughput cause greater incremental increases in the overall degradation total. This approach has been used previously across the literature [147] [201].

**Metric Block**

This block takes inputs from the other blocks and converts them into metrics for export and assessment. Base functions that this block will always carry out include the total number of cycles, analysis of average C-rates and power discharged. For different applications, additional subsystems can be included such as calculating payment transactions or system availability. In other applications more complex metrics are available that can define the SOC and C-Rate ranges that the ESS operates over, something that is explored further in Section 3.9.

## 3.7.1   Simulation Times

To illustrate how effective the newly developed models are at simulating different applications for significant periods of time, the total simulation time was recorded for a range of different applications over the course of a year for the FESS, BESS and HESS models, with the results shown in Table 3.5

Of all the combinations shown in Table 3.5, none exceed 10 minutes to simulate an entire year. The FESS model is generally faster, which is the result of the BESS model being slightly more complex due to the real-time degradation simulation.
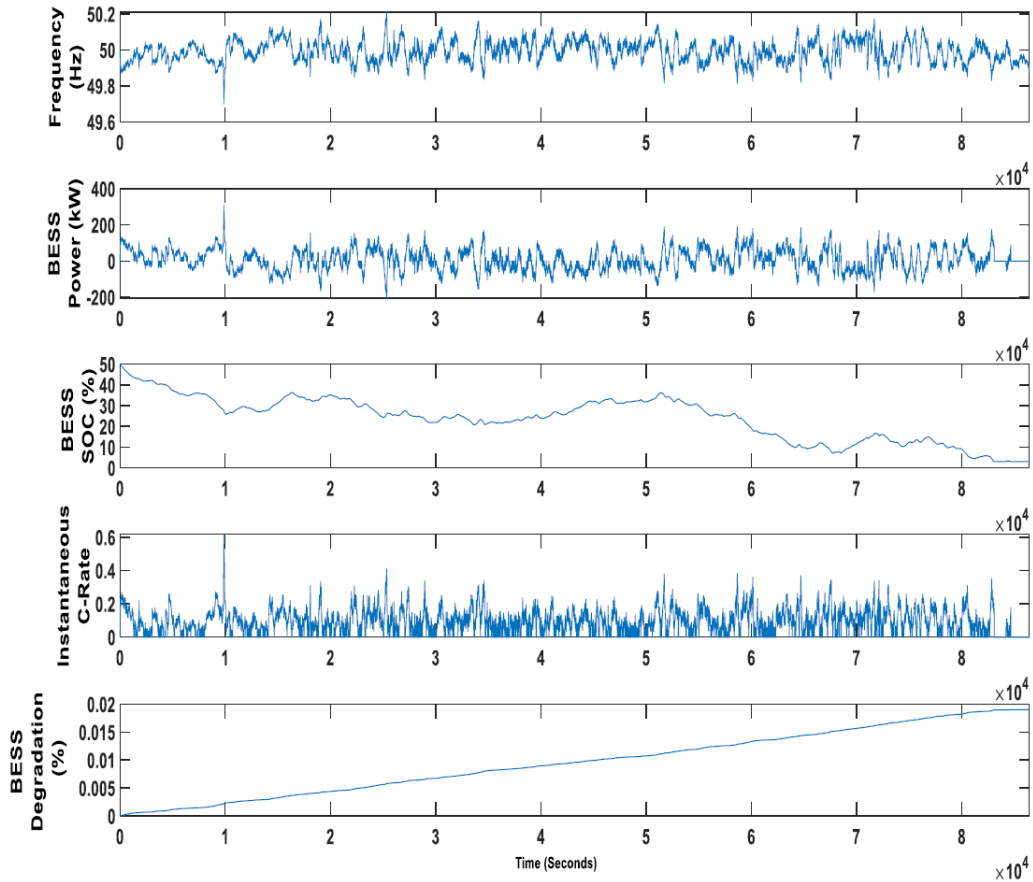
Figure 3.21: Example simulation output showing BESS degradation
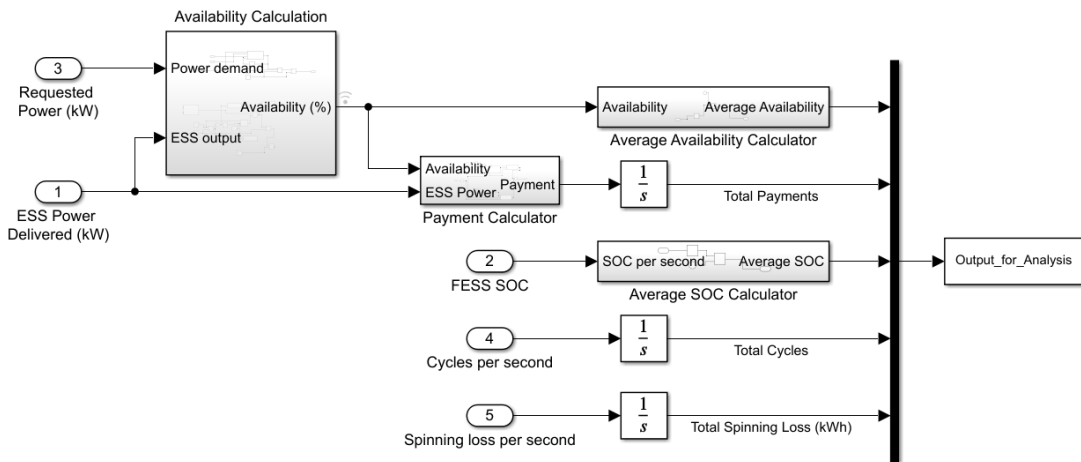


Figure 3.22: Metric block from Simulink model

The fact that 20 years of operation can be simulated in the worst case in under 3.5 hours is significant, as it means complex techno-economic analyses can be conducted quickly for multiple applications, offering an important tool in feasibility studies.

## 3.8   Verification of BESS Model

Using the data available from Willenhall ESS, a verification exercise was undertaken to validate the developed BESS model against a real-world system. To verify that the model is operating correctly, two validation exercises were performed. For the purposes of this verification exercise, two SOC readings utilized by Willenhall were used to validate the model. The first is termed 'BMS' and represents the in-built battery management system reading provided by Toshiba. The second is derived from a dual sigma point kalman filter implementation, termed 'DSPKF', and is taken from work previously conducted to produce a more reliable and accurate reading of large-scale battery systems SOC [202].

Firstly, 6 power profiles representing periods of time where the Willenhall ESS provides different levels of constant outputs were extracted from the monitoring system. These power profiles were then used as the input to the model, with the SOC of the model and the two Willenhall SOC readings then compared to determine the root mean square error (RMSE) of each verification exercise. These are referred to in this chapter as 'step-change profiles'.

Following that, the SOC data for 6 different 30-minute periods of the Willenhall installation providing DFR were extracted, with the matching frequency profile for these periods used as the input to the DFR battery model discussed previously in Section 3.7. RMSE values were then derived for each of the 6 DFR verification exercises between both the BMS and DSPKF measurements for SOC. These are referred to in this chapter as 'Frequency response profiles'.

The time periods used in this assessment were chosen based on an initial exploration of appropriate operational characteristics. The step-change profiles were chosen to represent different levels of power and changes of charge/discharge. The frequency profiles were chosen based on periods of time that the Willenhall ESS was operating with the correct level of service provision and providing the correct DFR service.

RMSE is a method that can be used to measure modelling errors and has been used extensively across a variety of different applications. For battery modelling, it is commonly used to compare battery metrics such as SOC as presented in various studies [203] [204] [205]. The available literature suggests that an RMSE in the region between 0.50% to 2.00% is considered to be an accurate approximation of the SOC that is being compared.
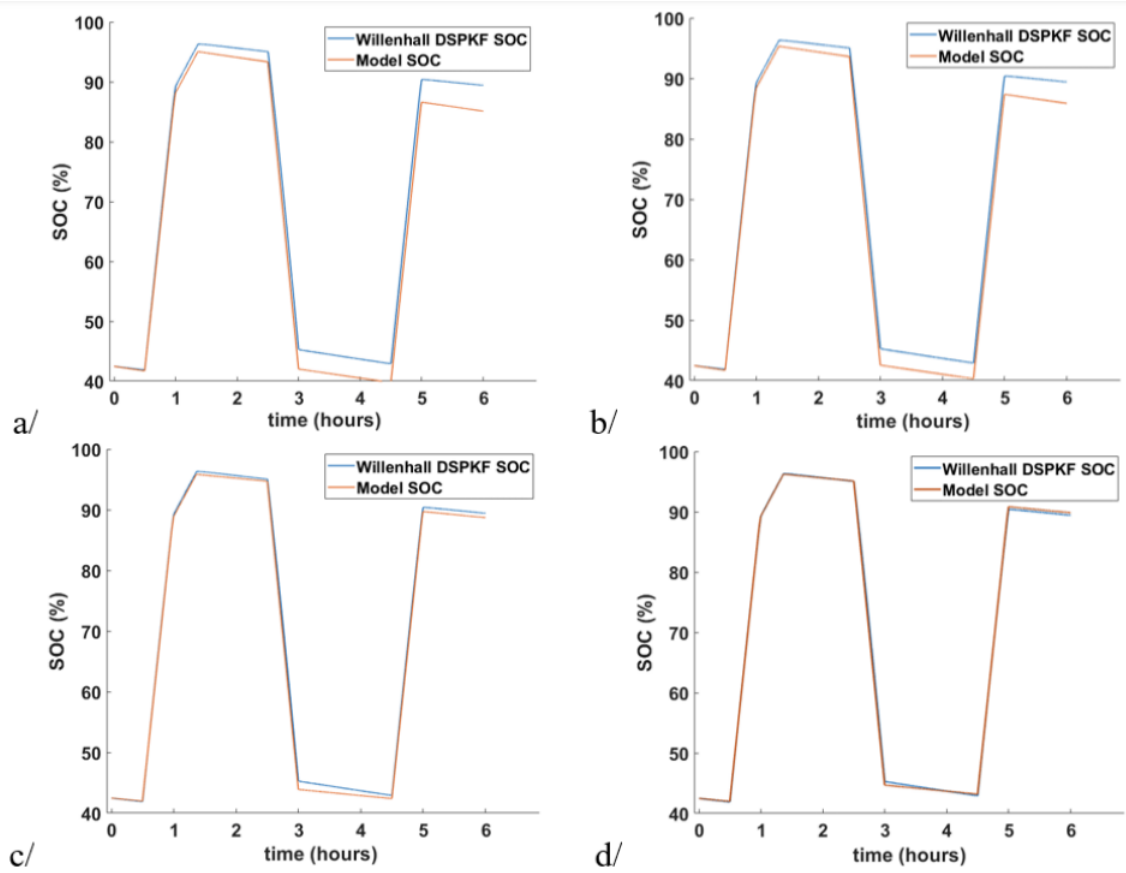
Figure 3.23: SOC profiles for Verification 3 as the variables are modified per 'sets' in Table 3.6 – a) Set 1 b) Set 3 c) Set 7 d) Set 10

In [204] a li-ion BESS connected to the grid is discussed, with RMSE used to verify the accuracy of the model in regards to capacity fade whilst [202] assesses the accuracy of a state of charge estimation system by using RMSE as a basis of accuracy. In [206], RMSE is used to assess uncertainty in forecasting wind speeds compared to subsequent power curves from wind turbines, with the RMSE broken down into 'bias' and 'variance of the error' to show the impact of different component factors on the RMSE.

### 3.8.1 Initial Model Refinement

As the Willenhall ESS site has been operational for several years now, it is unlikely that the efficiencies and discharge rates initially quoted are still valid today. Therefore, a degree of refinement was necessary to manually tune certain variables within the model with a view to decreasing the RMSE across the range of verification exercises. The variables that were varied to decrease the overall RMSE were the charging efficiency, discharging efficiency, and the self-discharge rate of the Willenhall ESS.
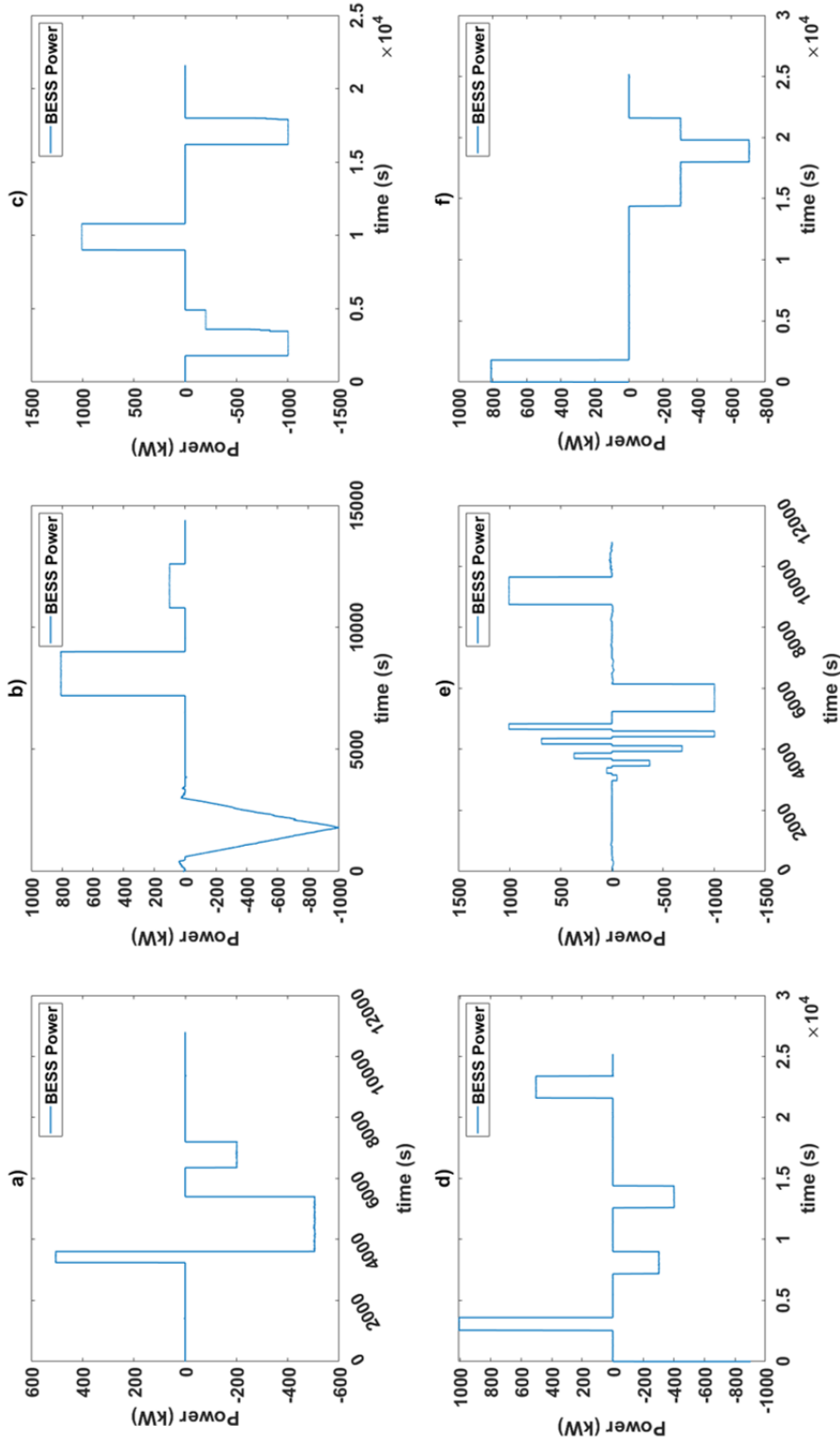
Figure 3.24: Power profiles used to verify the performance of the MATLAB/Simulink model a) Verification 1 (14/01/2022) b) Verification 2 (03/11/2021) c) Verification 3 (12/10/2021) d) Verification 4 (14/10/21) e) Verification 5 (17/08/21) f) Verification 6 (20/01/22)

Table 3.6: Model refinement process example showing variable increments

| | Set 1 | Set 2 | Set 3 | Set 4 | Set 5 | Set 6 | Set 7 | Set 8 | Set 9 | Set 10 |
|---|---|---|---|---|---|---|---|---|---|---|
| Charging Efficiency | 0.97 | 0.975 | 0.975 | 0.975 | 0.98 | 0.98 | 0.98 | 0.985 | 0.985 | 0.987 |
| Discharging Efficiency | 0.97 | 0.97 | 0.975 | 0.975 | 0.975 | 0.98 | 0.98 | 0.98 | 0.99 | 0.991 |
| Self-Discharge Modifier | 0.015 | 0.015 | 0.015 | 0.0125 | 0.0125 | 0.0125 | 0.01 | 0.01 | 0.01 | 0.01 |
| RMSE | 2.819% | 2.509% | 2.338% | 1.799% | 1.497% | 1.330% | 0.835% | 0.593% | 0.427% | 0.422% |

An example of how this process was conducted is shown in Table 3.6 and the accompanying Figure 3.23. This preliminary exercise aimed to derive the settings that best represented the current reality of the physical system. The refinement exercise was conducted across the entire range of verification sets, Verification 3 is used as an example illustrating how this process was conducted. In Table 3.6, the 'sets' referred to are the sets of values used for that particular instance of the refinement process.

## 3.8.2 Step Change Verification

To validate the model's response to power profiles that are simple step-change events, a set of 6 varying profiles as seen in Figure 3.24 were simulated with the resulting SOC curves compared with each Willenhall ESS SOC monitoring system.

Each individual comparison of SOC profiles for the step change verification is contained within the appendix (Figure A2 to Figure A13) showing the curves from which the RMSE values were derived. In Table 3.7, the RMSE for each set of verification data is shown. The top row shows the RMSE between the two systems already in operation at Willenhall (an average RMSE between the two systems of 1.41%), the closest correlation being Verification 1 with 0.78% and the furthest apart being Verification 5 with 1.72%. This shows that there is still variance even between the two systems in operation at Willenhall, although generally, they are well-matched.

Of the two SOC system measurements, the model matches most closely with the DSPKF algorithm with an average RMSE of 0.94% across the 6 verification exercises. However, the RMSE when compared to the BMS algorithm is only slightly larger at 0.96%. Under the BMS comparison, the lowest RMSE is 0.27% in Verification 1, whilst the highest is 1.62% under Verification 6. Under the DSPKF comparison, the lowest RMSE is 0.25% in Verification 5 compared to its highest at 1.74% in Verification 4. These results suggest that the model is performing accurately when asked to operate according to step change load profiles.
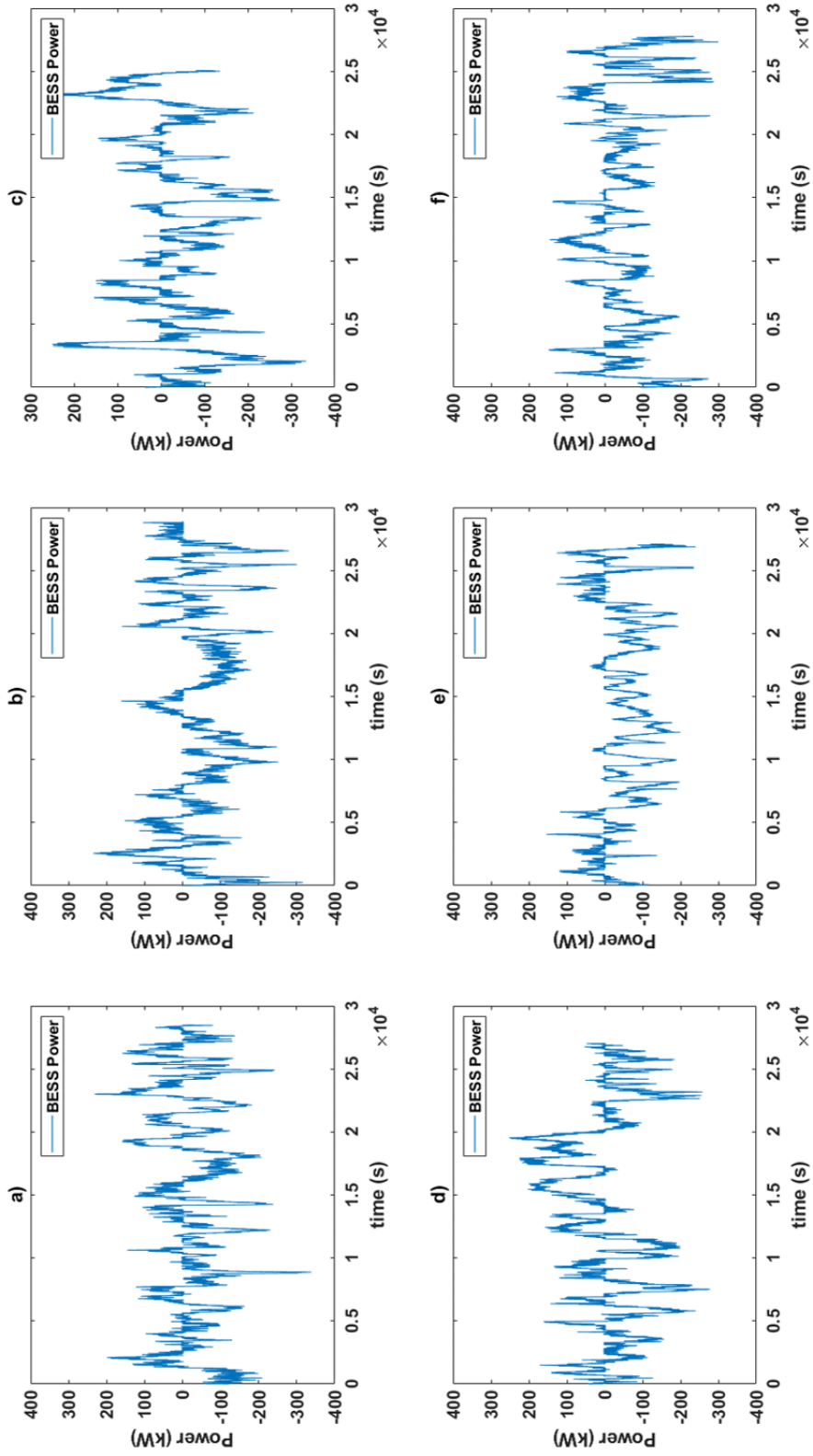
Figure 3.25: Frequency profiles used to verify the performance of the MATLAB/Simulink model a) Verification 7 (03/09/2021) b) Verification 8 (21/09/2021) c) Verification 9 (05/09/21) d) Verification 10 (26/09/21) e) Verification 11 (15/09/21) f) Verification 12 (13/09/22)

Table 3.7: RMSE values when comparing the SOC at each point between Willenhall BMS, Willenhall DSPKF and the MATLAB/Simulink model for the Step-Change power profiles

| Comparison | V1 | V2 | V3 | V4 | V5 | V6 | Average |
|---|---|---|---|---|---|---|---|
| BMS/DSPKF | 0.78% | 1.53% | 1.66% | 1.29% | 1.72% | 1.50% | 1.41% |
| BMS/Model | 0.27% | 1.06% | 1.00% | 1.53% | 0.28% | 1.62% | 0.96% |
| DSPKF/Model | 0.72% | 0.81% | 0.42% | 1.74% | 0.25% | 1.71% | 0.94% |

### 3.8.3   Frequency Response Verification

To validate the model's ability to interpret frequency signals and convert this into an accurate service and resulting SOC profile, a set of 6 varying profiles as seen in Figure 3.25 were simulated with the resulting SOC curves compared with each Willenhall ESS SOC monitoring system.

Once again each individual comparison of SOC profiles for the frequency response verification is contained within the appendix (Figure A14 to Figure A25) showing the data from which the RMSE values were derived.

The RMSE values for each verification exercise when performing frequency response load profiles are shown in Table 3.8. The first row shows the RMSE values when comparing the two SOC monitoring systems at Willenhall with each other, where they achieve an RMSE of 1.26% on average across the 6 frequency response load profile verification sets. They match most closely with each other under Verification 12 and differ the most under Verification 10.

For this set of verifications, the model again most closely matches the DSPKF algorithm with an average RMSE of 1.16% compared to the average RMSE of 1.61% when compared to the BMS. Compared with the DSPKF algorithm the most accurate verification set is Verification 7 and the least accurate verification set is Verification 8. Compared with the BMS the most accurate verification set is Verification 7 whilst the least accurate is Verification 11. The results again suggest that the model is performing accurately when compared to the real-life installation performing the same DFR service. The RMSE is slightly higher for the frequency verification when compared to the step-change profiles, which is likely due to the more complex response expected from the model although it still maintains a low overall RMSE.

### 3.8.4   Discussion

The SOC calculation section of the developed BESS model has been verified against the Willenhall ESS installation resulting in ranges of 0.27%-2.20% RMSE when performing Step-Change load profiles and ranges of 0.25%-2.78% when performing

Table 3.8: RMSE values when comparing the SOC at each point between Willenhall BMS, Willenhall DSPKF and the MATLAB/Simulink model for the frequency response profiles

| Comparison | V7 | V8 | V9 | V10 | V11 | V12 | Average |
|---|---|---|---|---|---|---|---|
| BMS/DSPKF | 1.20% | 1.39% | 1.09% | 1.99% | 1.08% | 0.79% | 1.26% |
| BMS/Model | 0.56% | 2.78% | 1.85% | 1.24% | 1.97% | 1.28% | 1.61% |
| DSPKF/Model | 0.25% | 1.91% | 1.81% | 0.71% | 1.54% | 0.74% | 1.16% |

frequency response services. The average RMSE across all 12 verification exercises was 1.29% when compared to Willenhall BMS and 1.05% when compared to the Willenhall DSPKF algorithm. The levels of RMSE determined by this analysis suggest that the model is performing accurately when compared to the real-life installation. The model matches most closely with the DSPKF algorithm which has been shown previously to be the more accurate measurement of the Willenhall ESS SOC [202].

## 3.9 Analytical Framework Overview

In this section, a detailed overview of the different analytical options available within the modelling framework that has been developed is provided, with commentary on how this can be used to inform ESS design and operation. In the literature review presented earlier in this chapter, existing methods for cycle counting were discussed, and within this section, the novel cycle counting method is utilised and the effect this has on the model's ability to provide detailed operational characteristics is presented.

Within this section, the example of a HESS consisting of a 500kWh/1C BESS and a 50kWh/5C FESS providing a DFR service of 500kW is utilised. Further analysis of the effect that changing control systems has on the way that the BESS and FESS operate is contained within Chapter 5. The information contained in this chapter concentrates purely on the mechanics of how the model works, and what options for data processing are available as a result of the implementation of the cycle counting method.

The method presented has been developed to provide greater granularity for the number of cycles experienced during operation to enable a wider range of analysis on how metrics such as C-Rate and SOC affect the degradation of a BESS. Where previously in [149] the cycle counting was conducted so that the cycle number incremented in steps of 0.5 according to a charging and discharging accumulator, this method concentrates solely on total energy throughput for a given second and converts this into an equivalent partial cycle occurring over a 1s period as shown in
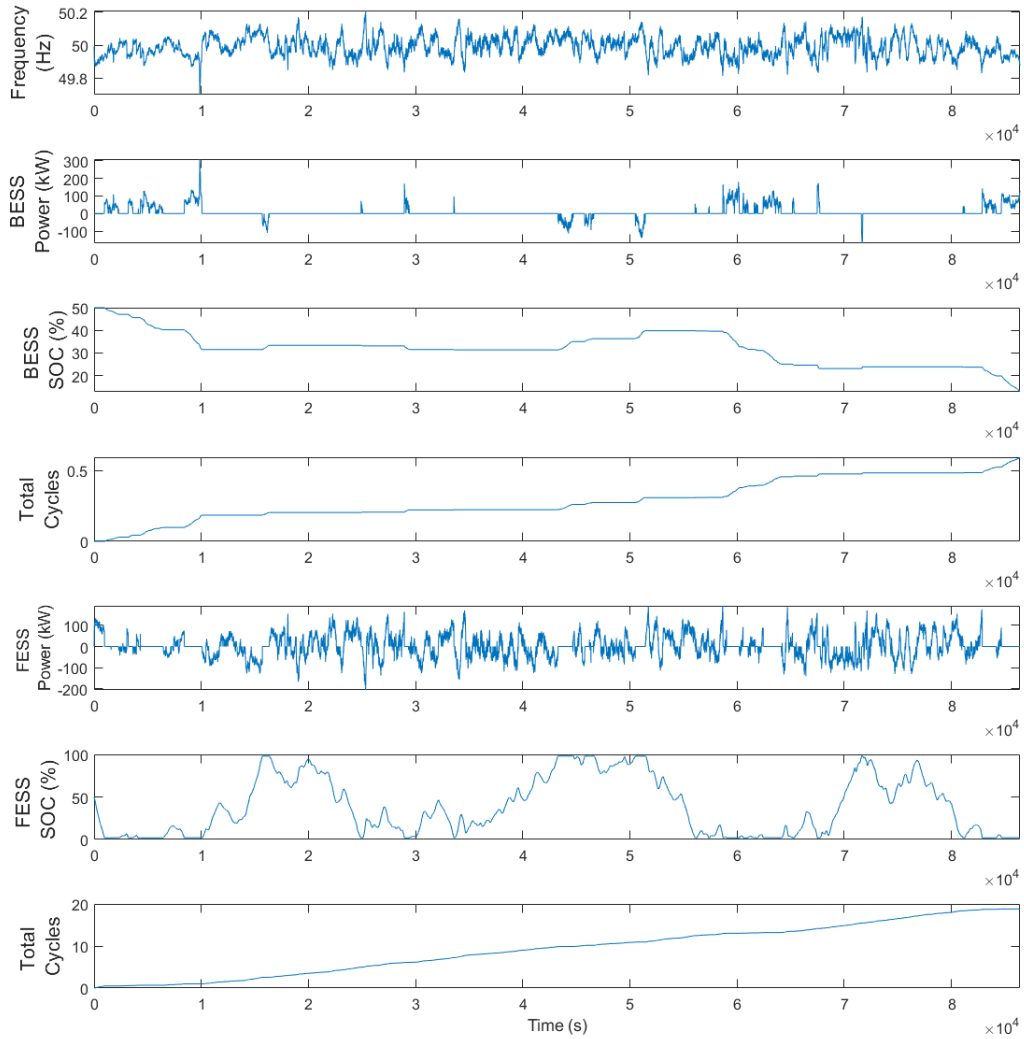
Figure 3.26: Cycle counting algorithm output example

Equation 3.7, where the change in SOC is determined over each 1 second period as a proportion of 100% SOC.

$$EPC = \frac{\frac{\mathrm{dSOC}}{\mathrm{d}t}}{100} \tag{3.7}$$

$$Cycles = \int_0^t EPC \tag{3.8}$$

The output of this, an equivalent cycle for any given second of operation, can then be either continuously integrated to give cycles over the length of the simulation as in Equation 3.8, or used on a second-by-second basis for further analysis. This ability to extract cycles on such a granular level represents a complex and effective

91
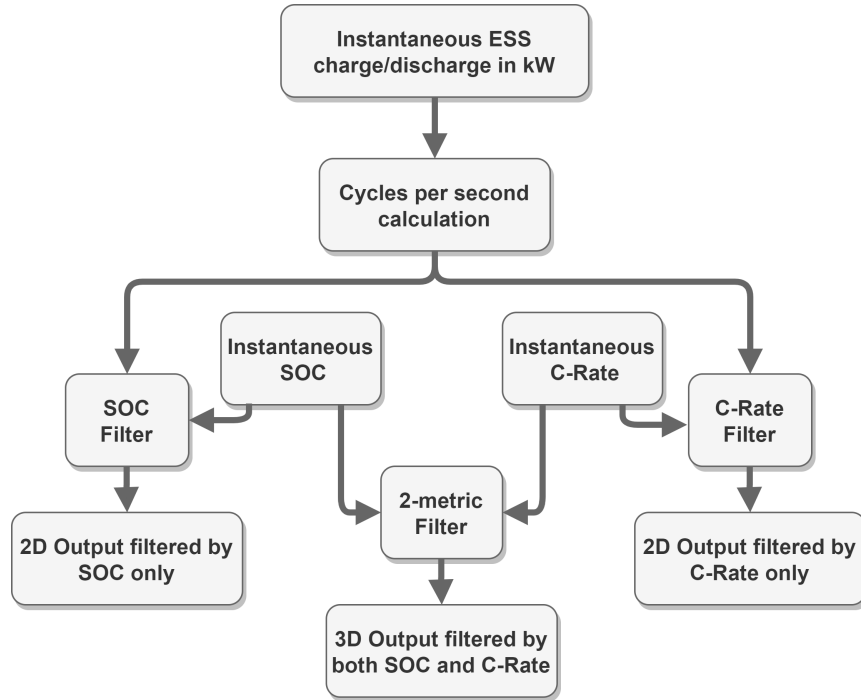
Figure 3.27: Flow diagram showing the filtered analysis approach for 5 equal bins of SOC and C-Rate

tool with which to analyse how the ESS operates for a given application. An example of how this cycle counting happens within the simulation is shown in Figure 3.26 demonstrating the operation of the hybrid FESS/BESS system providing DFR. The total cycles shown represent the cumulative equivalent partial cycle across the simulation duration. It can be seen that with the algorithm in operation for just over one day using frequency data from January 2019, the cycles are counting upward for every individual charge/discharge event that each ESS experiences. From this example, the BESS is shown to only experience 0.6 equivalent cycles whilst the FESS experiences 19.1 equivalent cycles.

The flow diagram in Figure 3.27 illustrates how the output of this equation can then be filtered further to provide a more detailed overview of the operation of the ESS. The example shown uses dividers shown in Table 3.9 but this can be set with higher or lower levels of granularity as required. Note that in Table 3.9 the columns are separate from each other and there is no link between values on the same row. The equivalent partial cycles are assigned and summed for each individual range (also referred to as a 'bin') providing a view of how frequently the ESS is operating within the specified ranges. These bin sizes can be modified to provide more or less granularity depending on the level of assessment required. Each equivalent cycle can be determined to have occurred at a given SOC and a given C-Rate. In this context, this is the instantaneous C-Rate as represented in Equation 3.9 where $P_t$ is the power output by the ESS at time $t$ and $E_{ESS}$ is the rated energy capacity of

Table 3.9: Dividers used in ESS operation analysis example

| FESS C-Rate | BESS C-Rate | FESS SOC | BESS SOC |
| --- | --- | --- | --- |
| 0-1 | 0-0.2 | 0-20% | 0-20% |
| 1-2 | 0.2-0.4 | 20-40% | 20-40% |
| 2-3 | 0.4-0.6 | 40-60% | 40-60% |
| 3-4 | 0.6-0.8 | 60-80% | 60-80% |
| 4-5 | 0.8-1 | 80-100% | 80-100% |
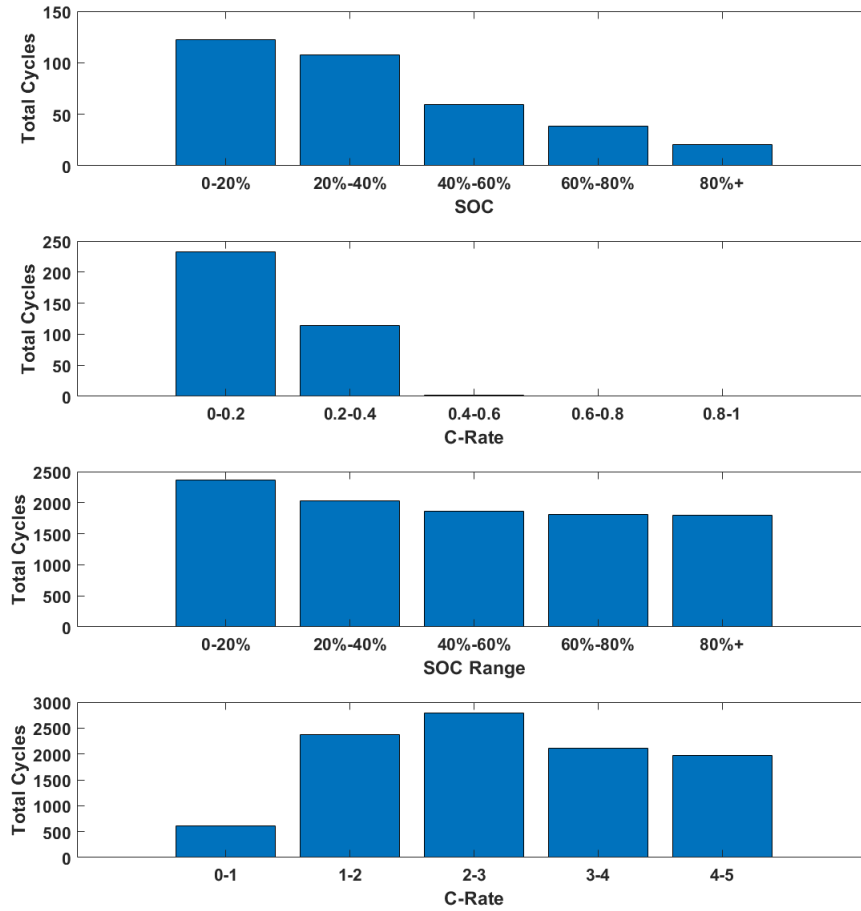


Figure 3.28: Separately filtered number of cycles at varying SOC and C-Rate ranges for a FESS and BESS

the ESS. This illustrates that whilst a system will be rated at a given C-Rate, it can provide power at any C-Rate up to and including this value, i.e. a 1C BESS may provide power in the region of 0-1C.

$$C_{inst} = \frac{P_t}{E_{ESS}} \tag{3.9}$$

The outputs shown in Figure 3.28 and Figure 3.29 illustrate the type of op-
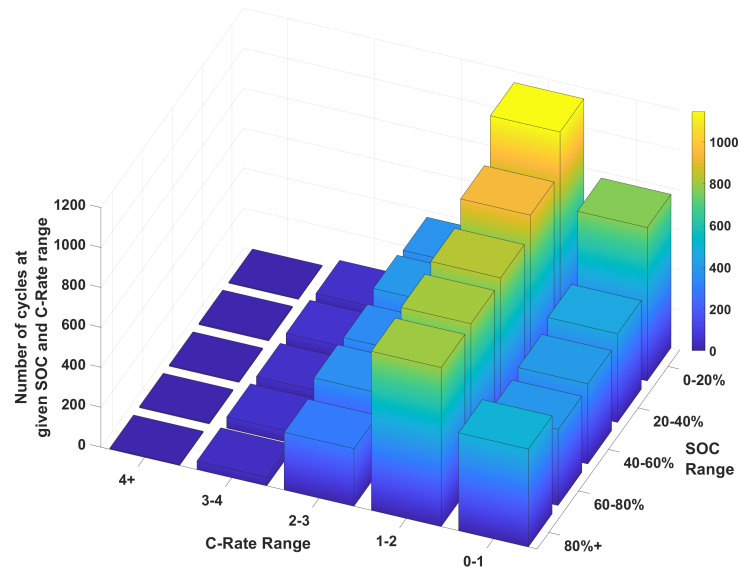
Figure 3.29: Combination filtered number of cycles at varying SOC and C-Rate ranges for a FESS

erational visualisations that are available when utilising this model. Figure 3.28 illustrates the basic level of filtering, where each microcycle is allocated separately to an SOC range and a C-Rate range. This provides a good overview of how an ESS is operating based purely upon one metric at a time. However, Figure 3.29 shows a much more detailed representation of ESS operation, where the SOC and C-Rate for each microcycle are allocated to a combined matrix, giving a two-variable representation of the ESS operation. Many large scale BESSs come with specific warranties that specify operational restrictions to avoid certain regions of C-Rate and SOC, and this analytical framework can be easily used to determine whether these operational restrictions are feasible for a given application and keep the operation of the ESS within warranty requirements.

Additionally, it is commonly found in the literature that higher C-Rates result in faster degradation, and this method of visualisation can be used to determine the C-Rate that an ESS is most commonly operating at and with this information develop control mechanisms or size hybrid equipment in order to control the operation of the ESS in desired ranges. This novel modelling and visualisation framework provides a foundation for tailoring control schemes and configurations to keep the ESS operating in certain regions of SOC or C-Rate, something that is discussed further within Chapter 5 where these visualisations are used to inform the development of novel HESS control schemes.

Table 3.10: Scenarios used for cycling degradation experiment

|      | Settings |
|------|----------|
| CS-1 | BESS only |
| CS-2 | FESS acting as a filter for response requests before BESS operates |
| CS-3 | FESS operating when frequency is outside of the 49.9-50.1Hz range, BESS inside range |
| CS-5 | 50:50 split of any given request between BESS and FESS |
| CS-6 | 30-second average power provided by FESS, BESS provides the difference between average and instantaneous |
| CS-7 | 30-second average power provided by BESS, FESS provides the difference between average and instantaneous |

### 3.9.1   Degradation Modelling Verification

This section details the verification undertaken to demonstrate that the degradation mechanism used within the MATLAB/Simulink model presented in this chapter is a good approximation of real-world degradation rates. This experiment is currently ongoing, and the intermediate results are presented in this section. Currently, the cells have simulated 189 days of frequency response service provision.

For this analysis, multiple different control strategies were utilised to produce load profiles that have then been applied to individual DMEGC (Model:INR18650-29E) lithium-ion cells. The scenarios studied are detailed in Table 3.10, all using a 0.5MW 1C BESS with a 0.5MW 8C FESS delivering a 0.5MW DFR service. The control strategies are explained in depth within Chapter 6. This section does not seek to provide commentary on the effects of changing control strategies and instead uses these different strategies to expose the cells to different levels of degradation.

Table 3.11 shows the equivalent number of cycles experienced under each control strategy at each iteration number of the experiment. The cycles contained in the table are the cumulative sum of the equivalent partial cycles from Equation 3.7.

Shown in Figure 3.30a are the results of the cycling experiment as of the completion of the 9th iteration of the test profile. A capacity check was performed at the end of each iteration. When these results are compared to those contained in Figure 3.30b it is apparent that the degradation is following a similar trajectory to that predicted by the model.

In the experimental results, there is a degree of uncertainty over the first 4 iterations due to the cell being exposed to cycling for the first time and beginning to normalise, whereas in the simulated results this is not accounted for and hence stays along a more linear path. It should also be noted that these test profiles represent the same load profile being repeatedly cycled, hence the result in general will be more linear than what could be expected from a real-world response service profile.

Table 3.11: Equivalent cycles at each iteration number for each control scheme

| | Iteration 1 | Iteration 2 | Iteration 3 | Iteration 4 | Iteration 5 | Iteration 6 | Iteration 7 | Iteration 8 | Iteration 9 |
|---|---|---|---|---|---|---|---|---|---|
| CS1 | 105.5 | 211.0 | 316.5 | 422.0 | 527.5 | 633.0 | 738.6 | 844.1 | 949.6 |
| CS2 | 79.0 | 158.0 | 237.0 | 315.9 | 394.9 | 473.9 | 552.9 | 631.9 | 710.9 |
| CS3 | 30.4 | 60.9 | 91.3 | 121.7 | 152.2 | 182.6 | 213.0 | 243.5 | 273.9 |
| CS5 | 37.1 | 74.2 | 111.3 | 148.4 | 185.5 | 222.6 | 259.7 | 296.8 | 333.9 |
| CS6 | 89.1 | 178.3 | 267.4 | 356.5 | 445.7 | 534.8 | 623.9 | 713.0 | 802.2 |
| CS7 | 76.4 | 152.8 | 229.1 | 305.5 | 381.9 | 458.3 | 534.6 | 611.0 | 687.4 |
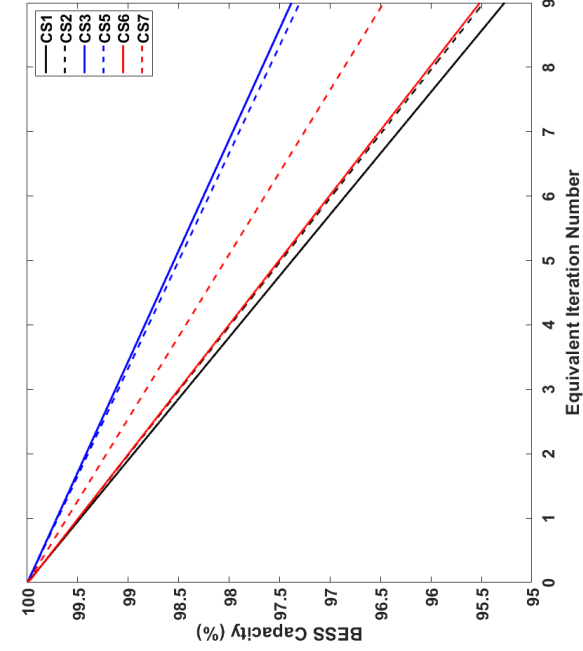
(a) Experimental Results
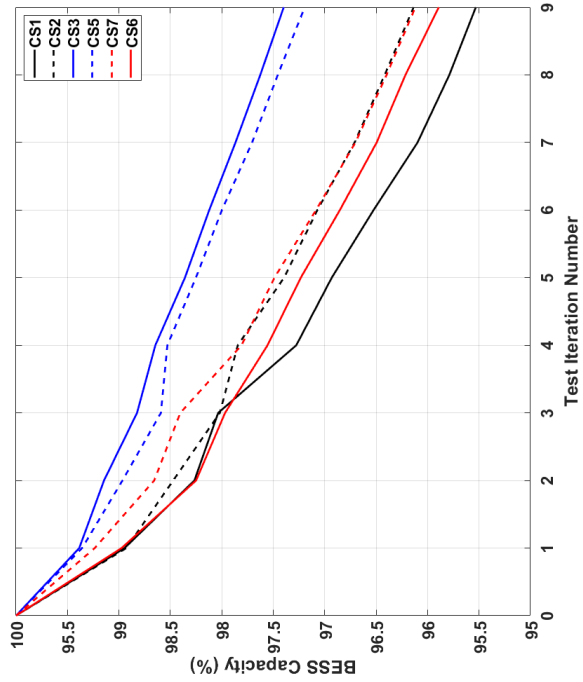
(b) Simulated Results

Figure 3.30: Degradation experiment showing the capacity of the cells after each iteration as a % of its rated capacity for a) Intermediate results of cycling experiment across different control strategies b) Simulated degradation results for identical inputs to the cycling experiment

Table 3.12: Predicted Cycles for Simulated Degradation to reach 80%

| Control | Iteration at 80% | Cycles Per Iteration | Total Cycles |
|---|---|---|---|
| CS-1 | 41 | 105.5 | 4325 |
| CS-2 | 47 | 79 | 3713 |
| CS-3 | 70 | 30.4 | 2128 |
| CS-5 | 65 | 37.1 | 2411 |
| CS-6 | 44 | 89.1 | 3920 |
| CS-7 | 47 | 76.4 | 3590 |

Table 3.13 shows the results as of the 9th iteration for each control strategy tested, along with the simulated results and the difference between the two methods. In terms of the final degradation value after 9 iterations, the largest deviation is found in CS-2 which finishes at a degradation level 0.66% lower than the simulated result. However, to assess the accuracy across all iterations, an RMSE analysis was carried out comparing each individual simulated iteration degradation level with the corresponding experimental level. The result of this is also shown in Table 3.13.

Another exercise was conducted to extrapolate the results of the simulated exercise to determine how many cycles each control strategy would complete before reaching 80% capacity, which is shown in Table 3.12. These results illustrate how the differences between the control strategies can allow the cells to operate for a longer duration of time before reaching end of life, with the maximum number of iterations achieved as 70 for CS-3. The manufacturer data sheet does not provide information on cycles to reach 80% of the original capacity, however it does show that after 1500 cycles the cells will have reached 87% of their original capacity [207]. This falls in line with the predicted values in Table 3.12.

From the results so far, an overall average RMSE of 0.43% has been produced, suggesting a strong correlation between the degradation being simulated by the model and that being experienced when real-world cells are subjected to the same cycling patterns. When looking at individual values of RMSE for each control strategy utilised, the least accurate is CS-6 which has an RMSE of 0.60%, showing that even at the lowest achieved correlation between simulated and experimental results there is still a high degree of accuracy achieved.

**Conclusions**

Intermediate results have been presented to illustrate the process being undertaken to verify the degradation modelling detailed in this thesis. These results suggest that the model is accurately representing the degradation rate of Li-ion BESSs and gives more certainty to the reliability of the results obtained. Throughout the work presented here, both the calculated degradation rate and the total number of cycles

Table 3.13: Overall results from intermediate degradation verification

|  | Experimental Result | Simulation Result | Difference after 9 iterations | Overall RMSE |
|---|---|---|---|---|
| CS-1 | 4.47% | 4.72% | -0.25% | 0.43% |
| CS-2 | 3.86% | 4.52% | -0.66% | 0.41% |
| CS-3 | 2.60% | 2.62% | -0.02% | 0.20% |
| CS-5 | 2.81% | 2.70% | 0.11% | 0.30% |
| CS-6 | 4.11% | 4.48% | -0.37% | 0.60% |
| CS-7 | 3.88% | 3.54% | 0.34% | 0.50% |

have been used as indicators of ESS lifetime to provide increased reliability to the results and to enable any outliers to be identified.

## 3.10 Conclusions

A detailed overview of the options available when modelling an ESS has been presented, along with commentary on related areas such as degradation modelling, techno-economic analysis and cycle counting. All of this information has been combined in order to develop a new FESS and BESS model for use in the rapid simulation of ESS applications.

The modelling and simulation framework presented in this chapter represents a novel blend of simplistic and modular modelling tools with complex sub-systems to add outputs to the overall system. It has been shown that when compared to a real-life installation, the BESS model can accurately approximate the SOC profile of the Willenhall ESS installation when responding to identical inputs, a significant milestone that illustrates the effectiveness of the overall philosophy behind the modelling framework.

The fast computational speeds of the developed models have been presented, showing that under 4 different applications, the maximum simulation time experienced was 9.9 minutes for a year of simulation. This chapter has shown that the new model can balance speed and technical accuracy to great effect, allowing a wide range of applications to be assessed in greater depth than traditional longer-duration simulations would allow.

Additionally, the novel microcycle identification and analysis system has been introduced, offering a range of different options for visualizing the intricacies of ESS operations and providing the foundation for further works to use these tools to refine operational parameters such as control schemes or ESS configurations in order to ensure the ESS remains within optimal regions of operation.

Finally, preliminary results from an experimental cycling exercise were presented

and discussed. After 9 iterations of the experiment, it has been shown that the model is a good approximation for the level of degradation experienced across a range of different operational modes with an overall RMSE of 0.43%.

# Chapter 4

# Export Limitation: Unlocking the Potential of Distributed Generation Using Energy Storage

## 4.1 Introduction

As previously discussed within Chapter 1, the increasing deployment of DG is causing significant hurdles for both DG sites and network owners and operators alike. With parts of the network increasingly reliant on ELS agreements to restrict the level of connection for DG owners, this results in the full potential of many new renewable generation sites not being reached. In this chapter, a literature review of utilising ESSs for wind generation curtailment is introduced. With minimal previous work being conducted in the field of ELS mitigation, parallels are drawn between the studies presented for grid-level curtailment and the locally limited generation sites showcased in this chapter. A novel scheme for reducing or removing the impact of ELSs is then introduced for the first time, firstly with a generalised higher level study followed by a real-world case study that includes a full techno-economic assessment comparing the effectiveness of BESS and FESS in delivering this application.

The main objective of this chapter is to explore the possibilities of ESSs being deployed effectively to alleviate export limitation issues and enhance the techno-economic performance of DG sites. Specifically, the work seeks to verify the suitability of FESSs and BESSs to perform this service both on a theoretical and real-world basis. It also aims to provide an economic framework to enable the research and development of FESSs that can be realistically deployed in this scenario.

The wind speed data utilised in this chapter was provided by the industrial sponsor for this project. As such, it reflects a specific period of time (January 2018 to December 2018). If alternative data sets were utilised then it is expected that

only minor changes to the results would occur, as the wind speed in the UK remains consistent year on year [208].

The key difference between the research presented in this chapter and the previous extensive body of work that has looked into wind curtailment is that ELSs are completely local with no involvement in forecasting or receiving payments for having their generation forcibly reduced. There are two distinct sub-categories of reduction in export of a wind farm;

- Curtailment - This is enforced upon a wind generation site due to grid stability issues such as excess generation being present on the system at a national level. It is compensated in the form of curtailment payments proportionate to the size of the generation site.

- Limitation - This is enforced upon a wind generation site where there is insufficient local infrastructure to support the full capability of the site. There are no compensation payments for this type of reduction.

In essence, export limitation represents a permanent enforced decrease in the capacity factor of the site. This work represents an important and novel step in increasing the understanding of an emerging issue and providing a viable energy storage-based solution for mitigating their impact and raising the capacity factor back to the intended levels.

### 4.1.1 Export Limitation Schemes

Export limitation in the context of U.K. Distribution Network Operators can best be explained with reference to Figure 4.1, which shows how an ELS works in practice, limiting the export of the site in real-time and preventing it from breaching the agreed limit. In this example, a site is limited to an export level of 0.2MW despite being capable of generating power in excess of this (0.3MW), thus resulting in a significant reduction in energy exported (14.2% less energy over the course of the 4000s of operation in this example). When considering different levels of limitation, the more limited the system is, the more potential for increasing the overall capacity factor there is. This is due to more excess energy being available for charging an energy storage device to then subsequently be discharged when the output drops back below the export level.

Capacity factor is a common metric for measuring the overall output of a generation site as a proportion of the theoretical maximum a continuous peak-rated output of the site would yield over the course of a year and is calculated as given in Equation 4.1 where $E_{\text{actual}}$ is the total amount of energy generated by the site in MWh and $P_{\text{rated}}$ is the rated power of the site in MW. Capacity factor has been

used extensively as a metric for improvements to generation sites throughout the literature [209] [210] [211].

$$Capacity \ Factor = \frac{\int_T^0 P_{out}dt}{P_{rated}T} = \frac{E_{actual}}{P_{Rated} \times 24 \times 365} \tag{4.1}$$

Governed by Engineering Recommendation G100 [18], the two main characteristics of ELSs are that the exported active power must be reduced to less than or equal to the maximum export capacity within 5 seconds and that the whole system must be fail-safe so that should any part of the ELS management system fail, the export will be ceased completely. It therefore acts as a constant limiter on the export of a given site, causing particular issues when a Distribution Network Operator needs to impose stricter requirements at a generation site due to upstream capacity, potentially leading to significantly oversized equipment, unfulfilled generation potential, and loss of potential revenue and lower return on investment. The main technical specifications of G100 are summarised below;

- The ELS must reduce the exported active power to less than or equal to the agreed export limit within 5 seconds

- The system must be fail-safe, both in terms of component failure and inadvertent breaches of the export limit. This means that if any component of the export limitation system fails then the exported active power will be reduced within 5 seconds.

## 4.2   ESSs for Wind Curtailment Avoidance

In terms of local, site-specific restriction of DG export levels, there is very little previous work conducted in the field. This is likely due to the fact it is still an emerging problem which will become increasingly relevant as local Distribution Network Operator networks reach their capacities. Of the literature available, a focus is found on strategies for investing in both DG and Distribution Network Operator network improvements such as found in [212], which presents a modelling scenario where curtailment rules, Distribution Network Operator incentives and local renewable generators are balanced according to the game theory principle. Whilst this is an interesting study and raises some good points about the balance between various stakeholders, there is no reference to ESSs which could be proposed as part of the solution. A similar theme is found in [213] where energy trading between generation sites is proposed as a solution to reducing constraints on local distribution networks, but once again there is no suggestion of utilising energy storage to assist in reducing such constraints.
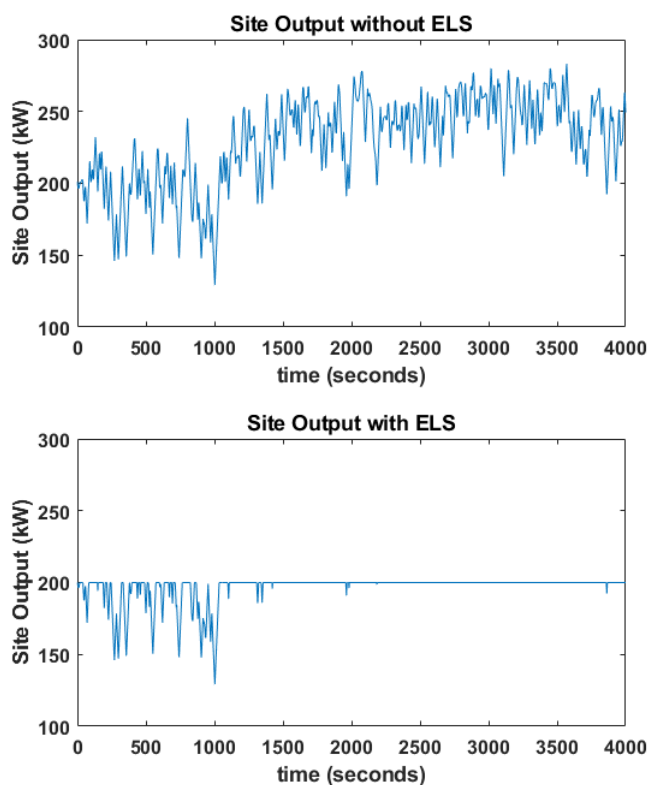
Figure 4.1: Example of ELS operation

The main previous work in locally limited DG is discussed in [214] which comments upon the fact that there has been very little exploration of the issues faced by DG sites. It proposes smarter connection schemes such as the 'Flexible Plug and Play' scheme trialled by UK Power Networks from 2012 to 2014, which concentrated purely on connection-based innovation with no focus on deploying energy storage to assist in relieving curtailment issues beyond a limited simulation trial [215]. This project was funded with almost £10m back in 2011, suggesting that there is significant commercial interest in managing these issues. Clearly, there is a significant opportunity for the investigation of novel use of ESSs to alleviate local distribution curtailment issues.

A study in [216] looks at transmission-limited wind generation sites in the United States, with an important aspect representing the TCC analysis that suggested a BESS could be economically beneficial up to a ceiling of $780/kW. Whilst the focus of this study is still on a much larger scale than those sites subjected to ELSs in the U.K., it illustrates the importance of performing sensitivity analysis on the ESS costs under differing scenarios. A similar study is undertaken within [217] which investigates the impact of the income provided by the BESS at different costs on the NPV of the system. The key takeaway from these studies is that sensitivity analysis is a key aspect of any wind generation-related economic study and should be utilised effectively wherever possible.

Grid-scale wind curtailment in the U.K. is increasing, with more than £500m spent on paying wind farms to stop generating in 2021, a significant increase from over £200m in 2020 [218]. It is important to consider some of the main pieces of literature available as parallels can be drawn between the methods used at the grid level and potential solutions that can be used in local-level studies.

In [173], three different methods of dealing with wind curtailment are proposed consisting of direct curtailment, network investment, and electrolysis (essentially representing energy storage in this scenario). Taking a whole system approach, it analyses the economic benefit of each technique based upon the resulting NPV. The study is quite high level and broad in its execution but raises the interesting point of comparing changes in NPV according to different scenarios.

Another important area to note is the work presented by [219], which focuses solely on the control and operation of a wind turbine to directly reduce curtailment by variation in torque control in tandem with pitch angle modifications to good effect. Something that has not been discussed, however, is utilising this ability to vary the output of a turbine in order to maximise the effect of an ESS being introduced, combining the two methods to produce a better techno-economic solution.

In many studies, the aim of introducing an ESS to a wind generation site is to smooth the power output of the site, an objective that aligns well with restricting the output of a site to fall in line with export limitation. Three key studies in this area are [74], [98] and [220]. Firstly, in [74], a BESS integrated with a wind generation site is minimized in order to reduce costs and increase economic performance, whilst maintaining the correct level of technical performance. It also looks into the optimal topology of BESS installation at a large wind farm, concluding that a BESS that is distributed throughout the site rather than in one location is more effective. It claims that a BESS is a suitable candidate for wind smoothing applications such as the export limitation mitigation discussed in this chapter. However, it neglects to discuss the effect that operating this service has on the lifetime of the BESS, which represents significant scope for further work in this field, something this thesis will build upon.

Within [220], a FESS is utilised for wind power smoothing. This study claims a significant benefit to utilising FESSs for wind smoothing applications, although the smoothing achieved is minimal due to the objective being more closely related to reducing the power spectrum variance when exporting to the grid. Despite this though, it suggests that a FESS can effectively provide this type of support and thus warrants further investigation in this chapter.

When considering other potential ESS technologies for wind power smoothing, [221] discusses the potential for supercapacitors to provide a smoothing service. Whilst it claims good results when utilising supercapacitors, the investigation is

somewhat limited in its scope and focuses more on the transient characteristics that can be better supported with the shorter storage duration times of supercapacitors. The study concludes that longer-term storage would be required to effectively provide a preset power output, as the work in this thesis sets out to do, suggesting they would be unsuitable for consideration.

## 4.3 Export Limitation Mitigation using a FESS

In this section, a detailed assessment of using FESSs to alleviate export limitations caused by local distribution restraints is presented for the first time, with the objective of unlocking further techno-economic potential that is currently unable to be realised when subjected to an ELS.

Export limitation on a local scale is only going to become more of an issue as the demand for more DG installation increases. The UK government is currently looking to loosen restrictions on the deployment of onshore wind [222] [223] which will lead to increasing levels of deployment of wind generation. This work presents a timely investigation into allowing new installations to consider additional methods to extract the maximum amount of value from their existing or proposed generation site. It also allows previously discounted sites to be considered for the deployment of new onshore wind generation sites.

The financial benefits of utilising flywheels in this way are also presented for the first time. The work contained in this section can cause a significant impact on the viability of generation sites across Great Britain. The key technical metrics that will be assessed within this study are as follows;

- Capacity factor increase - For this study, the capacity factor for the base site with no ESS has been calculated followed by the CF for the site with the ESS introduced. The capacity factor increase is then determined by calculating the difference between the two values.

- Limited time proportion - The limited time proportion represents the amount of time that the wind generation site is limited under the terms of the ELS as a proportion of the total operational time, as shown in Equation 4.2 where $t_{\text{limited}}$ is the duration of time that the export is limited and $t_{\text{operational}}$ is the total time the system is operational for. It can be used as a metric to determine how the introduction of the FESS is affecting the duration of time that the site is operating without any restrictions.

- FESS Cycles - The total amount of cycles experienced by the FESS, an important metric to monitor the lifetime of the system which has initially been

Wind Generation
(4 X 250kW turbines)

Local distribution
network operator
substation

Export Limitation
Panel
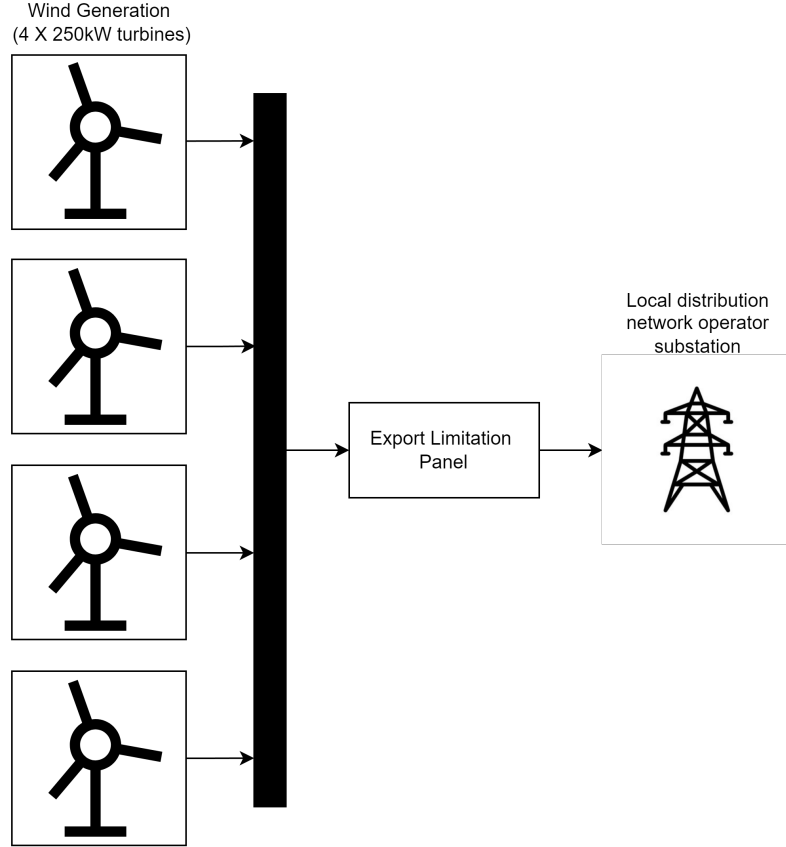
Figure 4.2: Export limited site diagram with no FESS

set as a limit of 100,000 cycles before a replacement for all the work contained within this thesis unless otherwise stated.

$$LTP(\%) = (1 - \frac{t_{limited}}{t_{operational}}) \times 100 \tag{4.2}$$

## 4.3.1 Study Overview

In this study, a 1MW wind power site is considered using real-world wind data to simulate a year of generation in a MATLAB/Simulink model as previously discussed in Chapter 3. The wind generation site has been modelled based on 4 co-located turbines using the publicly available power curves of the WindTechnik WTN250 [224]. Basic site diagrams showing the system without a FESS present and with a FESS installed are shown in Figure 4.2 and Figure 4.3 respectively.

A sensitivity analysis has been conducted on the level of export limitation the site is subjected to. This consisted of limiting the output by 5%, 10% and 20% of the total site output. For instance, a 1MW site subjected to a 20% export limitation would be allowed to export a maximum instantaneous power of 0.8MW. The technical performance of the system is then assessed when varying the energy-to-power ratio of the FESS, with three different power capacities considered (0.05MW,

Wind Generation
(4 X 250kW turbines)

FESS

Local distribution
network operator
substation

Export Limitation
Panel
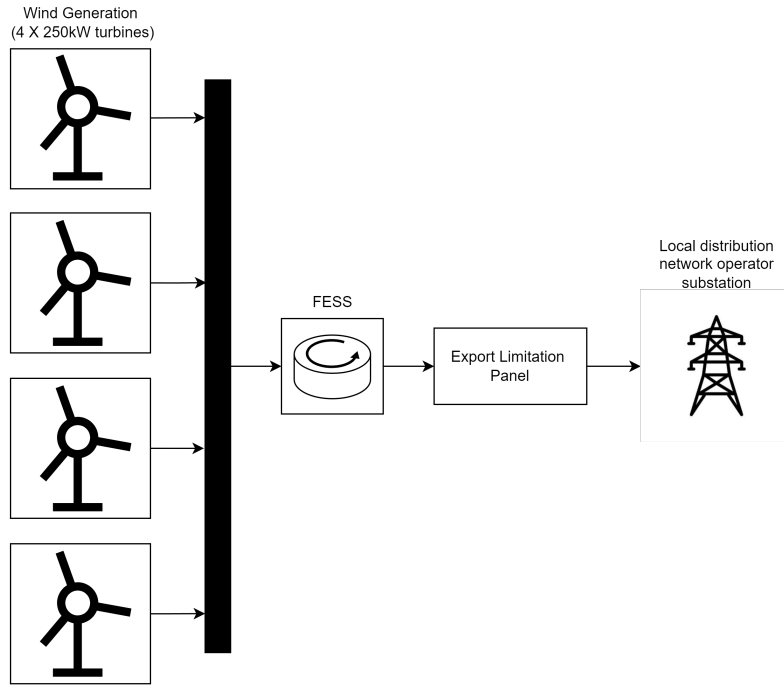
Figure 4.3: Export limited site diagram with FESS installed

0.1MW and 0.2MW). Throughout this chapter, FESSs that are specified with different power or energy ratings are referred to as different FESS configurations.

The energy-to-power ratio of an ESS is referred to as C-Rate within this thesis as previously discussed in Chapter 2, in line with the definition commonly used for BESSs. This value is varied between maximum C-Rates of 1C and 20C to represent changing the energy capacity of the system, illustrated in Table 4.1. Subsequently, an economic analysis is performed to evaluate the viability of introducing the FESS in terms of real-world benefit. This is an important metric to consider as it can provide guidance about the specifications that they will be required to design FESSs to in order to participate in different markets, and encourage further research to achieve the required specifications.

Subsequently, an economic analysis is performed to evaluate the viability of introducing the FESS in terms of real-world benefit. The income generated by the site has been set as £0.06/kW in line with available data from both existing wind generation sites consulted as part of this study, and publicly available information [225]. With the current energy picture being uncertain, this value has been chosen as a conservative option in order to produce a more robust set of results. The wind data was provided by the industrial sponsor for this project in collaboration with several existing wind generation sites where ELS is an issue.

Table 4.1: Different FESS configurations considered in the ELS Wind Generation study

| C-Rate | Energy capacity in kWh of the FESS at specified power ratings | | |
| --- | --- | --- | --- |
| | 0.05MW FESS | 0.1MW FESS | 0.2MW FESS |
| 1 | 50.00 | 100.00 | 200.00 |
| 2 | 25.00 | 50.00 | 100.00 |
| 3 | 16.67 | 33.33 | 66.67 |
| 4 | 12.50 | 25.00 | 50.00 |
| 5 | 10.00 | 20.00 | 40.00 |
| 6 | 8.33 | 16.67 | 33.33 |
| 7 | 7.14 | 14.29 | 28.57 |
| 8 | 6.25 | 12.50 | 25.00 |
| 9 | 5.56 | 11.11 | 22.22 |
| 10 | 5.00 | 10.00 | 20.00 |
| 11 | 4.55 | 9.09 | 18.18 |
| 12 | 4.17 | 8.33 | 16.67 |
| 13 | 3.85 | 7.69 | 15.38 |
| 14 | 3.57 | 7.14 | 14.29 |
| 15 | 3.33 | 6.67 | 13.33 |
| 16 | 3.13 | 6.25 | 12.50 |
| 17 | 2.94 | 5.88 | 11.76 |
| 18 | 2.78 | 5.56 | 11.11 |
| 19 | 2.63 | 5.26 | 10.53 |
| 20 | 2.50 | 5.00 | 10.00 |
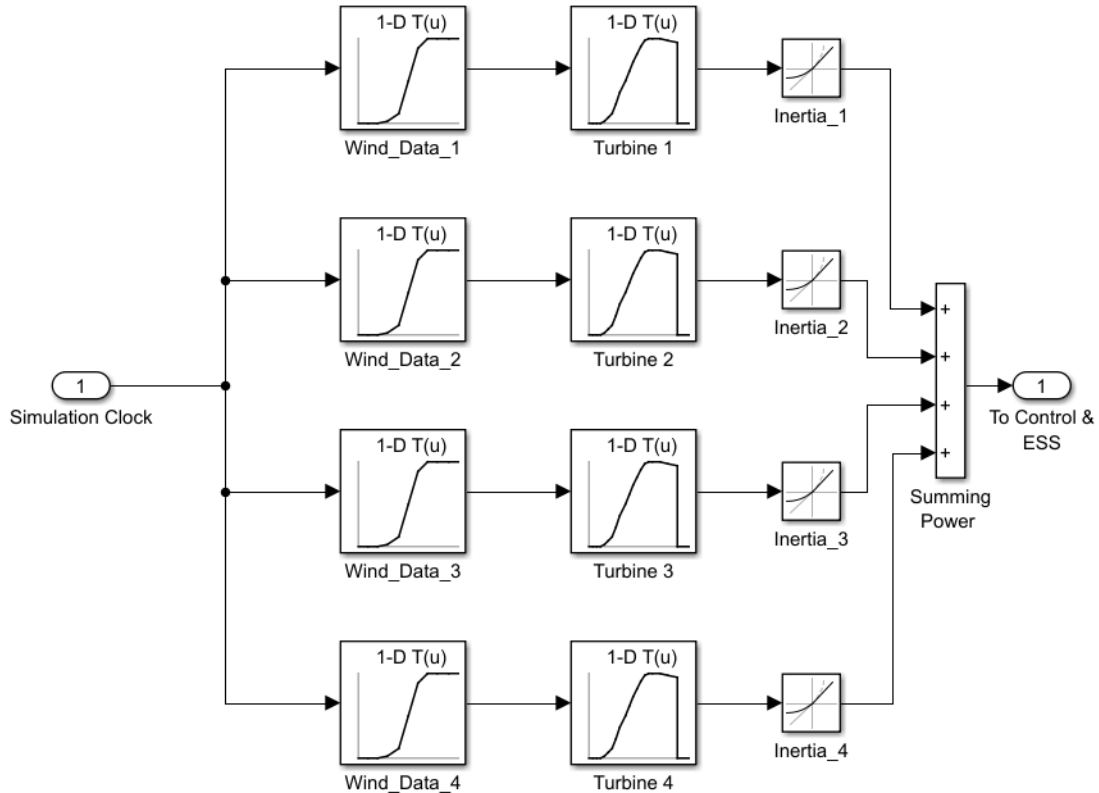
Figure 4.4: Application block for wind generation simulation

## 4.3.2 Wind Site MATLAB/Simulink Model

Following on from the model outlined in Chapter 3, this section describes the specific elements that enable the model to be utilised for wind generation site simulation. An overview block diagram has previously been discussed in Figure 3.10.

Firstly, Figure 4.4 shows the application block for a wind generation site. In this scenario, any number of wind turbines and associated wind profiles across a given site can be utilised to generate the overall output power of the site, in this example, there are four 250kW turbines stationed at the site. The input data utilised was provided by the industrial sponsor of this project at a frequency of 10 seconds which was subsequently interpolated to provide 1 second data. A slew rate block has been included for each turbine to represent the inertia of the system. The slew rate is set at -4.5/4.5 and was determined through a process matching the simulation output data to the known output data provided by the industrial sponsor.

The other major difference with the model discussed previously in Chapter 3 is in the control block. For this application, the request is fed through a different calculator that takes the calculated output power from the application block and compares it with the site limit. If the output power is higher than the limit, it attempts to charge the ESS and if the output power is lower than the limit then it
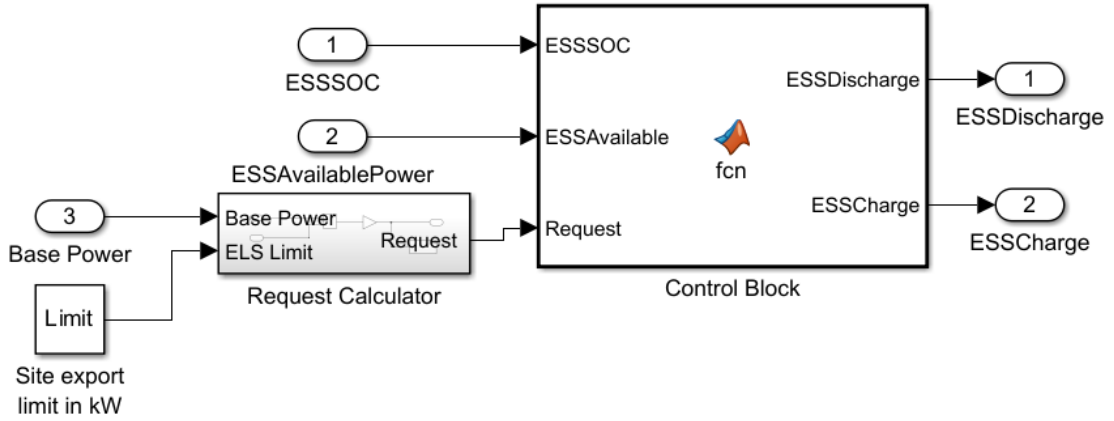
Figure 4.5: Control block for wind generation simulation

attempts to discharge the ESS. This is represented in Equations 4.3 and 4.4, where $P_{\mathrm{dis}}$ is the discharge power of the ESS in kW, $P_{\mathrm{cha}}$ is the charge power of the ESS in kW, $SOC_{\mathrm{low}}$ and $SOC_{\mathrm{high}}$ are the low and high limits of the ESS SOC range, $SOC_{\mathrm{ESS}}$ is the current SOC of the ESS, $P_{\mathrm{base}}$ is the output of the site before any adjustments due to ELS in kW, and $P_{\mathrm{limit}}$ is the export limit of the site in kW.

$$P_{dis} = \begin{cases} |P_{base} - P_{limit}| & SOC_{low} \leq SOC_{ESS} \leq SOC_{high} \text{ and } P_{base} \leq P_{limit} \\ 0 & \text{otherwise} \end{cases} \tag{4.3}$$

$$P_{cha} = \begin{cases} |P_{base} - P_{limit}| & SOC_{low} \leq SOC_{ESS} \leq SOC_{high} \text{ and } P_{base} \geq P_{limit} \\ 0 & \text{otherwise} \end{cases} \tag{4.4}$$

The remaining aspects of the model are the same as previously explained in Chapter 3.

### 4.3.3 Technical Analysis

A sensitivity analysis was performed over a range of C-Rates for three power capacities and varying levels of limitation. To demonstrate how the system operates within MATLAB/Simulink, Figure 4.6 shows the simulation output for a 20% limited site, with a 5C 0.2MW FESS installed to assist with export limitation.

The FESS is seen to be charging whenever the site output power exceeds the ELS threshold until it reaches its SOC high limit, at which point the remaining excess power will be dissipated by an ELS panel. The FESS then discharges when the output power falls below the agreed export limit.

In the following analysis, the x-axis on Figures 4.7-4.10 shows varying levels of
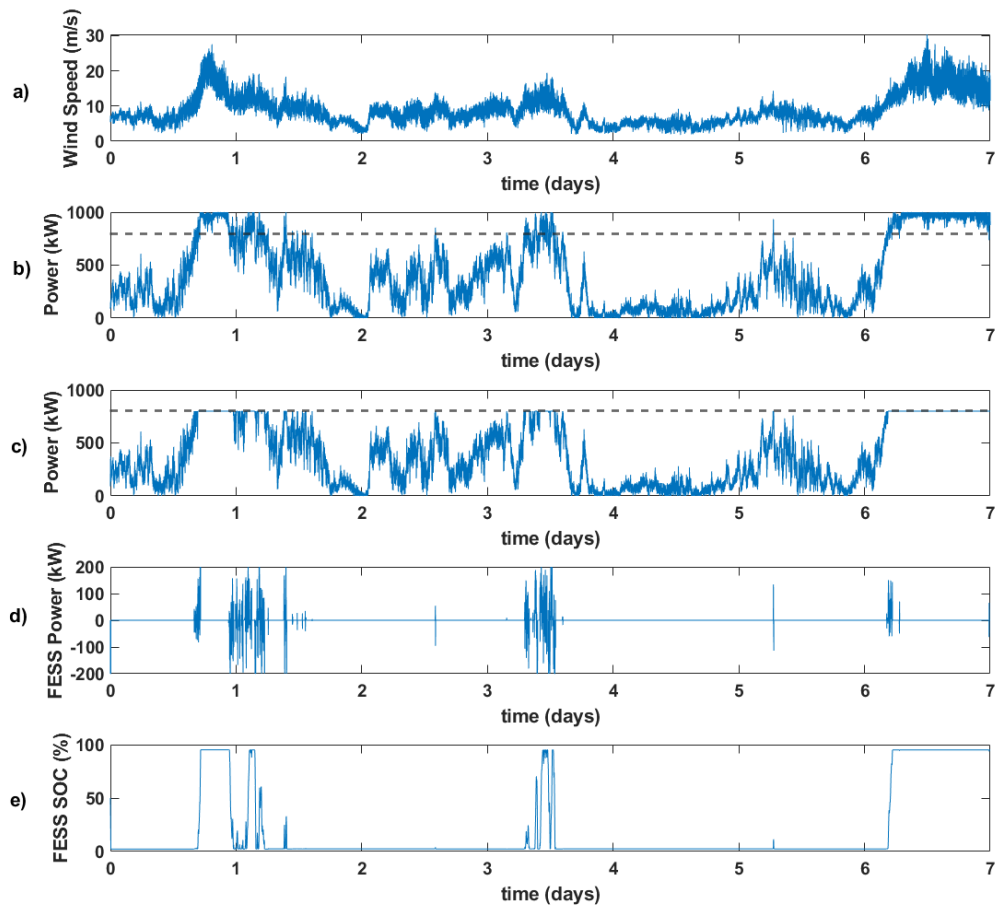
Figure 4.6: Example simulation output for ELS site simulation showing a) Wind Speed b) Site output without any ELS scheme in place c) Site output with ELS and integrated FESS d) FESS output power e) FESS SOC
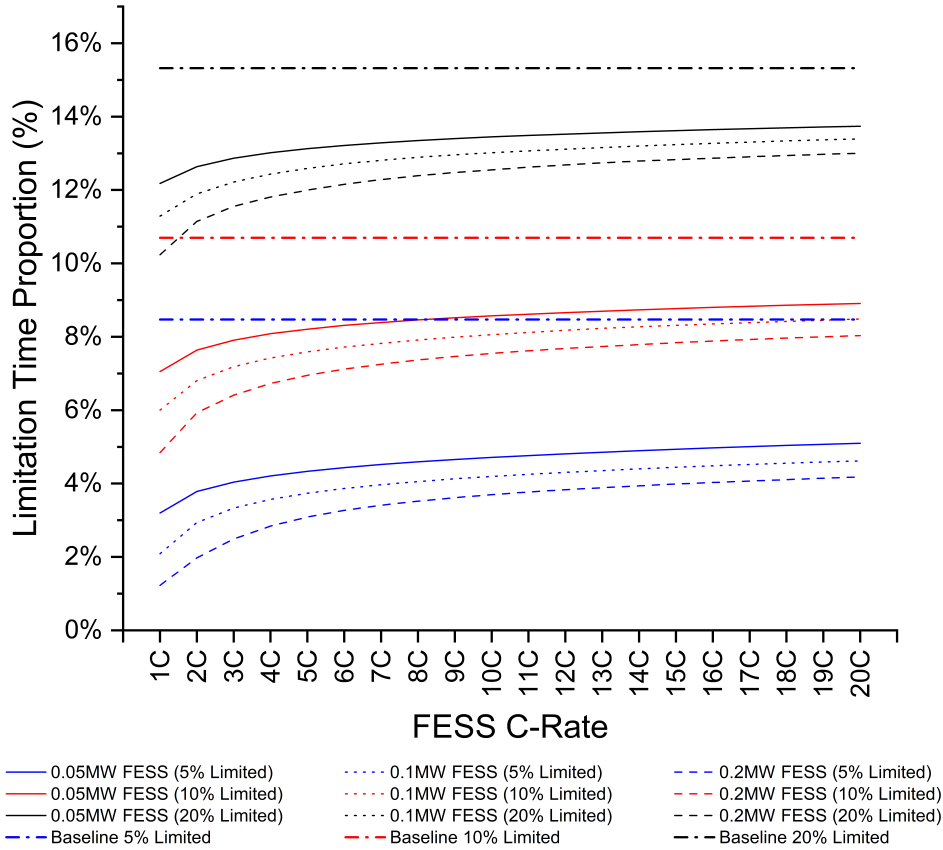
Figure 4.7: Limited Time Proportion (%) for different levels of limitation and FESS sizes over a range of C-Rates including baseline without any FESS for each limitation level

C-Rate. The results are presented for three different levels of FESS power capability (0.05MW, 0.1MW and 0.2MW). Thus, the changing C-Rate is varying the energy capacity of the system. For example, a 0.05MW FESS at 1C will have an energy capacity of 0.05MWh, whilst at 20C this will represent an energy capacity of 0.0025MWh as previously shown in Table 4.1.

The first of the three technical criteria to be assessed is limited time proportion, with the results shown in Figure 4.7. This metric gives a good idea of how often the FESS is operating for a given set of conditions and how sensitive the system is to changes in C-Rate (and therefore energy capacity as power is fixed).

From Figure 4.7 it is clear that for all three levels of limitation, a significant reduction in the amount of time spent being limited can be achieved. It is also clear that regardless of the level of limitation, the lower C-Rate configurations perform best but then plateau rapidly to suggest that increasing the C-Rate further does not have a significant detrimental effect on performance, suggesting that the application could be taken on by a wide range of flywheel specifications. Whilst it is acknowledged that the results would likely continue to improve at even lower C-Rates, such specifications are very uncommon in FESSs and therefore the minimum

C-Rate considered was maintained at 1C.

When the site experiences a smaller degree of limitation, then the impact from introducing a FESS becomes more apparent suggesting that the more oversized the generation in relation to the site export limit, the less potential there is for improving the site performance through this method. From a baseline of 8.5% limited time proportion, introducing varying sizes of FESS reduces this to between 1.2% and 5.1% limited time proportion. At the lowest point, the limited time proportion of 1.2% suggests that the site is almost operating at its full potential. Even for higher levels of limitation, there is still a significant reduction available by using a FESS, with the 20% limitation level showing a reduction from 15.3% to a range of 10.2% to 13.7% depending on C-Rate and rated power.

Interestingly, in scenarios where the energy capacity is equal but with different configurations (for instance a 4C 0.1MW FESS has the same energy capacity as a 2C 0.05MW FESS) they do not perform at the same level, with the higher power system performing better. For the example previously mentioned, a 2C 0.05MW FESS at a limitation level of 5% shows a limited time proportion of 3.8% whilst the 4C 0.1MW FESS at the same level of limitation has a limited time proportion of 3.8%. This shows that whilst the energy capacity is important, a higher power rating also allows the system to contribute more effectively.

In Figure 4.8 the total amount of cycles that the FESS is subjected to per year is shown. From the literature review, it was found that a FESS can commonly withstand at least 100,000 cycles before the end of life whilst in some cases can withstand significantly more.

Considering the results with this in mind, it is clear that under all but 3 of the simulated scenarios, the FESS will not come close to reaching 100,000 cycles over a 25-year lifetime. However, the three configurations with a 0.05MW flywheel would reach between 106,000 and 111,000 cycles in 25 years of operation. Even with these values, it is likely that when considering the information in Table 2.2, the majority of FESSs would be able to be designed to withstand these levels of cycling as 100,000 cycles are generally quoted as the lower threshold of allowable cycles.

The final metric to be discussed is capacity factor increase. This shows the effect that the changing levels of limitation have on the overall capacity factor of the site, and will subsequently lead to how much more income the site can generate. The results of this study are shown in Figure 4.9

For all of the studied FESS configurations and limitation levels, the capacity factor increase decreases as the C-Rate is increased with a significant decrease when comparing low C-Rate systems to higher C-Rate ones. However, after an initial rapid decrease in capacity factor increase as the C-Rate is increased from 1C, all of the configurations experience a plateau where further increasing of the C-Rate does not
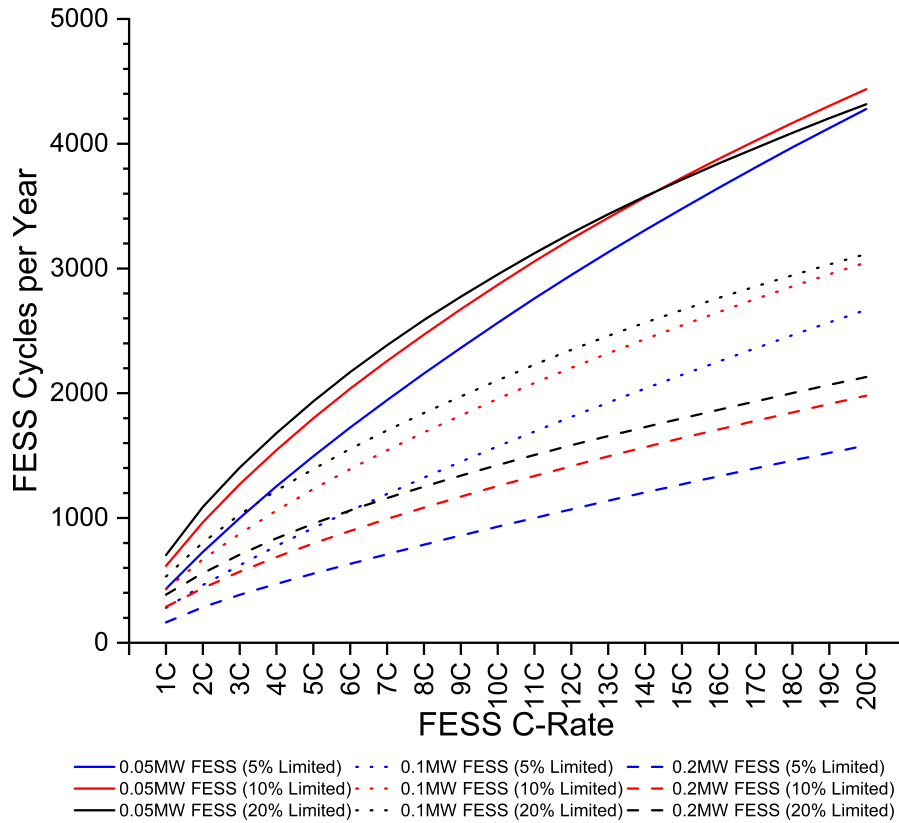
Figure 4.8: Cycles per year experienced by the FESS for different levels of limitation and FESS sizes over a range of C-Rates including baseline without any FESS for each limitation level

result in a significant reduction in capacity factor increase, suggesting again that a wide range of FESS configurations can be suitable for this application. Additionally, as limitation is increased, all systems experience immediate reductions in the CFI that they provide although this feature is again more prominent at lower C-Rates than higher ones.

It is interesting to note that whilst the 0.2MW FESS achieves the two best capacity factor increase results under the 20% and 10% limitation scenarios, it is then the 0.1MW FESS under the 20% and 10% limitation scenarios that produces the next best results rather than the 0.2MW FESS under 5% limitation. This suggests that the 5% level of limitation does not contain a sufficient duration of time where the export is limited to provide scenarios where the FESS is justified.

When considering different levels of limitation, the more limited the system is the more potential for increasing the overall capacity factor there is. This is due to more excess energy being available for charging the FESS to then subsequently be discharged when the output drops back below the export level. At its peak, a capacity factor increase of 0.44% can be achieved. Whilst the numbers for these increases appear small, considering the scale of the site the value becomes clear.
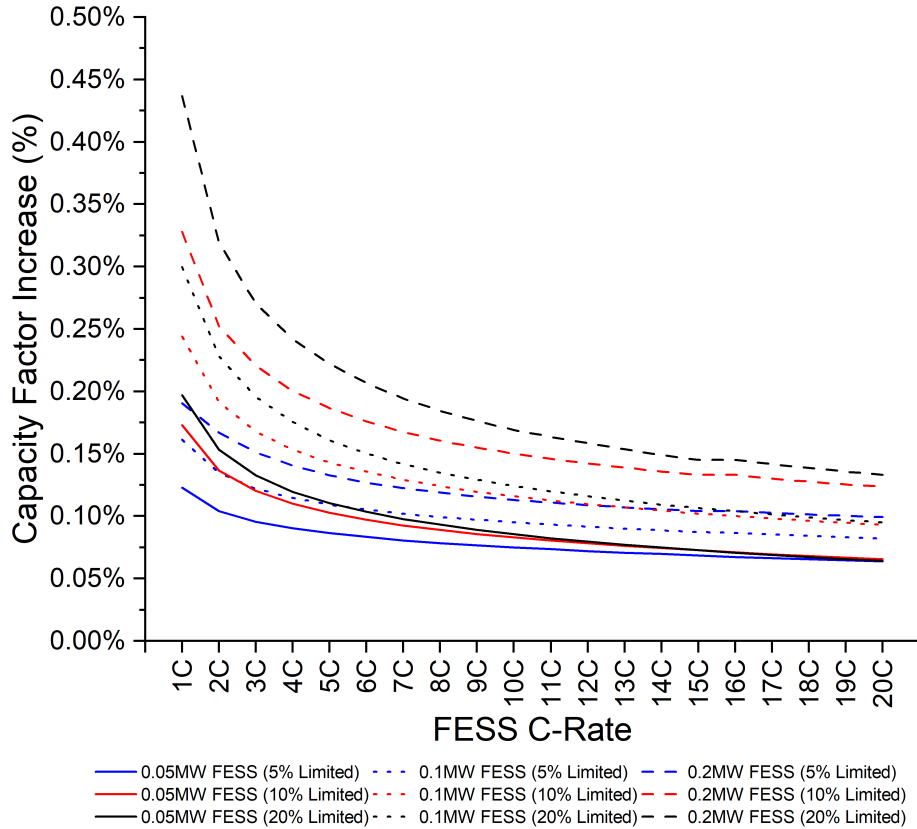
Figure 4.9: Capacity Factor Increase (%) for different levels of limitation and FESS sizes over a range of C-Rates

A capacity factor increase of 0.44% for a 1MW site would result in an additional 38.5MWh of generation over the course of a year. The lowest increase of 0.07% would lead to an additional 6.1MWh of generation over the course of a year.

## 4.3.4 Economic Analysis

In order to verify the real-world viability of the systems being analysed, an economic analysis was conducted. This economic analysis is based upon comparing the difference between the baseline NPV of the system without an energy store, and the new NPV that could be achieved with an ESS present to produce a net present value change. This is calculated as shown previously in Equation 3.2 over a period of 25 years, with the additional income of the wind site from export of additional energy enabled by the ESS included in the $C_{income}$ part of the equation.

For the initial assessment, the TCC was set at £500/kW along with a discount rate set at 5% in order to provide a baseline for further analysis. This value was provided by the industrial sponsor for this project at the time of writing as an approximate cost for their system. This TCC has been set to provide an initial baseline result, with the TCC then varied to show the ranges of values for TCC that
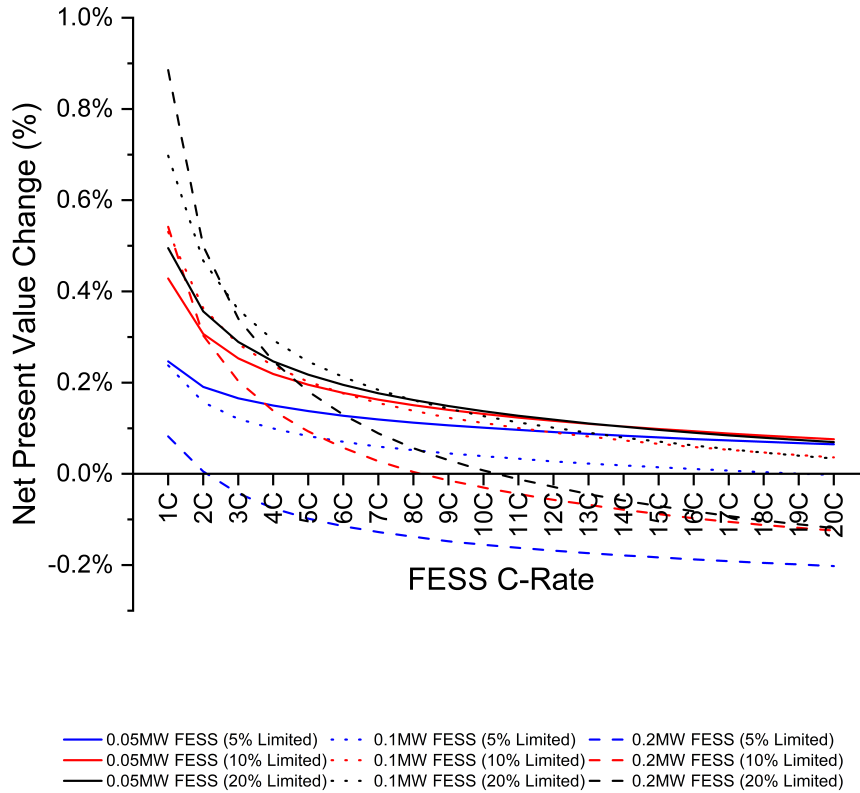
Figure 4.10: NPV change for varying FESS and site configurations across a range of different C-Rates with discount rate of 5% and TCC of £500/kW

should be targeted in order to provide an economically viable product. The NPV change has been calculated for varying C-Rates at a TCC of £500/kW, with the results of this baseline study shown in Figure 4.10.

It is clear that the lower end of the C-Rate spectrum creates the most favourable increase in NPV, before beginning to plateau around the 4-10C range depending on the configuration being assessed. Across the range of C-Rates studied, the level of limitation and energy capacity has a significant impact on which C-Rate will provide the most significant economic benefit, with the following configurations representing the greatest increase at the given C-Rate ranges;

- 1C-2C - 0.2MW FESS (20% limited)

- 3C-7C - 0.1MW FESS (20% limited)

- 8C-13C - 0.05MW FESS (20% limited)

- 14C-20C - 0.05MW FESS (10% limited)
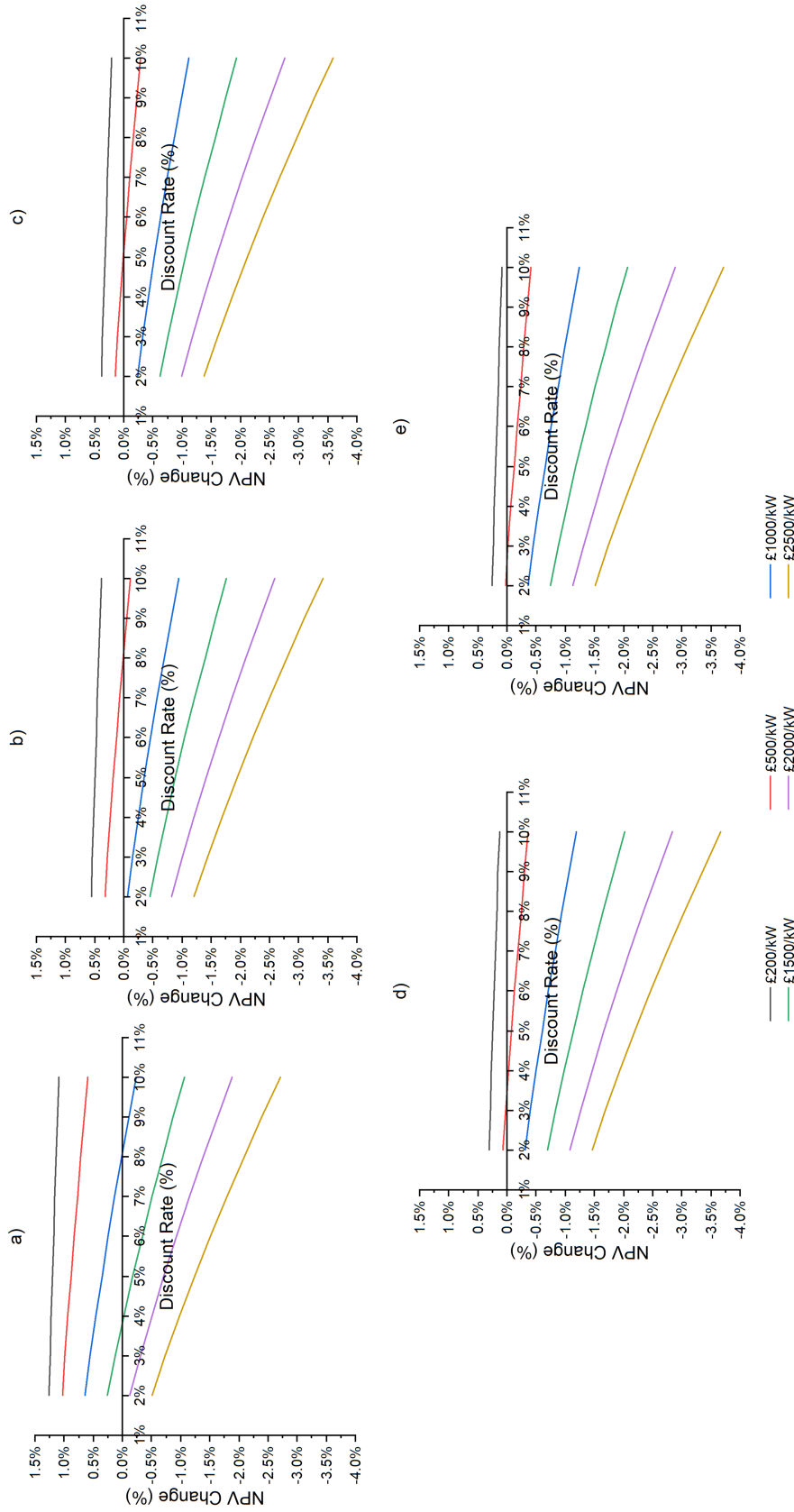
Figure 4.11: NPV change for a 0.2MW FESS installed at a site limited by 20% based on varying levels of discount rate and TCC for a) a 1C system b) a 5C system c) 10C system d) 15C system e) 20C system

These results are particularly interesting, as it shows that in the lower C-Rate ranges the larger FESS systems are more favourable, as well as there being a greater advantage from higher levels of limitation. However, as the C-Rate is increased this changes until at 11C a lower level of limitation coupled with the smallest FESS power rating becomes the best performing configuration. Again these results show that at this TCC a wide range of different FESS configurations can be introduced to add value to a site.

However, the results are not uniformly positive. The 0.2MW FESS in a 5% limited system fares particularly badly with only a 1C and 2C FESS providing a positive NPV change under these conditions. Additionally, the other two levels of limitation for a 0.2MW FESS fall into negative NPV change at different points. Here then we have at one end of the spectrum a 0.2MW FESS (20% limited) providing the biggest NPV increase but at the other end providing a negative change to NPV highlighting the fine line between positive and detrimental effects from deploying energy storage systems. It is therefore evident that it is important to ensure the energy storage technology, energy capacity and power capacity are all carefully chosen depending on the scenario at an individual site.

Following on from this a sensitivity analysis was conducted for the 0.2MW FESS under 20% limitation, varying the TCC between £200/kW and £2500/kW and varying the discount rate between 2% and 10%. The results of this are shown in Figure 4.11.

Firstly consider the varying levels of TCC. This has a big impact on the overall level and direction of NPV change compared to the baseline. If the TCC could be reduced down as low as £200/kW then the change to NPV would be positive regardless of the required discount rate or indeed C-Rate. However, all of the discount rate combinations for £2000/kW and above result in exclusively negative NPV changes.

An interesting point to note is that the lower the TCC gets the less vulnerable the system is to changes in the discount rate. Taking the 1C system as an example, the £200/kW TCC only varies by 0.176% between its highest and lowest NPV change whilst the £2500/kW TCC varies by 3.21%. The discount rate, therefore, becomes a more important metric as the TCC of the system is increased. Whilst the NPV increases are small, they still represent a positive impact and are dependant on the level of economic return that site owners require, as well as the level of risk they are willing to accept. These results provide the foundation for further analysis in this field, looking into increasing the impact of ESS deployment and enhancing the economic impact.

### 4.3.5   Alternative Energy Storage Economic Assessment

It is prudent to analyse the significantly more mature technology of Li-ion BESSs in order to compare their economic performance for this application and determine whether the FESS can provide a legitimate advantage over the generally cheaper and more commonly deployed Li-ion BESS. The technical performance of a BESS for this application will be looked at in more detail in the following section.

For this assessment, the BESS C-Rate was set as 1C to represent the most common type of system configuration with the energy capacity varied between 20kWh and 200kWh. The same simulations were then conducted as in the previous section, with the TCC of the BESS set as £400/kWh in line with current industry economic conditions, representing the whole TCC including aspects such as battery cells, power electronics and integration costs.

Figure 4.12 shows the results of this study. Across the range of capacities studied and over all three levels of export limitation the BESS will actually cause a negative economic impact on the site apart from under a small number of specific combinations. This is in sharp contrast to the results from the FESS study, where multiple different combinations experienced a positive NPVC across the entire range of C-Rates studied.

When deployed in the lowest level of export limitation, the BESS does not provide a positive NPVC under any configuration. This is because the additional income generated does not outweigh the cost of multiple replacement systems being required over the operational lifetime due to excessive cycling, which in this study is considered as the point at which the system reaches 10,000 cycles. Under the 10% limited scenario, the BESS provides a positive NPVC for energy capacities of 90-110kWh and 130-150kWh, whilst in the 20% scenario a positive NPVC is provided for 150kWh and 180-190kWh. Even when the NPVC is positive, the peak value achieved is 0.09%, much lower than many values achieved by the FESS.

Rather than the smooth exponential lines from Figure 4.10, the NPVC for the BESS configurations studied fluctuates significantly as the energy capacity is increased. This is due to the balance between additional income from the extra capacity and additional costs from the number of cycles experienced by the system. This is further illustrated in Table 4.2, which highlights the results from BESS capacities of 140kWh to 160kWh at a 20% limitation rate. This shows that due to the years before replacement increasing beyond 5 years from 140kWh to 150kWh there is a significant drop in lifetime cost, improving the NPVC. However, at the next energy capacity, the increased cost of the system due to a larger energy capacity is counteracted by a minimal increase in yearly income, resulting in a drop in NPVC.

Figure 4.13 shows the number of years that the BESS will be operational before
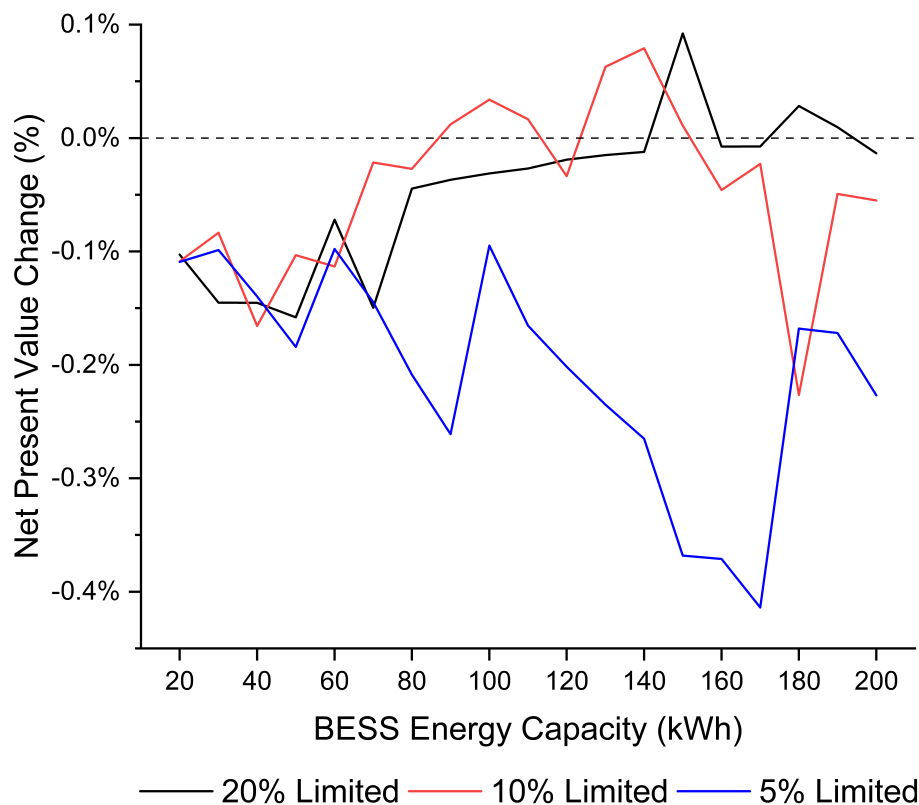
Figure 4.12: NPV change for varying BESS energy capacities under differing levels of export limitation

requiring replacement. This application places a significant strain upon a BESS which results in a reduced lifetime. As previously discussed in Section 2.2, it is likely that all of the FESS configurations studied would not need replacement during the 25-year operational lifetime. This is the key area in which the FESS is shown to be a superior energy storage technology for use in this application.

There are circumstances where this could change, for instance, if the BESS cycle lifetime was significantly enhanced, the replacement costs would then not impact the NPVC and the overall outlook for BESSs for this application would be improved.

Table 4.2: Simulation results from a BESS performing export limitation at a 20% limitation level for selected energy capacities

| BESS Size (kWh) | CFI | Years before replacement | Total Lifetime Cost (£) | Yearly Income (£) | NPVC |
|---|---|---|---|---|---|
| 140 | 1.64% | 4.98 | 672000 | 28519 | -0.01% |
| 150 | 1.69% | 5.17 | 600000 | 29360 | 0.09% |
| 160 | 1.74% | 5.34 | 640000 | 30325 | -0.01% |
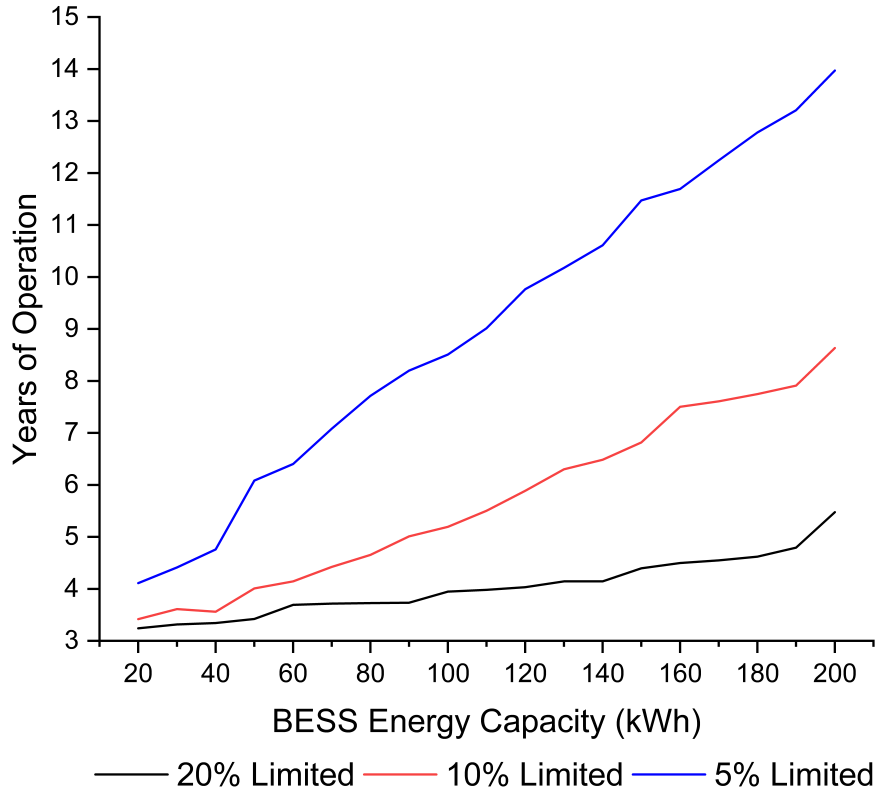
Figure 4.13: Years of Operation before BESS would need replacement due to excessive cycling

Additionally, if the BESS cost was reduced sufficiently that the replacement costs were minimal then the same effect would occur. These are two areas that will need to be pursued for a BESS to be competitive with a FESS in this application.

## 4.3.6 Discussion

A novel application of FESSs has been introduced and analysed from both a technical and economical perspective. The scale of the issue that this work seeks to address has been highlighted, showing how this application has the potential to generate additional income for new and existing sites across Great Britain. Flywheels are ideally suited to perform this service due to their rapid response time, high power capabilities and resistance to cycle-based degradation.

In terms of technical performance, increases to the overall capacity factor of the site can be achieved up to 0.44% for a 1MW site being limited by 20%. Additionally, the duration of time that the site is export limited for can be reduced dramatically under a wide range of FESS configurations and operational restrictions. The FESS is also shown to experience a number of cycles that it is more than capable of handling over the course of its lifetime.

In terms of economic performance, a peak increase to the NPV of the site of 0.85% was achieved at a £500/kW TCC whilst a sensitivity analysis conducted shows that the relationship between the discount rate and TCC and the effect this has on the economic viability of introducing a FESS. The key takeaway from this section is that as the TCC is reduced the effect of increasing discount rates on the NPV change is reduced. From the analysis conducted it is clear that aiming for a TCC of £500/kW in the short term with an aim to reduce this as low as possible will provide the greatest range of options for deploying varying configurations of FESS.

Now referring back to the information presented in Chapter 2 and Figure 2.14, where it was shown the mean value for FESS TCC within the studied literature was £780/kW, it can be concluded that at this price point, there would only be a limited selection of scenarios where a FESS could be implemented, although it is not far off the required level to begin entering regions where significant economic value can be achieved. Some existing systems on the market could likely be deployed for this application, especially if they fall at the lower end of the TCC range.

Finally, the study looked at the impact that BESSs could have when being deployed for this application, focusing on the potential economic return from the site. It was shown that in only 9/57 studied combinations of BESS energy capacity and level of limitation could a BESS can be deployed and achieve a positive economic impact. Even when a positive economic impact is achieved, the peak impact achieved is minimal at 0.09%. This is due to the excessive cycling required by this application, with the maximum lifetime of the BESSs studied being 13.9 years.

## 4.4 Case Study

The previous section represented a generalised view of the potential for energy storage to be deployed at export-limited sites. This section now explores a case study using operational and economic data from a generation site subjected to an ELS located within the UK. This allows the economic conclusions to be re-assessed in a real-world scenario, which can provide greater clarity on the required techno-economic specifications for a FESS to be deployed for this application.

The site in question has the following main operational criteria;

- The turbine is rated to deliver a maximum power output of 300kW

- The site export limit is 250kW.

- The turbine can be set via pitch control to modify the output power of the turbine. The set point for the output power is referred to in this study as 'Targeted site output'.
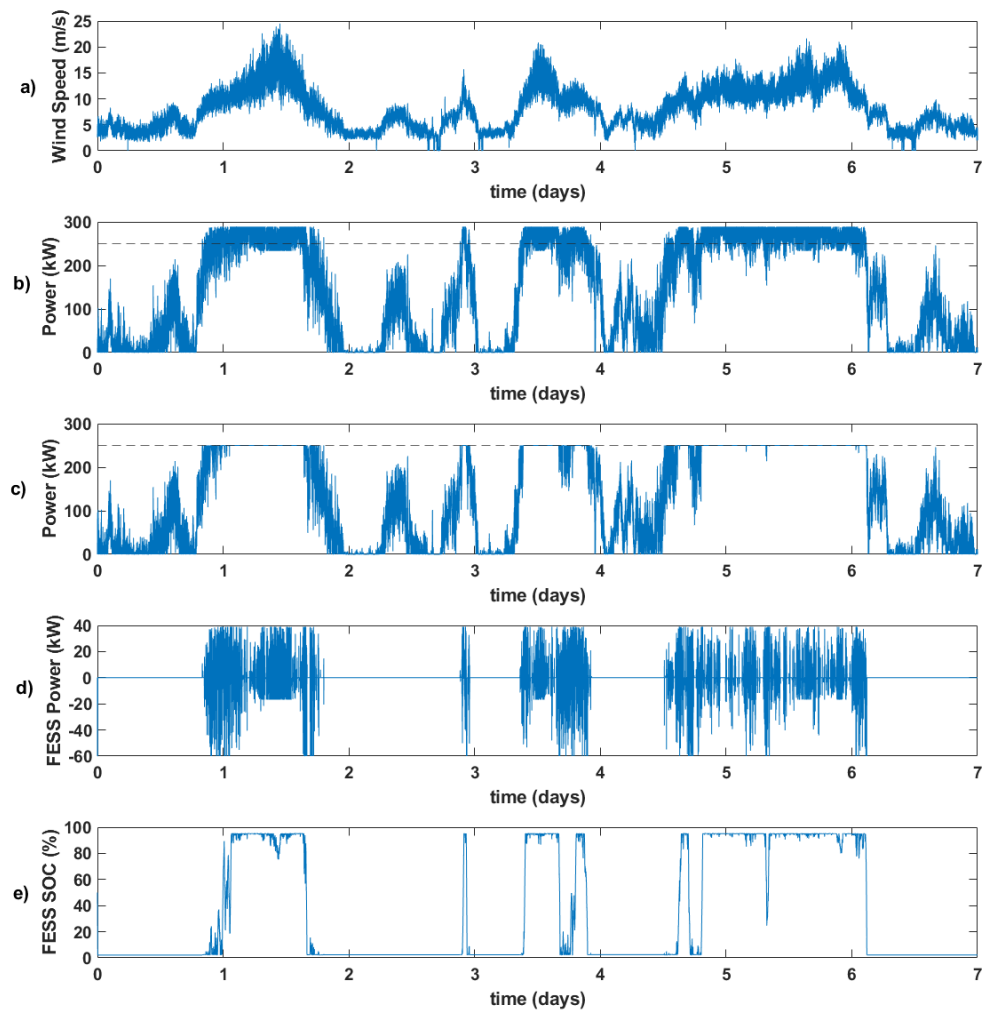
Figure 4.14: Example simulation output showing FESS operating to reduce export limitation issues showing a) Wind Speed b) Site Output without ELS c) Site Output with ELS and FESS d) FESS Power e) FESS SOC

Wind speed data for the site was made available at a resolution of 10 seconds. This data was linearly interpolated to create data of 1-second resolution. Linear interpolation was chosen in line with the approach taken across multiple studies in similar areas [226–229]. It is considered that within the 10-second time frame, the inertia of the system will not react sufficiently to any very short-duration fluctuations to a degree that would affect the validity of the simulation. An example simulation output showing a FESS operating to maintain the site output at 250kW is shown in Figure 4.14

With a site that has the ability to generate power in excess of its agreed export limit, this study is an ideal opportunity to showcase the technical and economic

Table 4.3: ESS configurations used for ELS Case Study

| Identifier | ESS Type | Energy Capacity (kWh) | C-Rate |
|---|---|---|---|
| F1 | FESS | 7.5kWh | 8 |
| F2 | FESS | 22.5kWh | 8 |
| F3 | FESS | 37.5kWh | 8 |
| B1 | BESS | 30kWh | 1 |
| B2 | BESS | 60kWh | 1 |
| B3 | BESS | 90kWh | 1 |

benefits that can be achieved by introducing an ESS. For this case study, three configurations of FESS will be compared against three configurations of BESS to show the impact of utilising the two different technologies for this application and the effect that their relative strengths and weaknesses have on the operation of the system.

The case study has been conducted using the specifications of the OXTO Flywheel, an 8C 60kW, 7.5kWh modular FESS. Table 4.3 summarises the configurations studied. The approach taken is to represent the installation of 1, 3 and 5 individual flywheel units at the site, and compare this against a range of different BESS configurations. The BESS configurations have been chosen to represent small modular systems in the same way as the FESS configurations, across a range of power ratings that would be suitable for this application given that the maximum additional power to be absorbed at any one time is 50kW. It is not considered useful to utilise an 8C BESS for this comparison as such systems are uncommon and as such prohibitively expensive, therefore for the BESS analysis it was determined most appropriate to play to the relative strengths of the BESS to ensure a fair comparison. Additionally, utilising a 1C FESS would not be appropriate as the majority of commercial FESS systems are higher C-Rate units.

An economic study is then undertaken to determine the required TCC at which the FESS and BESS configurations would be viable for installation at the site based upon the requirement of providing a positive NPV change.

### 4.4.1 Performance Analysis

As with the previous study, the main performance statistics that will be considered are limited time proportion and capacity factor increase whilst also considering the degradation that takes place on the BESS during the course of operation.

Each metric has been assessed over a range of targeted site outputs, with the aim of looking at whether the ESS can offer greater benefits if the site is continu-
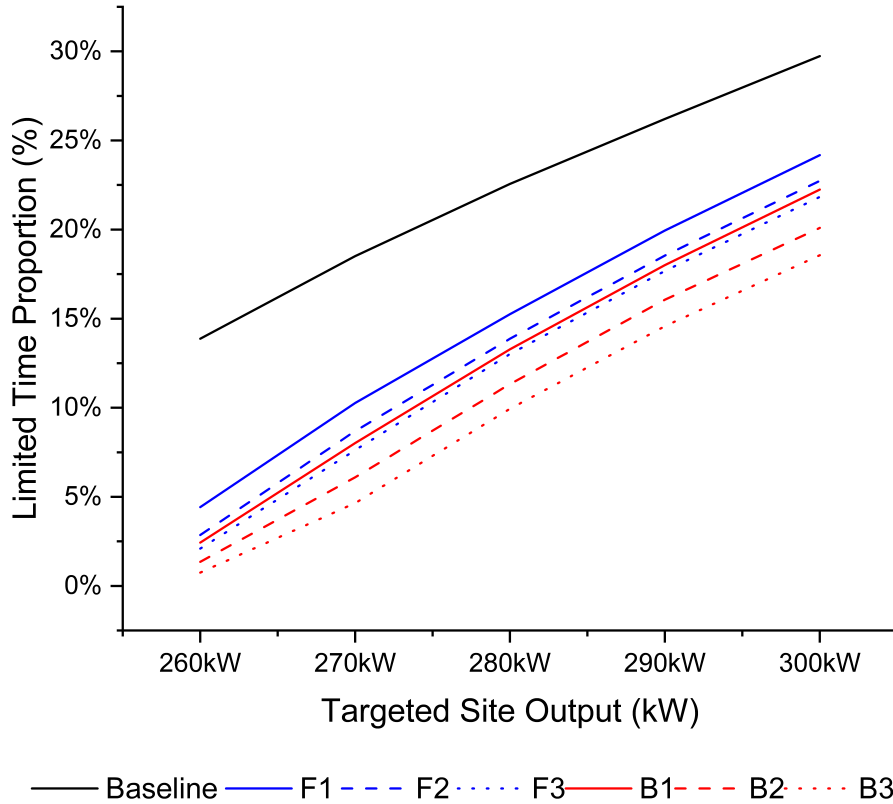
Figure 4.15: Limited Time Proportion for varying FESS and BESS sizes across different target outputs

ously generating above the export limit. In this example, the ELS panel would be operating at the grid connection point, with any energy that is over 250kW instantaneous power and is not absorbed by the ESS being 'dumped' into a resistor bank to maintain the output within the export limit. This study aims to capture as much of that energy that would otherwise be wasted as possible.

Initially, looking at the limited time proportion for this site as shown in Figure 4.15, it is clear that the introduction of any ESS technology or configuration will result in an immediate reduction in LTP, with the effect slightly lessening as the target output is increased.

Comparing the two different ESS technologies it is apparent that in general terms the BESS is more adept at reducing the limitation experienced by the site, reducing by more than the best performing FESS in 2 of the 3 configurations. This is likely due to the greater levels of energy capacity available that enables the BESS to operate for longer durations of excess power duration before becoming fully charged. In fact, the only situation in which the FESS will work better than the BESS is when the FESS has a higher energy capacity when comparing configuration F3 with B1. From this standpoint, it appears that the application is largely technology agnostic
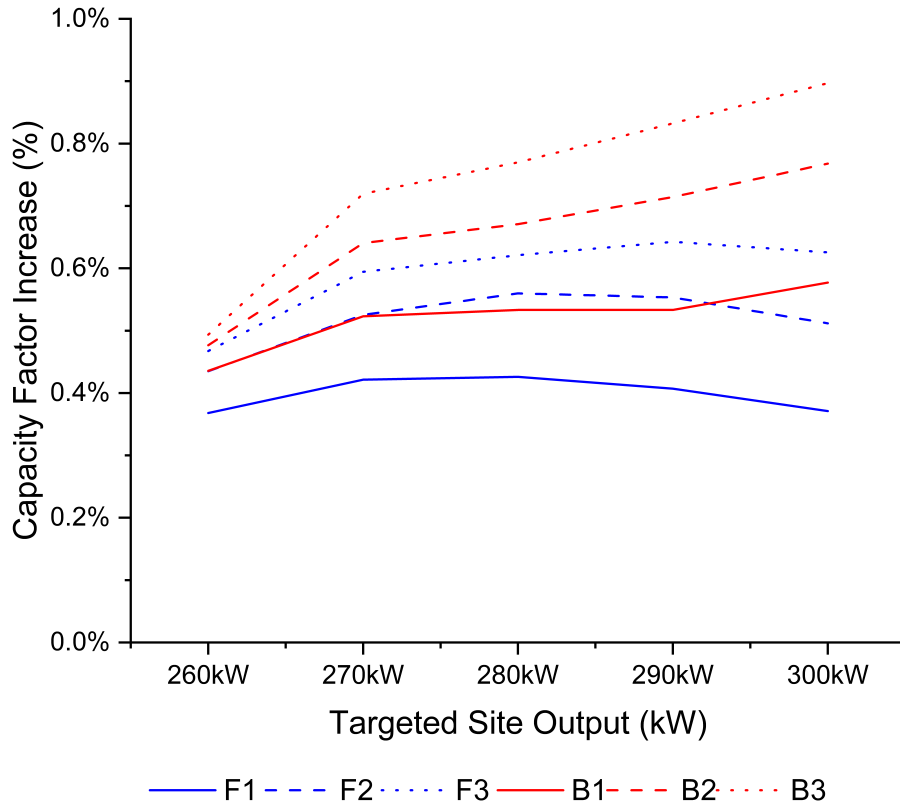
Figure 4.16: Capacity Factor Increase for varying FESS and BESS sizes across different target outputs

with equal performance available depending on energy capacity.

Capacity factor increase for the analysed configurations is shown in Figure 4.16, This metric is where the differences between the two technologies begin to become a bit more apparent with a clear, albeit relatively small, difference in the shape of the two sets of curves.

For all of the FESS configurations, the capacity factor increase peaks in the region of 270-290kW targeted site output before beginning to fall back down whilst for the BESS configurations there is a continuous trend upwards as the targeted site output is increased. The reason for this difference between the two systems is that because of their higher C-Rates, the FESSs charge much quicker when the export level is above the limit, meaning they reach fully charged status sooner and hence are able to manage the higher targeted site output less effectively than the BESSs.

Once again there is a clear correlation between the energy capacity and effectiveness in improving capacity factor increase, with the highest energy capacity BESS configuration (B3) achieving a peak increase of 0.9% (representing an additional 23.6MWh of energy over the course of a year), whilst the highest energy FESS configuration provides a peak increase of 0.63% (an additional 16.6MWh of energy over
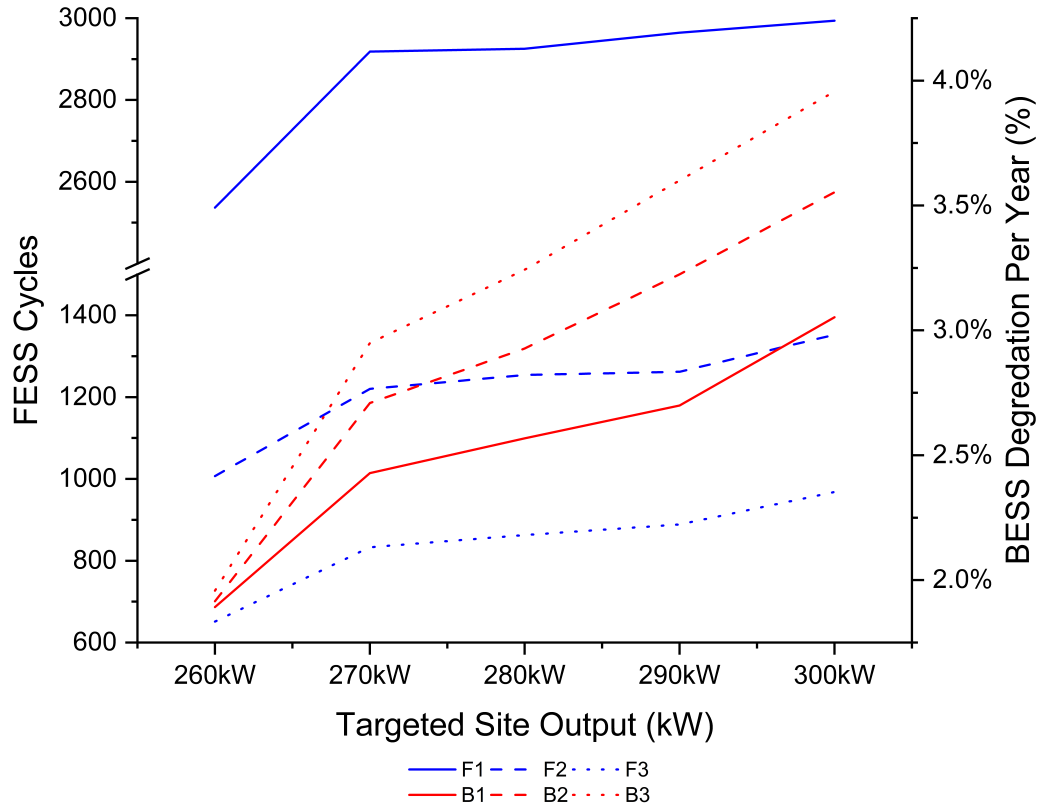
Figure 4.17: Cycles and Degradation for varying FESS and BESS sizes across different target outputs

the course of a year).

Finally, Figure 4.17 shows the cycles experienced by each FESS per year and how much degradation each BESS configuration experiences.

First let us consider the FESS cycle numbers, which across all configurations peak at 2925 cycles across a single year (configuration F3 for 300kW target output). Extrapolating this across the expected 25-year lifespan would result in just over 73,000 cycles, well below the marketed cycle limit across the flywheel manufacturer industry (as shown in Table 2.2). This suggests that all the configurations studied can easily handle this application without the need for anything more than standard levels of maintenance.

However, when considering the level of BESS degradation experienced each year, the lowest value is 1.9% per year for configuration B1 at a 260kW target output. Even at this lowest level of degradation, the BESS would still only be expected to last into its 11th year of operation before it would require replacement due to degradation. In addition to this, at the worst levels of degradation, the BESS would last just over 5 years before requiring a replacement.

It is in this last set of analyses that the issue with installing BESSs over FESSs
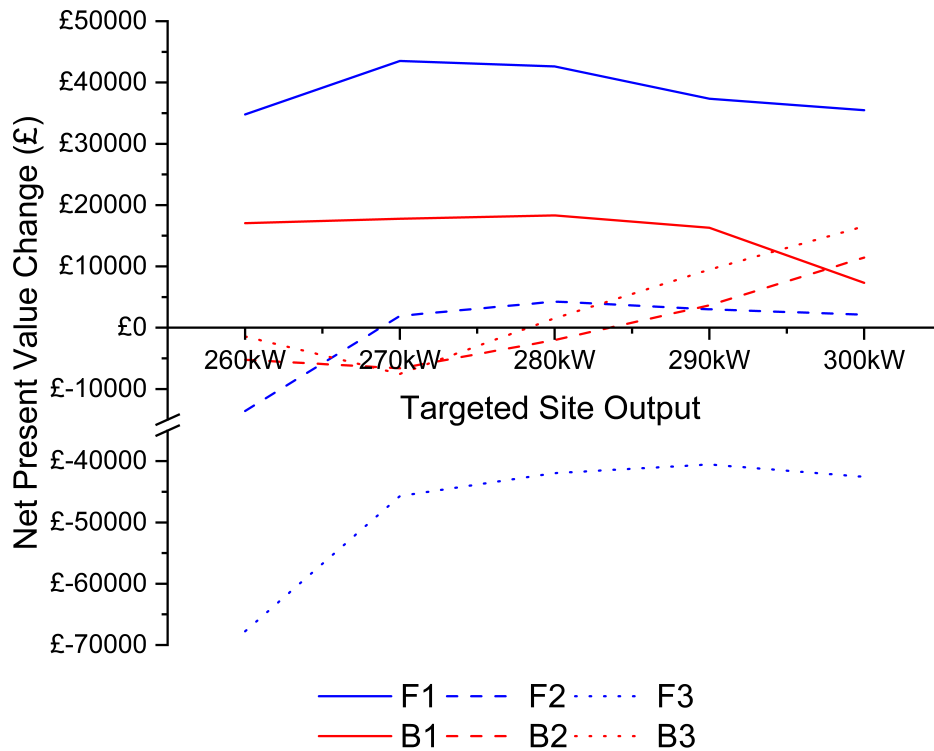
Figure 4.18: NPV change for varying FESS and BESS sizes across different target outputs

for this application becomes apparent. Whilst the BESS can perform technically better than the FESS, when we begin to consider the effect that this application has on the lifetime of the BESS the drawbacks outweigh the positive effects. This factor is particularly important when considering the economics of the site.

## 4.4.2   Economic Analysis

To further inform the results of the technical analysis and the comparison between BESSs and FESSs for this application, an economic analysis was performed using the same theories as discussed earlier in this chapter. Firstly, the NPV for each combination studied so far at a TCC of £500/kW and a discount rate of 5% is shown in Figure 4.18 to provide a baseline economic analysis to build from.

It is seen in Figure 4.18 that of the configurations assessed, configuration F1 (a 7.5kWh 8C FESS) is the best performing from the initial economic assessment. The low cost of installing just one of the modular FESSs coupled with the diminishing returns of installing further FESS modules results in the net present value change becoming worse as the FESS is increased in size. It is also important to note that configuration F1 peaks at 270kW target output, with any further increase in targeted

output bringing the NPVC down rather than up. This is because the FESS is now sitting at 100% SOC for longer periods of time, rendering it less effective than when capturing more of the available additional energy at the lower target outputs. The key aspect to be aware of to explain why this impacts the NPV in this way, it is important to note that at the higher targeted site outputs, the base NPV that is being compared against is also increasing, and the resulting drop in NPVC at the higher target outputs is actually the result of the relative increase becoming smaller.

When considering the BESS configurations, they are grouped together far more closely than the FESS configurations. B1 is the best performing by a narrow margin (£18,000 NPVC compared to £17,000 NPVC for B3), but is also the only configuration where the NPVC falls at the higher target outputs. This is due to the complex trade-off between increasing income from the additional energy available, and the resulting increase to degradation from the BESS being required to operate more frequently. Where for B1, an additional replacement BESS is required when the target output reaches £300/kW, this does not happen for B2 and B3, although it can be observed happening initially at the step between 260kW and 270kW target outputs. This is an important aspect to note, as it highlights the importance of sizing these systems appropriately in order to avoid negative impacts and generate the greatest NPVC.

The best-performing combinations of both FESS and BESS were then analysed under a discount rate and TCC sensitivity study to investigate over what range of values each system can provide a positive economic impact. The two configurations being investigated further consisted of configuration F1 with a 270kW target output, and configuration B1 with a 280kW target output. In this section, reference will also be made to the previous study conducted in this chapter, including specifically Figure 4.11. Firstly, the results for the FESS are considered, as shown in Figure 4.19.

When comparing the results in 4.19 with those produced in Figure 4.11 it is evident that for this case study the reality is actually much more favourable for the introduction of a FESS. For this 8C system, a positive NPVC can be achieved across a wide range of different TCC values and discount rates, suggesting that other C-Rates beyond the 8C system used in this study could potentially have an even more significant impact.

As the TCC is increased, the related improvements to NPV are reduced, but even at a TCC of £1000/kW, above the mean value taken from the literature review in Chapter 2, there is still the potential for providing a positive NPVC all the way up to a discount rate of 7%. It is also important to note that the economic performance in this case study, using an 8C FESS, is significantly better across the entire range of values when compared to the 5C and 10C systems shown previously in Figure 4.11.
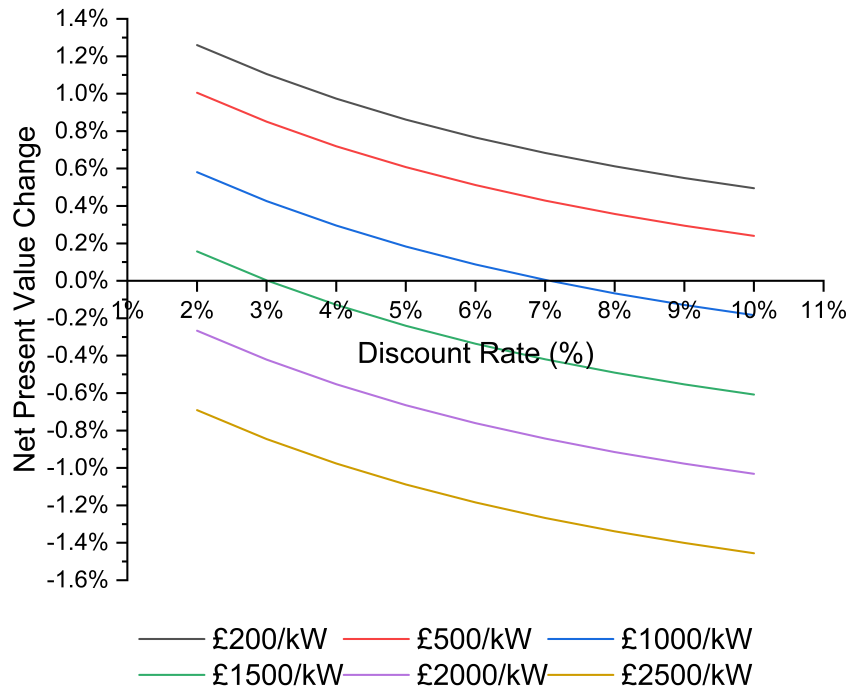
Figure 4.19: NPV change for varying discount rates and TCCs for a 7.5kWh 8C FESS at a site with a targeted output of 270kW

This suggests that actually, a wider range of FESSs could be viable in real-world scenarios than previously suggested.

Conversely, for the BESS sensitivity analysis, the results do not look quite as promising. Referring back to the previous subsection (specifically Figure 4.17), it is clear that the impact of the degradation on the BESS is having a significant impact on the ability for the BESS to provide a positive economic impact.

Only under a £200/kW TCC does the BESS provide a positive NPVC across the entire range of discount rates, and will only provide positive NPVC at a TCC of £500/kW for a discount rate of 2% and 3%. It appears that unless the BESS can be deployed at a lower TCC than the current approximation of around £400/kW, then it would have a negative impact on the economic performance of the site.

### 4.4.3 Discussion

A case study has been presented exploring the techno-economic potential of both FESSs and BESSs for assisting a real-world site operating under ELS restrictions. This study has been vital in providing context to the theoretical work conducted in the first part of the chapter.

From a technical perspective, the BESS configurations performed generally better than the FESS configurations due to the increased energy capacity from the
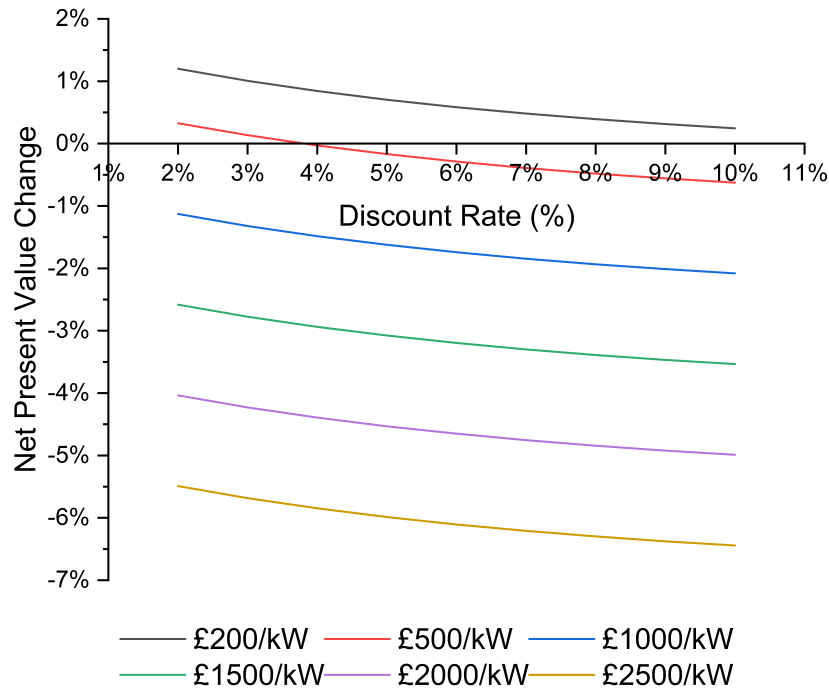
Figure 4.20: NPV change for varying discount rates and TCCs for a 30kWh 1C BESS at a site with a targeted output of 280kW

configurations studied. However, the performance gap is not significant enough to indicate a preference for one ESS technology or the other. Additionally, there is the potential for different configurations from different manufacturers to perform either better or worse than those discussed in this chapter. The key takeaway from a technical perspective is the evidence that an ESS can be introduced to effectively assist an export limited site on a smaller local scale with the potential to improve performance at many sites across Great Britain currently operating under such schemes.

In terms of the economic sensitivity analysis, it has been shown that the excessive strain placed upon a BESS being used for this application and the subsequently required replacement rates of the BESS units has a significant impact on its ability to be economically viable. The FESS on the other hand can easily withstand the required cycle rates and provides a strong economic performance across a range of different TCC and discount rate values. This study provides real impactful data to build upon when considering an emerging area of research, whilst also informing the industry on the impact that can be achieved for DG owners and FESS developers alike.

# 4.5 Chapter Conclusions

This Chapter presented a first-of-its-kind study into the feasibility of utilising FESSs to mitigate the effect of ELSs at a wind generation site. At a high level, it has been shown that there is significant potential for FESSs to be applied to this area with them providing a solid technical level of performance across a range of different scenarios.

First, a detailed theoretical techno-economic study was conducted to explore the potential for implementing FESS into a site subjected to ELS. The results of this study showed that across a wide range of FESS configurations and economic parameters, a significant benefit can be introduced by installing a FESS. This is important in opening up a new area of research for implementation of FESSs as well as the exploration of other storage technologies and is significant in showing the potential gains that can be achieved.

These studies have been conducted for specific wind speed profiles, and hence if profiles from different locations were utilised the results may vary. However, using the varying levels of limitation has shown how these ESSs operate under different conditions. At sites with more sustained periods of high wind speeds then the Limited Time Proportion would be higher, meaning larger energy stores would be more suitable whilst at sites with less wind energy available would likely lead to smaller energy stores being more appropriate.

The case study, presented in the second half of this chapter, shows that the research presented is viable in a real-world scenario with the potential to provide a positive techno-economic impact to DG sites across Great Britain. It has been shown for the site studied that whilst a FESS can have a positive economic impact across a wide range of parameters, a BESS can only be profitable in a narrow band of circumstances due to excessive cycling requirements. The work presented here can have a significant impact on both real-world DG sites and FESS manufacturers, as well as providing direction for future research into the development of FESSs and the type of system that will need to be developed to fully realise the potential of this application.

A key outcome of this study is the detailed guidelines surrounding the economic considerations of this application. For the first time, an outlook of the required TCC for their systems to be viable for deployment in this field is produced, something that provides a strong basis for further investigation for other applications. The theoretical research has been shown to be sound with a detailed real-world case study.

At the beginning of this chapter, the objective of exploring the potential for FESSs to be installed to effectively enhance export limited generation sites was

discussed. This objective has been comfortably met, with a wide range of sound conclusions drawn from the work presented, ultimately showing that FESSs are suitable for this type of application. Additionally, the economic framework objective of this chapter has also been met, providing extensive data on the technical and economic parameters that will need to meet in order for FESSs to be able to be deployed for this application.

# Chapter 5

# Flywheels as Standalone Providers of Frequency Response Services

## 5.1 Introduction

One of the most prominent applications that ESSs are being developed and deployed for is providing frequency response services. By far the most popular ESSs to be deployed for this purpose are BESSs [53]; however, with such services, BESSs do have specific drawbacks when used for this application due to their high susceptibility to cycle based degradation [230]. On the other hand, higher C-Rate ESSs cannot provide the service for long enough to be viable as standalone systems due to reaching high or low SOC limits too quickly to sustain long periods of frequency deviation in a single direction.

This section concentrates specifically on the DFR service offered by NGESO [231], an existing frequency response service for the Great Britain grid with extensive publicly available data. This represents a good benchmark for assessing the effectiveness of ESSs delivering frequency response services in general. The chapter begins with a literature review of ESS provision of frequency response services, specifically concentrating on the use of FESSs for this purpose although the application of HESSs is also discussed.

The main technical contribution of the chapter comes in the form of a techno-economic analysis of a standalone FESS providing DFR, showcasing both the benefits and challenges that are faced when attempting to use FESSs for this application. The study is then evolved into a hybrid study, introducing varying sizes of BESS to be co-located with the FESS (creating a HESS) to analyse the effect that hybridisation has on the techno-economic performance of the site.
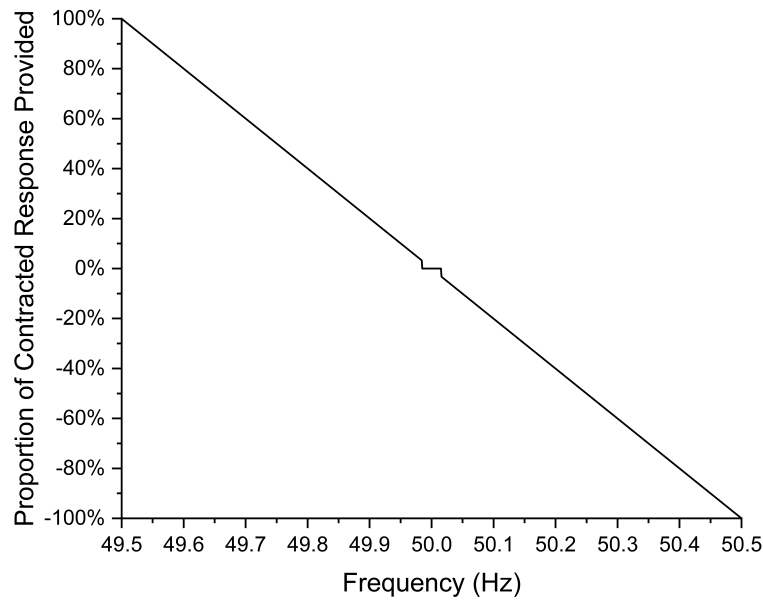
Figure 5.1: DFR Response Envelope

## 5.2 Literature Review

DFR is a service offered for the Great Britain grid and is defined in relation to the response envelope shown in Figure 5.1. The basic premise of the service is that as the frequency deviates further from the rated frequency of 50Hz, the contracted ESS will provide higher proportions of either the rated charging or discharging power [231]. The central region of Figure 5.1 represents the 'dead-band' where no response is required from the ESS.

The main metric for measuring an ESSs ability to provide DFR is termed 'Availability' and is expressed as a percentage of time that the output of the ESS matches the requested output from the service, as shown in Equation 5.1 where $P_{\text{DFR}}$ is the power requested by the service, $P_{\text{ESS}}$ is the power provided by the ESS, and $t_{\text{end}}$ is the overall contracted delivery period, or in the context of this research, the simulation time end as the service is being modelled on a 24/7 basis. This metric is highly important, as it is used as a basis for determining whether payment is provided for that service period, with payments reducing as soon as the availability drops below 95% [232]. The ESS will drop below 100% availability when it either reaches its low SOC limit and is unable to discharge if requested to do so or if it reaches its high SOC limit and is unable to charge when requested to do so.

Throughout this thesis, the approach has been taken to simulate the 24/7 delivery of these services in order to provide easily comparable results between different operations and help inform the ongoing development of these services. For a real-
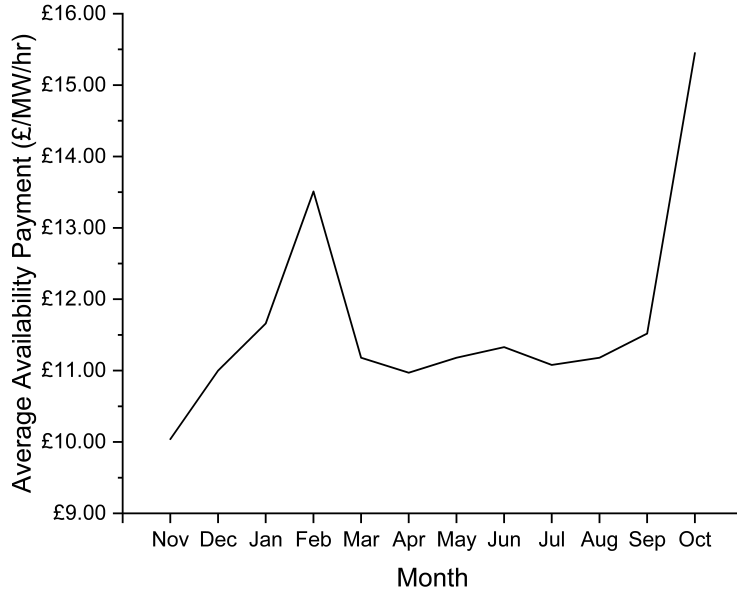
Figure 5.2: Average availability payments to ESS units between November 2020 and October 2021

world installation, the provision of the service would be subject to operator success in bidding for delivery periods, alongside other revenue opportunities in the balancing and wholesale markets. The maximum available revenue to a site performing this service would be to participate in all periods, and hence if a ESS solution can be found that achieves 100% availability across a whole year then this could have a significant impact on ESS deployment. Additionally, the connection costs of a grid-connected ESS mean that the benefits of providing a service, even at a low availability fee, would outweigh not providing the service by covering the connection costs.

$$A_{vail}(\%) = \frac{\sum_{t=0}^{t_{end}} x}{t_{end}} \begin{cases} x = 1 \ P_{DFR} = P_{ESS} \\ x = 0 \quad otherwise \end{cases} \tag{5.1}$$

Payment for this service is based upon a tendering process, and Figure 5.2 shows the average availability price across all accepted tenders from ESS units between November 2020 and October 2021. This time period has been chosen to align with the frequency data used throughout this thesis, which covers the same period of time. The overall average availability payment is £11.67/MW/hr, which is the value that will be used in all financial calculations going forward.

Another service commonly discussed within literature is enhanced frequency response which is a separate service that was offered by NGESO and that has since been discontinued. Whilst the service itself will not be offered out for auction again,

there still exists a wide range of research on the topic which can be used to inform research into DFR and other frequency response services.

The relevant research for BESSs providing DFR falls into two broad areas, economic-based studies and studies concentrating on degradation effects from providing the service including how best to mitigate against this.

In terms of nomenclature, 'Frequency Response' is often referred to as 'Frequency Regulation'. However, these terms are also often used to refer to responding to very short-duration frequency events, rather than the continuously operating services discussed in this thesis. This type of frequency regulation is not within the scope of the work contained in this thesis.

A key study in [233] discusses the market within the New York Independent System Operator portion of the electrical grid in North America. Whilst there is no technical study undertaken and the paper is more focused on explaining the mechanisms available, there is an important aspect raised that claims an energy storage system would be expected to see over 6,000 cycles per year operating as a frequency regulation service. Clearly, this would be excessive for some forms of ESS susceptible to cycle-based degradation.

A significant area of research focuses on extending the life of a BESS being used for frequency response services. In [159] the approach taken is to use a specific control mechanism to maintain the BESS SOC within a certain range. Whilst the study concluded that a positive NPV was achievable, this came with the caveat that no BESS control method led to a lifetime longer than 5.9 years, however, this is based on simulated rather than experimental data and hence should be treated with caution. This thesis defines end-of-life as a reduction to 80% of the original battery capacity.

A similar study into BESS degradation whilst performing frequency response services is undertaken in [234] where different methods of control and participation are analysed to determine their effects on the degradation of a Li-ion BESS. In this paper, it is claimed that the maximum lifetime achieved was 13.5 years under favourable conditions, with the shortest lifetime achieved being just 4.8 years. Again, this suggests a significant interest in the area of extending the lifetime of BESSs providing frequency regulation, and that more work needs to be undertaken to begin to consistently achieve longer lifetimes. This work is again simulation-based, however, this does allow more direct comparisons with the simulation-based studies in this thesis.

Continuing in the area of battery energy management, the works in [235] and [236] discuss various methods of managing the SOC of a BESS whilst providing enhanced frequency response. Both studies consist of in-depth technical assessments with [235] then also considering revenue possibilities when combining with other

services. Again, this work concentrates on the control of the BESS to extract maximum performance, whereas consideration could also be given to the hybridisation of the system to provide a performance boost.

In terms of studies on FESSs providing frequency response services as a standalone unit, there is minimal literature available due to their perceived unsuitability for this application. The main area of research that has parallels with that contained in this thesis is the work on frequency regulation, where FESSs have been regularly investigated for instantaneous frequency event management [110] [117] [31]. One such study is the work in [237] which discusses high-speed flywheels for voltage and frequency support, and concludes that the FESS is well suited to the application. In [238], a hardware-in-the-loop approach is presented for utilising flywheels for frequency support, with the results claiming again that a FESS is suitable for deployment in this area. A key aspect to take away from this work is the fact that the FESSs are suggested to be fast-acting in response to frequency deviations, and if this ability can be extended to providing continuous rather than instantaneous support, then they could have a significant impact and suggests an area of work that is worthwhile further exploration.

By far the most relevant piece of work previously conducted in the field of BESS/FESS hybrids is that presented in [102]. This work looks at utilising FESSs to counter the ageing of a BESS providing frequency response. Whilst this study is promising, especially in its conclusion of a circa 20% extension of battery lifetime, there are significant gaps that can be exploited and improved upon. The main area that is not considered by the work is that the analysis is conducted on a generic level, with little analysis of the actual performance of the system in providing the service. Additionally, the ageing cycles are repeated short-duration events, rather than a long-scale simulation exposing the system to different types of charge profiles. Finally, no economic analysis is conducted to determine whether this battery life extension would be offset by the cost of introducing the flywheel. Clearly, there is significant scope for a far more in-depth study from both a technical and economic perspective.

Generally, then, it can be seen from the literature that a gap exists for both the provision of frequency response services by very short duration storage such as FESSs, and for the hybridisation of systems to extract maximum techno-economic benefit.

## 5.2.1 NPV Calculations

Throughout this chapter, and continuing throughout the rest of the work contained in this thesis, reference is made to calculating the NPV of the system. This equation

has previously been detailed in Equation 3.2 (in Chapter 3), and for the purposes of this chapter the revenue of the site ($C_{\text{revenue}}$) is calculated as shown below in Equation 5.2

$$C_{revenue} = 0.5 A_{Fee} P_{ESS} P_{Factor} \begin{cases} A_{vail} > 95\% & P_{Factor} = 1 \\ 60\% < A_{vail} < 95\% & P_{Factor} = 0.75 \\ 10\% A_{vail} < 60\% & P_{Factor} = 0.5 \\ A_{vail} < 10\% & P_{Factor} = 0 \end{cases} \quad (5.2)$$

Where $A_{\text{Fee}}$ is the availability fee (set as £11.67 as detailed above), $P_{\text{ESS}}$ is the rated power being delivered by the site in MW and $P_{\text{Factor}}$ is the performance factor corresponding to the availability calculated for that period using Equation 5.1. The equation is multiplied by 0.5 to represent the calculation being calculated in half-hourly periods.

## 5.3 Techno-economic Analysis of FESSs Providing DFR

This section discusses the techno-economic assessment of both an independent FESS and a hybrid FESS/BESS system when performing DFR services providing novel results on the technical effectiveness of these systems to meet the required performance criteria and the required TCC to produce a system economically viable for operation in this market. The work contained in this section is important in both exploring the capabilities of standalone FESSs and in emphasising the advantages gained by considering hybridisation as an option when delivering these services.

### 5.3.1 FESS-Only Analysis

FESS configurations have been assessed by keeping the power rating constant and changing the C-Rate. In the first (FESS-only) analysis the system was matched as a 1MW service with a 1MW FESS with the C-Rate being varied to represent changing energy capacity. The simulations consisted of running a DFR service 24/7 across a year utilizing frequency data from November 2020 to October 2021. The C-Rates have been chosen to represent the range of FESS configurations available in today's market, ranging from 0.25C to 20C. Table 5.1 shows a summary of the different configurations used in the analysis.

Table 5.1: FESS Configurations analyzed in FESS-Only DFR study

| Configuration | Energy (kWh) | Power (kW) | C-Rate |
|---|---|---|---|
| A | 4000 | 1000 | 0.25 |
| B | 1000 | 1000 | 1 |
| C | 400 | 1000 | 2.5 |
| D | 200 | 1000 | 5 |
| E | 100 | 1000 | 10 |
| F | 66 | 1000 | 15 |
| G | 50 | 1000 | 20 |

**Technical Analysis**

The main performance metric for the system is to remain available for response services at least 95% of the time. If the system has no stored energy (0% SOC) then it is not available for export, if it has reached capacity for energy stored (100% SOC) then it is not available for import. The equation for availability has been defined previously in Equation 5.1.

Initially, the average availability was calculated across the 12 months studied (November 2020 to October 2021), with the results of this shown in Figure 5.3. The first conclusion to be drawn is that there is significant variability in the demands present from month to month, with some months such as March and December showing significantly lower availability than less strenuous months such as April and January. This is noted as it does highlight a certain degree of unpredictability inherent in providing this service.

Figure 5.3 shows that for time period studied the 95% target is achieved across all months for configurations A and B whilst failing to reach this for 3 out of 12 months for configuration C. Configuration D maintains an average availability of more than 90% across the year but all higher C-Rated systems fall below the 90% mark meaning they would be less desirable for the DFR service. This shows how important energy capacity is for providing this service, and suggests that more power-centric FESSs may not be suitable as standalone ESSs. The results contained in Figure 5.4 help inform this conclusion, showing the average availability falling dramatically as the energy capacity is reduced.

The energy throughput shown in Figure 5.4 illustrates how the changing C-rate affects the performance of the system for this metric along with average availability across the whole year. Configuration A will provide the best performance in this regard, with a steady decrease in energy throughput as the C-Rate is increased (due to their decreasing energy capacity) which is tied intrinsically to the availability of the system.

From the C-Rate analysis conducted, the range of viable C-Rates for a power-
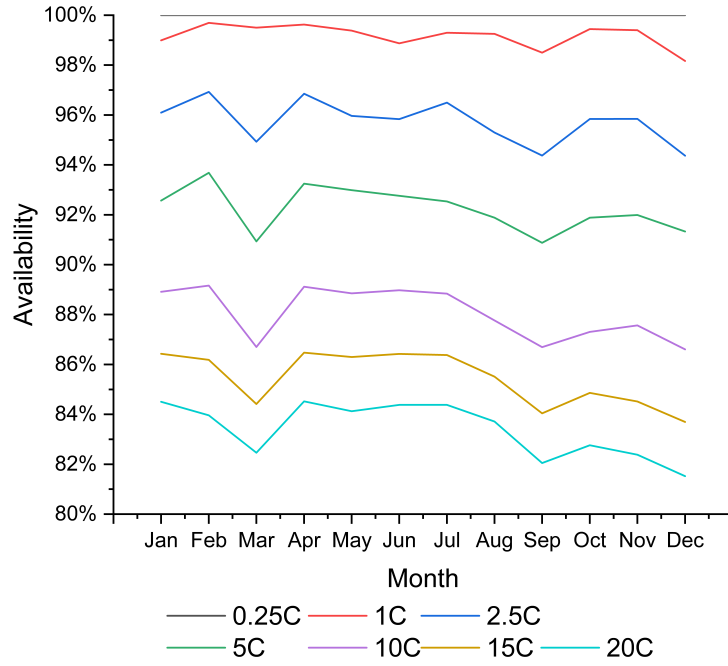
Figure 5.3: Availability per month for varying configurations of FESS
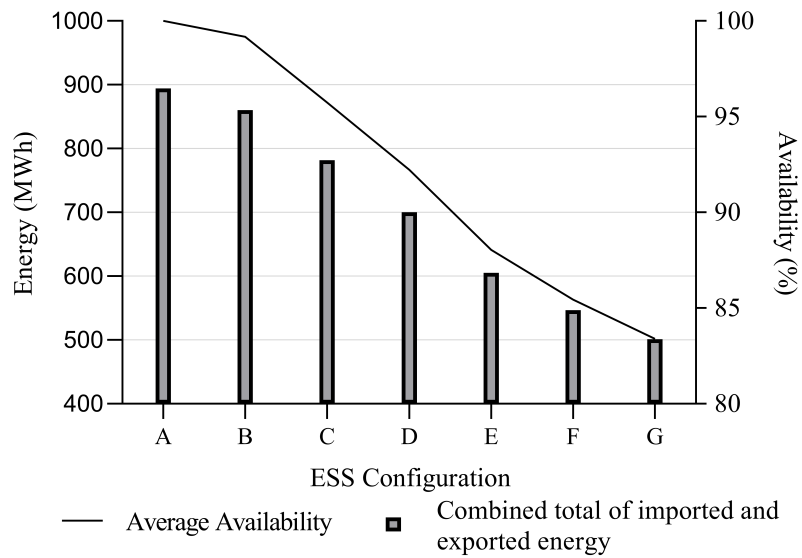


Figure 5.4: Average availability and energy throughput across the year for varying configurations of FESS

Table 5.2: Performance statistics for varying FESS configurations performing DFR

| Configuration | Average SOC (%) | Cycles per Year |
|---|---|---|
| A | 77 | 742 |
| B | 61 | 1322 |
| C | 54 | 2341 |
| D | 52 | 3828 |
| E | 51 | 6292 |
| F | 50 | 8373 |
| G | 50 | 10138 |

matched system is between 0.25 and 2.5C. When considering average availability across the year, this metric goes from 100% average availability for a 0.25C system to 99.18% for a 1C system. The only other system with an average availability above 95% is configuration C which recorded a 95.74% average availability across the year which is a fairly significant drop off in overall availability. Again, whilst this does not suggest the traditional configurations of FESS would work for providing this service, it does not rule out FESSs generally as there are similar configurations available on or coming to the market.

Table 5.2 shows the results of further performance monitoring tests. There is a clear increase in the number of cycles per year as the C-Rate is increased and with life cycle estimates for existing Flywheels previously discussed as ranging from 100,000 to 500,000+, flywheels at the lower end of this estimate may struggle to provide sufficient lifetime at higher C-Rates.

**Economic Analysis**

For the economic analysis, the FESS TCC was varied between £200/kW and £900/kW. This range of values was chosen after an iterative simulation process showed this range to sufficiently show the financial trends in both directions for analysis purposes and falls in line with the lower end of the power based TCCs detailed previously in Chapter 2. The results of calculating the NPV of the system over an operational period of 20 years for different TCC values and FESS configurations is shown in Figure 5.5. The discount rate was set at 8% for this study, intended to represent the fact that this application is already dominated by BESSs, and as such any competing technology would need to offer an attractive return in order to be considered.

At the lower end of the C-Rate scale, the 0.25C and 1C systems both cross the threshold into positive NPV from £500/kW and lower. This is likely to be achievable as further advancements in flywheel technology are made, but would only represent a marginally positive NPV. More strenuous targets would be the £400/kW threshold for a 5C system which would require more significant advancements to be made.
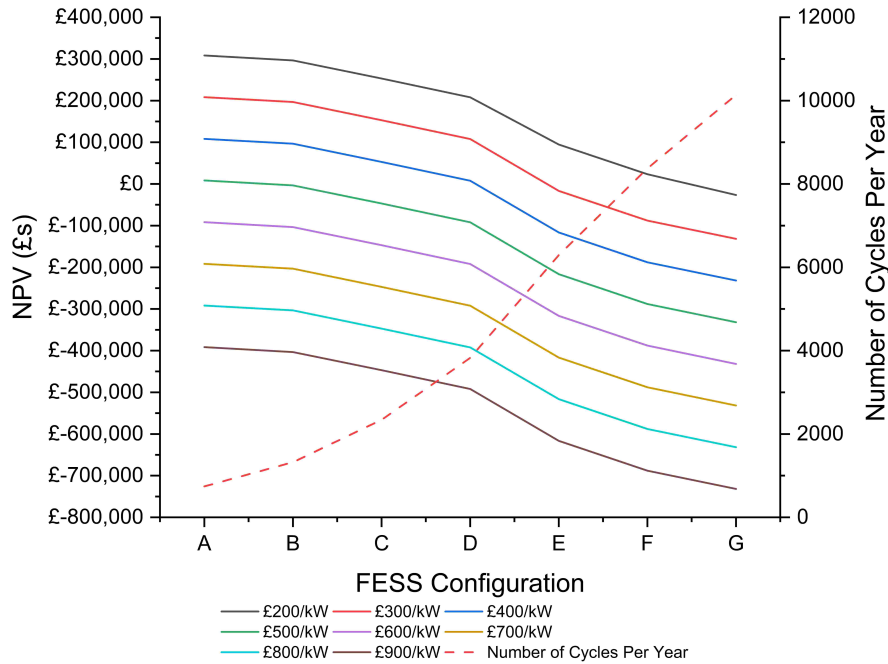
Figure 5.5: NPV for a 20-year lifespan for varying configurations of FESS

A 15C FESS only achieves positive NPV at a target price of below £250/kW whereas a 20C FESS would have to reach a target TCC of lower than £200/kW to achieve a positive NPV. This is not a realistic aim considering the previously discussed average £/kW value of £780/kW and therefore these should be considered unlikely candidates for providing this service.

There is a sizeable decrease in the economic prospects from configuration E to G, and this is mainly due to the rapidly increasing number of cycles leading to a potential for the system not achieving a 20-year lifespan.

The total cycle limit was been set at 100,000 to represent the lowest commonly referred value within the literature; however, a higher NPV could be achieved for the higher C-Rate systems if this limit were to be increased. For example, with configuration G experiencing 10,138 cycles per year, it would require a threshold set at 206,360 to increase the NPV by reducing the replacement system costs. This would not be an unreasonable cycle limit to assume considering the cycle limits stated by FESS manufacturers, and the study was repeated considering a 250,000 cycle limit.

The results of increasing the cycle limit available are immediately apparent in Figure 5.6 for configurations E, F and G. Whilst still seeing a decreasing level of NPV, the decrease is now much more shallow, as even the worst performing configuration (G) can now achieve a positive NPV under a £200/kW TCC. Whilst it is unlikely that this price point would become a reality, it now opens up a wider range of configurations for potential use in this application.
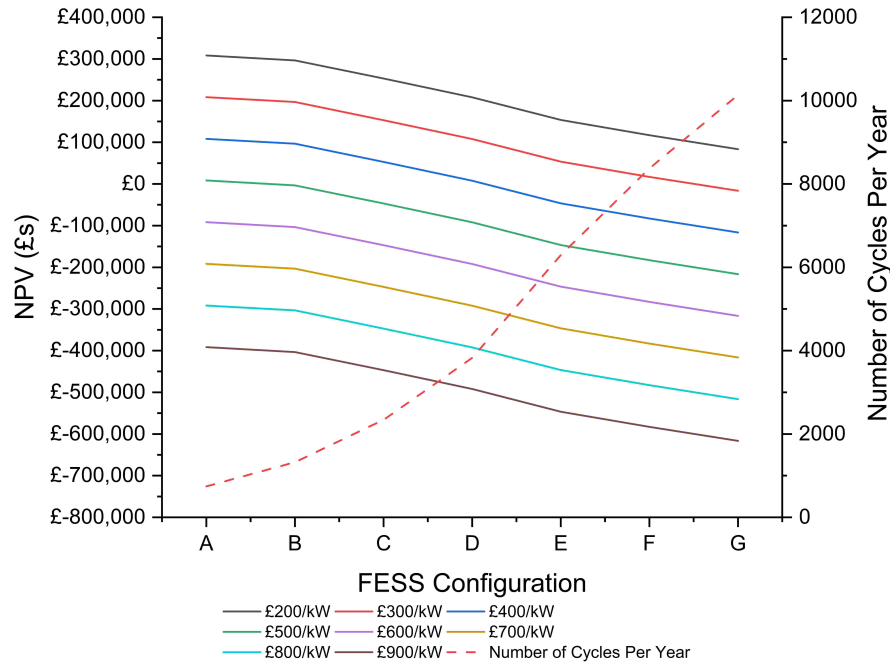
Figure 5.6: NPV for a 20-year lifespan for varying configurations of FESS with increased cycle lifetime

Whilst the 0.25C and 1C FESS both produce promising results with good technical and economic performance, they are of the less common energy-centric type of FESS. A likely target range for more widespread FESS configurations of 2.5-5C aiming for no more than £400/kW could provide a financially viable FESS-only DFR service. However, it must be considered that these results are associated with a discount rate of 8% and hence higher TCC values would result in a positive NPV if a lower level of profit was allowed for.

To illustrate this, a discount rate sensitivity study was conducted for configurations B, C and D which were identified as the most realistic options for FESS configurations under current market conditions. The discount rate was varied between 2% and 10% with the results shown in Figures 5.7-5.9.

Immediately it becomes apparent that by reducing the discount rate, a far more promising picture for the viability of a FESS providing these services emerges. Even configurations C and D are able to provide significant positive NPV scenarios across a much wider range of TCC with lower discount rates.

The best-performing system is still configuration B, which can provide a positive NPV for all discount rates when the TCC is £400/kW or below, whilst when looking at the more realistic region of £700/kW the configuration can still provide a positive NPV across discount rates ranging from 2-4%. However, at £700/kW for configurations C and D, there are fewer positive results, with C providing positive NPV at discount rates of 2-3% and D only providing positive NPV at 2%.
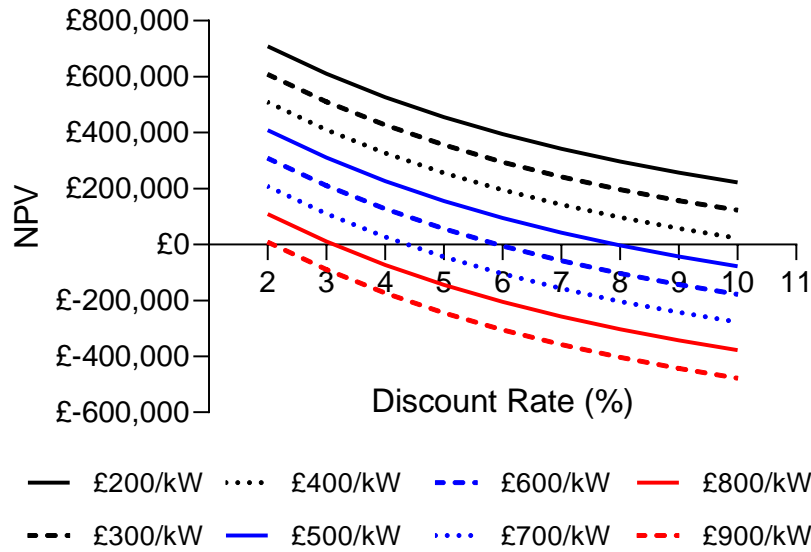
Figure 5.7: Discount and TCC Sensitivity Analysis for Configuration B

This sensitivity analysis highlights the fine line between economic viability and negative repercussions. For configuration B (the 1C system), 59.7% of the studied combinations resulted in a positive NPV, whilst for configuration C (2.5C system) this value is 51.4% and for configuration D (5C system) the value is 44.4%.

The information presented so far details an indication of the challenges when considering FESS capability of providing standalone DFR services. However, it is clear that the energy capacity of the FESS is a significant disadvantage when considering the higher C-Rate systems. The question then needs to be asked, for a system such as configuration D, which stands at the edge of achieving the requisite technical levels of performance, what can be done to increase the effectiveness of its implementation? It is from this starting point that this thesis now begins to consider the benefits of hybridisation of FESSs and BESSs to attempt to extract further value from the respective systems.

## 5.3.2 Hybrid Analysis

For this section, configuration D has been chosen to be studied further in a hybrid scenario, as this configuration represents a fairly common FESS C-Rate specification, as well as showing promising results without quite achieving the ideal level of 95% average availability. For this reason, it is an ideal candidate to take forward to understand the effects of hybridisation in this way, and determine if a better techno-economic performance can be achieved.

A key criterion of the hybridisation scheme is to ensure that the required power rating of the system (1MW) is maintained across all configurations. For this reason,
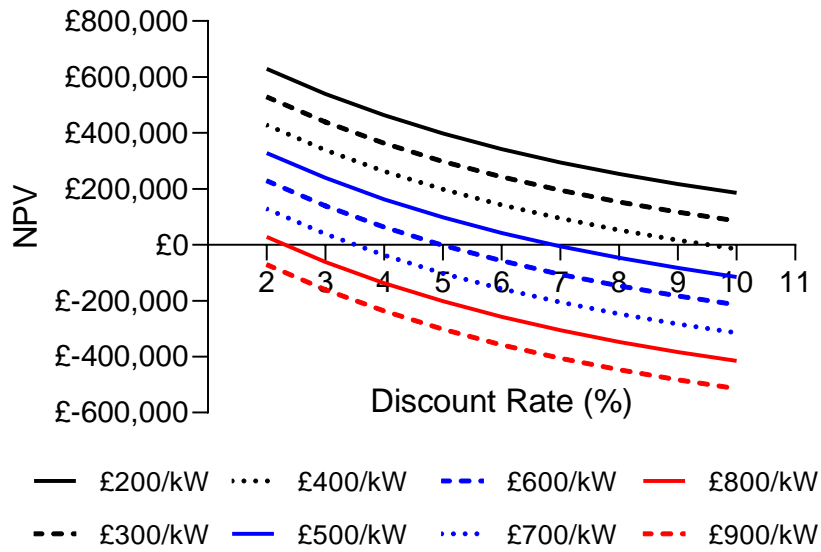
Figure 5.8: Discount and TCC Sensitivity Analysis for Configuration C
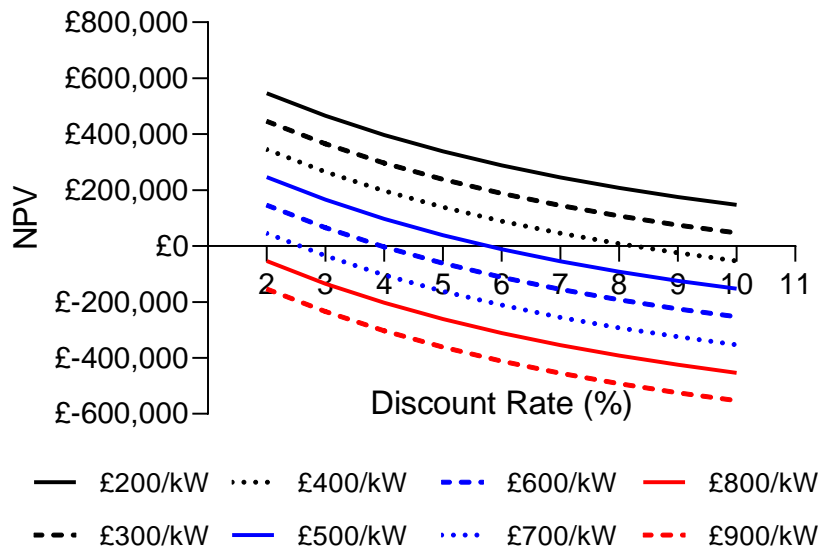


Figure 5.9: Discount and TCC Sensitivity Analysis for Configuration D

Table 5.3: Hybrid Configurations analyzed in HESS DFR study

|   | FESS kWh Rating | FESS kW Rating | C-Rate | BESS kWh Rating | BESS kW Rating | C-Rate |
|---|---|---|---|---|---|---|
| D | 200 | 1000 | 5 | - | - | - |
| H | 200 | 1000 | 5 | 50 | 50 | 1 |
| I | 200 | 1000 | 5 | 100 | 100 | 1 |
| J | 190 | 950 | 5 | 50 | 50 | 1 |
| K | 180 | 900 | 5 | 100 | 100 | 1 |
| L | 160 | 800 | 5 | 200 | 200 | 1 |

two different approaches have been taken, with the configurations to be studied shown in Table 5.3. The first approach, with configuration H and I, represents an additional quantity of BESS being introduced on top of the existing FESS that was analysed as configuration D. The second approach consists of decreasing the size of the FESS and replacing this with different amounts of BESS capacity as shown with configurations J, K and L.

The control strategy for the hybrid system operates such that the FESS will fulfil any request that it is able to, and only in the event of the FESS being unable to fulfil the request will the BESS operate. This control strategy is discussed in more detail in Section 6.2.

**HESS Technical Analysis**

Figure 5.10 shows the technical performance of the different hybrid configurations. The main aspect to note is the fact that the average availability over the course of a year increases by at least 1.5% across all configurations, with the peak increase occurring under configuration L which achieves an average availability of 94.1%. Were the energy capacities of the BESS portions to be increased further then this would have a knock-on effect of increasing the average availability.

Additionally, there are positive increases to the overall energy throughput of the system, illustrating the hybrid configurations' abilities to operate for longer periods of time before reaching SOC limits.

The remaining performance characteristics are shown in Table 5.4 and show a similar pattern of slight performance benefits from the introduction of a hybrid system.

As the FESS size is reduced, the number of cycles it is exposed to increases, with configuration L expected to complete 89,900 cycles over 20 years. It is clear that further reductions in FESS size beyond that specified in configuration L would likely result in a cycle limit of 100,000 being reached before the specified 20-year lifetime and hence having a potentially significant impact on economic viability if
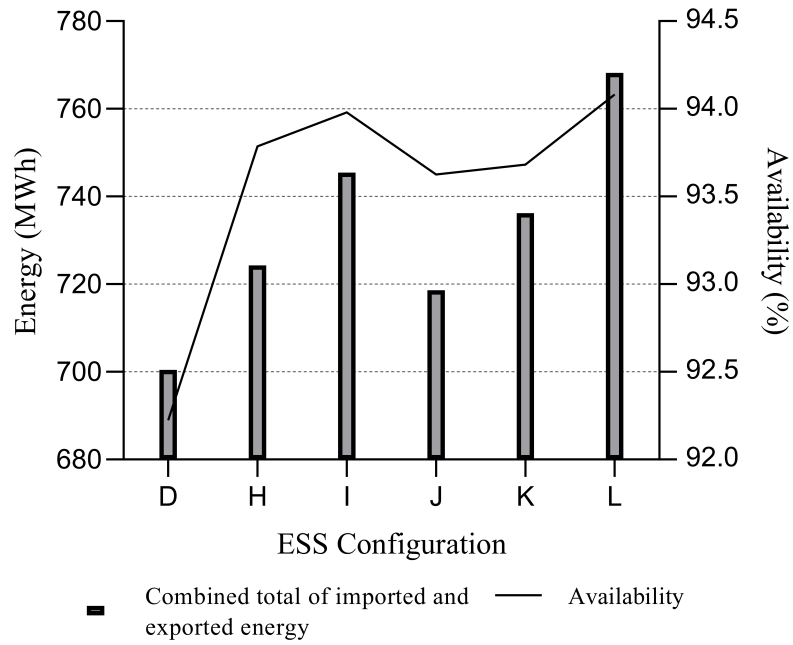
Figure 5.10: Average availability and energy throughput across the year for varying configurations of HESS

Table 5.4: Performance statistics from hybrid configurations study

| Configuration | Average SOC Flywheel | Average SOC Battery | FESS Cycles | BESS Cycles |
|---|---|---|---|---|
| D | 51.82 | - | 3828 | - |
| H | 49.29 | 47.61 | 3829 | 434 |
| I | 49.29 | 48.38 | 3829 | 429 |
| J | 49.27 | 47.55 | 3973 | 458 |
| K | 49.25 | 48.32 | 4130 | 477 |
| L | 49.20 | 48.57 | 4495 | 478 |

using a system that specified this lower cycle limit.

The number of BESS cycles for all configurations leads to a 20-year cycle expectancy of between 8580 (configuration I) and 9560 (configuration L). In this study, the cycle limit has been assumed to be 10,000 before system replacement would be required and therefore any excess cycling beyond this limit could have a significant impact on economic viability. However, some literature suggests cycle limits lower than this, and that should be taken into account when considering the data produced here. The cycle intensity should be a key consideration when sizing ESS for frequency response services and the balance between the two different ESS technologies cycle capacities that make up the HESS should be carefully managed, with any ESS utilised being chosen with specific cycle limits in mind.

**HESS Economic Analysis**

For the economic portion of this analysis, the FESS TCC has been set to £780/kW in line with the average found previously in the literature review. From the baseline NPV for configuration D at this TCC, further analysis has been undertaken to assess the impact of BESS TCC and discount rate on the feasibility of hybridisation from an economic standpoint. The results of this analysis are shown in Figures 5.11 - 5.13.

This analysis reveals several interesting trends. For analysed TCC values of £600/kW and above configuration J is the option that consistently performs best. This is due to the small amount of BESS required for this configuration, so the benefits provided are less affected by the higher TCC.

In the other direction, at lower TCC values, configuration L provides the highest NPVC again due to the complex balance between increase in performance and cost. As the BESS cost goes below the FESS cost, it becomes more beneficial to replace more of the FESS with quantities of BESS. Thus there is a balancing act to be achieved depending on the relevant costs of each component.
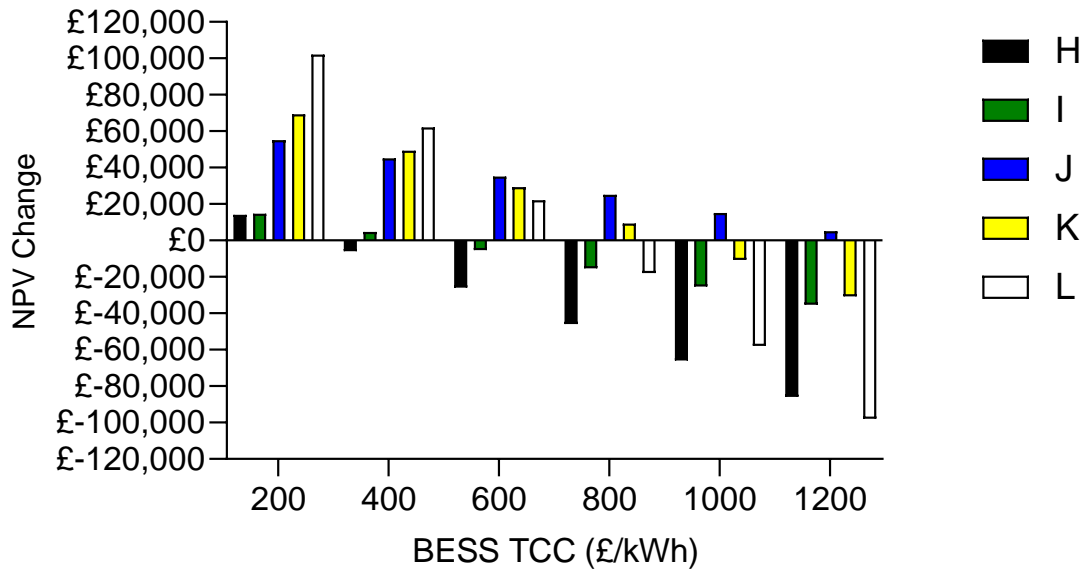
Figure 5.11: NPV Change under different HESS Configurations for a discount rate of 4%
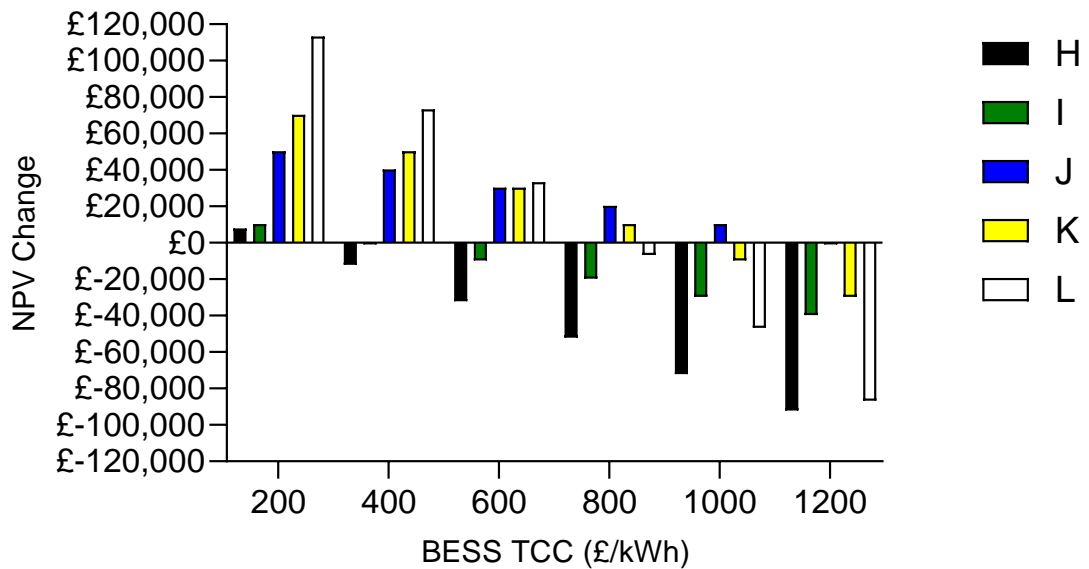


Figure 5.12: NPV Change under different HESS Configurations for a discount rate of 6%
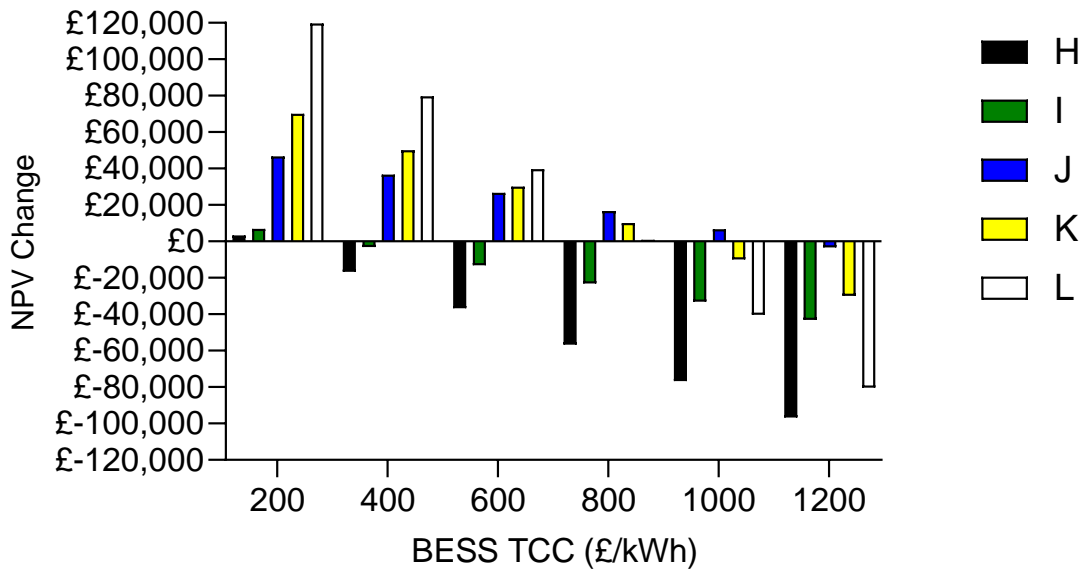
Figure 5.13: NPV Change under different HESS Configurations for a discount rate of 8%

Additionally, it is interesting to note that at the lower end of the BESS TCC values, increasing the discount has a positive effect on the NPVC. This runs counter-intuitively to the common understanding of NPV; however, it is easily explained by acknowledging that as the discount rate is changed, the baseline NPV of configuration D is also changing. Consequently, the effect of hybridisation is actually having more of a positive effect as a ratio of the original NPV.

This conclusion now leads us to consider the actual NPV achieved by these systems, and whether the increases seen under these varying scenarios are sufficient to make the selected configuration (D) economically viable. To illustrate this, the base NPV values when using a TCC of £780/kW for the FESS and the best-performing value of £200/kW for the BESS are shown across varying discount rates in Figure 5.14.

Despite the hybridisation improving the NPV in all of these scenarios, the NPV remains negative unless the discount rate is reduced to 2%. This leads to the conclusion that whilst the NPV can be improved, the system as a whole is still likely to not be economically viable.

To further explore this, the section will conclude by considering the effect that hybridisation has on configurations B and C. To do this, the analysis previously conducted was repeated for both configurations in order to replicate the results shown previously in Figure 5.14 but for the two new configurations. Once again, the FESS TCC was set as £780/kW with the BESS TCC set as £200/kW to illustrate the best case scenario for BESS impact when installing with a FESS of average

152
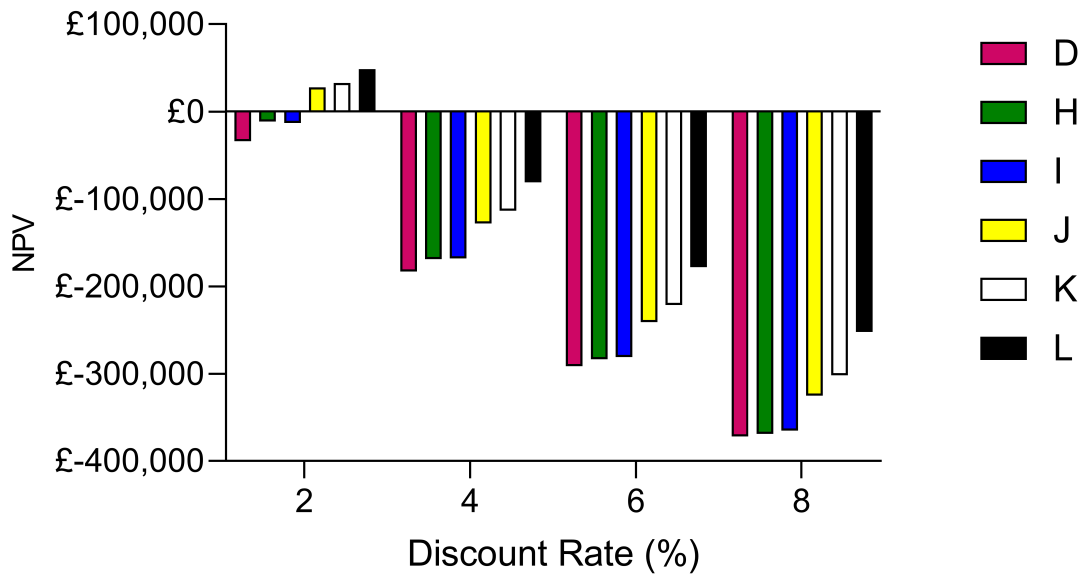
Figure 5.14: Total NPV under different HESS Configurations for varying discount rates from a baseline of Configuration D

cost. The results of this analysis are shown in Figure 5.15 and 5.16. The updated Configurations considered in this analysis are shown in Table 5.5

As expected, the hybridisation with Configuration B produces the highest overall NPV. However, the effect of hybridisation still remains fairly minimal, with a negative NPV only turning positive in one scenario in Figure 5.15, when considering a 4% discount rate for which configuration Q can provide a positive NPV when configuration B does not.

The impact is also not uniformly positive. With Configuration B and C already performing to a higher economic level than Configuration D, there are scenarios where the introduction of a BESS at as low a TCC as £200/kW will have a negative impact on the overall NPV even at the lowest discount rate. This is due to the fact that in these configurations, the addition of the BESS components does not provide a sufficient technical performance boost to offset the additional economic cost.

### 5.3.3 Discussion

Under current economic conditions, it is unlikely that a FESS could be deployed as a standalone system providing DFR. At the price point of £780/kW, only configurations B and C can provide a positive NPV and even then this can only be achieved with a small discount rate of 2%. This suggests that a significant reduction in the cost of FESSs would be required in order for it to be deployed for this application. This section has however opened up the discussion around energy-limited assets for frequency response services, suggesting that the potential is there for deployment,

Table 5.5: Further Hybrid Configurations analyzed in HESS DFR study

|   | FESS kWh Rating | FESS kW Rating | C-Rate | BESS kWh Rating | BESS kW Rating | C-Rate |
|---|---|---|---|---|---|---|
| B | 1000 | 1000 | 1 | - | - | - |
| M | 1000 | 1000 | 1 | 50 | 50 | 1 |
| N | 1000 | 1000 | 1 | 100 | 100 | 1 |
| O | 950 | 950 | 1 | 50 | 50 | 1 |
| P | 900 | 900 | 1 | 100 | 100 | 1 |
| Q | 800 | 800 | 1 | 200 | 200 | 1 |
| C | 400 | 1000 | 2.5 | - | - | - |
| R | 400 | 1000 | 2.5 | 50 | 50 | 1 |
| S | 400 | 1000 | 2.5 | 100 | 100 | 1 |
| T | 380 | 950 | 2.5 | 50 | 50 | 1 |
| U | 360 | 900 | 2.5 | 100 | 100 | 1 |
| V | 320 | 800 | 2.5 | 200 | 200 | 1 |
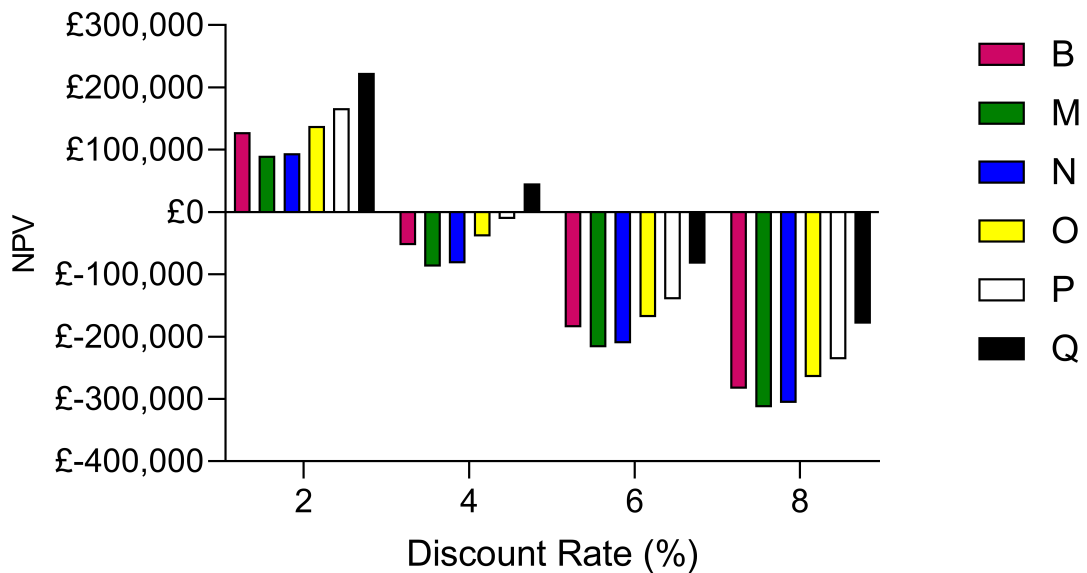


Figure 5.15: Total NPV under different HESS Configurations for varying discount rates from a baseline of Configuration B
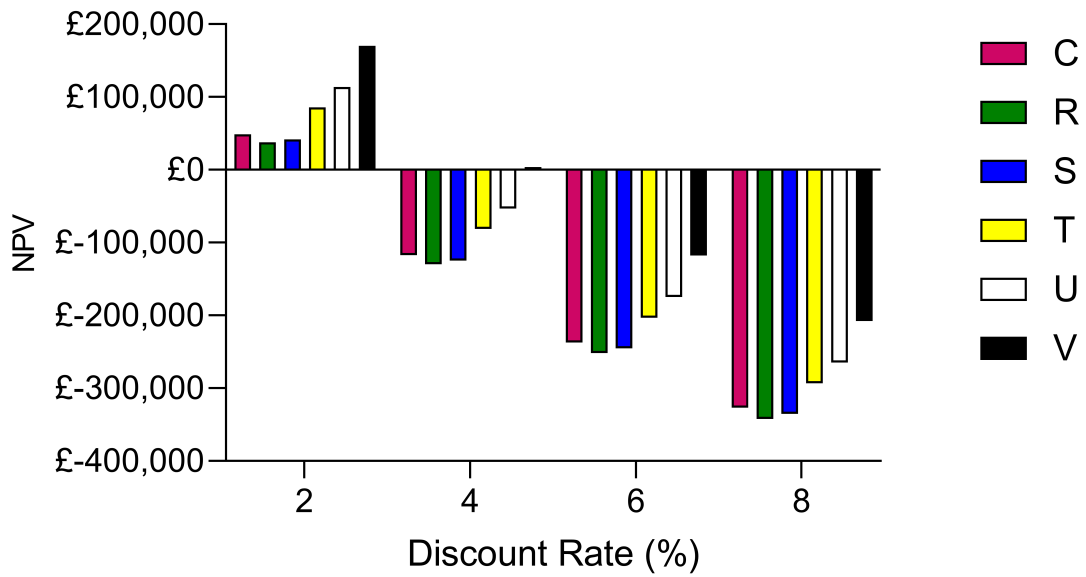
Figure 5.16: Total NPV under different HESS Configurations for varying discount rates from a baseline of Configuration C

but this would require further research and development in order to improve FESS energy capacities and lower costs. It has also provided a detailed set of targets for flywheel manufacturers to meet in both the costing and technical specifications in order to be able to competitively deploy their systems for this application.

In a hybrid scenario, as BESS TCC is increased the impact that it has on the overall NPV is lessened to the point where it will then cause a loss of NPV, with the same sensitivity being present in FESS TCC as well. What this part of the study shows, however, is that the balance between positive and negative techno-economic impact is dependent on many different factors. There are scenarios in which a FESS could operate as a standalone DFR service provider, just as there are then scenarios in which hybridisation with a BESS can improve its techno-economic performance.

However, this should not be taken for granted as a perfect solution as the variables involved have a significant impact on the performance of the site. There will be multiple crossover points between BESS and FESS configurations, discount rates, and TCC of the relevant ESSs where the economic impact swings between positive and negative.

### 5.3.4 Chapter Conclusions

This chapter focused upon the ability for FESSs to provide a DFR service for NGESO. This is an important study in understanding the ability of very short-duration energy storage such as flywheels to play a relevant part in frequency response markets across the world. The results from this study suggested that as a

standalone entity, a FESS with a low C-Rate will be most effective at providing the service, as the 0.5C system showed the best overall performance.

Realistically however, FESSs are rarely specified as high energy assets, and as such further analysis was performed on 1C, 2.5C and 5C systems to determine the conditions under which they can be profitable in providing DFR. The results from this analysis show that whilst the economic performance declines as the C-Rate is increased, there is still potential for a higher C-Rate FESS to provide a positive NPV, especially at lower values of TCC and discount rate. Overall, a comprehensive economic study has been produced over a range of different configurations and variables to illustrate how a FESS can be economically viable in this scenario.

Building upon this, a hybridisation study was undertaken to determine the effect of introducing a small amount of BESS to a standalone FESS. To do this, a configuration shown to have a negative NPV in the previous analysis was used to analyse whether this could become positive through the use of a BESS. In summary, the answer to this question was yes, however, this was only possible under very specific and limited scenarios of low discount rates and very low BESS TCC. It can be concluded from this section that whilst hybridisation can be beneficial, there are other scenarios where a negative impact can be produced. This is an important distinction to make, as it shows that sometimes introducing energy storage can have negative repercussions and as such should be carefully considered depending on application, cost and performance.

Using this work as a baseline, the following Chapter now moves forward into a more detailed assessment of hybrid systems and the ability to exploit further value from such systems through appropriate control and sizing.

# Chapter 6

# Hybridisation of Flywheels for Frequency Response Service Delivery

## 6.1 Introduction

After the introduction to hybridisation in the previous chapter, the contribution of this chapter focuses on the optimisation and operation of a HESS. Firstly, a suite of novel hybrid control methods is introduced and discussed. Two control schemes are then used to showcase the degradation mitigation analysis modelling framework that was introduced in Chapter 3, and the impact that this can have on designing and operating HESSs.

Following this, each control system is assessed on a technical basis before undergoing refinement to improve the performance of the control strategy. This comprehensive analysis using multiple analytical tools provides the first example of an in-depth review of novel hybrid control strategies, different approaches to the refinement of said control strategies, and the impact that these different strategies have on the overall economic potential of the site.

## 6.2 Using a FESS to Enhance a BESS Installation

For this section, the thesis now flips the question of the previous section to consider what impact a FESS can have on a BESS providing a DFR service. This research is particularly important, as BESSs are already widely deployed in this application and plan to be deployed for further similar applications. The possibility of extending BESS lifetime and the associated techno-economic benefits would be beneficial to

Table 6.1: Overview of studies conducted on the novel control strategies

| Control Strategy | Method | FESS Energy Range (kWh) | FESS C-Rate Range | FESS Power Range (kW) | Other Control Variables |
|---|---|---|---|---|---|
| CS-2 | GA | 10-100 | 4-15C | 40-1500 | None |
| CS-3 | Iterative | 30-100 | 4-8C | 120-800 | Lower and Upper frequency thresholds |
| CS-4 | Iterative | 100-1000 | 4C | 400-4000 | Lower and Upper frequency thresholds |
| CS-5 | Iterative | 15-200 | 4-12C | 60-2400 | % contribution from each ESS |
| CS-6 | GA | 10-100 | 4-15C | 40-1500 | Average power calculation ($t_{av}$) |
| CS-7 | GA | 10-100 | 4-15C | 40-1500 | Average power calculation ($t_{av}$) |
| CS-8 | Iterative | 83-200 | 4-12C | 1000 | Duration of time that each ESS operates per hour |

asset owners and the wider electricity grid by enabling assets to continue operating beyond their currently predicted lifespans. This also has environmental implications, by helping batteries to stay online longer it removes the requirement for more regular replacement and increased usage of the materials used in the construction of these systems.

In the following sections, the minimum FESS C-Rate considered is 4C. This is intended to represent the FESSs typical role as a very short duration energy storage. Whilst it is acknowledged that lower C-Rate FESSs do exist, they are far less common and therefore less relevant to the objectives of this section, which focuses on enhancing existing installations rather than providing a standalone service as detailed in the previous chapter. Note that in some cases where multiple similar figures are presented, the axis limits are not constant and therefore care should be taken when comparing figures.

Table 6.1 gives an overview of the approaches taken to studying each control strategy, along with the variables that were used in each process.

## 6.2.1 Novel Control Strategies Overview

Eight different control schemes have been assessed within this work, consisting of a BESS only baseline and 7 hybrid control schemes. Table 6.2 contains a description of each control strategy. The baseline control strategy consists of a 1MW/1MWh BESS delivering a 24/7 1MW service set at a TCC of £400/kW. Using this approach it can be shown how the key metrics such as availability, net present value and BESS degradation change according to hybrid configuration and control mechanism. The NPV is calculated using the same approach as previously defined in Section 5.2.1.

For all of the hybrid control strategies detailed in this section, the BESS specification is kept constant at 1MW/1MWh/1C. This has been fixed to allow direct comparison between the effects that the different strategies and FESS configurations have on the techno-economic performance of the BESS. This was not considered as a variable as the intention of this section is to represent the addition of a FESS to an already existing or pre-planned BESS installation.

Each control strategy has an associated control flowchart. In the following sections, each control strategy is presented with commentary on how it was developed and the goals of investigating the control strategy.

Where included, the SOC limits for the respective ESSs are shown in Table 6.3. These limits are based upon known operational conditions of the different ESSs, and the addition of such limits helps account for aspects such as cell balancing. The limits for the FESS were taken directly from the industrial sponsor's technical specifications whilst the limits for the BESS were taken from those currently in operation at Willenhall ESS.

In general, these strategies have been developed over the course of several years of iterative design and case studies. The knowledge gained from repeated simulations of different hybrid systems has been used to identify areas that could become control variables, which have then been tested and refined over the years to arrive at the 7 control strategies presented in this section. An example of each control strategy operating for 24 hours providing DFR as a 1000kW 1C BESS and 100kW 10C FESS is contained in the Appendix as Figures A26-A32 illustrating how each individual ESS participates in the response service.

Because this process has been iterative over a significant timescale, not all of the control strategies have been investigated in the same way. Initially, Genetic algorithms were utilised in order to explore the typical optimum ranges for the variables involved. Subsequently, the information gained from these studies was used to perform iterative investigations and provide greater insight into the effects of changing certain parameters. Once the control strategies have been introduced and explained, this chapter is broken down to discuss each control strategy in the manner

Table 6.2: Description of each control strategy to be assessed

| Control Strategy Designation | Description |
| --- | --- |
| 1 | A 1MW/1MWh battery was used as a baseline to compare with the remaining control schemes. The BESS delivers the required DFR power for all requests whilst it remains within SOC limits. No FESS is included. |
| 2 | The FESS acts as a filter to the BESS, responding to any request that it is available to meet. Only if the FESS cannot meet the power requirements is the request passed on to the BESS. |
| 3 | The FESS takes on any requests outside of a designated frequency range, with the BESS responding to any requests inside the range. For example, a FESS could meet any requests below 49.9Hz and above 50.1Hz, whilst the BESS meets any requests in the 49.9-50.1Hz range. |
| 4 | The FESS takes on any requests inside of a designated frequency range, with the BESS responding to any requests outside the range. For example, a BESS could meet any requests below 49.9Hz and above 50.1Hz, whilst the FESS meets any requests in the 49.9-50.1Hz range. |
| 5 | Any power request is split between the two systems according to the ratio of the FESS maximum power output to the agreed service. For example, a 1MW service and a 0.2MW FESS would have each power demand split at a ratio of 5:1 between BESS and FESS. |
| 6 | The FESS provides the 30-second rolling average of the requested power, with the BESS making up any difference between the power delivered by the FESS and the instantaneous request. |
| 7 | The BESS provides the 30-second rolling average of the requested power, with the FESS making up any difference between the power delivered by the BESS and the instantaneous request. |
| 8 | The responsibility for providing the service alternates between the two systems over a set period. For example, a FESS will deliver the service for 30 minutes followed by the BESS delivering for the next 30 minutes. |

Table 6.3: SOC Limits used for individual ESS models

|  | FESS | BESS |
| --- | --- | --- |
| $SOC_{low}$ | 2% | 5% |
| $SOC_{high}$ | 98% | 95% |
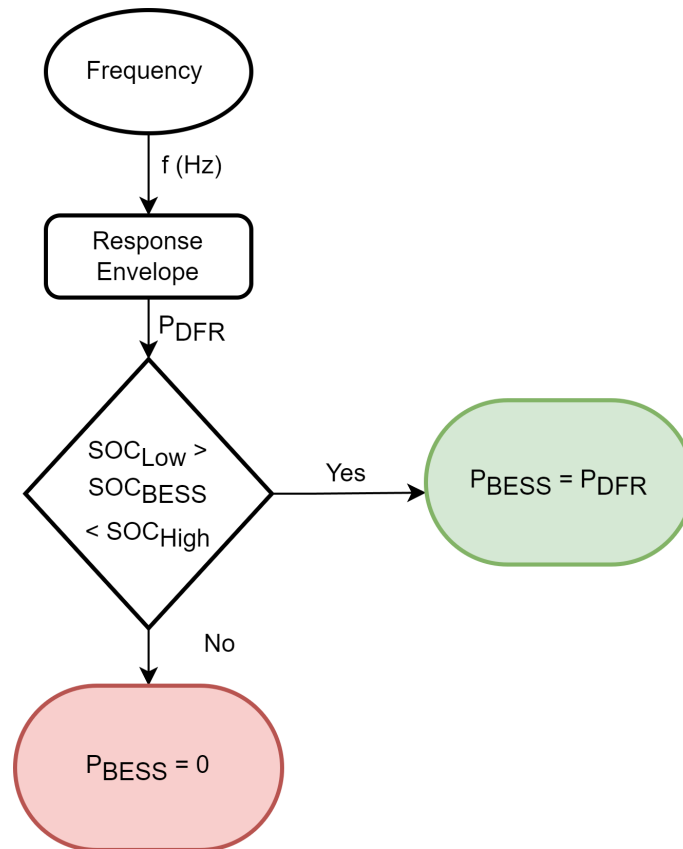
Figure 6.1: Control flowchart for Control Strategy 1

in which they were originally assessed with a concluding section tying together the results of the separate studies.

Many of the control strategies discussed here could be extended with fallback options for when requests are not met and additional control measures; however, the strategies presented are intended to be a baseline investigation into the possibilities available, with future works expected to refine and extend the most promising strategies.

**Control Strategy 1**

This is the baseline control strategy against which all other strategies will be measured. For this reason, this strategy consists solely of a BESS, enabling each hybrid system to be compared to determine whether it causes a positive or negative effect. Unless otherwise stated, this consists of a 1MW/1MWh/1C BESS delivering a 1MW service. The control flowchart is shown in Figure 6.1.

This strategy is the most basic of the set, where the BESS is asked to provide a power determined by the frequency and response envelope ($P_{\mathrm{DFR}}$) and as long as the energy associated with that request ($E_{\mathrm{Req}}$) is less than or equal to the energy currently available in the relevant direction in the BESS (either charging or
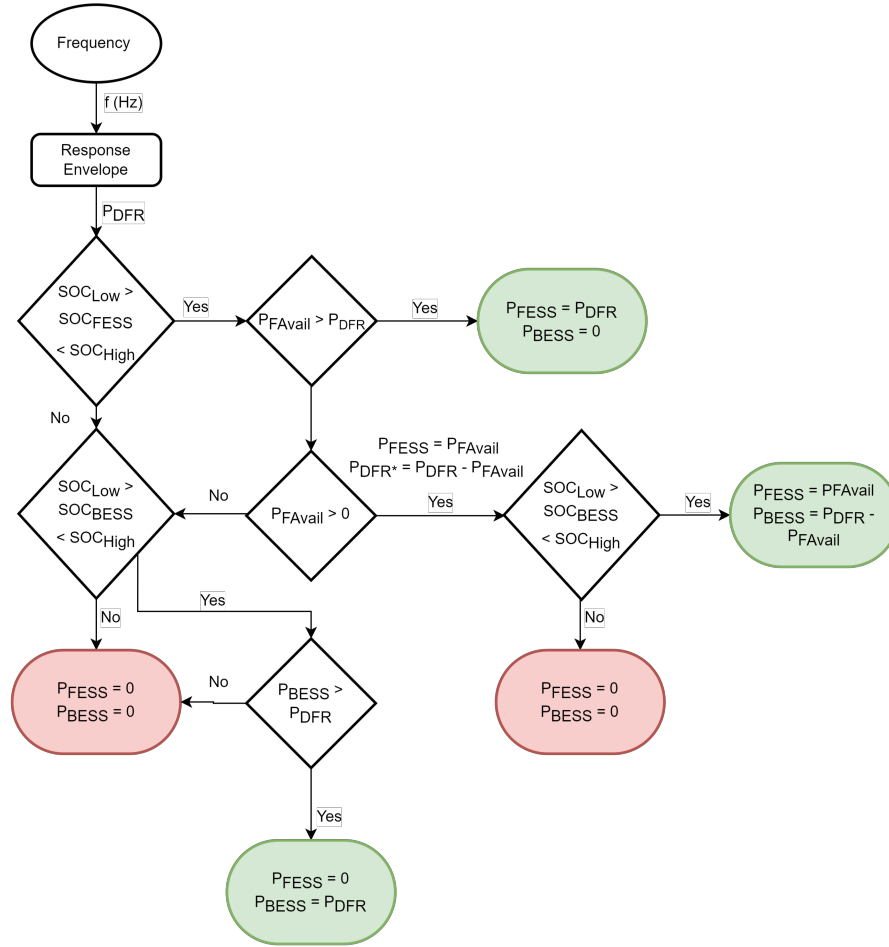
Figure 6.2: Control flowchart for Control Strategy 2

discharging) ($E_{BESS}$) then the BESS can respond so that $P_{BESS}$ is equal to $P_{DFR}$. The request will not be fulfilled if the BESS does not have the spare capacity in the relevant direction to accommodate the energy $E_{Req}$.

**Control Strategy 2**

This control strategy was developed as the initial method of implementing a hybrid system, this consists of asking the FESS to take on any request that it can with the BESS only activating when the FESS is unable to. The philosophy for this strategy is to try and allow the BESS to operate as little as possible whilst still maintaining high availability. Figure 6.2 shows the control flowchart for this strategy.

The approach to this strategy is broadly the same as that in CS-1 but with the additional step of the request passing through the FESS. The FESS is asked to provide a power determined by the frequency and response envelope ($P_{DFR}$) and as long as that request is less than or equal to the power currently available in the relevant direction in the FESS (either charging or discharging) ($P_{FESS}$) then the FESS can respond so that $P_{FESS}$ is equal to $P_{DFR}$. In this scenario, $P_{BESS}$ would

be equal to zero, and the request is wholly met by the FESS.

There are then occasions where the FESS is not able to meet the entire request, such as when the FESS is sized lower than the service being provided. In this scenario, $P_{\text{FESS}}$ will be equal to the maximum amount of power that the FESS can provide, and the new request that the BESS sees is the difference between what the FESS can provide and the requested power. If the BESS can meet this request, then the request is met through a combination of the two ESSs, and if not then the request is not met.

Finally, if the FESS has reached its high or low SOC threshold and hence cannot provide any response, then the request that the BESS sees is simply $P_{\text{DFR}}$ as with CS-1.

## Control Strategy 3

The third control strategy was developed as part of testing to determine if there were ways of reducing the impact on BESS degradation by only cycling it in certain regions. To this end, it was noted that there was the potential for splitting the requests up by the frequency associated with them and hence allowing the maximum power experienced by each ESS to be controlled. Figure 6.3 shows the control flowchart.

This strategy is the first to have a filter stage before the ESSs are instructed to operate. Each request is separated according to the frequency, and directed to either the BESS or FESS depending on what boundaries have been set. For this control strategy, the BESS will take on any request within a set range, and the FESS will take on any request outside of a set range.

To give an example, if the upper threshold ($f_{\text{high}}$) was set to 50.1Hz and the lower threshold ($f_{\text{low}}$) was set to 49.9Hz, then a frequency of 49.95Hz would be directed to be responded to by the BESS and a frequency of 49.8Hz would be responded to by the FESS. From the point that the request is assigned, there is no interaction between the two ESSs, with the request being solely delivered by either the FESS if the frequency is within the assigned range, or by the BESS if the frequency is outside the assigned range.

## Control Strategy 4

This control strategy is the reverse of CS-3, again developed with the aim of controlling how the BESS is operated within set regions. Figure 6.4 shows the control flowchart.

For this control strategy, the FESS will take on any request within a set range, and the BESS will take on any request outside of a set range, the opposite allocation
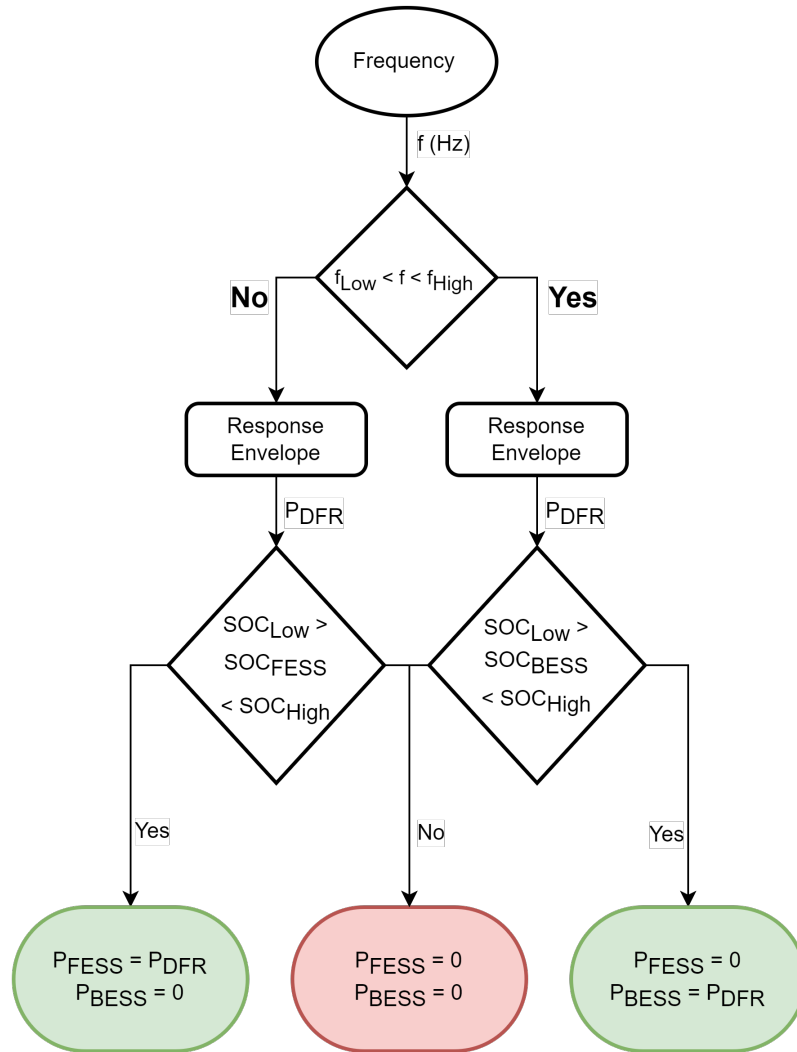
Figure 6.3: Control flowchart for Control Strategy 3

to CS-3. Figure 6.4 shows the flowchart for how this strategy is executed, where $f_{\text{Low}}$ is the lower frequency threshold, $f_{\text{High}}$ is the high-frequency threshold, $P_{\text{DFR}}$ is the required power requested by the response envelope and $P_{\text{BESS}}$ and $P_{\text{FESS}}$ are the power output from the BESS and FESS respectively.

To give an example, if the upper threshold ($f_{\text{high}}$) was set to 50.1Hz and the lower threshold ($f_{\text{low}}$) was set to 49.9Hz, then a frequency of 49.95Hz would be directed to be responded to by the FESS and a frequency of 49.8Hz would be responded to by the BESS. From the point that the request is assigned, there is no interaction between the two ESSs, with the request purely dealt with based upon the ability of the assigned ESS to accommodate it.

**Control Strategy 5**

This strategy takes a different approach to the same philosophy detailed in CS-3 and CS-4. Instead of splitting the request according to frequency, it is always distributed

164
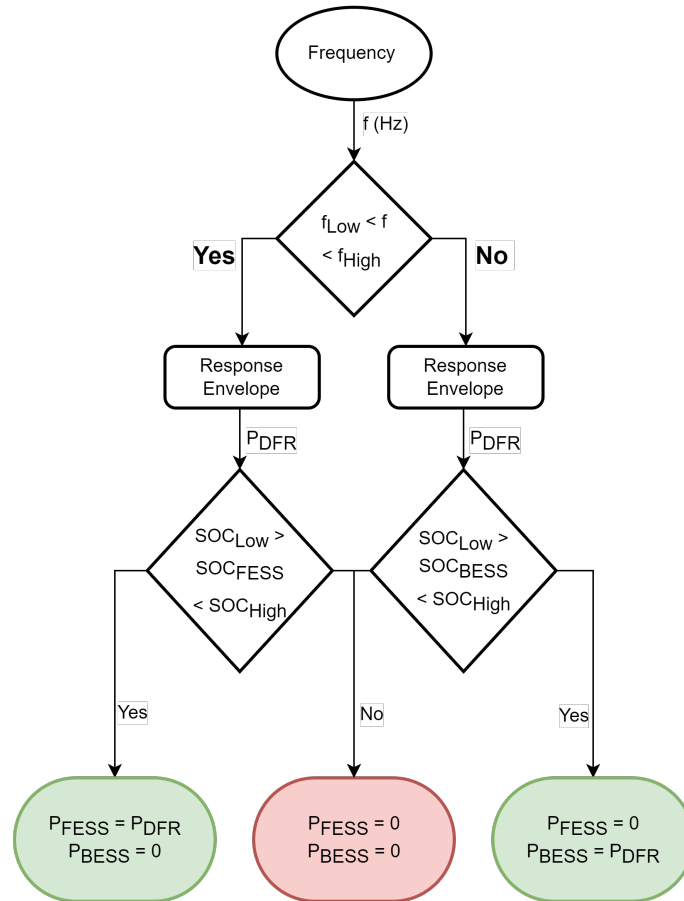
Figure 6.4: Control flowchart for Control Strategy 4

between the two ESSs according to a set ratio as in Figure 6.5.

As an example of the operation of the system, if a 1MW/1MWh/1C BESS and a 0.2MW/0.05MWh/4C FESS were paired together, then the ratio would be set at 5:1 between the BESS and the FESS. Once the power has been proportionally separated, the ESSs do not interact and both must provide the full requested power for the overall request to be met. If either ESS fails to provide the requested power then the overall request will not be met.

**Control Strategy 6**

This strategy was developed with the objective of smoothing out the operation of the ESSs, by using the average request as well as instantaneous requests. This operates in tandem with reducing the power throughput that the BESS experiences by only assigning it the difference between the average and instantaneous power. Figure 6.6 shows the control flowchart

For this strategy, the 30-second average of requested power is calculated ($P_{Av}$) and assigned to the FESS. The BESS control unit is then provided with $P_{DFR}$ and $P_{Av}$ with which it calculates the difference between the two to produce $P_{Dif}$. The
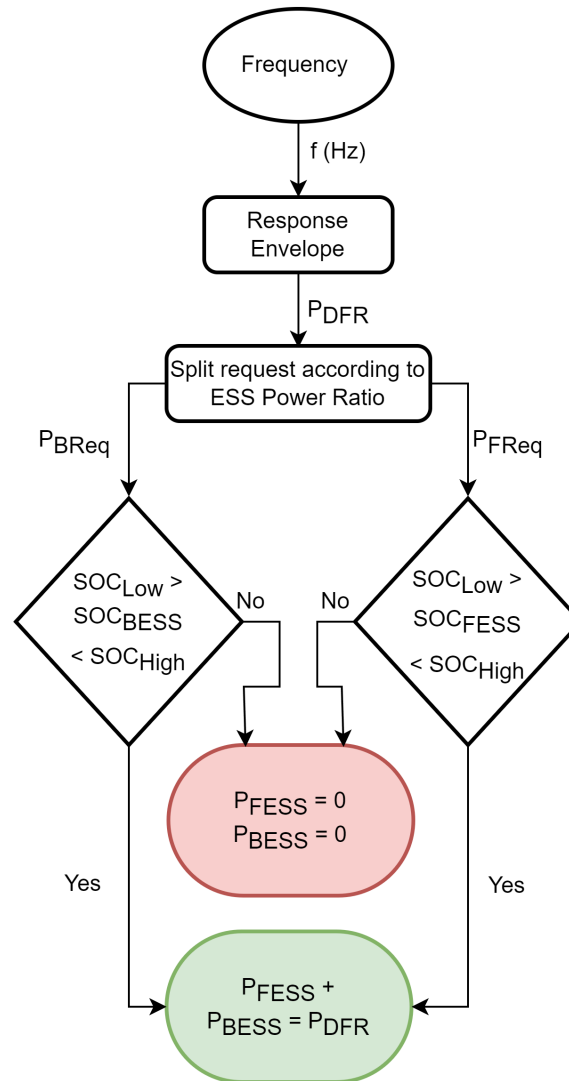
Figure 6.5: Control flowchart for Control Strategy 5 *note that if either branch results in a 'no' decision then this overrides the control and sets the output to the 'zero' outcome*

average power is a simple rolling average of the previous 30 seconds of requested power and is not predictive, with an example power profile for the baseline and average powers shown in Figure 6.7. From this point, the two ESSs are independent and both must provide the power requested of it in order for the overall request to be met.

**Control Strategy 7**

This strategy was developed as the opposite of the strategy described as CS-6. The roles of the BESS and FESS are reversed to assess whether this method provides an improvement in availability and degradation. Figure 6.8 shows the control flowchart.

For this strategy, the 30-second average of requested power is calculated ($P_{\mathrm{Av}}$) and assigned to the BESS. The FESS control unit is then provided with $P_{\mathrm{DFR}}$ and
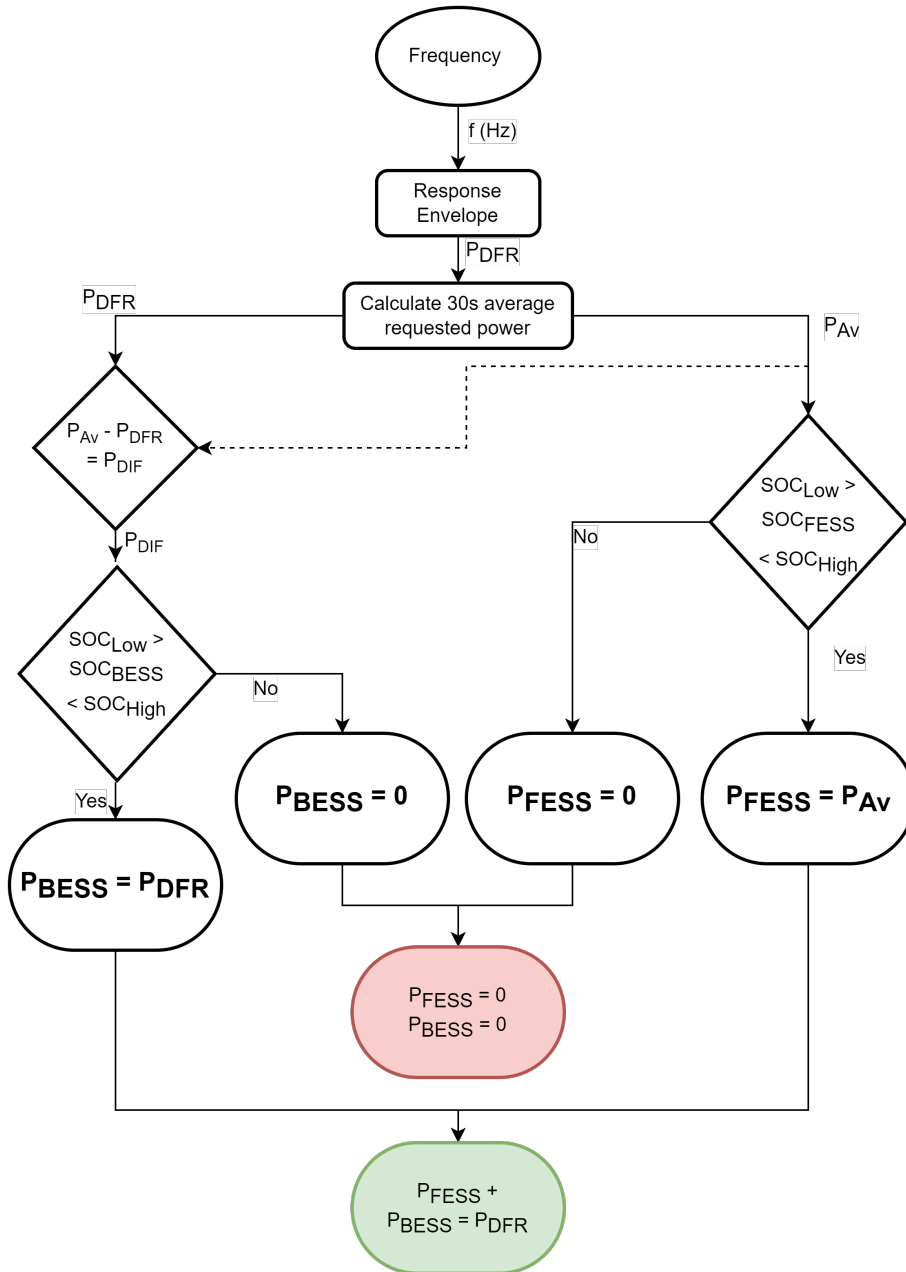
Figure 6.6: Control flowchart for Control Strategy 6

$P_{\mathrm{Av}}$ with which it calculates the difference between the two to produce $P_{\mathrm{Dif}}$. From this point, the two ESSs are independent and both must provide the power requested of it in order for the overall request to be met.

**Control Strategy 8**

The final control strategy was developed by considering operational time as a control variable. For this method, the ESS which is responsible for delivering the requested power is varied at set intervals, such as every 30 minutes, as shown in Figure 6.9.

For this control strategy, each ESS operates independently for the given time frame in the same manner as with CS-1, only alternating between ESS responsibil-
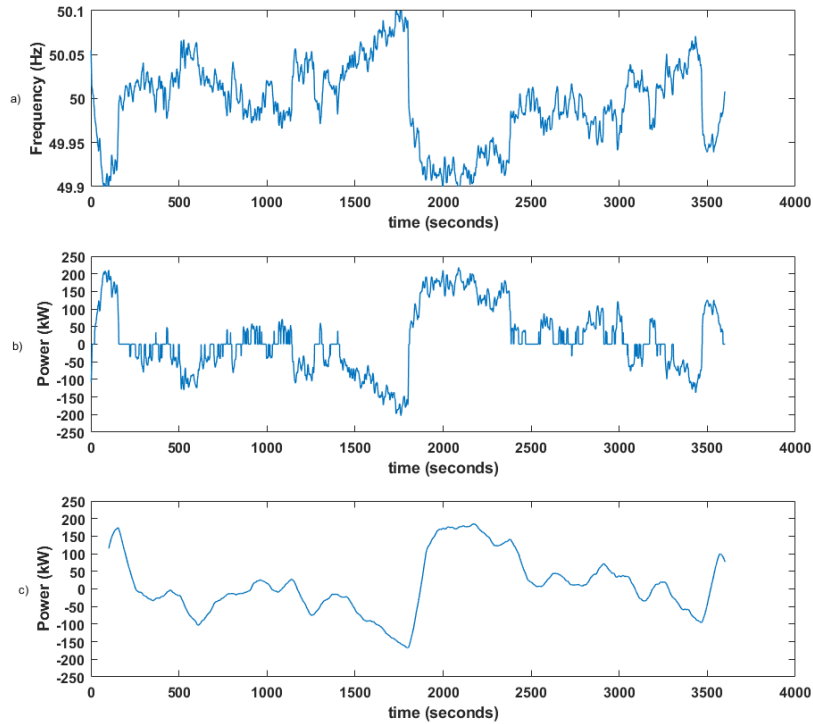
Figure 6.7: Example simulation output for CS-6 showing a) Frequency b) Baseline power request ($P_{DFR}$) c) Average power request ($P_{Av}$)

ity.n If the ESS responsible for service provision at that time cannot provide the requested power then the request will not be met.

**Discussion**

The range of novel control strategies developed as part of this thesis has been introduced and their operation explained. Represented in this section is a significant endeavour to develop strategies to extract the maximum impact from the hybridisation process and thus improve the techno-economic viability of the whole system.

It is important to note that several control strategies execute the control in such a way that if either one of the ESSs fails to provide the requested power then the other ESS does not compensate for this and hence the overall output is set to zero. This approach was taken for ease of implementation purposes, however, these control strategies could be expanded upon by allowing each ESS to compensate for the other in the future. The potential impact of this would be twofold. Firstly, the average availability of the system would likely increase leading to increased revenue. However, the degradation of the battery would likely increase from becoming more active and therefore result in negative economic implications.

From this point onwards, the control strategies will be analysed and optimised
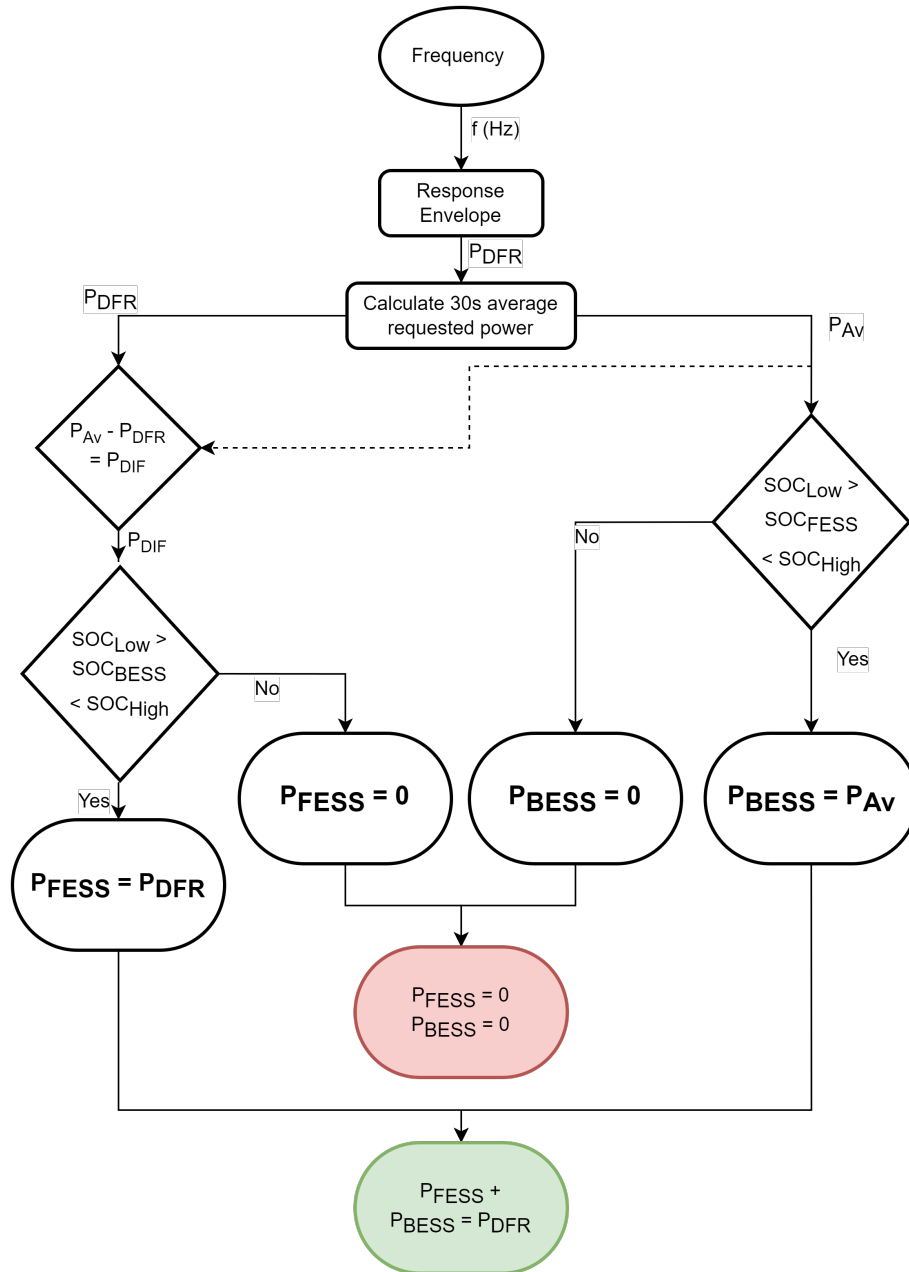
Figure 6.8: Control flowchart for Control Strategy 7

in order to assess their effectiveness in improving the techno-economic performance achieved by CS-1.

## 6.2.2  Degradation Mitigation Modeling Framework

Before the control strategies are assessed in detail, this section details the complexities of the modelling framework previously discussed in Chapter 3 and how it can be used to inform the decisions that are made with regard to refining each individual control strategy. This visualisation was key in designing the control strategies discussed in the previous section, as it allows the areas of operation to be clearly
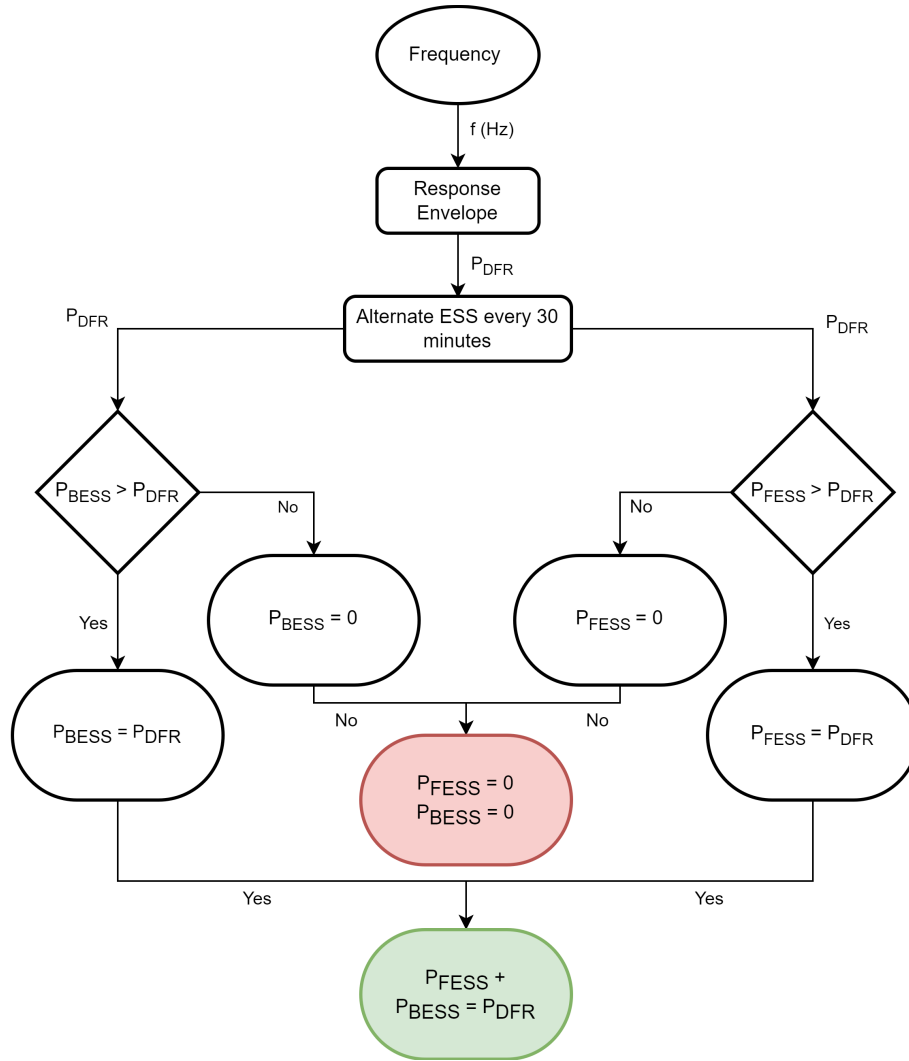
Figure 6.9: Control flowchart for Control Strategy 8

visualised in order to inform decisions on the control set points and philosophy. The main objective from these visualisations is to illustrate how different control schemes can try and maintain BESS operation at low C-Rates and SOC values in the region of 20-80%. These have been shown throughout literature as operating regions more beneficial to extending battery lifetime due to reduced heat losses and unwanted side reactions [142] [239] [240].

Chapter 3 gave a brief introduction to the 3-D data analysis possible within the modelling framework, including an example of this in Figure 3.29. This section will now present how the operation of the BESS can be visualised under three different control strategies, namely CS-2, CS-3 and CS-6. These three strategies have been chosen to highlight different areas of operation for the individual ESSs when control strategies are varied. In this analysis, the configuration studied consists of a 0.5MW/0.5MWh/1C BESS operating with a 0.25MW/0.05MWh/5C FESS to provide a 0.5MW DFR service and showcases the analysis possible from filtering the
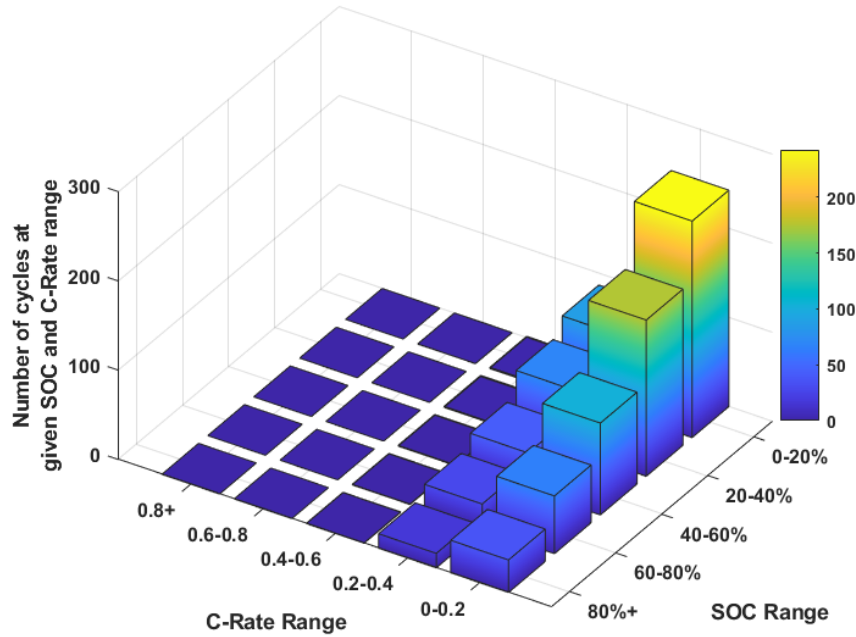
Figure 6.10: Total number of cycles at combined ranges of C-Rate and SOC for the BESS under CS-1

SOC operational ranges and C-Rate operational ranges into 5 separate ranges or 'bins'. The control strategies presented in this section have been selected to showcase the effects that different strategies can have on the operation of the two systems and this section is not intended to be an exhaustive exploration of all control strategies. Note that in the following sections, the axis limits are not constant between each figure, and therefore care should be taken when comparing different figures. The following figures were generated using the hybrid DFR model previously described in Chapter 3.

**CS-1**

Firstly, in order to provide context for the following graphs, the visualisation for CS-1 where the BESS is operating without any hybridization with a FESS is presented. This is shown in Figure 6.10 where it can be seen that the BESS is operating mostly in the 0-0.4 C-Rate region, concentrated mainly at lower SOC regions but with some activity across all SOC ranges.

**CS-2**

Figure 6.11 and Figure 6.12 illustrate the 3-D operation visualisation for the BESS and FESS respectively operating under CS-2. From the analysis presented, both ESSs perform the majority of their cycling at lower C-Rate ranges compared to
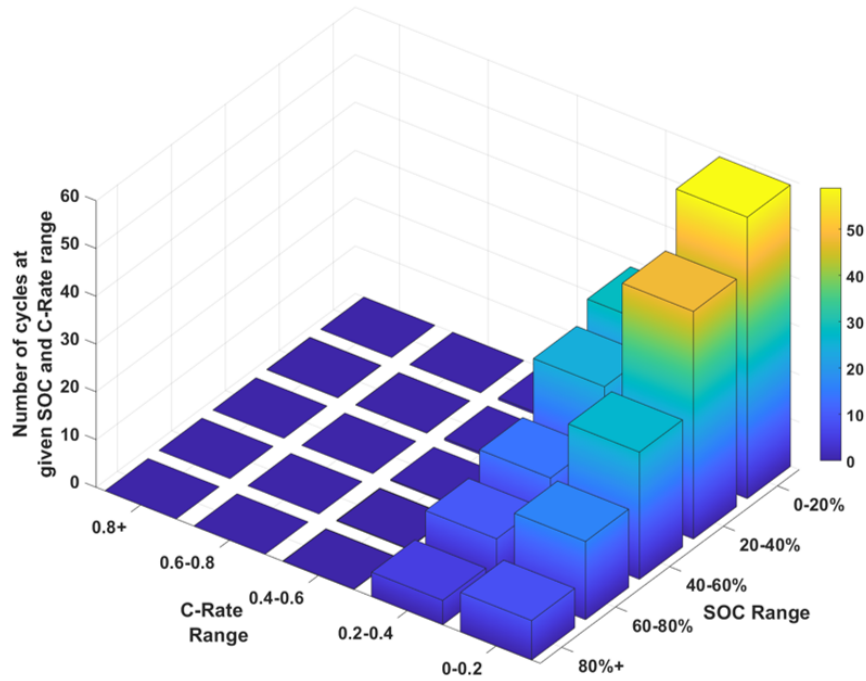
Figure 6.11: Total number of cycles at combined ranges of C-Rate and SOC for the BESS under CS-2

their overall C-Rating with the FESS operating across the whole spectrum of SOC ranges whilst the BESS tends to operate much more frequently in the 0-40% SOC range which could be detrimental in terms of battery degradation.

This visualization of the operation of the system provides a foundation for tailoring the operation of the systems to concentrate the activities of the ESS in specific favourable areas, potentially through the introduction of certain control schemes. In this specific example, the fact that the BESS operates almost exclusively in the 0-0.4C region and the FESS operates over the 0-3C range suggests both aspects of the hybrid ESS may be oversized from a power-rating perspective. Additionally, it can be used to design control strategies that manage the SOC in more beneficial ranges for extending battery life as opposed to the low SOC range demonstrated in this analysis.

**CS-3**

Figure 6.13 and Figure 6.14 show the same presentation of C-Rate and SOC range of operation but this time for CS-3. The impact of this change in the control strategy is significant, with the FESS now operating almost exclusively in the 2-3 C-Rate range with no cycles experienced above 4C which suggests the FESS could be alternatively sized at 4C rather than 5C with no performance impact and significant cost savings.

The BESS now operates in an even more concentrated region, with the majority of cycles taking place in the 0-0.2C and 0-20% SOC ranges. This suggests that
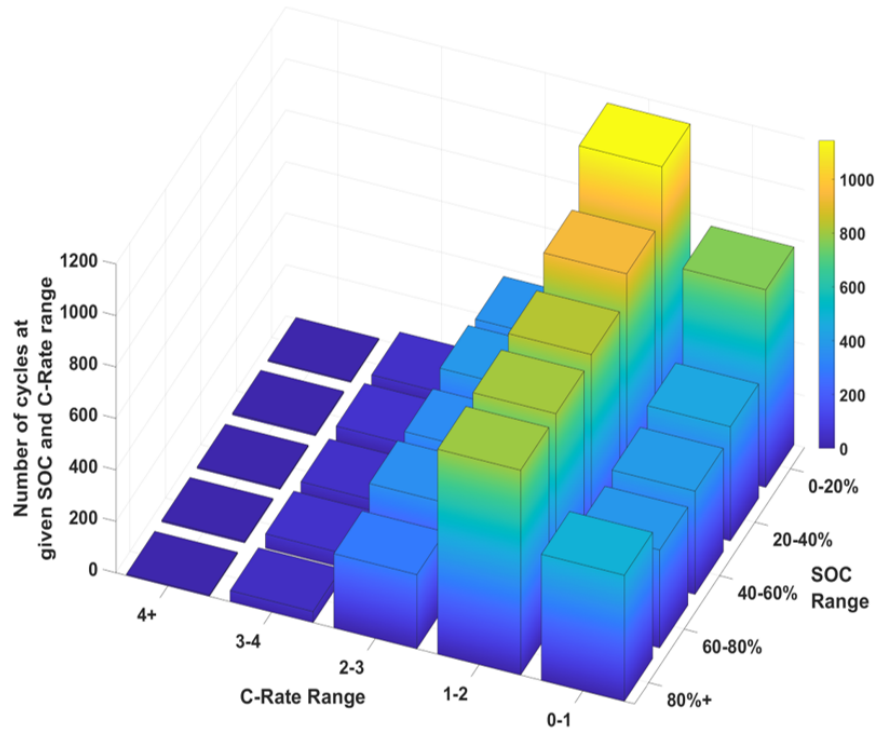
Figure 6.12: Total number of cycles at combined ranges of C-Rate and SOC for the FESS under CS-2

despite the lower number of cycles experienced in this application, the SOC will be maintained in a region that is generally considered throughout literature to have a detrimental effect on battery lifetime.

**CS-6**

Figure 6.15 and Figure 6.16 show the FESS and BESS operational statistics when operating under CS-6. For the FESS, the SOC range is still spread evenly across the spectrum whereas it operates mostly in the 4+ C-Rate range with small degrees of usage in the lower C-Rates. For this control strategy, the FESS is sized at an appropriate level with the system making use of the full range of power capabilities.

The activity from the battery is now almost exclusively within the 0-0.2 C-Rate with the SOC spread more evenly across the entire range of operation. This is likely to have a much better effect on battery lifetime than the other control strategies presented in this section. Additionally, the C-Rate being maintained mostly in the 0-0.2C and 0.2-0.4C ranges will also have a positive impact. However, this analysis does suggest that the battery is significantly oversized for this control strategy and likely could be specified as a lower C-Rate battery.
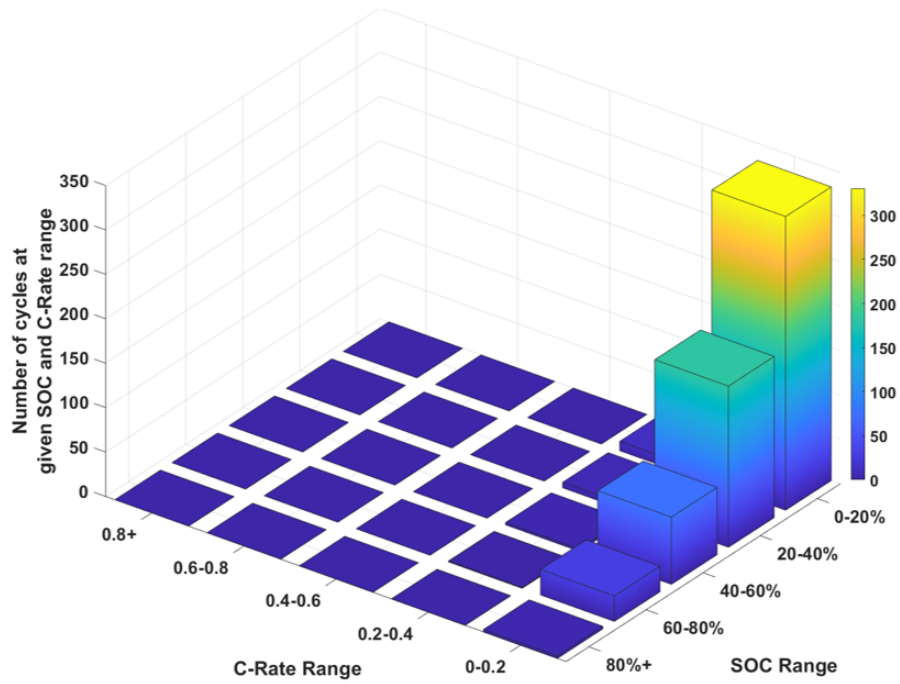
Figure 6.13: Total number of cycles at combined ranges of C-Rate and SOC for the BESS under CS-3
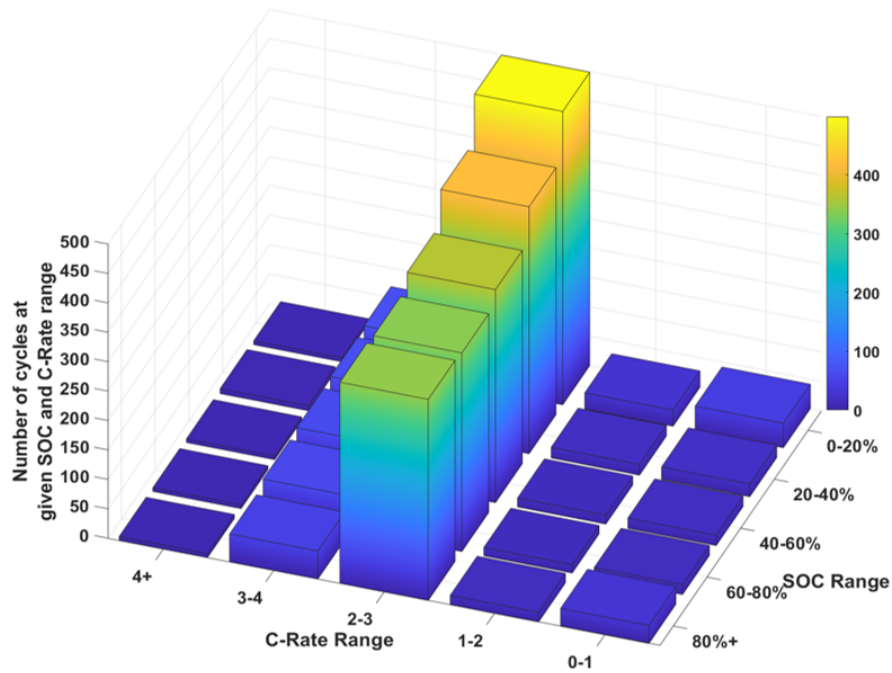


Figure 6.14: Total number of cycles at combined ranges of C-Rate and SOC for the FESS under CS-3
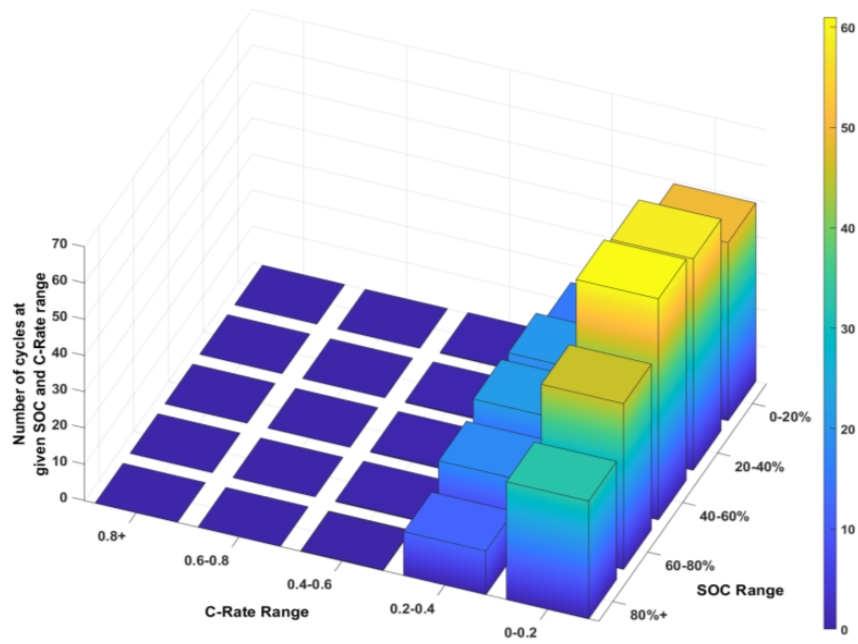
Figure 6.15: Total number of cycles at combined ranges of C-Rate and SOC for the BESS under CS-6
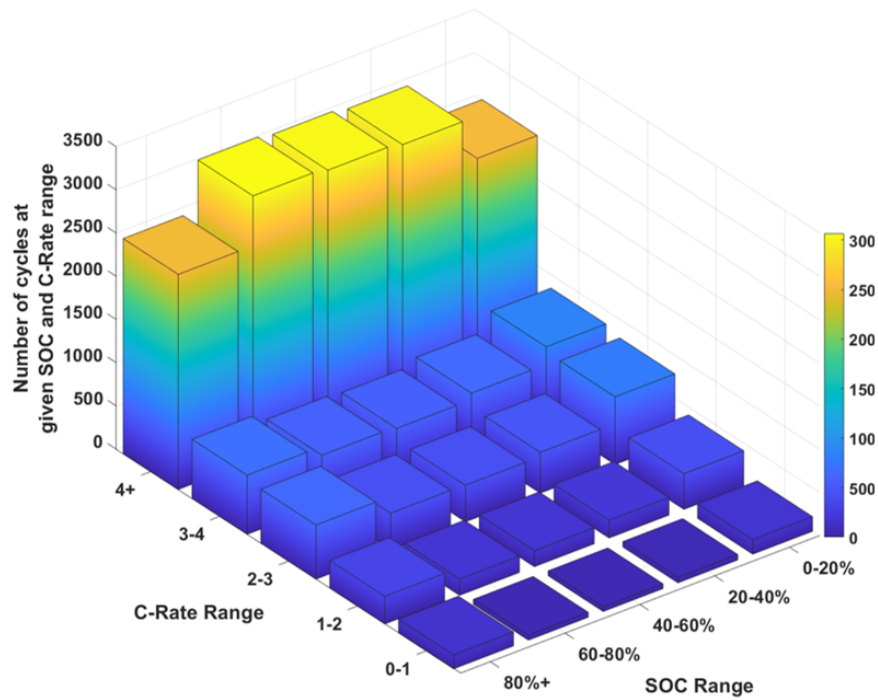


Figure 6.16: Total number of cycles at combined ranges of C-Rate and SOC for the FESS under CS-6

# 6.3 Genetic Algorithm Optimisation of Hybrid Control Strategies

In this section, a GA will be used to optimise the configuration of a FESS being used in CS-2, CS-6 and CS-7. This analysis is conducted based on an initial exploration of the variable space and provides the foundations for further iterative work in the following section of this chapter.

## 6.3.1 Study Overview

The analysis was conducted using the Genetic Algorithm toolbox within MAT-LAB/Simulink. The Genetic Algorithm has been used in this work in order to explore a wide range of FESS configurations in a bounded population set, offering a good degree of certainty in the optimal configuration whilst simultaneously providing economic performance data across the entire population range.

The reward value for the algorithm is the overall NPVC of the system. In the scenario presented in this work, the reward value needs to be maximized rather than minimised. The reward value is calculated by measuring the increase (or decrease) in NPV compared to CS-1. For this reason, the fitness function needs to be set up in such a way that negative values are not considered beneficial and calculate the reward value accordingly. The initial part of this process is to use Equation 6.1 ensuring that as the minimisation function decreases, the NPV change is maximized.

$$MinimisationFunction = \frac{1}{(1 + (NPV_{HESS} - NPV_{CS1}))} \qquad (6.1)$$

The drawback of this however that is if the NPVC becomes negative, then that would automatically be counted as a higher fitness than a positive NPVC. To counteract this, a subfunction was introduced to parse any negative NPVC values and assign higher fitness values as the NPVC becomes more negative. This function is shown in Figure A33 in the Appendix. The variables that the GA was given to optimise were FESS C-Rate and FESS energy capacity in kWh.

The constraints for the GA were determined based upon providing a sufficient range for the GA to operate across and be worthwhile, whilst simultaneously ensuring solid bounds to prevent excessive simulation durations. The lower FESS C-Rate of 4C was chosen to allow the optimisation to be based purely on power centric FESSs as a better representation of the most common FESS configurations, whilst the upper bound of 15C was chosen in the knowledge that energy capacity is still an important characteristic for this application. The energy capacity boundaries of 10-100kWh were similarly chosen to offer an appropriate range of values for the GA to explore whilst maintaining it in the range of representing a small number of

Table 6.4: Parameters used in the GA Optimisation process

| Parameter | Setting |
|---|---|
| Crossover Rate | 0.8 |
| Mutation Rate | 0.05 |
| Initial Population | 40 |
| Generations | 20 |

individual FESS units.

The crossover rate was set as 0.8 and the mutation rate was set to 0.05 in order to allow the GA to reach a solution within the generations specified without sacrificing exploration of outlying areas of the population. Considering the boundaries that have been set cover a total number of possible individuals of 1092, The population size was set as 40 with the maximum number of generations as 20, to give a total possible number of individuals as 800 and hence allow a thorough exploration of the available options without performing an exhaustive search. These parameters are summarised in Table 6.4.

## 6.3.2 Control Strategy 2

Control Strategy 2 was outlined in the previous section and consists of the FESS acting as a filter to the BESS, taking on any request that it is capable of either completely meeting or contributing to before passing on any remaining requests to the BESS.

Figure 6.17 shows the best configuration at each generation of the genetic algorithm where C-Rate refers to the rating of the ESS as defined previously in Equation 2.2. It is clear that the algorithm very quickly finds the best region for configuration settings before slightly refining the energy capacity. From generation 2 onwards no further advancement is made from the best configuration of 91kWh energy capacity and 4C C-Rate.

In terms of the actual performance of the control strategy, Figure 6.18 shows the NPV achieved across the generations.

A modest increase in NPVC was achieved across the GA, rising from an initial value of £1,115,000 to a peak value of £1,188,000. The significant positive NPVC achieved suggests the control strategy is highly effective in producing a system that balances technical performance with economic impact.

To illustrate how the NPVC changes across the range of values studied, Figure 6.19 shows all individuals studied across the GA and the NPVC values that they achieved. Each individual is a combination of the chosen C-Rate and energy capacity. It is clear that the algorithm spends the majority of its time looking at solutions
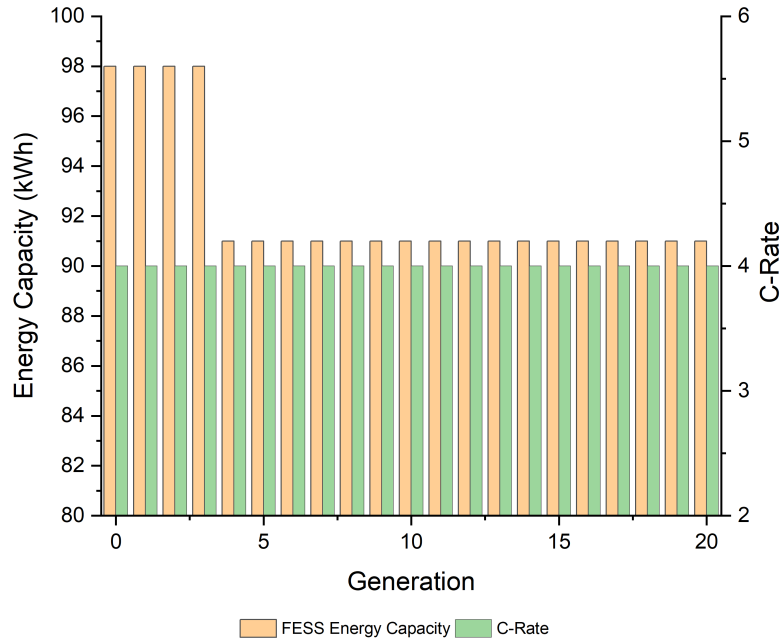
Figure 6.17: Best individuals per generation for CS-2

at the lower C-Rates, and that when higher C-Rate individuals are included in the population they represent dramatic reductions in the overall NPVC. It is interesting to note the ridged aspect of the graph, as the energy capacity is increased the NPVC tends to decrease up to a point where it experiences a sudden jump upwards, and this repeats multiple times. This represents the points where the additional energy capacity of the FESS is causing the BESS to cross the threshold of requiring an additional replacement over the course of the studied lifetime.

The results of Figure 6.19 give confidence that the outcome of the GA is the optimum solution within these bounds, with clear trends that indicate less favourable outcomes for individuals that were not generated as part of the algorithm process.

Finally, Figure 6.20 shows the number of times each individual was chosen over the course of the GA. This shows the convergence towards the low C-Rate, high energy capacity region of the population. Interestingly, the best individual selected (91kWh, 4C) was not the combination that was selected the most often by the GA, being selected 17 times compared to a 92kWh 4C individual being selected 18 times. The C-Rate selected most often was 4C, with the frequency of selection decreasing as the C-Rate rises. This ties up with the information presented previously in Figure 6.19, with the best regions in that figure lining up with the most frequently selected individuals in Figure 6.20.

Due to the nature of this control strategy, there is little further optimisation or sensitivity analysis that can be performed as the only main variables are the energy capacity and C-Rate of the FESS. Unlike the other control strategies, there are no
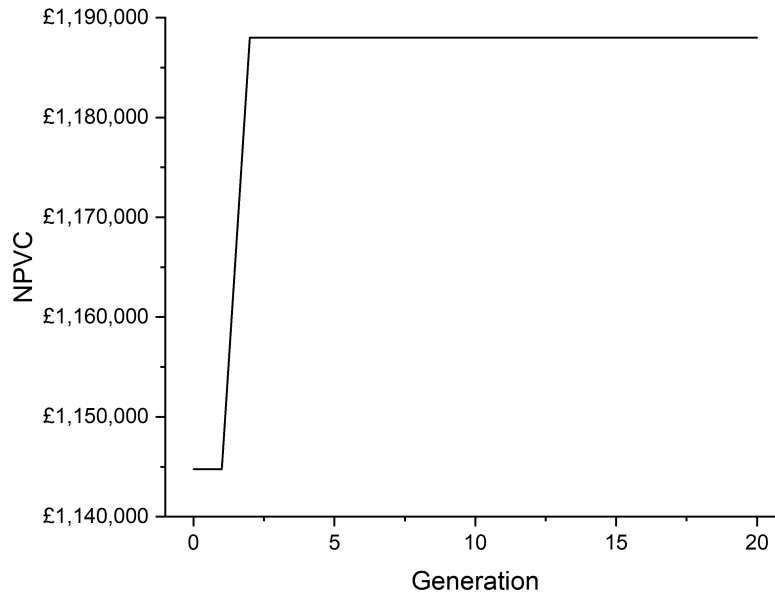
Figure 6.18: NPV achieved per generation for CS-2

variables within the strategy itself that can be tuned to produce different results. The results of the genetic algorithm, therefore, represent the best performance possible for this control strategy, showing a significant positive NPVC and making this strategy a worthwhile consideration for HESS control.

### 6.3.3 Control Strategy 6

Control Strategy 6 was outlined in the previous section and consists of the FESS delivering a 30-second average of the requested power whilst the BESS delivers the difference between the instantaneous and average request.

Illustrating how the genetic algorithm refined the configuration to achieve a better NPV, the best individuals per generation are shown in Figure 6.21. The figure reveals the minimal incremental modifications made by the genetic algorithm to determine the best configuration. Starting from an initial best individual of 25kWh and 6C, the final best individual is 28kWh and 4C. It can be seen that the best C-Rate is determined very quickly at generation 2, with no further modification suggesting confidence in this being the optimal C-Rate for this control strategy.

Shown in Figure 6.22 are the overall results of the GA, showing the positive NPVC increasing as the algorithm finds better configurations through the generations. There is a fairly modest increase from the initial generation to the final result, increasing from £943,000 to £1,152,000. Overall though this represents a slight decrease from the NPVC generated from the previously discussed GA for CS-2.
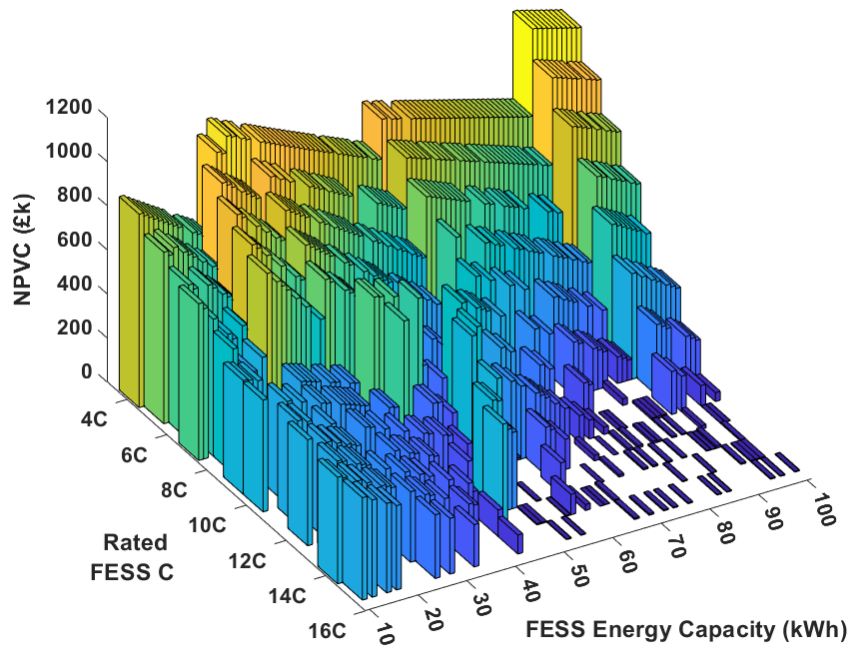
Figure 6.19: NPV achieved for all individuals studied for CS-2

It is interesting to note that the result of this GA has produced a significantly different best energy capacity than considered for CS-2, showing that if a manufacturer has a specific energy capacity unit, then it is important that they tailor the control strategy to make the most of the specifications, with CS-2 producing the best energy capacity of 91kWh compared to 28kWh in CS-6. A FESS with a lower energy capacity may be unsuitable when utilising CS-2, but instead, be able to provide a good economic improvement if CS-6 is considered instead.
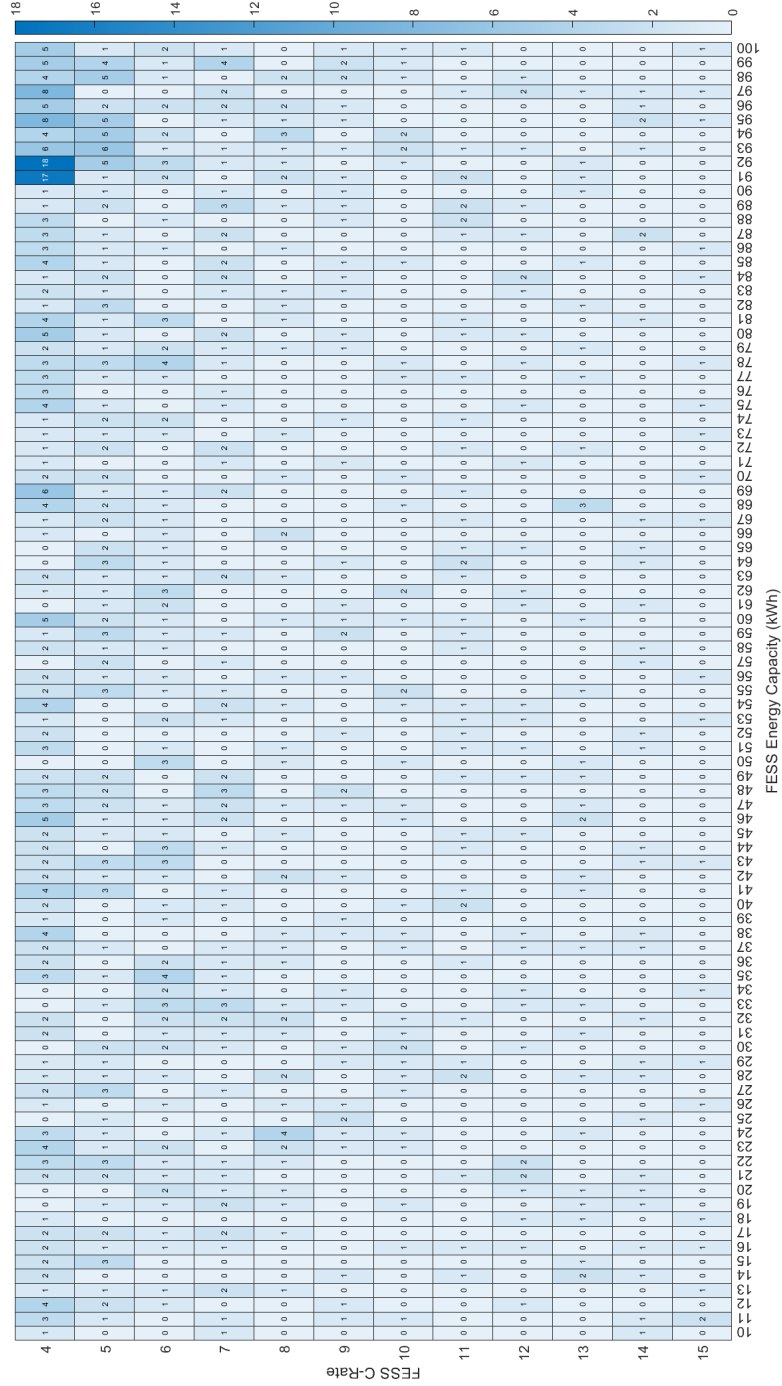
Figure 6.20: Heat map showing the GA exploration of CS2
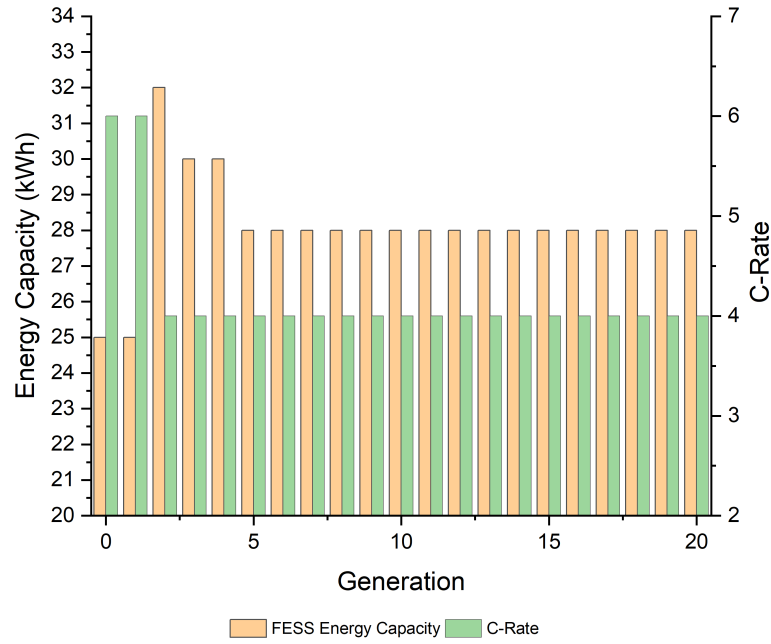
Figure 6.21: Best individuals per generation CS-6, $t_{\mathrm{av}} = 30$s

Once again it can be seen from Figure 6.23 that there are multiple local maximum points as the NPVC rises and falls whilst the C-Rate and energy capacity are varied. With increasing C-Rate the economic benefits decrease, whilst for energy capacity the NPVC fluctuates up and down as the capacity is increased.  The region of combinations with high C-Rate and high energy capacity is the worst performing.

As with CS-2, the heat map showing the exploration of the individuals is shown in Figure 6.24.  The individuals chosen most regularly are concentrated in the low C-Rate, low energy capacity region, with the eventual best individual selected the most times (32 times).  As the C-Rate and energy capacity increase, the rate at which individuals were selected is reduced, with very few selected in the upper regions of the population due to their poor performance, as seen in Figure 6.23.
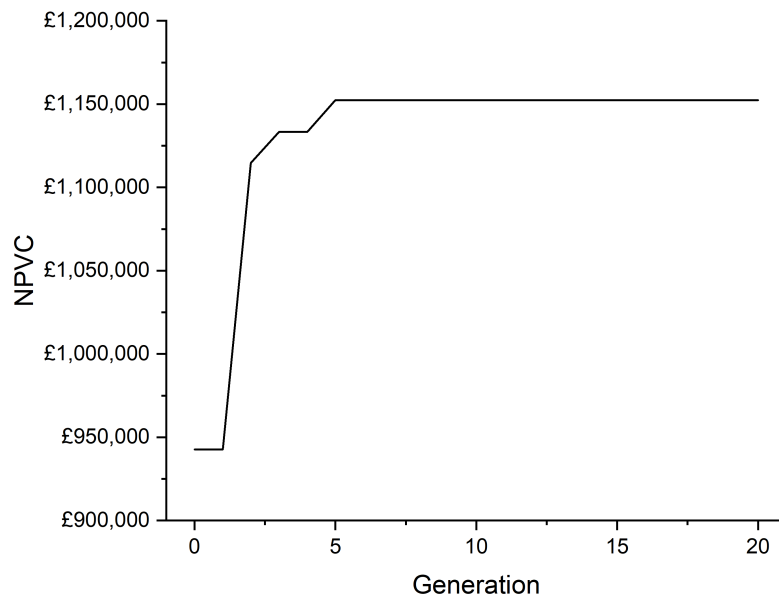
Figure 6.22: Maximum positive NPVC at each generation of the GA , $t_{av} = 30$s
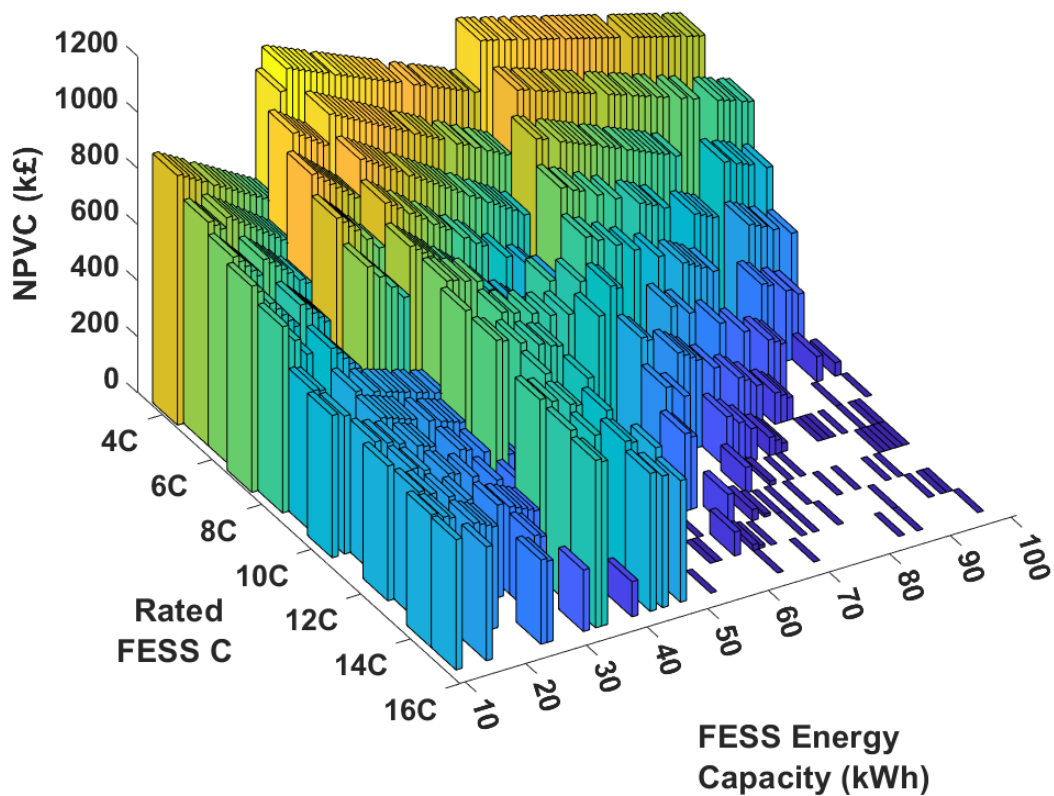


Figure 6.23: NPV achieved for all individuals studied for CS-6 , $t_{av} = 30$s
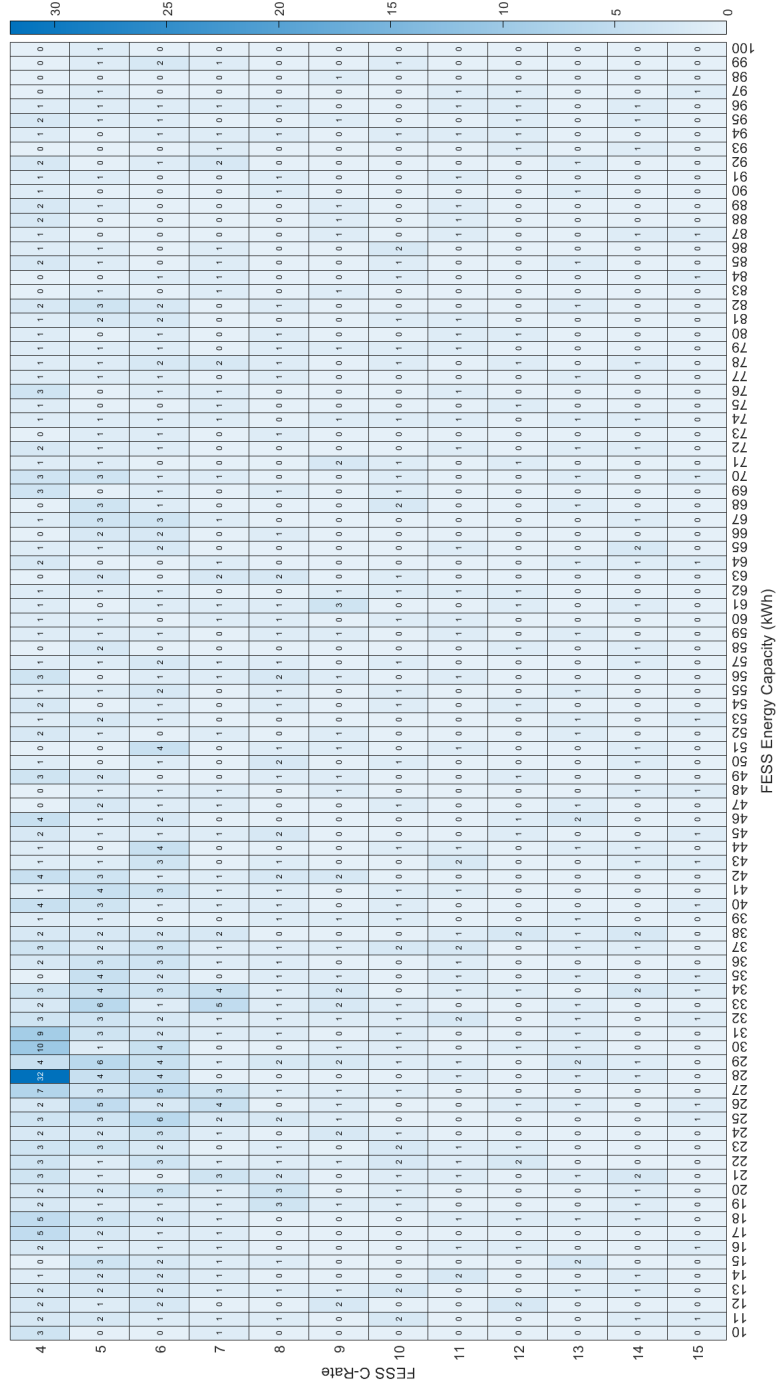
Figure 6.24: Heat map showing the GA exploration of CS6, $t_{av} = 30s$
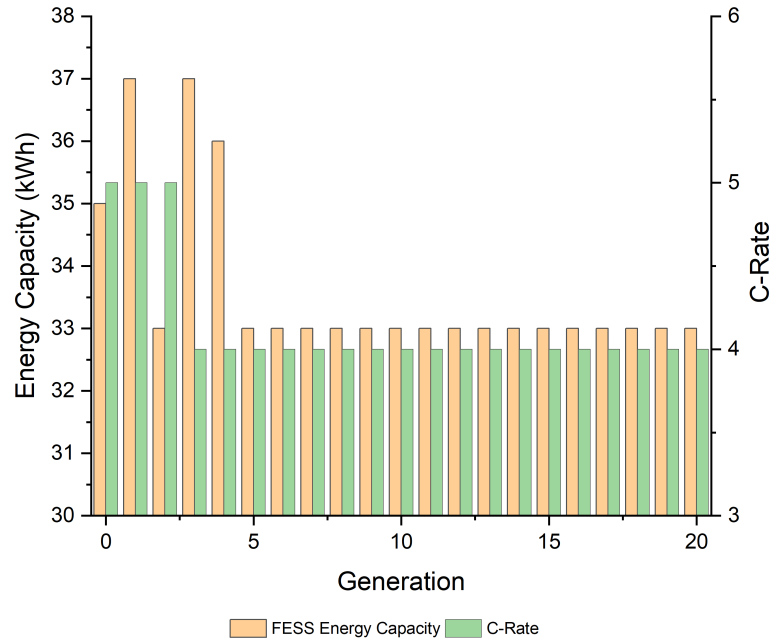
Figure 6.25: Best individuals per generation CS-6 , $t_{av} = 120s$

**Control Strategy Settings Sensitivity Analysis**

In relation to this control strategy, it is important to note that the main variable in the control settings is average power calculation time in seconds ($t_{av}$). In the initial genetic algorithm, this was set to 30 seconds and resulted in a positive NPVC being achieved.

To explore the impact that the control strategy settings have on the performance of CS-6, the genetic algorithm was conducted two more times, this time with $t_{av}$ set to 120s and 300s. These values of $t_{av}$ were chosen after initial exploration of the variable space showed that beyond these values further variation in results was not achieved.

Initially looking at $t_{av}$ set to 120s, Figure 6.25 shows the best individuals per generation. Again, the GA settles on the best configuration fairly early in the run, reaching its final configuration at generation 5. The C-Rate initially starts out at 5C before dropping to 4C as before, whilst the energy capacity varies between 37kWh and 33kWh as the algorithm progresses. Compared to when $t_{av}$ was set to 30s, this GA has resulted in a very similar individual being chosen, differing from the previous best configuration by just 5kWh.

Figure 6.26 shows the resulting NPVC at each generation of the GA. Again, a modest increase is seen across the generations, culminating in a NPVC of £1,115,000. This is slightly less than when setting $t_{av}$ to 30s, but still a significant increase in NPV compared to the CS-1 baseline for a slightly different FESS configuration.
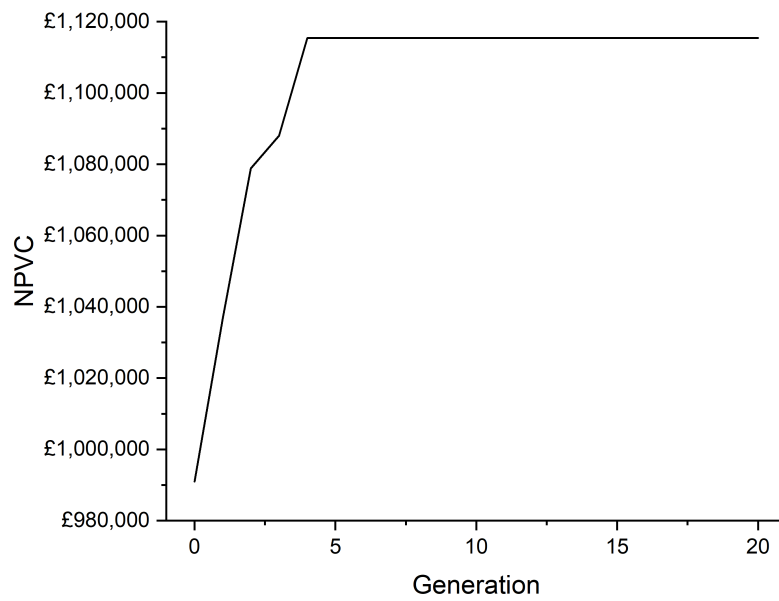
Figure 6.26: Maximum positive NPVC at each generation of the GA, $t_{av} = 120$s
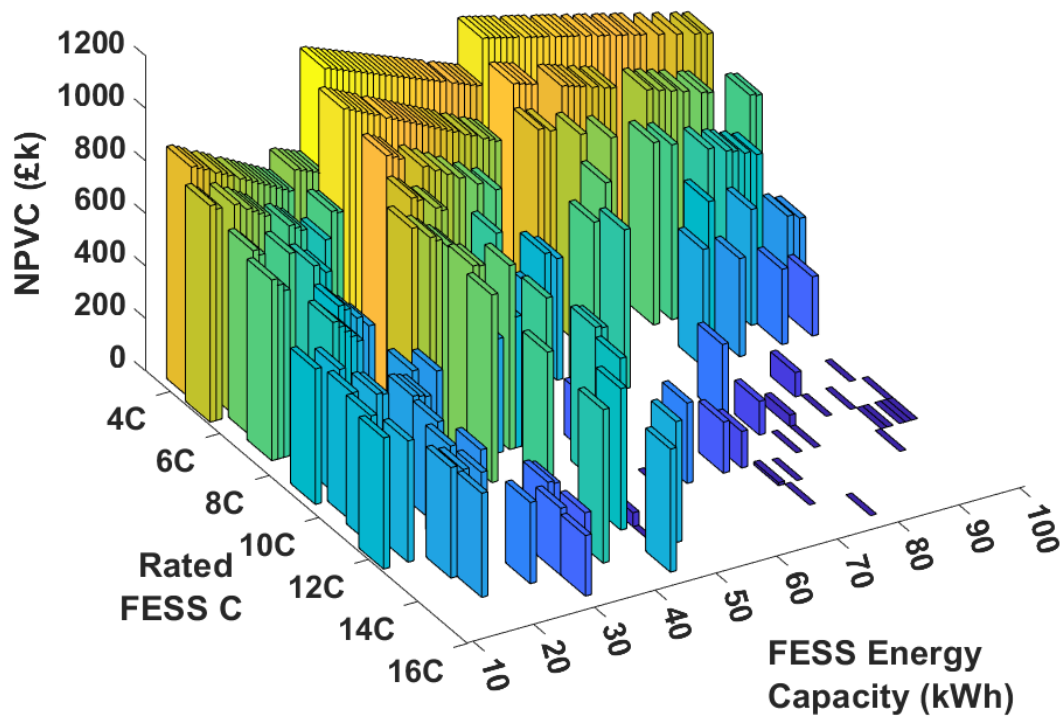


Figure 6.27: NPVC achieved for all individuals studied for CS-6 , $t_{av} = 120$s
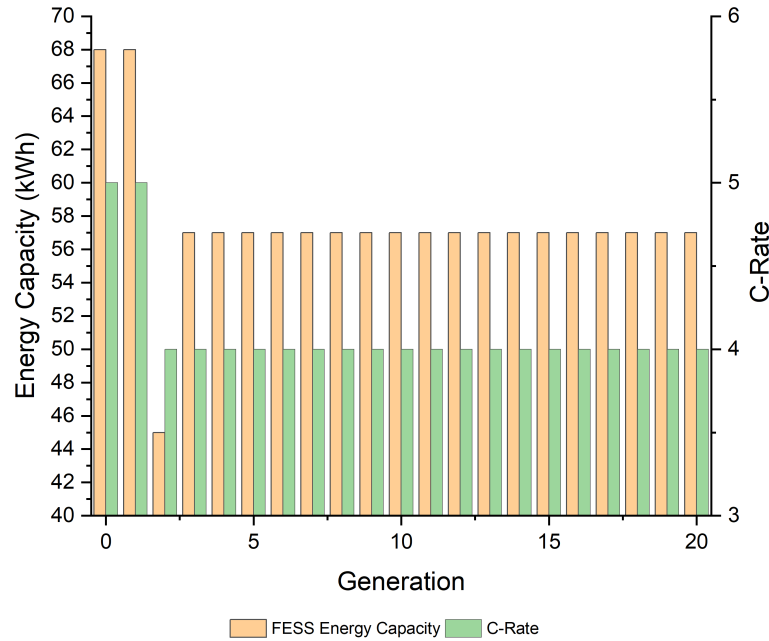
Figure 6.28: Best individuals per generation CS-6 , $t_{av} = 300$s

The range of values achieved across all individuals with these settings is shown in Figure 6.27, where it follows a very similar pattern to that seen previously with $t_{av}$ set to 30s. The NPVC fluctuates up and down with increasing energy capacity, whilst experiencing a steady decrease as C-Rate is increased. Once again the upper region of high C-Rate and high energy capacity is the worst performing.

Finally, Figure 6.28 shows the best configuration per generation for a $t_{av}$ setting of 300s. The algorithm determines a 57kWh 4C system to be the best configuration under these settings. This is quite different from the configurations for the 30s and 120s $t_{av}$ settings, up from 28kWh and 33kWh respectively suggesting the longer average calculation requires a higher energy capacity to manage.

Figure 6.29 shows the results concerning peak NPVC. This time the algorithm makes significant improvements, from a starting NPVC of £908,000 to a final value of £1,080,000. Once again, this is a reduction from both the 30s and 120s $t_{av}$ settings, but not by a significant amount. The energy capacity being 57kWh suggests that once again there is a significant range of FESS energy capacities that could be considered to provide a strongly positive NPVC, as long as the control strategy is set up accordingly thus opening up this application to a wider range of systems.

Whilst the pattern of results shown in Figure 6.30 is similar to that seen previously for the other control settings, it illustrates the slight shift in the optimal region now that the average power contribution is 300 seconds.

In order to fully explore the available control options under this strategy, a new GA was performed. This time, the FESS C-Rate was set to 4C as this is the most
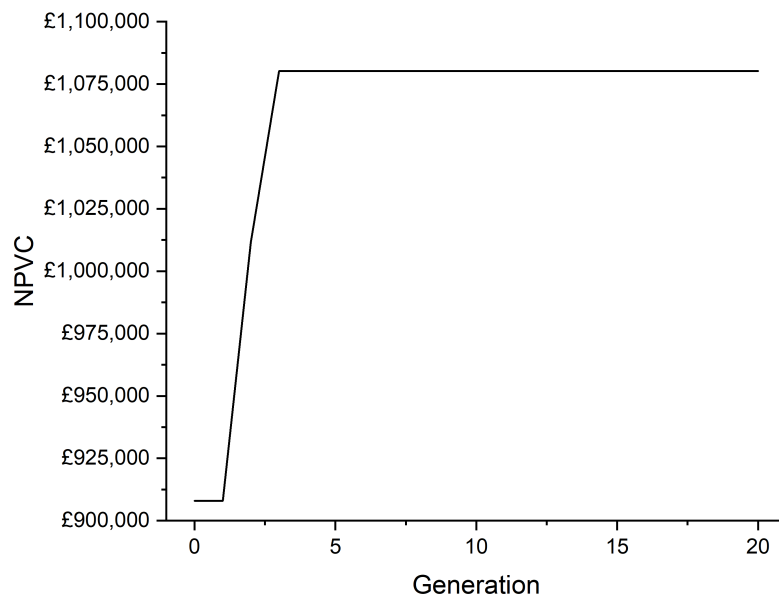
Figure 6.29: Maximum positive NPVC at each generation of the GA , $t_{\mathrm{av}} = 300\mathrm{s}$
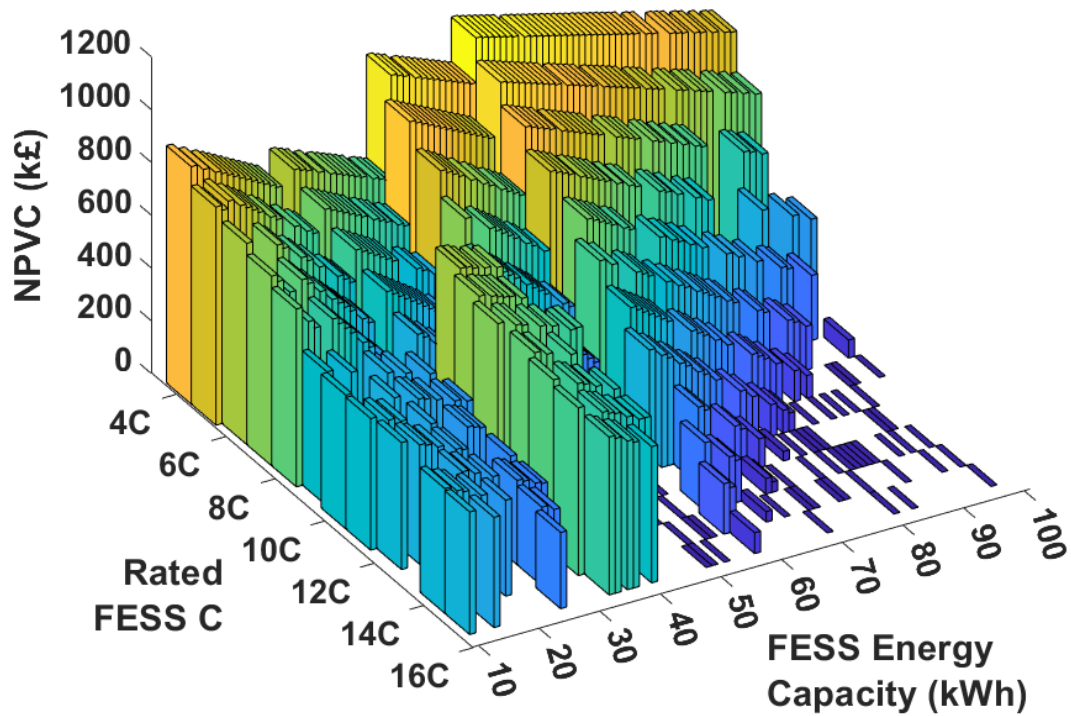


Figure 6.30: NPVC achieved for all individuals studied for CS-6 , $t_{\mathrm{av}} = 300\mathrm{s}$
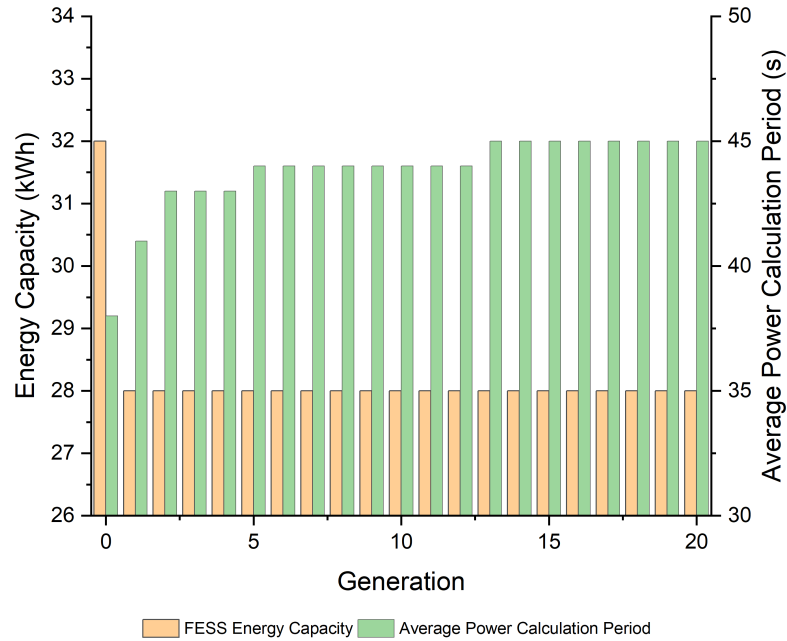
Figure 6.31: Best individuals at each generation of the CS-6 GA when varying $t_{\mathrm{av}}$

commonly produced value of the previous analysis. In its place, the second variable becomes $t_{\mathrm{av}}$, between boundaries of 10s and 60s. The FESS energy capacity remains as a variable but this time restricted between 20kWh and 40kWh, again replicating the range over which the 30s and 120s studies determined the optimal configurations to be within.

From Figure 6.31 it can be seen that the energy capacity is set very early in the algorithm, with the only significant refinement coming in the form of varying $t_{\mathrm{av}}$. The optimal setting is calculated by the 13th generation as 45 seconds whilst the energy capacity is determined to be 28kWh, the same as previously identified for setting $t_{\mathrm{av}}$ as 30.

Considering how this affects economic performance, Figure 6.32 shows the improvement across the generations. Comparing the final peak NPVC to previous studies is a small improvement over the previously calculated maximum value (£1,152,000 for $t_{\mathrm{av}}$ set at 30) to the new value of £1,155,000.

Overall then, this is an effective control strategy for generating significant extra value for a BESS site performing frequency response services with only a small-sized installation of FESS.

### 6.3.4 Control Strategy 7

The last control strategy to be optimised by GA is CS-7. This control strategy is the reverse of CS-6, with the BESS now providing an average power and the
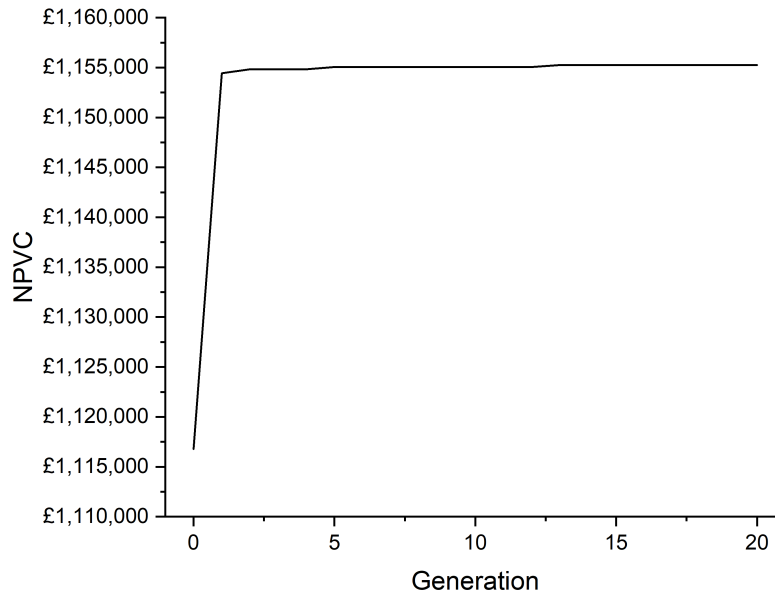
Figure 6.32: Maximum positive NPVC at each generation of the CS-6 GA when varying $t_{av}$

FESS supplementing this with the difference between the average and instantaneous request.

The GA was initially conducted with a $t_{av}$ of 30s, as in the previous section. Figure 6.33 shows the best individuals per generation for this GA run.

In sharp contrast to the previous GA runs in this chapter, Figure 6.33 shows a high level of change throughout the course of the algorithm, considering a total of 7 different configurations to be the best performing at different generations. Interestingly, there is a brief period where a 9C system is deemed to be the best performing before the 4C system is reconsidered at a different energy capacity. What this suggests is that for this control strategy, there is a wide range of different configurations that can provide similar economic impacts. The energy capacity also fluctuates quite significantly between 10kWh and 27kWh, before settling on 11kWh. This can be further illustrated when comparing with Figure 6.34.

The increase over the course of the algorithm is minimal in this instance, but the key takeaway from Figure 6.34 is that all of the best individuals at each generation fall within the range of £526,000 to £548,000 NPVC. Despite significantly different combinations of energy capacity and C-Rate being assessed, there is minimal difference in the overall NPVC. This indicates that this control strategy presents a method for allowing a wider range of FESS configurations to be deployed. Note that the figures in this subsection contain different axis limits than those presented previously in this section.

190
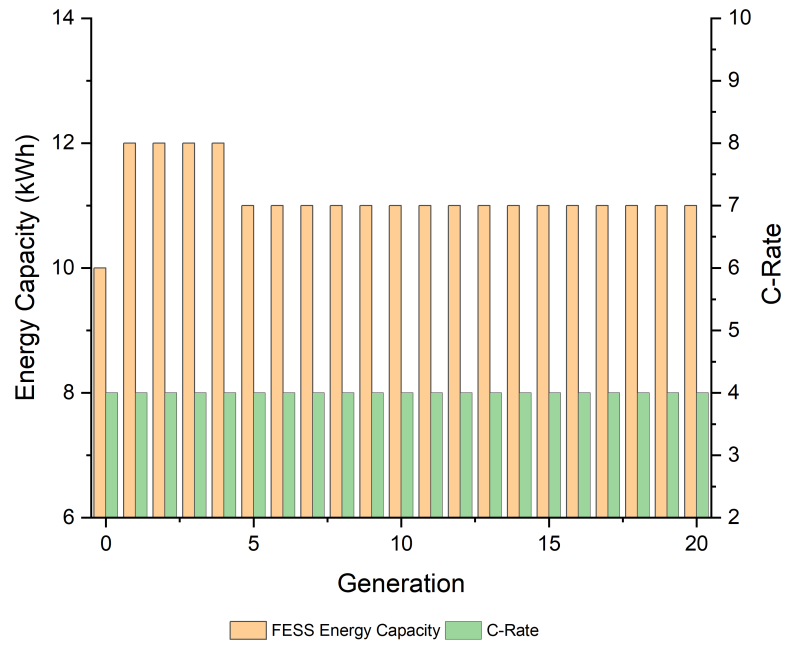
Figure 6.33: Best individuals per generation CS-7, $t_{\mathrm{av}} = 30\mathrm{s}$
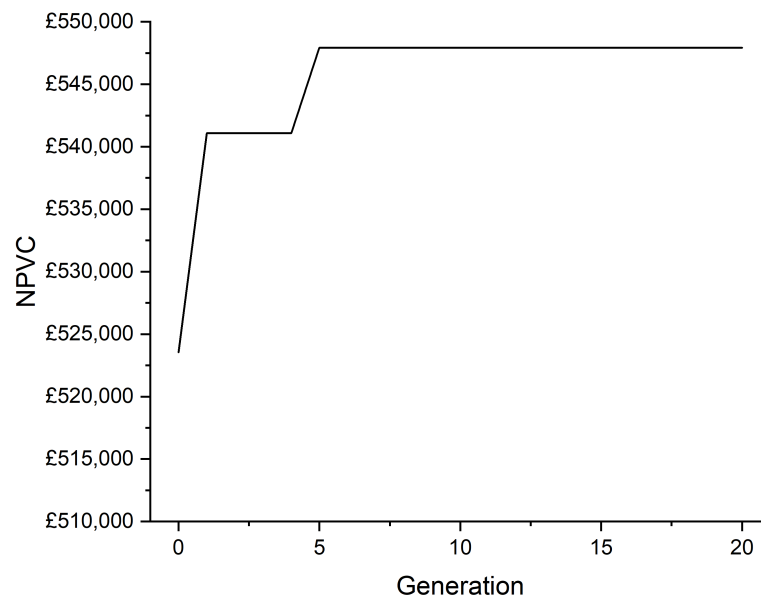


Figure 6.34: NPVC per generation CS-7, $t_{\mathrm{av}} = 30\mathrm{s}$
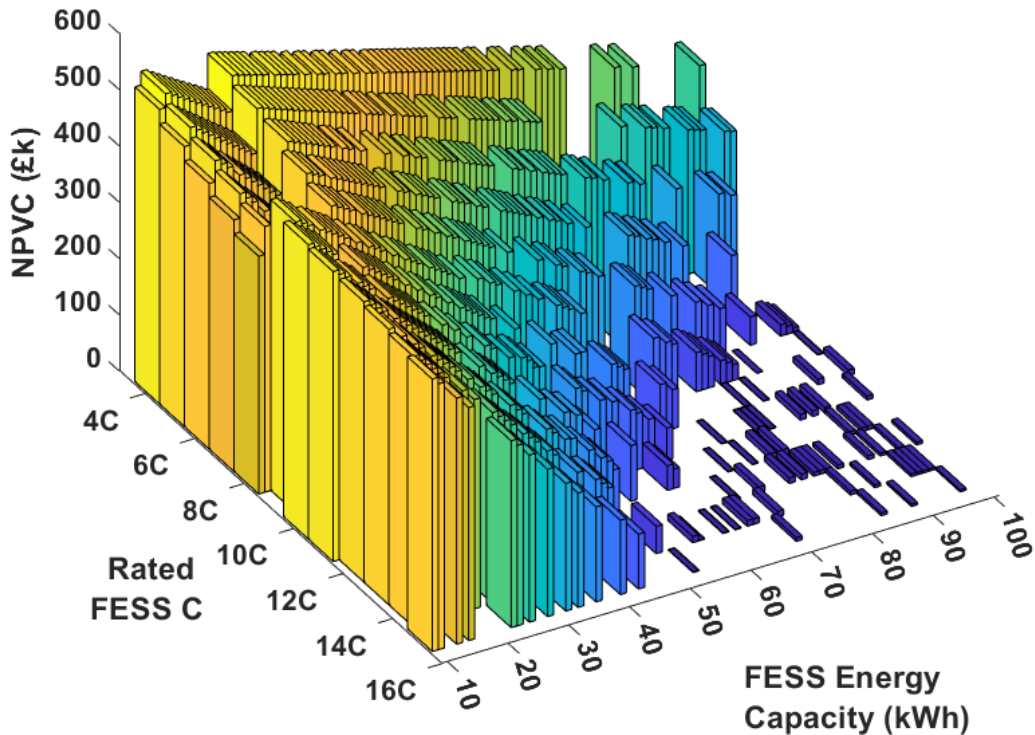
Figure 6.35: NPVC achieved for all individuals studied for CS-7, $t_{\mathrm{av}} = 30$s

When looking at the NPVC achieved by each individual studied, shown in Figure 6.35, it is clear that this control strategy is less able to accommodate a wide range of different combinations of C-Rate and energy capacity than those previously studied. However, at the lowest levels of energy capacity, the resulting NPVC does not vary significantly as the C-Rate is changed. Whilst the NPVC is lower than achieved for CS-6, it still provides significant extra value but with the added benefit of being suitable for delivery by a wider range of FESS C-Rate configurations. There is however a much more rapid and linear drop off as the energy capacity is increased, suggesting this control strategy is most suited to lower energy systems.

Figure 6.36 shows the number of times each individual within the population was chosen. Again, there is a clear concentration in the low C-Rate, low energy capacity region of the chart with the eventual best configuration being chosen the most times. It shows that the algorithm has tested a wide range of individuals whilst narrowing down to the optimum region for this population set.

Table 6.5: Results of the genetic algorithm for CS-7 under different control settings

| Setting | FESS kW Rating | FESS C-Rate | NPVC |
|---------|----------------|-------------|----------|
| 120s | 10kWh | 9C | £538,000 |
| 300s | 10kWh | 9C | £538,080 |

**Control Settings Sensitivity**

As in the previous section, the GA was conducted again for $t_{av}$ settings of 120s and 300s. The final results of these algorithms are shown in Table 6.5 with Figures A34-A37 in the Appendix showing the algorithm progress charts.

Interestingly, when the duration is modified a higher C-Rate of FESS becomes the dominant configuration, with both of the two further settings assessed resulting in the best configuration of a 10kWh 9C FESS. The increased value of $t_{av}$ leads to a slight drop in NPVC with almost identical results between the two different settings. 300s performs slightly better than 120s but to such a marginal degree that it suggests there is little economic benefit to modifying the settings for this control strategy.

However, from these results, it can be concluded that this control strategy offers another avenue for different configurations of FESS to be deployed, albeit with a significantly lower NPVC than achievable under different control strategies. There is very minimal difference in achieved NPVC when adjusting the control strategy settings.

### 6.3.5 Discussion

Three control strategies have been analysed and optimised using genetic algorithms in this section. In terms of economic benefit, it has been shown that CS-2 will result in the best impact from introducing a FESS whilst CS-6 can also provide a similar level of impact. CS-7 did not produce as significant an economic benefit but is still able to provide an NPVC in excess of £500,000.

The key talking point from this section however is the illustration that these financial benefits are not limited to a narrow range of FESS C-Rate and energy capacity configurations. It has been shown throughout the work that whilst different specifications may produce lower levels of economic benefit, they can still provide a significant impact.

The best configurations found for each individual control strategy so far are shown in Table 6.6. CS-2 provides the best economic performance, however, it is clear from the results shown that by changing the control strategy a wide range of different FESS configurations can be deployed for this application and still provide

Table 6.6: Summary of genetic algorithm control strategy optimization results

|     | FESS Energy Capacity | FESS C-Rate | NPVC | Control Settings |
| --- | --- | --- | --- | --- |
| CS1 | N/A | N/A | -£966,000 | N/A |
| CS2 | 91kWh | 4C | £1,188,000 | |
| CS6 | 28kWh | 4C | £1,152,000 | $t_{\mathrm{av}} = 30$s |
| CS6 | 28kWh | 4C | £1,155,000 | $t_{\mathrm{av}} = 45$s |
| CS6 | 33kWh | 4C | £1,115,000 | $t_{\mathrm{av}} = 120$s |
| CS6 | 57kWh | 4C | £1,080,000 | $t_{\mathrm{av}} = 300$s |
| CS7 | 11kWh | 4C | £548,000 | $t_{\mathrm{av}} = 30$s |
| CS7 | 10kWh | 9C | £538,000 | $t_{\mathrm{av}} = 120$s |
| CS7 | 10kWh | 9C | £538,080 | $t_{\mathrm{av}} = 300$s |

economic benefits.

Overall, it has been shown that there is significant promise to utilising different control strategies to maximise economic impact whilst also acknowledging that a significant range of different types of FESS can be deployed depending on the control strategy utilised.
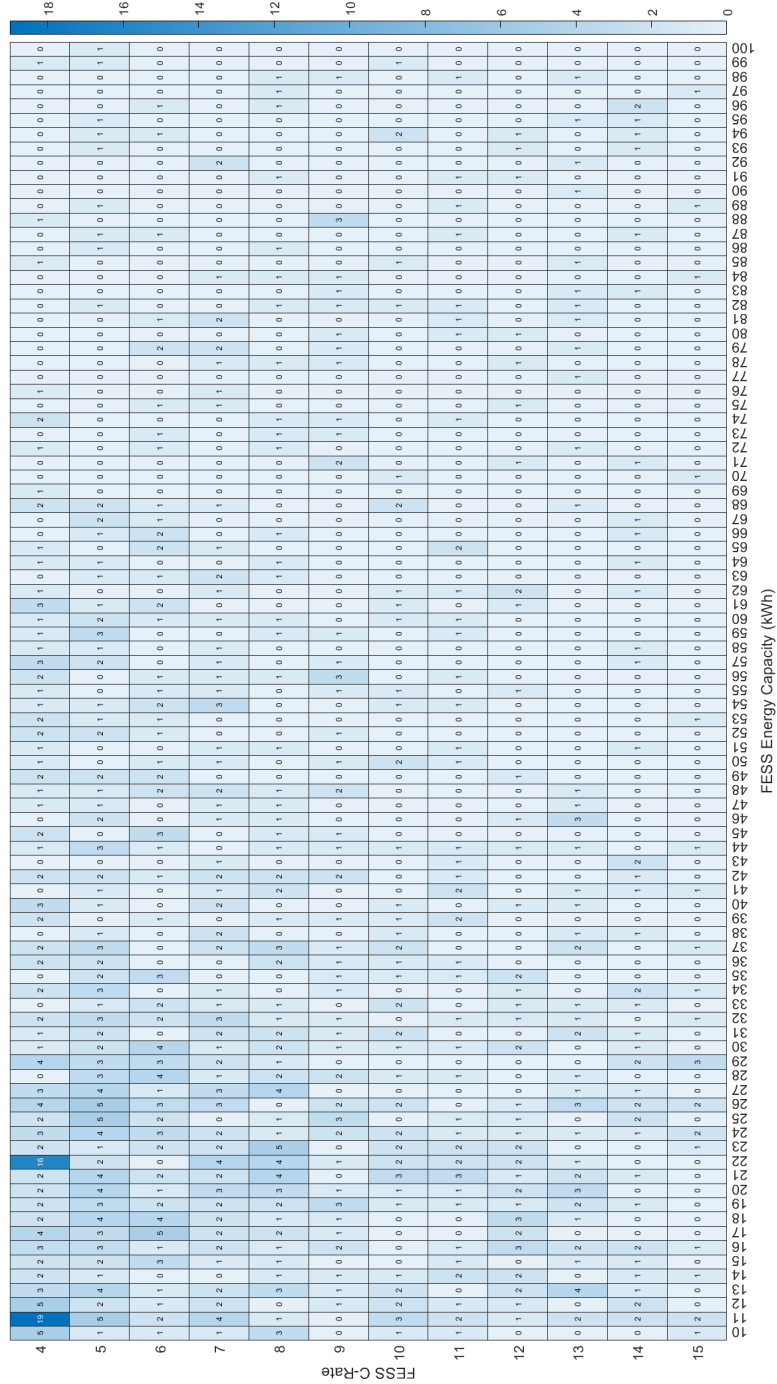
Figure 6.36: Heat map showing the GA exploration of CS-7, $t_{av} = 30s$

## 6.4 Techno-Economic Analysis of Remaining Control Strategies

As with the previous work explored in this chapter, the baseline which each control strategy is to be measured against consists of a 1MW/1MWh BESS delivering a 24/7 1MW service (CS-1). Using this approach it can be shown how the key metrics such as availability, net present value and BESS degradation change according to hybrid configuration and control mechanism.

### 6.4.1 Initial Assessment

The starting point for this section was taken as a 60kWh 4C FESS, which was determined as the optimal solution for CS2 and CS6 in the previously published paper [241]. As part of the process of writing this thesis, it was decided that the FESS cost used in this earlier analysis did not fall in line with the values used in other studies conducted subsequently (a FESS TCC of £2400/kW) due to using information available from the technical sponsor at the time of original publication. For this reason, the genetic algorithm study was revised to line up with the rest of the information presented in this thesis using a FESS TCC of £780/kW as determined in Section 2.5. As the FESS specification used is purely a starting point and undergoes significant sensitivity analysis, it has remained the initial specification studied in this section. For reference, the original study as a whole is available at [241]. The results of a year-long simulation using these specifications for each control strategy are shown in Table 6.7.

The key metrics that will be discussed in this section are as follows;

- Net Present Value Change - As previously discussed, this is the change in NPV when the hybrid system is compared to the baseline NPV of the BESS-only control strategy (CS-1)

- Threshold TCC - This is the highest TCC value at which a system will achieve a positive NPVC. It is important in determining at what point a system becomes economically viable. Unless otherwise stated, these calculations are performed using a discount rate of 5%.

- Availability and BESS degradation - As with previous studies, these two metrics are the primary technical criteria for measuring performance, with their definitions unchanged from earlier studies.

This initial set of simulations can be used to identify which control strategies are viable to investigate further and refine to their specific strengths. The baseline to

Table 6.7: Initial results of control strategy analysis showing availability, cycles and BESS degradation for a 1MW 1C BESS and 60kWh 8C FESS

|  | CS-1 | CS-2 | CS-3 | CS-4 | CS-5 | CS-6 | CS-7 | CS-8 |
|---|---|---|---|---|---|---|---|---|
| Availability | 96.33% | 95.83% | 94.25% | 86.40% | 96.95% | 96.93% | 96.77% | 90.00% |
| BESS Cycles | 1304 | 525 | 986 | 305 | 986 | 609 | 1297 | 638 |
| FESS Cycles | 0.0 | 7998 | 1872 | 7165 | 2730 | 7995 | 1513 | 4516 |
| Degradation | 2.6% | 1.0% | 2.0% | 0.5% | 2.0% | 1.2% | 2.5% | 1.3% |
| NPV (£ks) | -966 | 14 | -405 | -260 | 73 | 96 | -539 | -528 |

which all subsequent control strategies will be compared is CS-1 (BESS only) where it can be seen that the average availability is 96.33% and a high overall degradation over the course of 1 year is 2.6% due to the high cycle count (1304 over 1 year).

This is a prohibitive amount of degradation for the service to be viable as the system would need replacing frequently, and so this is one of the key areas that will be assessed with the remaining control systems. CS-2, CS-6 and CS-7 have been optimised and discussed in the previous section.

CS4, where the FESS takes control of all requests within a set frequency band and the BESS takes control of all requests outside of that band, shows the lowest amount of BESS degradation over the course of a year, decreasing from 2.6% when a BESS is operating alone to 0.5% under this control strategy. However, it also has a very low availability, which will result in poor economic performance. This control strategy is therefore worth investigating further to determine whether it can be modified to provide a stronger overall performance.

Alternatively, CS-3 represents a low amount of degradation reduction for the BESS with a value of 2.0% over the course of a year. Considering that this control strategy does not offer greater availability than other control strategies studied that provide a much greater degradation reduction, this control strategy does not represent a promising option. However, it will be explored briefly to verify that changing control settings cannot extract greater performance benefits.

CS-5 shows excellent availability and a moderately reduced level of BESS degradation. However, the lack of FESS cycles present in this control strategy suggests that it could be utilised in a more significant role to reduce the degradation further. This will be investigated further to determine if changing the FESS size can provide a more balanced solution.

Finally, CS-8 also represents a potentially exploitable initial assessment, offering reduced BESS degradation with low average availability. This control strategy can be further investigated to assess whether the availability can be increased by modifying either the duration for the alternating energy storage operations or by evaluating different configurations of FESS.

Table 6.8: BESS Degradation for varying frequency threshold settings under CS-3

| BESS Degradation (%) | | Lower Frequency Threshold (Hz) | | | | | |
|---|---|---|---|---|---|---|---|
| | | 49.95 | 49.94 | 49.93 | 49.92 | 49.91 | 49.90 |
| | 50.05 | 0.5 | 0.5 | 0.5 | 0.5 | 0.5 | 0.5 |
| | 50.06 | 0.8 | 0.8 | 0.8 | 0.8 | 0.8 | 0.8 |
| Upper Frequency | 50.07 | 0.9 | 1.1 | 1.1 | 1.1 | 1.1 | 1.1 |
| Threshold (Hz) | 50.08 | 0.9 | 1.2 | 1.4 | 1.4 | 1.4 | 1.4 |
| | 50.09 | 0.9 | 1.2 | 1.5 | 1.7 | 1.7 | 1.7 |
| | 50.1 | 0.9 | 1.2 | 1.5 | 1.8 | 1.9 | 2.0 |

Table 6.9: Availability for varying frequency threshold settings under CS-3

| Availability (%) | | Lower Frequency Threshold (Hz) | | | | | |
|---|---|---|---|---|---|---|---|
| | | 49.95 | 49.94 | 49.93 | 49.92 | 49.91 | 49.90 |
| | 50.05 | 84.63 | 82.73 | 80.98 | 79.29 | 77.66 | 76.05 |
| | 50.06 | 89.47 | 87.41 | 85.59 | 83.96 | 82.41 | 80.63 |
| Upper Frequency | 50.07 | 88.35 | 91.60 | 89.77 | 88.10 | 86.60 | 85.19 |
| Threshold (Hz) | 50.08 | 86.08 | 90.87 | 93.23 | 91.64 | 90.23 | 88.91 |
| | 50.09 | 84.14 | 88.92 | 93.45 | 94.45 | 93.14 | 91.77 |
| | 50.1 | 82.46 | 87.24 | 91.81 | 95.53 | 95.32 | 94.25 |

## 6.4.2 Control Strategy 3

Control Strategy 3, as discussed in the previous section, utilises the BESS to respond to any requests when the frequency is within a set range, whilst the FESS responds to any requests where the frequency is outside of this range. The results of the initial assessment were not favourable for this control strategy, with a high level of degradation and a lower availability than found in the majority of the other control strategies studied.

**Control Settings Sensitivity**

The key variables within the control strategy consist of the high and low-frequency boundary thresholds. To explore whether increased technical performance can be achieved, these values were varied as shown in Table 6.8 and Table 6.9 with the same 60kWh 4C FESS configuration.

In general, these results do not show significant improvements over the initial assessment. Whilst in some areas there is a minimal improvement to average availability along with a slight decrease to BESS degradation, these performance benefits are not significant enough to allow this control strategy to compete with others discussed in this thesis. From a viewpoint of attempting to balance the trade-off between availability and degradation from this control strategy, the combination

Table 6.10: Excerpt of NPVC results from frequency threshold variation for CS-3, rounded to the nearest £k

| NPVC (£k) | | Lower Frequency Threshold (Hz) | | | | |
|---|---|---|---|---|---|---|
| | | 49.94 | 49.93 | 49.92 | 49.91 | 49.90 |
| | 50.07 | 497 | 620 | 528 | 438 | 355 |
| Upper Frequency | 50.08 | 623 | 785 | 745 | 667 | 581 |
| Threshold (Hz) | 50.09 | 507 | 776 | 488 | 462 | 395 |
| | 50.1 | £411 | £674 | £530 | £586 | £561 |

of 49.94Hz/50.07Hz may represent the best compromise. The main reason for this conclusion is that with a degradation of 1.1% and average availability of 91.60%, there is scope to improve the technical performance of the site whilst maintaining a level of degradation similar to other control strategies.

However, the impact of these metrics on the overall NPVC of the system is a complex balance between increasing availability whilst preventing excessive degradation, and the best economic solution is often not necessarily the best technical performing solution. To verify this, the NPVC was calculated with a TCC of £780/kW, and the results are shown in Table 6.10. Note that this analysis was performed over a smaller range of values, with setting combinations that did not achieve a minimum of 90% availability discounted on a technical performance basis.

From this analysis, it can be seen that when the economics are considered, the best control settings are a combination of 49.93/50.08Hz. There is a complex balance between degradation and availability, as availability is increased it brings about an increase in degradation, thus both increasing income and expenditure.

Taking these control settings as the starting point, the energy capacity and C-Rate can now be varied to assess how this affects both the average availability and the NPVC. With the control settings fixed, the degradation of the BESS will remain constant even as the FESS capacity is varied.

**Energy Capacity and C-Rate Sensitivity**

To fully explore the potential improvement of this control strategy, a range of different FESS configurations were assessed for techno-economic performance under the previously determined control settings. Figure 6.37 shows how the availability of the site changes when varying the C-Rate and energy capacity.

The results of this analysis are very interesting, showing that as the energy capacity of the system is increased the subsequent effect of varying the C-Rate has no impact on average availability. However, at lower energy capacities there is a significant positive impact from reducing the C-Rate.

Following this, an NPVC assessment was conducted to verify the economic per-
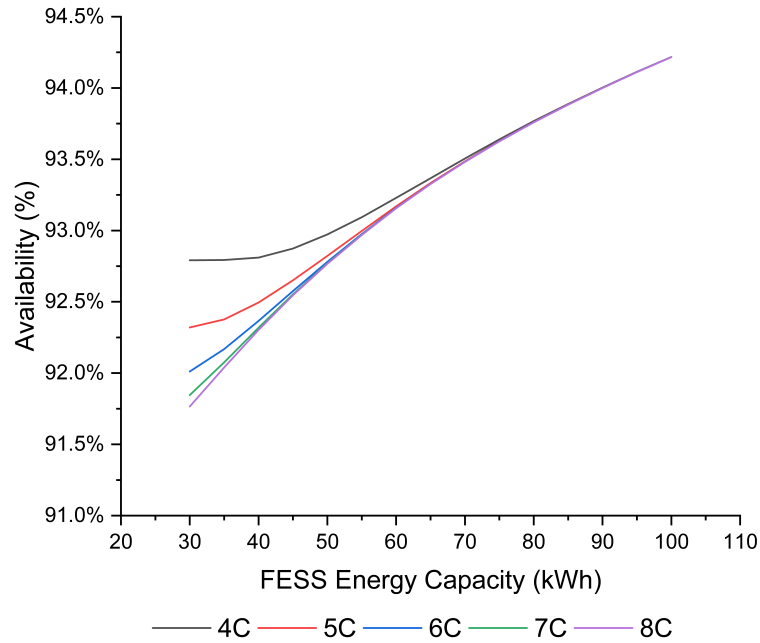
Figure 6.37: Average availability for CS3 of varying FESS energy capacities and C-Rates

formance of the systems, with the TCC set as £780/kW to represent an average value and a 5% discount rate. The results of this study are shown in Figure 6.38.

The best-performing system economically is the 4C 55kWh system, with a total NPVC of £785,000, with this value falling as the energy capacity is increased and a sharp drop happening as the energy capacity is decreased. This step change occurs due to the system crossing the threshold for increased availability payments as the energy capacity of the FESS is increased. For a 5C system, the peak energy capacity remains the same, however for the 6C, 7C and 8C systems, the peak energy capacity is 50kWh with the overall NPVC declining as the C-Rate is increased. However, it should be noted that all of the C-Rates and energy capacities shown in Figure 6.38 provide a good level of NPVC, with the lowest value of £335,000 being provided by an 8C 45kWh FESS. This indicates that a significant range of different FESS configurations could be deployed using this control strategy.

The threshold TCC, being the TCC at which the site provides a positive NPVC at a discount rate of 5%, is shown in Figure 6.39. It can be seen that the threshold TCC for this system under this control strategy is £4,350/kW. It can be concluded therefore that despite initial doubts over the viability of this control strategy, it can in fact provide a positive NPVC over a range of configurations and up to a high threshold TCC when considering common FESS costs.
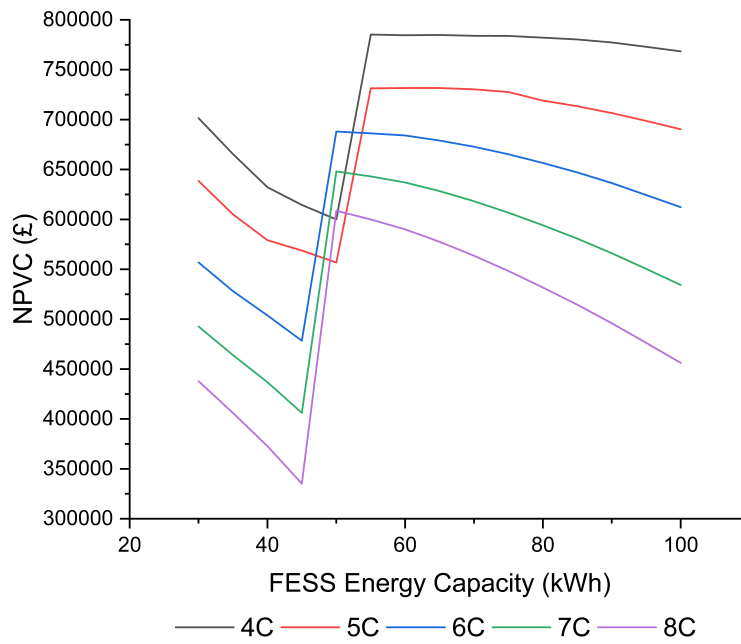
Figure 6.38: NPVC for CS3 of varying FESS energy capacities and C-Rates
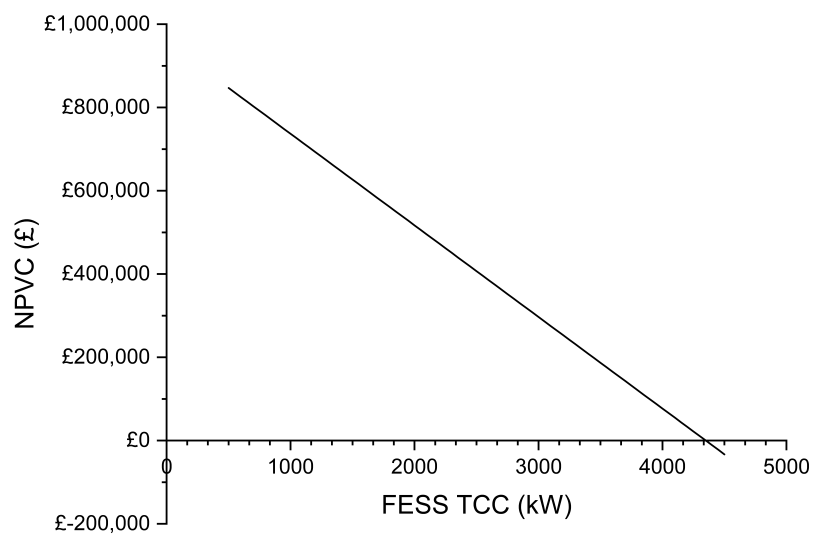
Figure 6.39: NPVC of a 50kWh 4C system across different TCC values
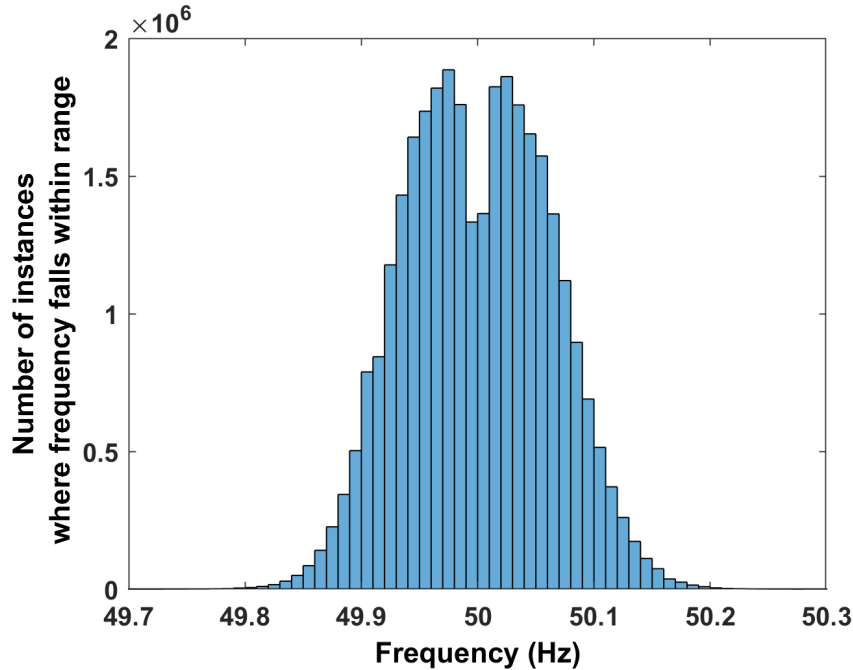
Figure 6.40: Histogram showing the number of instances the grid frequency falls within given ranges (a bin width of 0.01) over the course of a year between November 2020 and October 2021

### 6.4.3 Control Strategy 4

As discussed in Table 6.2 and shown in Figure 6.4, this control strategy operates by assigning all of the power requests derived from a frequency within a set threshold to the FESS, and anything outside of this threshold to the BESS. For the initial assessment of this control strategy, the thresholds have been set as 49.9Hz for the lower band limit and 50.1Hz for the upper band limit, meaning any frequency response in the 49.9-50.1Hz range will be delivered by the FESS and anything outside will be delivered by the BESS.

As can be seen from Figure 6.40 which shows a histogram of the frequency over the period November 2020 - October 2021, this would cover a vast amount of the time in which the service would be expected to operate, with the majority of the frequency instances falling within this 49.9Hz-50.1Hz range and minimal activity outside of it.

**Energy Capacity Sensitivity**

The first step to assessing how the performance of this control strategy can be improved is to determine the performance over a wide range of different FESS configurations. The simulation was therefore executed over a range of 100kWh to 1MWh FESS maintaining the C-Rate at 4C resulting in a power range of 400kW to 4MW. Note that for this control strategy, an initial study on varying C-Rates was carried
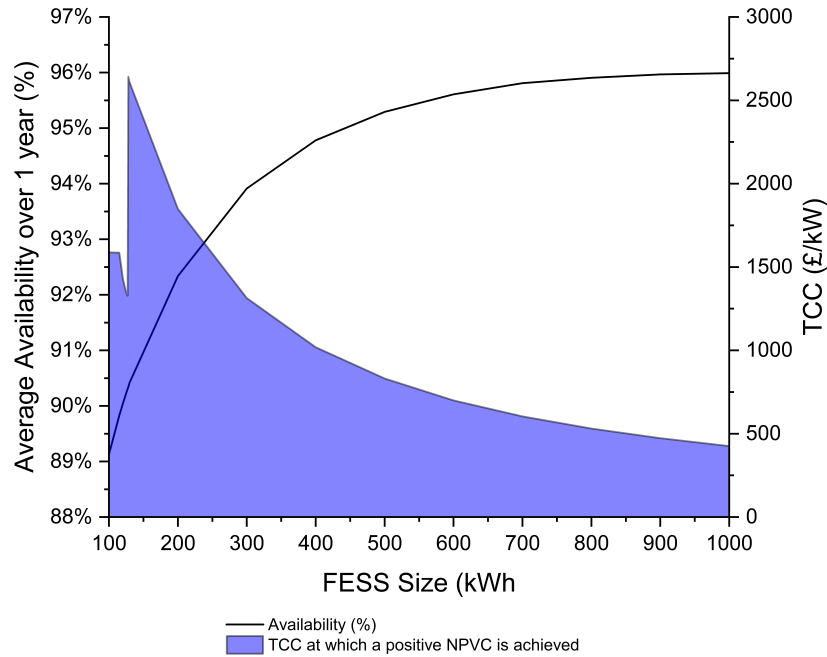
Figure 6.41: Average availability and threshold cost for FESS to provide a positive NPVC across varying FESS sizes for CS-4. The shaded area represents values of TCC where a positive NPVC would be achieved

Table 6.11: Excerpt of NPVC results from frequency threshold variation for CS-4 using a 128kWh 4C system, rounded to the nearest £k

| NPVC (£k) | | Lower Frequency Threshold (Hz) | | |
|---|---|---|---|---|
| | | 49.92 | 49.91 | 49.9 |
| Upper Frequency Threshold (Hz) | 50.08 | £658 | £653 | £592 |
| | 50.09 | £935 | £998 | £1007 |
| | 50.1 | £816 | £907 | £953 |

out and showed that increasing the C-Rate did not provide any performance benefit and purely resulted in increased costs and therefore decreased economic value.

The results of varying the FESS energy capacity are shown in Fig. 6.41 where both average availability and the threshold TCC for a positive NPVC are displayed. As the energy capacity of the system is increased the availability increases in line with this, plateauing at 96% availability. Conversely, as the energy capacity is decreased the threshold for positive NPVC increases to a peak of £2,641/kW for a 128kWh system before dropping again as the energy capacity is decreased further.

This sheer drop occurs as the system reaches a point of generating significantly less income due to low availability. It subsequently rises again when decreasing beyond this point as there is a minimal further reduction in income but a continuous reduction in TCC as the FESS gets smaller.
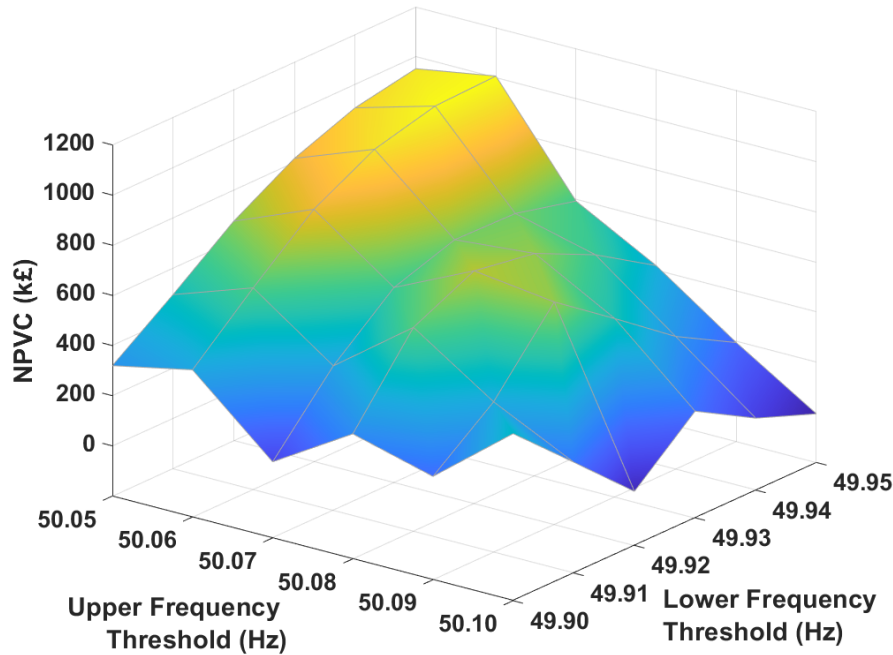
Figure 6.42: NPVC for varying high and low-frequency threshold set points for CS-4 using a 128kWh 4C system

**Control strategy Settings Sensitivity**

Taking the results from the previous section into account (utilising a 128kWh system), the simulation was then run with varying settings for the high and low-frequency boundaries, taking into account the histogram shown in Fig. 6.40. and noting that as the frequency range for FESS operation is reduced, they will be asked to operate with increasing regularity, with a steep increase in operating time as the frequency gets closer to 50Hz.

The low boundary was varied between 49.9Hz and 49.95Hz in 0.01Hz intervals, and the high boundary was varied between 50.05Hz and 50.1Hz also in 0.01Hz intervals. The TCC was set to be £780/kW as determined previously in Chapter 2. The resulting NPVC was then plotted for each combination of high and low-frequency boundaries, as seen in Fig. 6.42. with Tables 6.11 showing the values for the upper region of the graph.

For all of the set point combinations, there is an increase to the overall NPV. However, for the 49.9/50.09Hz and the 49.91/50.09Hz combination the NPVC is greater than the original 49.9/50.1Hz combination. This asymmetry takes advantage of sacrificing a small amount of degradation for an increase in average availability. These results suggest that further improvements can be made by re-performing the energy capacity sensitivity analysis conducted previously with the two new pairs of set points. The 49.9/50.09Hz is the best-performing combination, representing an

Table 6.12: Excerpt of BESS Degradation results from frequency threshold variation for CS-4

| BESS Degradation | | Lower Frequency Threshold (Hz) | | |
| --- | --- | --- | --- | --- |
| | | 49.92 | 49.91 | 49.9 |
| Upper Frequency Threshold (Hz) | 50.08 | 1.0% | 1.0% | 0.9% |
| | 50.09 | 0.8% | 0.7% | 0.7% |
| | 50.1 | 0.6% | 0.5% | 0.5% |

Table 6.13: Excerpt of Average Availability results from frequency threshold variation for CS-4

| Average Availability | | Lower Frequency Threshold (Hz) | | |
| --- | --- | --- | --- | --- |
| | | 49.92 | 49.91 | 49.9 |
| Upper Frequency Threshold (Hz) | 50.08 | 92.6% | 92.4% | 91.4% |
| | 50.09 | 91.1% | 91.4% | 91.3% |
| | 50.1 | 89.5% | 90.2% | 90.3% |

increase of £1,007,057.

In Table 6.12, which details the level of degradation the experiences under each combination of settings, it can be seen that a significant reduction in overall BESS degradation can be achieved for all combinations, but with the most significant reductions being achieved when the Upper-Frequency Threshold is set at 50.1Hz as this is when the BESS will be operating the least. Where lower levels of degradation are present this would lead to an extended BESS lifetime and subsequent improvements to the economic performance of the site.

In Table 6.13, which details the average availability under each combination of settings, it can be seen that there is no significant variation between all of the combinations. Whilst the availability peaks at 92.6% with the 50.08/49.92Hz combination, this only drops by 3.1% when considering the worst combination (50.1/49.92Hz). Whilst the availability has been improved from the initial assessment, it still does not reach the ideal level of 95% average availability which is a significant drawback of the strategy.

**Re-assessing energy capacity**

The previous energy capacity sensitivity analysis was repeated this time using firstly a 49.9/50.09Hz and secondly a 49.91/50.09Hz set point combination. Figure 6.43 shows a focused view of Figure 6.41, displaying the 100-140kWh region of the results where the peak for all three studied frequency combinations occurs. For the
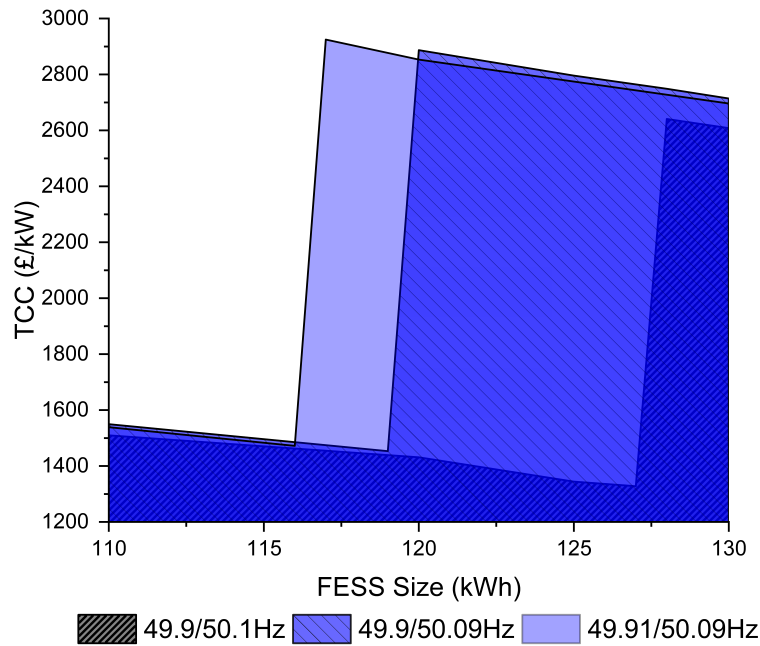
Figure 6.43: Threshold TCC for a FESS to provide a positive NPVC at varying energy capacities for CS-4

49.9/50.09Hz combination, the FESS size with the highest possible TCC to provide positive NPVC at a 5% discount rate occurs at 120kWh compared to the previously determined 128kWh for the 49.9/50.1Hz combination, and additionally will now provide a positive NPVC up to a value of £2,887/kW compared to a previous value of £2,641/kW.

When using set points of 49.91/50.09Hz the FESS size which provides the highest possible TCC for a positive NPVC is 117kWh which can provide a positive NPV up to a value of £2,925/kW. This indicates that the 49.91/50.09Hz pairing represents the best setting for this control strategy.

For the two variations on set point combinations, the sudden fall in TCC for a positive NPVC occurs at a lower energy capacity than in the original set point combination. Changing the set points in this way transfers a small amount of the energy throughput from the FESS to the BESS, sacrificing a minimal increase in degradation for an increase in availability.

**Current economic implications**

As previously discussed, literature places the TCC for a FESS across a wide range of values. To give a representation across this range, the simulation was executed using different TCC values as well as using the control settings determined above and taking the optimal FESS configuration for the 49.91/50.09Hz set point. The NPVC for a range of different TCC values was produced and plotted in Figure 6.44.
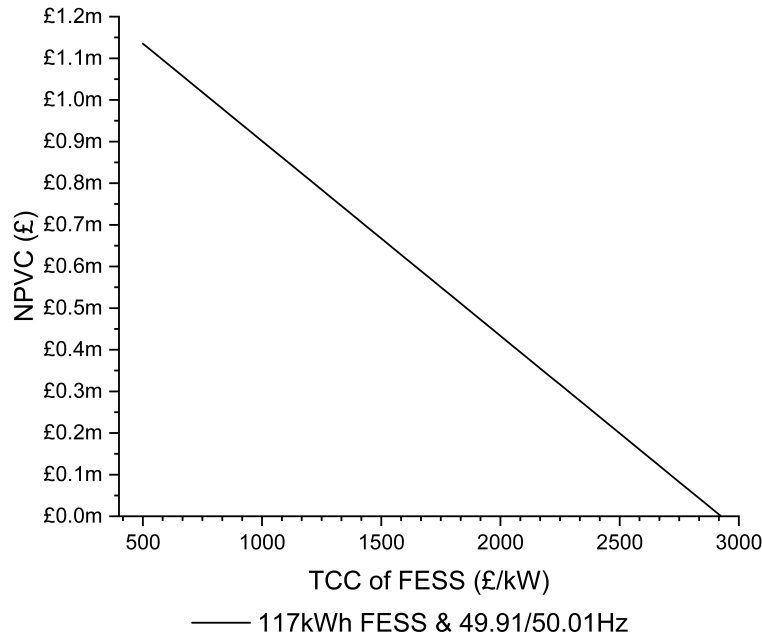
Figure 6.44: NPVC when introducing a 117kWh FESS of varying TCC for CS-4

The chart shows as expected that as the TCC increases the scale of positive NPVC is reduced with a linear relationship identified. Assuming a TCC at the lower end of the available literature, the hybridisation under this control strategy would increase the NPV of the system by £1,135,000 at £500/kW. Even at a value of £2000/kW, the NPV would be increased by £433,311, showing a strong case for the effectiveness of this control strategy (CS-4) despite the lower-than-ideal level of availability. At a TCC of £780/kW the NPVC is £1,004,000.

### 6.4.4 Control Strategy 5

For this control strategy, the power demand is split according to the power rating of each HESS component. Under the initial simulation, this control strategy achieved an average availability of 96.95% and a total BESS degradation of 2.0%. The are two main variables that will affect the effectiveness of this control strategy, the FESS energy capacity and the FESS C-Rate.

The initial set of simulations was performed with CS-5 set to split the power request according to the ratio of 100% of the FESS Max Power to the overall service, as discussed in Table 6.2. Example ratios are shown in Table 6.14. The maximum contribution that the FESS will provide at any one time, regardless of its power rating, is 50%.

Table 6.14: Examples of the ratio of demand split for varying levels of FESS rated power

| Fess Rated Power (kW) | FESS Contribution | BESS Contribution |
|---|---|---|
| 200 | 20% | 80% |
| 300 | 30% | 70% |
| 500 | 50% | 50% |
| 700 | 50% | 50% |

Table 6.15: Availability under different FESS configurations for CS-5

| FESS Energy Capacity (kWh) | 4C | 8C | 12C |
|---|---|---|---|
| 15 | 96.77% | 96.82% | 96.85% |
| 50 | 96.94% | 96.90% | 96.62% |
| 100 | 96.97% | 95.92% | |
| 150 | 96.80% | | |
| 200 | 96.26% | | |

## C-Rate and Energy Capacity sensitivity analysis

Shown in Table 6.15 and 6.16 are the performance results from varying the energy capacity between 15kWh and 250kWh and the C-Rate between 4 and 16C. Note that the greyed-out sections of the tables represent hybrid combinations that are not relevant for this control strategy as the FESS contribution would render the BESS irrelevant and hence is an unrealistic scenario to consider.

The results show that there is a minimal impact on overall availability when the configuration of the FESS is varied, with the average availability ranging from 95.92% to 96.97% for the configurations tested. On the other hand, there is a significant impact on the BESS degradation when the FESS configuration is varied, ranging from 0.5% to 2.5% suggesting that in certain scenarios this control strategy actually causes increased degradation in the BESS compared to the BESS only strategy of CS-1.

This is likely due to the reduction in output causing it to reach SOC limits less often and hence operating for longer, with the FESS not taking enough of a share of the power to provide any benefit. However, in some cases, the degradation is significantly reduced extending the life of the BESS and increasing the average availability at the same time.

Table 6.16: BESS Degradation under different FESS configurations for CS-5

| FESS Energy Capacity (kWh) | 4C | 8C | 12C |
|---|---|---|---|
| 15 | 2.5% | 2.3% | 2.1% |
| 50 | 2.1% | 1.5% | 1.0% |
| 100 | 1.5% | 0.5% | |
| 150 | 1.0% | | |
| 200 | 0.5% | | |
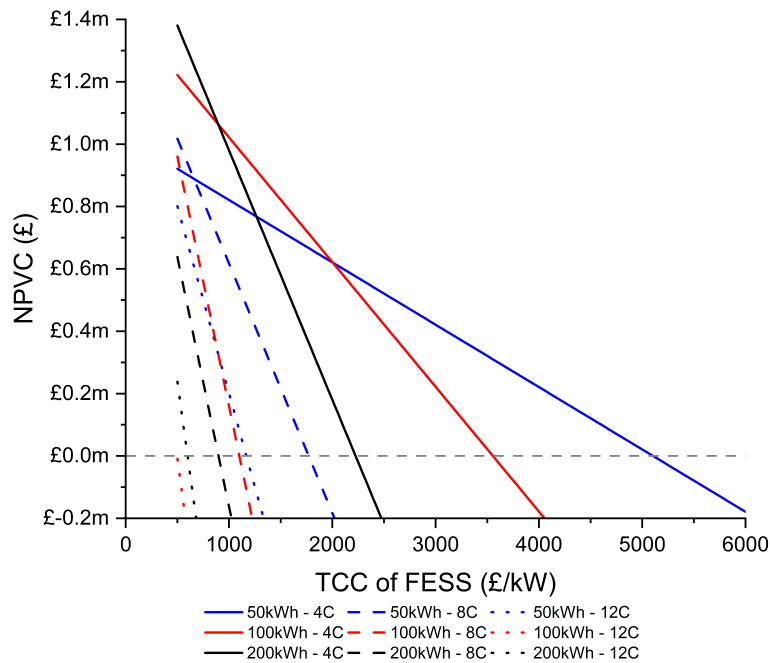


Figure 6.45: NPVC for varying TCC across different FESS configurations for CS-5

**TCC sensitivity analysis**

To further analyse the effectiveness of this control strategy, a TCC sensitivity analysis has been conducted. This was conducted for FESS sizes of 50kWh, 100kWh and 200kWh at varying C-Rates of 4, 8 and 12. The results of this analysis are shown in Fig. 6.45. showing the NPVC for TCC values ranging between £500/kW and £6000/kW. The discount rate is again set to 5% for this analysis.

Of the configurations tested, the 200kWh 4C system shows the highest available NPVC at a TCC of £500/kW but drops sharply downwards as the TCC is increased. The configurations considered have a TCC profitability threshold between £595/kW and £5,855/kW with the exception of the 100kWh 12C configuration which does not achieve a positive NPVC above £500/kW. Tthe majority of the systems considered have threshold TCC values that fall into the range of TCC values previously identified in Chapter 2 as commonly specified FESS values, namely in the range of

£500-2,500/kW. This suggests that it is likely that many of the FESSs currently available could result in a positive techno-economic performance when implemented in this way.

Looking at the leading edge of the graph, the best configurations of FESS for this control strategy are as follows;

- Between £500/kW and £875/kW the 200kWh 4C system is the best performing.

- Between £875/kW and £1,975/kW the 100kWh 4C system is the best performing.

- Above £1,975/kW the 50kWh 4C system is the best performing, becoming negative above £5,105/kW

This suggests that for this control strategy, the lower C-Rate configurations are more economically viable in general, with the energy capacity to be installed being dependant on what the current TCC is.

### 6.4.5   Control Strategy 8

When utilising this control strategy, the ESS responsible for delivering the service is alternated based upon a set duty period. In the initial assessment, this was set to alternate for 30 minutes of delivery from each ESS in turn. For example, the FESS will be asked to deliver 100% of the requested power for 30 minutes, followed by the BESS being asked to deliver 100% of the requested power for 30 minutes.

Fig. 6.46, shows how the BESS degradation varies according to the duration of time that the FESS is asked to operate with the BESS degrading more the less time the FESS operates for. Even with the FESS operating for 30 minutes of every hour, this control strategy cannot achieve the same high reductions in BESS degradation as achieved previously with CS-4 and CS-5. However, it still achieves modest reductions in degradation with any time length above 15 minutes of FESS operation per hour resulting in an overall BESS degradation of less than 10% per year.

**C-Rate and Energy Capacity sensitivity analysis**

The main variables of this control strategy are the FESS contribution duration, the FESS energy capacity and the FESS C-Rate. However, this initial assessment started from the point of a 60kWh 4C FESS that provided a maximum of 240kW of power, meaning it could not provide the required service in the periods that it was active. For this reason, in this section a power-based sensitivity analysis was
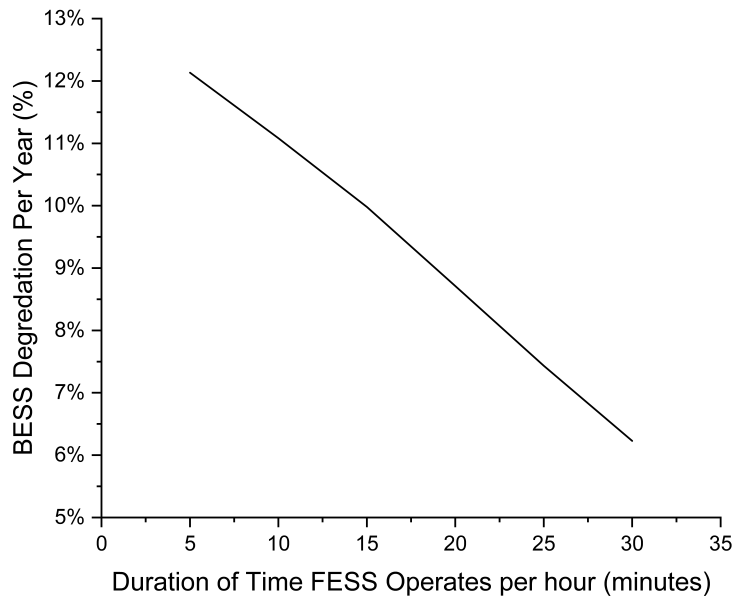
Figure 6.46: BESS Degradation per year for varying settings of FESS duration of operation per hour for CS-8

conducted with the power set at 1000kW and the C-Rate set at 4, 8 and 12C, thus changing the energy capacity of the FESS.

The proportion of an hour that the FESS is active for was also varied between 20 and 30 minutes with the average availability for these simulations shown in Fig. 6.47. An initial economic assessment is also shown in Fig. 6.47, setting the FESS TCC at £780/kW to determine how profitable each combination of C-Rate and FESS contribution duration could be at this cost.

Average availability experiences a steady decline for all 3 variations of C-Rate, with only the 4C system being able to provide an availability above 95% at the lower FESS duration end of the scale. It can be seen that the best results at this TCC are achieved with a FESS contribution duration of 23 minutes, and the overall positive NPVC reduces as the C-Rate of the FESS is increased beyond this point.

In the opposite direction, there is a sharp drop off once the duration is dropped below 23 minutes, due to the BESS degradation remaining high enough that an additional replacement system is required within the studied time frame. The best-performing system is the 4C system which peaks at £465,000 when the FESS contribution is 23 minutes per hour. The peak for the 8C system is £357,000 and for 12C is £275,000.

Following this, a threshold TCC for positive NPVC assessment for this level of FESS contribution duration was carried out for the range of C-Rates with the results shown in Fig. 6.48. There are only 5 combinations of active FESS time and FESS
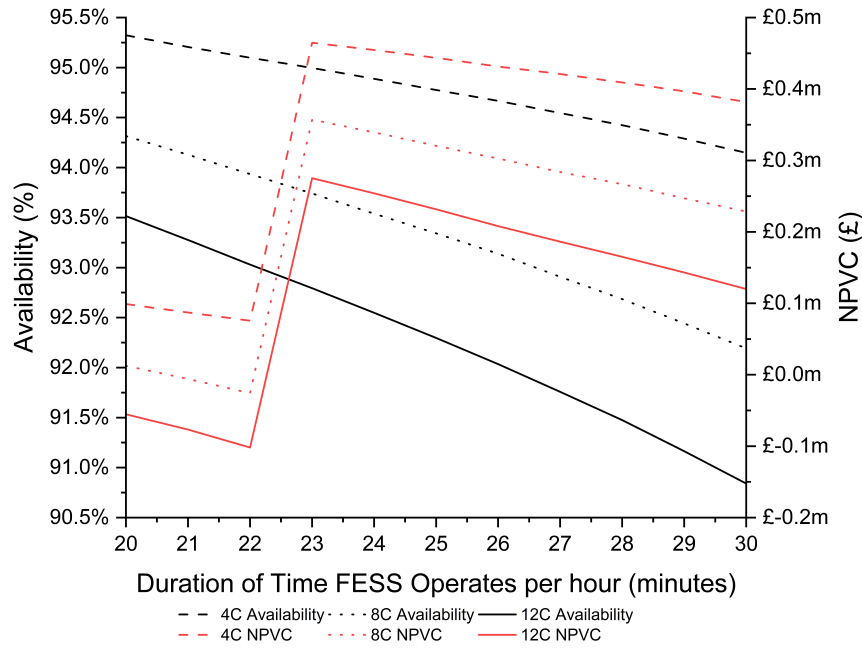
Figure 6.47: a) Average Availability and b) NPVC for different C-Rates of a 1MW FESS, across a range of different FESS operational duration

C-Rate that produce a negative NPVC.

Figure 6.48 shows that the positive NPVC threshold TCC for all three systems falls in the £1,105-£1,244/kW range, a position that places it in the middle of the range of existing FESS TCC within the current literature. This suggests that all three systems have a chance of introducing a positive NPVC under current costs, with the potential to increase this positive change further as the TCC is reduced. The 4C system represents the best-performing configuration, however, the 8C and 12C configurations also perform well enough that systems that fall into the higher C-Rate ranges could be considered under this control strategy.

## 6.4.6 Discussion

A range of different control strategies for hybrid energy storage systems delivering DFR have been presented. It has presented a core methodology around designing and optimising hybrid control strategies to maximise both technical and economic performance. All of the hybrid control strategies provided some degradation reduction in the initial analysis, ranging from a year-long BESS degradation of between 2.65% and 12.4% for the hybrid systems compared to a baseline of 13.15%.

The control strategies that had not previously been analysed by the GA simulations were investigated further, undergoing refinement and economic analysis. They showed potential improvements to the NPV of the site across all analysed control schemes, often being provided by significantly different FESS configurations.
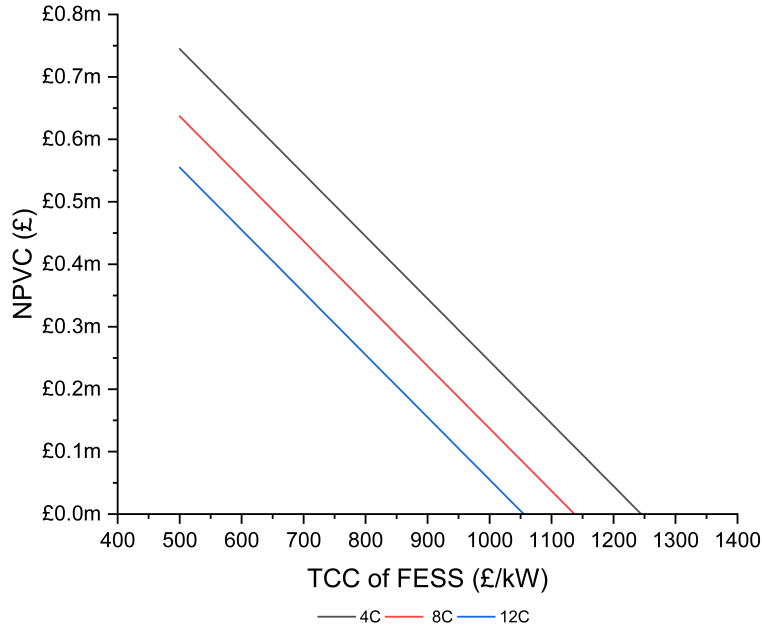
Figure 6.48: NPVC for varying TCC across different FESS configurations for CS-8

Finally, the TCC at which a FESS will need to be produced to provide an economic benefit has been explored in depth. The control strategy that produced the best economic performance was Control Strategy 5 with a peak NPVC of £1,509,000. The range of threshold TCC for a positive NPVC was between £550/kW and £5,855/kW across all control strategies. However, the majority of the systems considered were concentrated in the region of a £1,000-£2,500/kW threshold TCC for positive NPVC, which falls in line with common values throughout the literature for FESS TCC, and as such shows significant potential for the deployment of FESSs in this area. It has been demonstrated that a wide range of FESS configurations at different TCCs can add significant techno-economic value to an existing or proposed BESS site providing DFR services.

## 6.5 Chapter Conclusions

The main contribution of this chapter was the development of a series of novel control strategies for a HESS performing a DFR service. Different techniques have been used to explore the effectiveness of the best-performing strategies. Overall the analysis showed the importance of choosing the correct control strategy depending on the configuration of the system and economic priorities. Many of the control schemes studied resulted in significantly different best configurations for the FESS, ranging between 28kWh to 1000kWh and 4C to 12C, all providing improvements to either BESS degradation, average availability, or in many cases both.

Table 6.17: Summary of control strategy economic analysis

|     | FESS Energy Capacity | FESS C-Rate | NPV | NPVC | Control Settings | Ident |
| --- | --- | --- | --- | --- | --- | --- |
| CS1 | N/A | N/A | -£966,190 | N/A | N/A | N/A |
| CS2 | 91kWh | 4C | £221,710 | £1,188,000 | | R1 |
| CS3 | 55kWh | 4C | -£180,950 | £785,000 | 49.93/50.08Hz boundaries | R2 |
| CS4 | 117kWh | 4C | £38,080 | £1,004,000 | 49.91/50.09Hz boundaries | R3 |
| CS5 | 50kWh | 4C | £134,800 | £1,101,000 | | R4 |
| CS5 | 100kWh | 4C | £139,940 | £1,106,000 | | R5 |
| CS5 | 100kWh | 8C | -£172,060 | £794,000 | | R6 |
| CS5 | 200kWh | 4C | -£163,700 | £802,000 | | R7 |
| CS6 | 28kWh | 4C | £186,100 | £1,152,000 | $t_{av} = 30s$ | R8 |
| CS6 | 28kWh | 4C | £189,060 | £1,155,000 | $t_{av} = 45s$ | R9 |
| CS6 | 33kWh | 4C | £149,200 | £1,115,000 | $t_{av} = 120s$ | R10 |
| CS6 | 57kWh | 4C | £114,010 | £1,080,000 | $t_{av} = 300s$ | R11 |
| CS7 | 11kWh | 4C | -£418,260 | £548,000 | $t_{av} = 30s$ | R12 |
| CS8 | 1000kWh | 4C | -£501,400 | £465,000 | | R13 |
| CS8 | 1000kWh | 8C | -£609,090 | £357,000 | | R14 |
| CS8 | 1000kWh | 12C | -£691,090 | £275,000 | | R15 |

In terms of economic analysis, the best-performing configurations and settings from each control strategy have been used to produce the NPVC at a TCC of £780/kW with the results shown in Table 6.17. Depending on the control system utilised the best performing FESS configuration varies significantly, which illustrates the significant impact that very short duration energy storage such as flywheels can have on the performance of an existing BESS installation. This conclusion is important as it shows that a vast range of FESS configurations can be viable for this application, giving key guidance to manufacturers looking to enter this market.

Finally, an emphasis has been placed on the threshold TCC that is required to be achieved in order to allow FESSs to become commercially viable in this application. Throughout the range of different configurations and control settings, the resulting threshold TCC to provide positive NPVC varied between £1,099/kW and £5,105/kW. Caution should be taken with the upper limits of this range as the values do represent outliers as illustrated in Figure 6.49 which shows the NPVC at varying TCC values for all of the scenarios detailed in Table 6.17. This graph provides a foundation for determining what levels of economic impact different FESS configurations can provide at varying levels of cost.

One of the most important conclusions to derive from this study is its indication that even FESS systems that fall in the upper regions of costs can be effectively deployed in this area, albeit with significantly lower economic impact as the price is
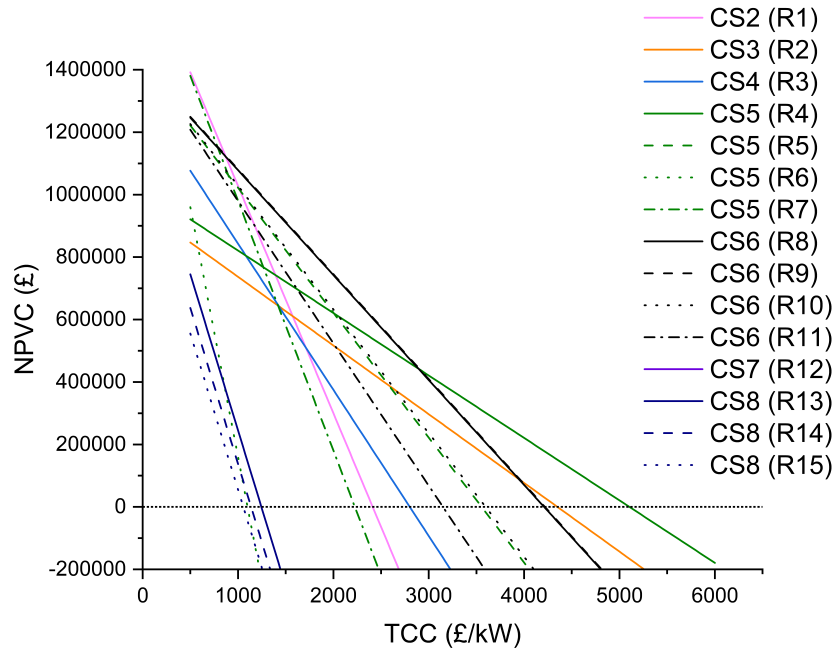
Figure 6.49: NPVC for varying Total Capital Costs of a FESS under different control strategies and settings (Refer to Table 6.17 for specific settings)

increased closer to the threshold. This gives a clear signal to industrial developers and manufacturers that there is potential in this technology and realistic goals for product costs to maximise impact.

# Chapter 7

# The Future of Frequency Response Services : A FESS perspective

## 7.1    Introduction

Whilst the previous chapter focused on the well-documented benchmark service of DFR, this chapter now moves focus to look at the new suite of frequency response services that have been introduced over the final 18 months of the work presented in this thesis [242]. These services have often been referred to as having been developed with a view of allowing a wider range of technologies to operate in the frequency response service market, and the first area that this chapter looks at is providing a novel investigation into this claim to determine whether very short-duration ESSs such as FESSs are suitable for being deployed under these new conditions.

The chapter then moves onto the development of a frequency response service profile designed specifically for delivery by a FESS in a first-of-its-kind study. A response envelope is developed from the ground up based upon characteristics present throughout the range of existing response envelopes before a sensitivity analysis is conducted to determine the viability of a range of different FESS configurations for delivering the new service.

Finally, an economic analysis is conducted looking at varying availability fees and how this would impact upon the viability of a FESS providing the developed service when compared with other similar studies for BESS installations and existing market conditions.

Table 7.1: Delivery statistics for new frequency response services

|  | DC Low | DC High | DR Low | DR High | DM Low | DM High |
|---|---|---|---|---|---|---|
| Executed Volume (GW) | 16.4 | 11.7 | 0.77 | 3.44 | 0.12 | 0.12 |
| Participants | 19 | 19 | 4 | 5 | 2 | 2 |
| Average Clearing Price (£/MW/h) | 30.8 | 3.02 | 28.8 | 34.9 | 5.00 | 8.2 |

# 7.2 Dynamic Containment, Moderation and Regulation

After the publication of the product roadmap for frequency response and reserve by NGESO in 2017, there has been a commitment to renew that range of frequency response services in order to develop a more flexible electricity system that can utilise the resources available efficiently and economically [243].

Table 7.1 shows delivery statistics relating to DC, DR and DM for July 2022. As the oldest active service, DC represents the largest operating market with significant volumes of participation. With DR and DM in their infancy the values associated with these services is likely to grow rapidly in the coming years. In fact, NGESO have stated that they will be aiming to procure around 1GW of all three services by an unspecified future date [244]. This, therefore, means that there are significant opportunities available for a wide range of asset owners to participate and contribute to these markets in the coming years. DC low is generally a higher price than DC high because it allows units to both export through DC low and stack services such as importing on the balancing mechanism.

Figure 7.1 shows the response envelope of the services being discussed in this thesis, with the individual services outlined as follows;

## 7.2.1 Dynamic Containment

DC was introduced in 2021 primarily as a post-fault service designed to react more quickly to frequency deviations [245]. The key operational feature of this service is that it only provides up to 5% of the rated power when the frequency is +/-0.2Hz from 50Hz hence the overall power output is considerably lower. This means there is a comparatively large 'dead-band' compared with DFR. Additionally, no charge management is allowed within the dead-band, with any charge management required being managed by submitting a baseline power for the following 1 hour delivery period. However, this baseline power must not take away from the available contracted power. For instance, a 10MW would only be able to provide 9MW of contracted power should the asset need to reserve 1MW for baseline power charge
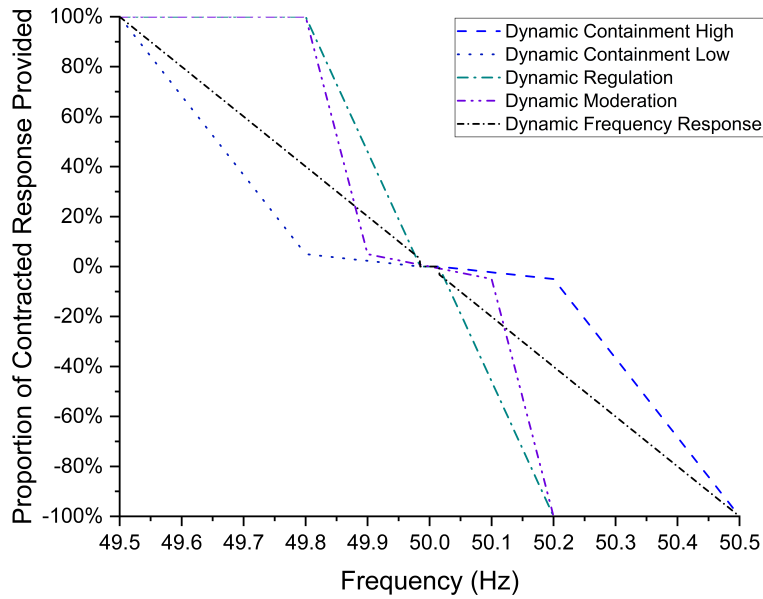
Figure 7.1: Response envelope for DC High and Low, DM, DR and DFR

Table 7.2: DC Service Parameters

| Service Specification | Detail |
|---|---|
| Dead-band | 49.985Hz to 50.015Hz |
| Dead-band delivery | 0% |
| Initial delivery | Between 0.015Hz and 0.2Hz up to 5% of rated power at 0.2Hz |
| Knee point | +/- 0.2Hz |
| Full delivery | +- 0.5Hz |

management. Reducing the contracted power available for service delivery reduces the revenue potential of the asset and is therefore not desirable. Full details of the DC service specification are shown in Table 7.2.

## 7.2.2    Dynamic Moderation

This service is designed to operate pre-fault managing larger imbalances in demand and generation when the frequency trends towards the limits of operational range and was introduced in May 2022 [246]. The ESS is required to deliver 30 minutes of service at any one time without the need to recharge. For instance, a 10MW service may be contracted to deliver a low-frequency response service and hence must have a minimum energy requirement of 5MWh. The service parameters are shown in Table 7.3.

DM has the potential to suit the high dynamic power capability of a FESS,

Table 7.3: DM Service Parameters

| Service Specification | Detail |
|---|---|
| Dead-band | 49.985Hz to 50.015Hz |
| Dead-band delivery | 0% |
| Initial delivery | Between 0.015Hz and 0.1Hz up to 5% of rated power at 0.2Hz |
| Knee point | +/- 0.1Hz |
| Full delivery | +- 0.2Hz |

Table 7.4: DR Service Parameters

| Service Specification | Detail |
|---|---|
| Dead-band | 49.985Hz to 50.015Hz |
| Dead-band delivery | 0% |
| Knee point | +/- 0.015Hz |
| Full delivery | +- 0.2Hz |

however, the high minimum duration of 30 minutes will result in periods of non-compliance due to insufficient energy storage. Non-compliance in this scenario refers to the fact that if an ESS could not provide 30 minutes of the agreed service at any time during the service period then it would be deemed to be non-compliant. For higher C-Rate assets which discharge fully in the region of seconds to minutes, this is unlikely to be achievable.

### 7.2.3  Dynamic Regulation

DR is also designed to operate as a pre-fault service continuously correcting smaller deviations in frequency and was introduced in April 2022 [247]. The ESS is required to provide 1 hour of continuous service without the need to recharge in any given direction. For instance, a 10MW service may be contracted to deliver a low-frequency response service and hence must have a minimum energy requirement of 10MWh. All systems are obliged to recover at least 20% of the total energy requirement in the following settlement period. The service parameters are shown in Table 7.4.

Due to the 1-hour requirement of continuous service, along with a minimum 1C energy capacity, it is unlikely that FESSs will be able to provide this category of service as it has been proposed. Higher energy capacity assets such as BESSs would likely be best suited to provide this service.

### 7.2.4   Literature Review

As these response services have either only just been introduced or are still being developed, there is a significant gap in completed research. The basic principles and considerations that were discussed in the literature review within Chapter 5 still hold true for the work contained in this chapter as the work still deals primarily with frequency response services.

Specifically relating to the new suite of services, the main piece of completed research comes from [248] with a sensitivity study looking into the required C-Rates for the provision of the range of new services. This paper claims that DC is generally a less demanding service than DFR, and that higher C-Rates (up to 10C) could be utilised effectively to provide the service. This suggests that there is a significant opportunity for short-term energy storage such as flywheels to provide this service. However, when considering the contract service delivery terms of DC the paper suggests that the higher  systems struggle with maintaining compliance due to long-duration frequency events where there is not enough energy in the ESS.

Additionally, [249] takes a more market-focused approach to analysing BESSs being utilised for the provision of DC. Rather than looking at technical performance, the study looks at the potential economic value in utilising a BESS for this purpose, concluding that a positive economic impact can be achieved. However, it is to be expected that BESSs will be able to adequately perform this service as they are the primary medium that DC has been designed for, and hence there still remains a gap for meaningful research into the performance of energy limited assets.

It is clear from the minimal research conducted that under the current requirements, very short-duration energy storage will still be unable to meaningfully participate in the frequency response service market. The work contained in this chapter builds upon this conclusion, looking specifically into the operation of FESS when considering no operational restrictions and using this as a basis to develop a service that can be effectively provided by very short-duration energy storage without the complex state of energy requirements opening up the opportunity for a much wider range of ESS technologies to provide such services.

## 7.3   Utilising FESSs for New Frequency Response Services

In this study, the services are represented as 24/7 delivery without considering partial-day block tendering or baseline energy management that would be required when providing the service in real-world conditions. This study instead focuses on the suitability of the response envelopes for delivery by flywheels and shows for the

first time how FESSs of varying C-Rates could provide these services.

The response envelope is one of the key defining characteristics of a frequency response service and directly affects the flow of energy to and from the storage system. It is therefore important to consider how a certain storage medium operates under each response envelope without operational restrictions as this study does in order to determine its overall potential at providing said service. Additionally for ESSs such as flywheels, continuous operation is a far more suitable approach, and therefore this investigation into the 24/7 operation of the existing response envelopes can help inform the development of a bespoke frequency response service.

Whilst the payment mechanism for these services is slightly different to that discussed previously with DFR, it has been kept consistent with DFR in this chapter in order to be able to provide like-for-like comparisons and allow commentary on the possibility for further development of the services.

## 7.3.1 Service Analysis

The initial service analysis does not contain an economic study, as this section is intended to focus specifically on the technical capability of a FESS to provide these services. Each service will be simulated over a year of 24/7 delivery for varying configurations of FESS, with the following metrics to be assessed will be as listed below. Tracking of non-compliance with the SOC rules is not included in this assessment.

- Availability - As defined previously in Chapter 5 and in Equation 5.1. The targeted average availability is 95%.

- Energy Throughput - The total amount of energy that passes through the ESS. This is an important metric to track when considering energy-limited storage such as flywheels, as it gives insight into how often the ESS is asked to operate.

- Energy Delivery Proportion - The total energy throughput of the ESS as a proportion of the overall energy requested by the service as given in Equation 7.1 where $E_{\text{deliv}}$ is the energy delivered by the system and $E_{\text{req}}$ is the total requested energy.

- Number of cycles - The total number of cycles that the ESS experiences.

$$\text{EDP } (\%) = (1 - \frac{E_{deliv}}{E_{Req}}) \times 100 \qquad (7.1)$$

The assessment conducted in this section uses the same model as previously outlined in Section 3.7, with the only modification compared the the FESS DFR
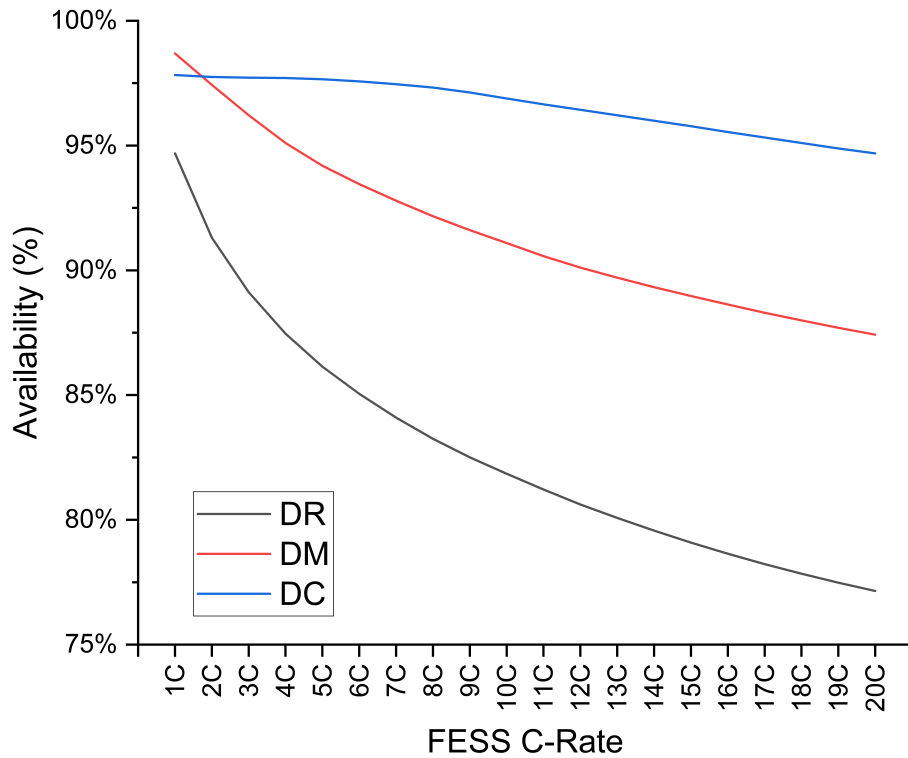
Figure 7.2: Average availability of a year-long simulation for varying FESS C-Rates performing DC, DR and DM

model being the replacement of the DFR service envelope within the application block with that of the relevant DC/DR/DM service envelope.

The average availability for varying C-Rates of FESS under the different service parameters is shown in Figure 7.2. For all services, the average availability peaks when being provided by a 1C system before falling as the C-Rate is increased. The 1C FESS achieves the best average availability when performing DM, reaching 98.69% availability, whilst once the C-Rate is increased beyond this the FESS is best at performing DC. The FESS can provide an average availability above 95% for C-Rates up to and including 18C when performing DC, up to and including 4C for DM, and fails to reach that threshold under any C-Rate for DR.

Figure 7.3 can be used to inform the results from Figure 7.2. It shows that the energy throughput for DR is significantly higher than for either DM or DC, which is a key reason for the lowered average availability, especially at the higher C-Rates (which have lower energy capacity). It can also be seen that there is a significant drop off in overall energy delivery proportion as the C-Rate is increased, representing the FESS no longer having enough energy capacity to handle the requests of the service. A key takeaway from this graph is that at the higher FESS C-Rates, the
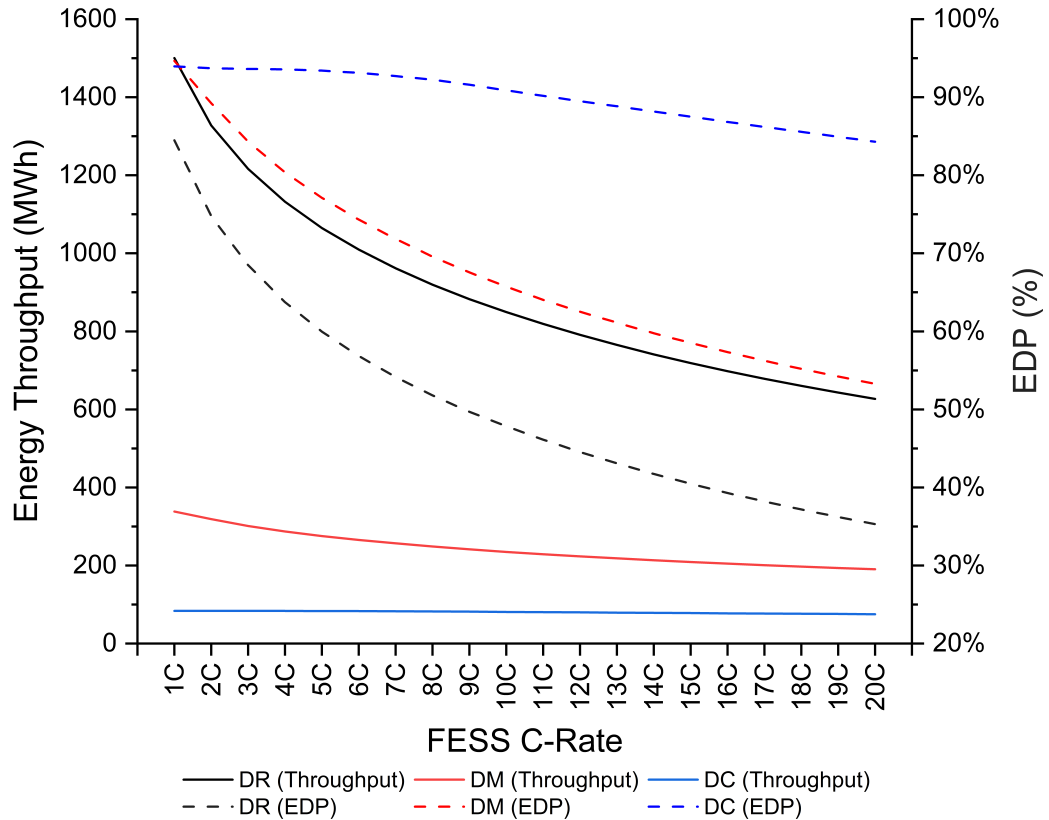
Figure 7.3: Energy throughput (MWh) and energy delivery proportion (%) from a year-long simulation for varying FESS C-Rates performing DC, DR and DM

FESS is unable to deliver high power responses for extended periods but is able to respond adequately when the frequency deviations are small, thus reducing the energy throughput and energy delivery proportion severely whilst only resulting in a modest reduction in average availability.

For instance, at 20C, a FESS provides only 35.3% energy delivery proportion over the year, but the availability is significantly higher at 77.1%, suggesting that the system is only managing to respond when the deviations are small and subsequently highlighting that whilst the availability remains high, the system is not providing the service required of it by the response envelope. The energy delivery proportion suggests that for DC, the FESS is able to provide a significant portion of the requested energy regardless of C-Rate as the energy delivery proportion starts at 94.0% for 1C and only falls to 84%.

Finally, Figure 7.4 shows that as the C-Rate is increased the number of cycles also increases. For DM and DC, the number of cycles never reach a level that could result in the lifetime of the FESS being shortened. Even with DR, it is unlikely that the peak number of cycles per year (12,531) would cause a problem for most FESSs, although some literature suggests cycle limits in the 100,000 range, which
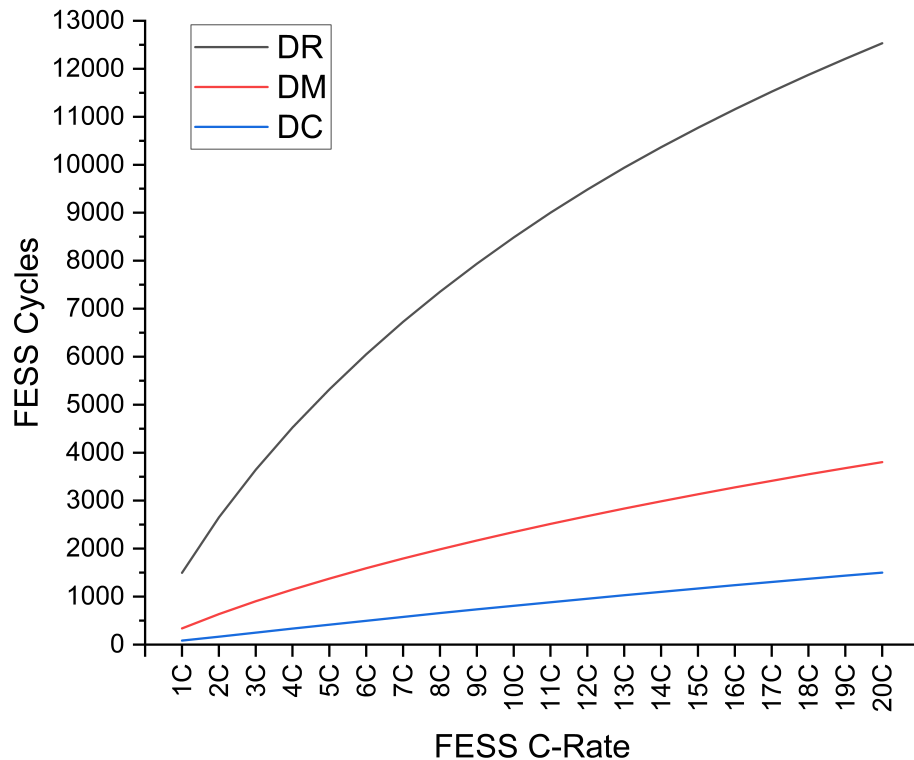
Figure 7.4: Cycles experienced during a year-long simulation for varying FESS C-Rates performing DC, DR and DM

would result in the FESS reaching the end of life in less than 10 years for all C-Rates above 13C. Higher cycle life FESSs would have no issues performing these services.

## 7.3.2  Hybridisation Impact Study

In order to achieve a higher level of average availability, a small amount of battery energy storage (0.1MWh/0.1MW/1C) was introduced to hybridise the system. This value of storage was chosen to represent a small system that could be easily co-located with a FESS installation without major additional works, unlike larger containerised systems such as the 1MW/1MWh/1C units previously studied in this thesis. The control was set to exclusively use the FESS to respond to the power demands, with the BESS only being requested to provide power if the FESS was not able to. The BESS will therefore only cover requests where it can either 'top-up' the FESS delivery by 0.1MW to deliver the requested power, or where the FESS cannot provide any power, the request must be 0.1MW of either charging or discharging power for the BESS to be able to meet it. For this study, average availability and energy delivery proportion will be considered as the primary metrics of if and how the addition of a BESS improves the service.
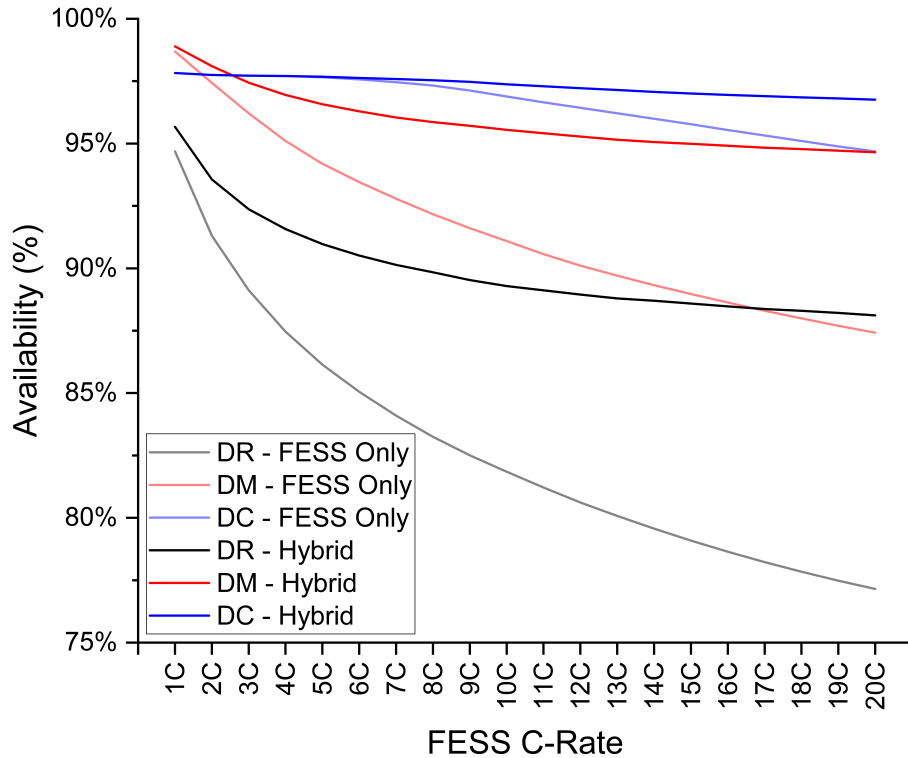
Figure 7.5: Average availability during a year-long simulation for varying FESS C-Rates performing DC, DR and DM both alone and hybridised with a 0.1MWh/0.1MW/1C BESS

In Figure 7.5 it can be seen that for all services there is an increase in availability when a BESS is introduced, as is to be expected. For some services, this increase is more significant than others. For example, when DR is considered, at the low C-Rate end of the analysis there is a minimal increase in average availability with an increase of 0.98% being seen at 1C, whilst a peak increase of 10.97% is seen at 20C. For DC, however, the impact is minimal, suggesting that hybridising for this service would not be worthwhile as the increase in availability only reaches a peak of 2.1% at 20C. The effect for DM falls between the two other services, with a moderate increase being achieved across the C-Rates by introducing the BESS, peaking at an increase of 7.3% at 20C.

Following on from this, Figure 7.6 shows how the energy throughput is changed by introducing a BESS for each service. Again taking into consideration the previous Figure 7.5, this provides context for the availability statistics, showing that as the overall energy throughput increases there is a correspondingly larger increase in availability. Looking again at DR, it is clear that the increases in energy throughput at the higher C-Rates are the primary driver for the increase in availability, with the additional energy capacity of the BESS becoming more important as the energy
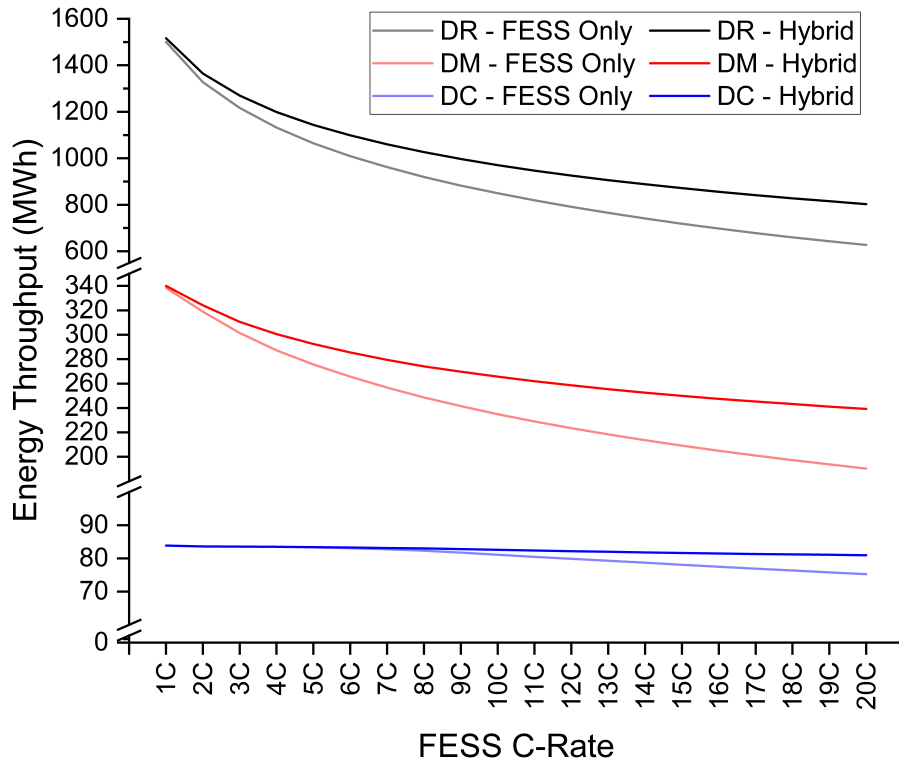
Figure 7.6: Energy throughput experienced during a year-long simulation for varying FESS C-Rates performing DC, DR and DM both alone and hybridised with a 0.1MWh/0.1MW/1C BESS

capacity of the FESS is reduced. For DM and DC there is a smaller increase in energy throughput by introducing the BESS, resulting in smaller increases to average availability.

It should be noted that the effectiveness of introducing this size of BESS is closely linked to the response envelope being tested. For DC, there is a very shallow incline in required power response meaning only a small amount of energy throughout occurs in the area where a 0.1MW BESS would be able to deliver the service (i.e when the power request is between 0-10%, which is the range the 0.1MW BESS can cover). However, for DR, there is a much steeper incline in required power response as the frequency deviates further from 50Hz, meaning the 0.1MW BESS will have more instances where it can utilise its full capabilities.

### 7.3.3 Discussion

In this study, the suite of new services from NGESO has been presented and discussed along with their suitability for provision by FESSs. The contractual service parameters for all three new services represent challenges for provision by energy-

limited assets such as FESSs. In order to encourage a wider range of energy storage medium participation, modifications would need to be made to aspects such as minimum delivery time.

To assess the suitability for a FESS to deliver the response envelope associated with each service, a C-Rate sensitivity analysis was undertaken. The results of this analysis showed that the most suitable response envelope for a FESS to deliver effectively is DC delivering both high and low services simultaneously, where the average availability was >95% up to and including an 18C system.

Conversely, for the DR response envelope, the FESS will never achieve >95% which has been shown to be due to the high levels of energy throughput required by the service which even the lower C-Rate FESSs cannot cope with.

Subsequently, a hybridisation exercise was undertaken to assess how the performance of the system could be improved by introducing a 0.1MWh/0.1MW/1C BESS. It was shown that for DR a significant improvement could be achieved in the average availability of the system, although for the majority of C-Rates, the 95% threshold could not be reached. For the other two services, DM and DC, more moderate improvements were achieved.

# 7.4 Designing a Bespoke Frequency Response Service for Delivery by FESSs

This section presents for the first time an investigation into designing a bespoke frequency response service for FESSs to perform. The service is represented as a continuous 24/7 service and the effectiveness is determined by the average availability over a year of the service being provided as previously discussed. Additionally, the energy throughput of the service has been assessed and compared with that provided by the existing frequency response services offered by NGESO in order to verify that the system is operating for a sufficient amount of time to be worthwhile. The initial analysis is performed on a 1MW/1MWh/1C FESS providing a 1MW service. Finally, a C-Rate sensitivity analysis has been performed to assess the effects of varying the C-Rate on the performance of the system.

The target for an effective service is that it should be available for a minimum of 95% of the operational time. The service should also be able to reach this availability at higher C-Rates with many of the existing or in-development FESSs having C-Rates in the region of 4-20C. It should also provide a total energy throughput in the same order of magnitude as that which would be provided by existing services, which has been chosen as a design criterion to ensure the service is operating frequently enough to contribute meaningfully to the balancing mechanism.

Table 7.5: Baseline results from a 1MWh/1MW/1C FESS providing 1MW of the existing frequency response services

| Service | Availability | Energy Throughput (MWh) |
|---------|-------------|-------------------------|
| DFR | 97.4% | 627 |
| DC | 97.8% | 84 |
| DR | 94.7% | 1546 |
| DM | 98.7% | 338 |

A baseline of how a 1MW/1MWh/1C FESS providing a 24/7 1MW service would perform delivering existing response profiles is shown in Table 7.5. Of the existing service profiles DM would provide the most suitable envelope to be delivered by the FESS, whilst also providing the lowest total energy throughput over the year of operation. DR is the worst performing as the only service below 95% average availability. It should be noted that the 24/7 delivery of these services is not practical under current market and service contract conditions, but it is included here as a representative benchmark for how the FESS can perform for different response profiles.

Additionally, DC is represented as performing both DC high and DC low concurrently for the same reason. The services designed in this study are proposed as 24/7 services as for FESSs, it is undesirable for them to be inactive for long periods of time due to spinning losses incurred and would therefore be more beneficial for it to be continuously operating. Finally, a dead-band (the zone where no power is imported or exported) between 49.985Hz and 50.015Hz is present at all times to mimic the most common approach taken by existing response envelopes and prevent excessive low-power cycling.

## 7.4.1 Initial Analysis

The initial analysis of a bespoke frequency response envelope consisted of varying the 100% power point ($f_1$ and $f_{-1}$ on Figure 7.7) for both the low and high-frequency ends of the spectrum with a 1MWh/1MW/1C system providing a 1MW service. A year-long simulation was conducted for each combination between 49.5-49.9Hz and 50.1-50.5Hz. The results of this simulation are shown in Table 7.6.

It is immediately apparent that as the 100% power point is moved further from 50Hz in both directions the average availability steadily increases. From a symmetrical 49.9/50.1Hz combination giving an average availability of 91.2%, the combination of 49.5/50.5Hz provides an average availability of 97.4% showing a significant improvement.
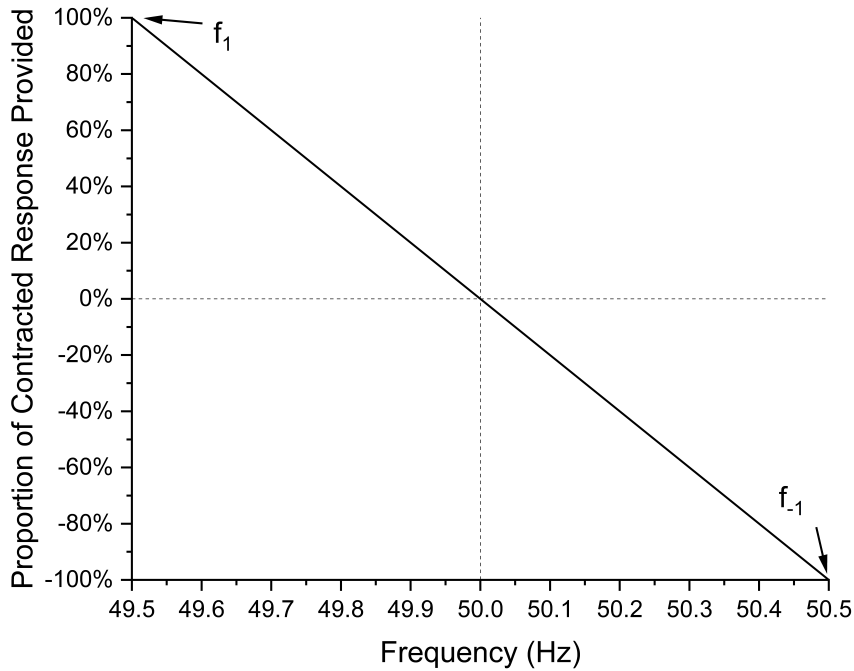
Figure 7.7: Response envelope example showing the points in the envelope that are varied for the initial analysis

There is also a degree of asymmetry to the results, with a higher availability produced when the high-frequency 100% power point is reached sooner than the low-frequency 100% power point. This leads to the maximum availability of 98.5% being achieved with a combination of 49.5Hz and 50.44Hz. However, if the asymmetry is increased too far then the average availability experiences a rapid reduction.

This asymmetry is due to the FESS experiencing spinning losses. By having a steeper charging curve, the spinning losses are constantly being countered with more energy being taken from the grid than discharged back. In this manner, the response envelope being slightly asymmetric uses the spinning losses to its advantage.

Taking this assessment as a baseline, the best-performing 100% power point combination was used to perform a C-Rate sensitivity analysis. The C-Rate was increased incrementally up to a value of 20C with the results of this analysis shown in Figure 7.8. There is a significant drop in average availability as the C-Rate is increased, with only a 1C and 2C system achieving average availability in excess of the required 95%. This suggests that the suitability of the envelope to more common FESS system characteristics like high power and low energy is poor and needs further tuning to enable it to perform at higher C-Rates.

Table 7.6: Average availability for varying high and low-frequency 100% power points

| Lower Frequency 100% Power Point (Hz) | Higher Frequency 100% Power Point (Hz) | | | | | | | | | | | | | | | | | | | | |
|---|---|---|---|---|---|---|---|---|---|---|---|---|---|---|---|---|---|---|---|---|---|
| | 50.1 | 50.12 | 50.14 | 50.16 | 50.18 | 50.2 | 50.22 | 50.24 | 50.26 | 50.28 | 50.3 | 50.32 | 50.34 | 50.36 | 50.38 | 50.4 | 50.42 | 50.44 | 50.46 | 50.48 | 50.5 |
| 49.9 | 91.2% | 91.0% | 90.5% | 89.8% | 89.0% | 88.3% | 87.6% | 86.9% | 86.4% | 85.9% | 85.4% | 85.0% | 84.7% | 84.4% | 84.1% | 83.8% | 83.6% | 83.4% | 83.2% | 83.0% | 82.8% |
| 49.88 | 92.0% | 92.1% | 91.8% | 91.3% | 90.6% | 89.9% | 89.1% | 88.4% | 87.8% | 87.2% | 86.7% | 86.2% | 85.8% | 85.5% | 85.1% | 84.8% | 84.6% | 84.3% | 84.1% | 83.9% | 83.7% |
| 49.86 | 92.2% | 92.8% | 92.9% | 92.6% | 92.0% | 91.4% | 90.6% | 89.8% | 89.1% | 88.5% | 87.9% | 87.4% | 87.0% | 86.5% | 86.2% | 85.8% | 85.5% | 85.2% | 85.0% | 84.7% | 84.5% |
| 49.84 | 92.2% | 93.1% | 93.5% | 93.6% | 93.3% | 92.7% | 92.0% | 91.2% | 90.5% | 89.8% | 89.2% | 88.6% | 88.1% | 87.6% | 87.2% | 86.8% | 86.5% | 86.1% | 85.9% | 85.6% | 85.3% |
| 49.82 | 91.9% | 93.0% | 93.8% | 94.2% | 94.2% | 93.8% | 93.3% | 92.5% | 91.8% | 91.1% | 90.4% | 89.8% | 89.2% | 88.7% | 88.2% | 87.8% | 87.4% | 87.0% | 86.7% | 86.4% | 86.1% |
| 49.8 | 91.5% | 92.8% | 93.8% | 94.5% | 94.8% | 94.7% | 94.3% | 93.7% | 92.9% | 92.2% | 91.5% | 90.9% | 90.3% | 89.7% | 89.2% | 88.7% | 88.3% | 87.9% | 87.5% | 87.2% | 86.9% |
| 49.78 | 90.9% | 92.3% | 93.5% | 94.5% | 95.0% | 95.2% | 95.1% | 94.7% | 94.1% | 93.3% | 92.6% | 92.0% | 91.3% | 90.7% | 90.2% | 89.6% | 89.2% | 88.8% | 88.4% | 88.0% | 87.7% |
| 49.76 | 90.4% | 91.8% | 93.1% | 94.2% | 95.0% | 95.5% | 95.6% | 95.5% | 95.0% | 94.4% | 93.7% | 93.0% | 92.3% | 91.7% | 91.1% | 90.6% | 90.1% | 89.6% | 89.2% | 88.8% | 88.4% |
| 49.74 | 89.9% | 91.3% | 92.6% | 93.8% | 94.8% | 95.5% | 95.9% | 96.0% | 95.8% | 95.3% | 94.7% | 94.0% | 93.3% | 92.7% | 92.0% | 91.5% | 90.9% | 90.5% | 90.0% | 89.6% | 89.2% |
| 49.72 | 89.4% | 90.7% | 92.1% | 93.3% | 94.4% | 95.3% | 95.9% | 96.3% | 96.3% | 96.0% | 95.5% | 94.9% | 94.2% | 93.6% | 93.0% | 92.3% | 91.8% | 91.3% | 90.8% | 90.3% | 89.9% |
| 49.7 | 88.9% | 90.3% | 91.5% | 92.8% | 93.9% | 94.9% | 95.7% | 96.3% | 96.6% | 96.6% | 96.2% | 95.7% | 95.1% | 94.5% | 93.8% | 93.2% | 92.6% | 92.1% | 91.6% | 91.1% | 90.7% |
| 49.68 | 88.5% | 89.8% | 91.0% | 92.3% | 93.4% | 94.5% | 95.4% | 96.1% | 96.7% | 96.9% | 96.8% | 96.4% | 95.9% | 95.3% | 94.7% | 94.1% | 93.4% | 92.9% | 92.3% | 91.8% | 91.4% |
| 49.66 | 88.2% | 89.4% | 90.6% | 91.7% | 92.9% | 94.0% | 94.9% | 95.8% | 96.5% | 97.0% | 97.2% | 97.0% | 96.7% | 96.1% | 95.5% | 94.9% | 94.3% | 93.6% | 93.1% | 92.6% | 92.1% |
| 49.64 | 87.8% | 89.0% | 90.2% | 91.3% | 92.4% | 93.4% | 94.5% | 95.4% | 96.1% | 96.8% | 97.3% | 97.4% | 97.2% | 96.8% | 96.2% | 95.6% | 95.0% | 94.4% | 93.8% | 93.3% | 92.8% |
| 49.62 | 87.5% | 88.6% | 89.8% | 90.9% | 91.9% | 93.0% | 94.0% | 94.9% | 95.7% | 96.5% | 97.1% | 97.6% | 97.6% | 97.3% | 96.9% | 96.4% | 95.8% | 95.2% | 94.6% | 94.0% | 93.5% |
| 49.6 | 87.2% | 88.3% | 89.4% | 90.4% | 91.5% | 92.5% | 93.5% | 94.4% | 95.3% | 96.1% | 96.8% | 97.4% | 97.8% | 97.8% | 97.4% | 97.0% | 96.5% | 95.9% | 95.3% | 94.7% | 94.2% |
| 49.58 | 86.9% | 88.0% | 89.1% | 90.1% | 91.1% | 92.0% | 93.0% | 93.9% | 94.8% | 95.6% | 96.4% | 97.0% | 97.6% | 98.0% | 97.9% | 97.6% | 97.1% | 96.6% | 96.0% | 95.4% | 94.9% |
| 49.56 | 86.7% | 87.7% | 88.8% | 89.7% | 90.7% | 91.6% | 92.6% | 93.4% | 94.4% | 95.2% | 96.0% | 96.6% | 97.3% | 97.8% | 98.1% | 98.0% | 97.7% | 97.2% | 96.7% | 96.1% | 95.5% |
| 49.54 | 86.5% | 87.5% | 88.5% | 89.4% | 90.3% | 91.3% | 92.2% | 93.0% | 93.9% | 94.7% | 95.5% | 96.2% | 96.9% | 97.5% | 97.9% | 98.3% | 98.1% | 97.8% | 97.3% | 96.7% | 96.2% |
| 49.52 | 86.3% | 87.2% | 88.2% | 89.1% | 90.0% | 90.9% | 91.8% | 92.6% | 93.4% | 94.3% | 95.1% | 95.8% | 96.5% | 97.1% | 97.7% | 98.2% | 98.4% | 98.2% | 97.8% | 97.4% | 96.8% |
| 49.5 | 86.1% | 87.0% | 88.0% | 88.8% | 89.7% | 90.6% | 91.4% | 92.2% | 93.0% | 93.8% | 94.6% | 95.4% | 96.1% | 96.8% | 97.4% | 97.9% | 98.4% | 98.5% | 98.3% | 97.9% | 97.4% |

Also in Figure 7.6 is the total energy throughput of each individual system in MWh. This metric is intrinsically tied to that of availability, but the key aspect to note is that even for a 20C system the energy throughput is still significant with 373.6MWh passing through the FESS over the course of a year. At its peak of 690.39MWh for a 1C system, the service will see more usage than all current services bar DR, with a very similar energy throughput to DFR but with an extra 1.1% availability across the year, showing that the refinement of the service to the flywheels advantages is working to enable it to provide a better service than existing ones.

## 7.4.2   Knee Point Analysis

Both DC and DM have 'knee points' where up to a certain frequency the power delivery is a small proportion of the overall contracted service, followed by a linear rise to the maximum power point. This section of the study focuses on placing a knee point into the response envelope and how this affects the average availability.

The maximum power points are set as 49.5Hz and 50.44Hz (points $f_1$ and $f_{-1}$ respectively on Figure 7.9) as determined in the previous section, with the power level of the knee-point set as 0.05% of the overall contracted service, replicating the setting used by DC and DM. The low and high knee-point frequencies (points $f_K$ and $f_{-K}$ on Figure 7.9) are varied between 49.85-49.95Hz and 50.05-50.15Hz respectively in increments of 0.01Hz. The results of this analysis are shown in Table 7.7.

The average availability once again increases as the knee-point is moved further away from 50Hz before decreasing again after a peak at 49.91/50.09Hz. In 90.08% of simulated combinations, the average availability was reduced by adding in a knee point. Despite this, some of the combinations represent a strong increase in average availability, peaking with the combination of knee points at 49.87Hz and 50.12Hz which provides an average availability of 99.89% across the year, meaning it will fail to meet the requested power of the grid for less than 10 hours over the course of the year. This combination shows the benefits of small asymmetry within the response envelope, causing the FESS to charge slightly more often than it discharges.

The total energy throughput for the year was also monitored during this assessment, with the values ranging from 518.4MWh (49.95/50.05Hz knee points) to 118.1MWh (49.95/50.15Hz knee points) as shown in Table 7.8.

For the combination that provided the highest average availability (49.87/50.12Hz), the total energy throughput was 160.9MWh, which would place it between the levels of energy provided by DM (83.9MWh) and DC (371.0MWh). This suggests that it operates sufficiently over the course of a year to be providing a worthwhile service to the Great Britain grid.
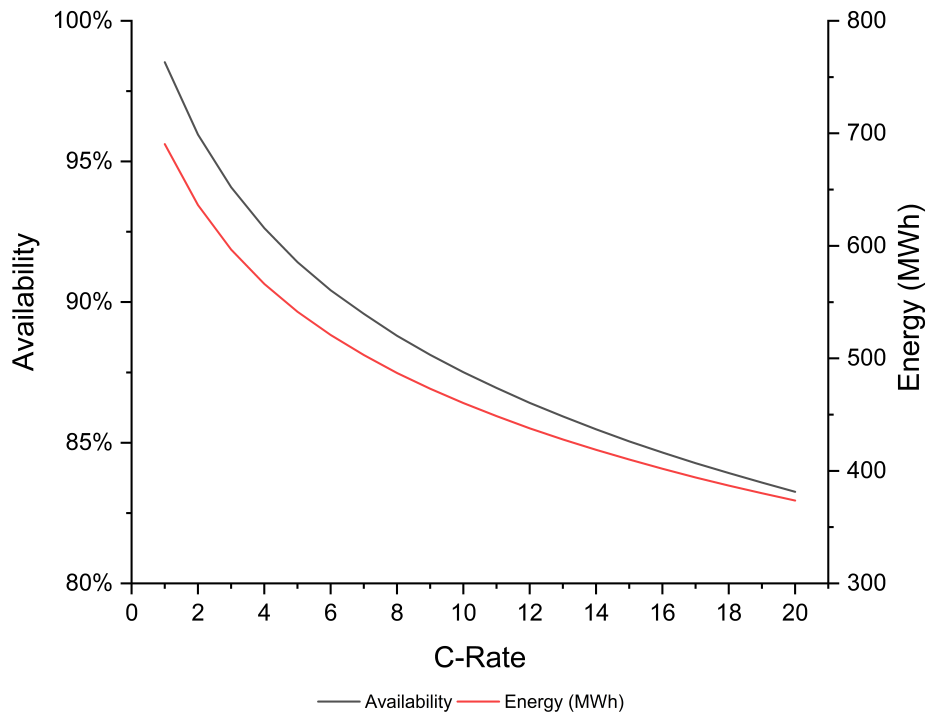
Figure 7.8: C-Rate sensitivity analysis when utilising 100% power points of 49.5/50.44Hz with a 1MW/1MWh/1C FESS providing a 1MW service
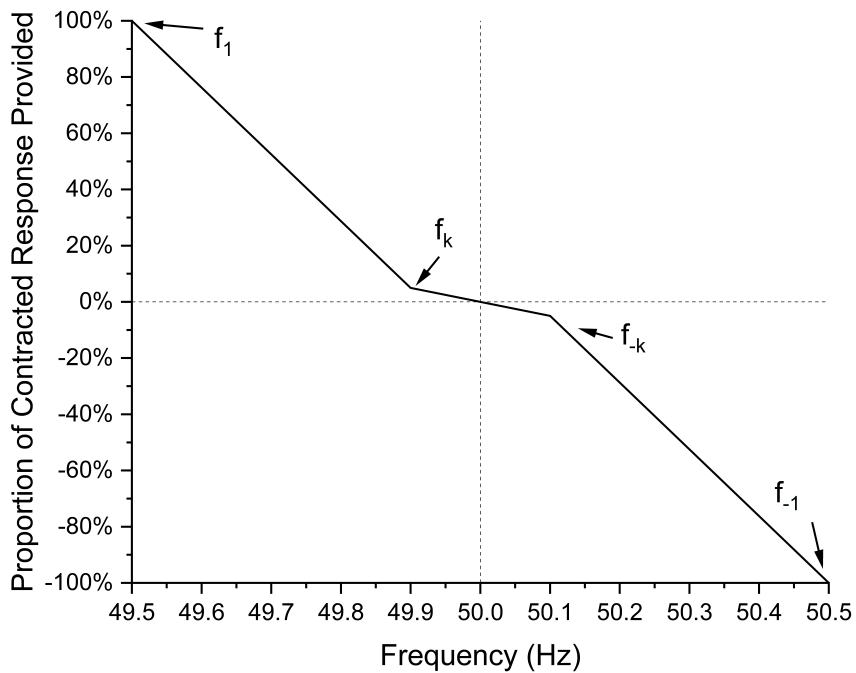


Figure 7.9: Response envelope example showing the points in the envelope that are varied for the knee point analysis

Table 7.7: Average availability for varying high and low-frequency knee points with the 10 combinations resulting in the highest average availability highlighted by a black outline

| $f_K$ (Hz) | $f_K$ (Hz) 50.05 | 50.06 | 50.07 | 50.08 | 50.09 | 50.10 | 50.11 | 50.12 | 50.13 | 50.14 | 50.15 |
|---|---|---|---|---|---|---|---|---|---|---|---|
| 49.95 | 97.65% | 95.90% | 93.32% | 91.17% | 89.40% | 87.96% | 86.82% | 85.80% | 85.12% | 84.58% | 84.13% |
| 49.94 | 97.99% | 98.71% | 95.99% | 93.48% | 91.42% | 89.78% | 88.45% | 87.25% | 86.46% | 85.83% | 85.30% |
| 49.93 | 95.73% | 98.12% | 98.82% | 96.11% | 93.69% | 91.75% | 90.22% | 88.84% | 87.92% | 87.15% | 86.55% |
| 49.92 | 93.70% | 95.93% | 98.31% | 98.85% | 96.22% | 93.96% | 92.14% | 90.53% | 89.48% | 88.61% | 87.88% |
| 49.91 | 92.03% | 94.01% | 96.22% | 98.54% | 98.86% | 96.33% | 94.25% | 92.33% | 91.08% | 90.11% | 89.31% |
| 49.9 | 91.18% | 92.51% | 94.46% | 96.59% | 98.80% | 98.81% | 96.05% | 94.27% | 92.81% | 91.66% | 90.72% |
| 49.89 | 90.10% | 91.31% | 93.05% | 94.98% | 96.99% | 99.09% | 98.24% | 96.22% | 94.61% | 93.27% | 92.20% |
| 49.88 | 89.22% | 90.37% | 91.95% | 93.66% | 95.55% | 97.87% | 99.43% | 98.17% | 96.35% | 94.91% | 93.69% |
| 49.87 | 88.54% | 89.62% | 91.10% | 92.67% | 94.37% | 96.48% | 97.99% | 99.89% | 98.10% | 96.46% | 95.18% |
| 49.86 | 87.97% | 89.02% | 90.39% | 91.87% | 93.40% | 95.37% | 97.05% | 98.71% | 99.79% | 98.01% | 96.55% |
| 49.85 | 87.50% | 88.75% | 89.81% | 91.19% | 92.64% | 94.16% | 95.77% | 97.38% | 98.93% | 99.69% | 98.06% |

Table 7.8: Energy Throughput (MWh) for varying high and low frequency knee points

| Energy Throughput | $f_K$(Hz) | | | | | | | | | | |
|---|---|---|---|---|---|---|---|---|---|---|---|
| | 50.05 | 50.06 | 50.07 | 50.08 | 50.09 | 50.10 | 50.11 | 50.12 | 50.13 | 50.14 | 50.15 |
| 49.95 | 518.4 | 462.4 | 382.7 | 317.0 | 264.5 | 203.9 | 190.8 | 162.1 | 143.9 | 129.6 | 118.1 |
| 49.94 | 487.9 | 457.6 | 382.3 | 316.9 | 264.4 | 223.1 | 190.8 | 162.1 | 143.9 | 129.6 | 118.1 |
| 49.93 | 405.3 | 404.0 | 379.3 | 316.9 | 264.4 | 223.0 | 190.8 | 162.1 | 143.9 | 129.6 | 118.1 |
| 49.92 | 336.6 | 336.6 | 336.0 | 315.1 | 264.4 | 223.0 | 190.7 | 162.1 | 143.9 | 129.6 | 118.1 |
| 49.91 | 282.0 | 282.0 | 282.0 | 281.8 | 263.5 | 223.0 | 190.7 | 162.1 | 143.9 | 129.6 | 118.1 |
| 49.9 | 239.5 | 239.5 | 239.5 | 239.5 | 239.3 | 222.7 | 185.3 | 162.1 | 143.9 | 129.6 | 118.1 |
| 49.89 | 206.7 | 206.7 | 206.7 | 206.7 | 206.7 | 206.5 | 185.3 | 162.1 | 143.9 | 129.6 | 118.1 |
| 49.88 | 181.4 | 181.4 | 181.4 | 181.4 | 181.4 | 181.3 | 181.3 | 162.1 | 143.9 | 129.6 | 118.1 |
| 49.87 | 161.8 | 161.8 | 161.8 | 161.8 | 161.8 | 161.8 | 161.7 | 160.9 | 143.9 | 129.6 | 118.1 |
| 49.86 | 146.3 | 146.3 | 146.3 | 146.3 | 146.3 | 146.3 | 146.3 | 146.3 | 143.8 | 129.6 | 118.1 |
| 49.85 | 133.9 | 133.9 | 133.9 | 133.9 | 133.9 | 133.9 | 133.9 | 133.9 | 133.9 | 131.0 | 119.0 |

$f_K$ (Hz)

Table 7.9: Bespoke Response envelope settings for 1C system

| Frequency (Hz) | Power Point |
|---|---|
| 49.5 | 1 |
| 49.87 | 0.05 |
| 49.985 | 0 |
| 50.015 | 0 |
| 50.12 | -0.05 |
| 50.44 | -1 |

Figure 7.10 shows the resulting response envelope with the existing services shown for reference, with Table 7.9 showing the settings determined to give the highest average availability for the 1C system. It can be seen that the response envelope created falls somewhere in the middle of existing services, showing that it could operate in a region where there is not currently a comparable service.

Following on from introducing a knee point, a second C-Rate sensitivity analysis was conducted with the results of this shown in Figure 7.11. Compared with the analysis shown in Figure 7.8 there is a much more shallow reduction in availability as the C-Rate is increased. At 10C (0.1MWh/1MW) there is still an average availability above 95% whilst still providing 138.54MWh of energy throughput across the year, showing that it is possible to have a high power, low energy FESS that can provide an effective frequency response service which is critical in allowing the more common specifications of FESS to operate in the frequency response service market.

Again, Figure 7.11 also shows the energy throughput across the year. This time, in contrast with Figure 7.8, the energy throughput stays in a much narrower range across all studied C-Rates with the lowest throughput being for a 20C system (122MWh) and the highest being for a 1C system (161MWh). The closest base service in terms of energy throughput is DC with a value of 83.9MWh, and importantly when compared to the bespoke designed service there is an improvement of 2.49% availability (from 97.8% to 99.89%) whilst providing almost double the energy throughput. This is an excellent indicator of the advantages gained from designing a service specifically for a FESS or other very short-duration storage rather than treating all ESS technologies as equal.

Figure 7.12 shows the number of cycles experienced per year under the initial response envelope discussed in Section A and under the subsequent envelope discussed in this section.

When comparing how the two response envelopes translate into FESS cycles, it is clear that at higher C-Rates the amount of cycling required by the FESS may be prohibitive even for a cycle-resistant storage medium such as flywheels. Taking the lower end of the quoted spectrum of cycle limits as 100,000 cycles, this
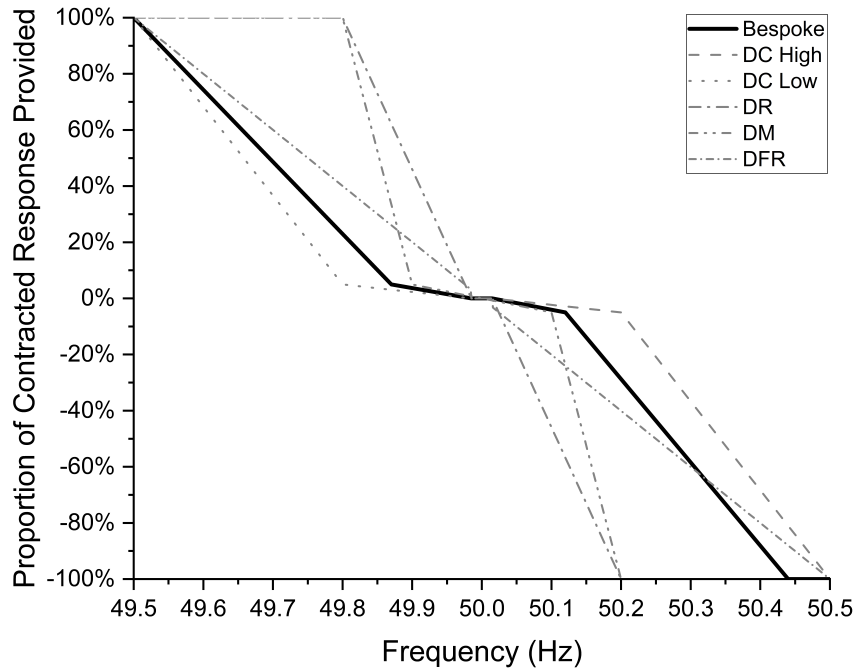
Figure 7.10: New frequency response envelope most suitable for provision by a 1MW/1MWh/1C FESS providing a 1MW service with existing frequency response service envelopes shown for reference
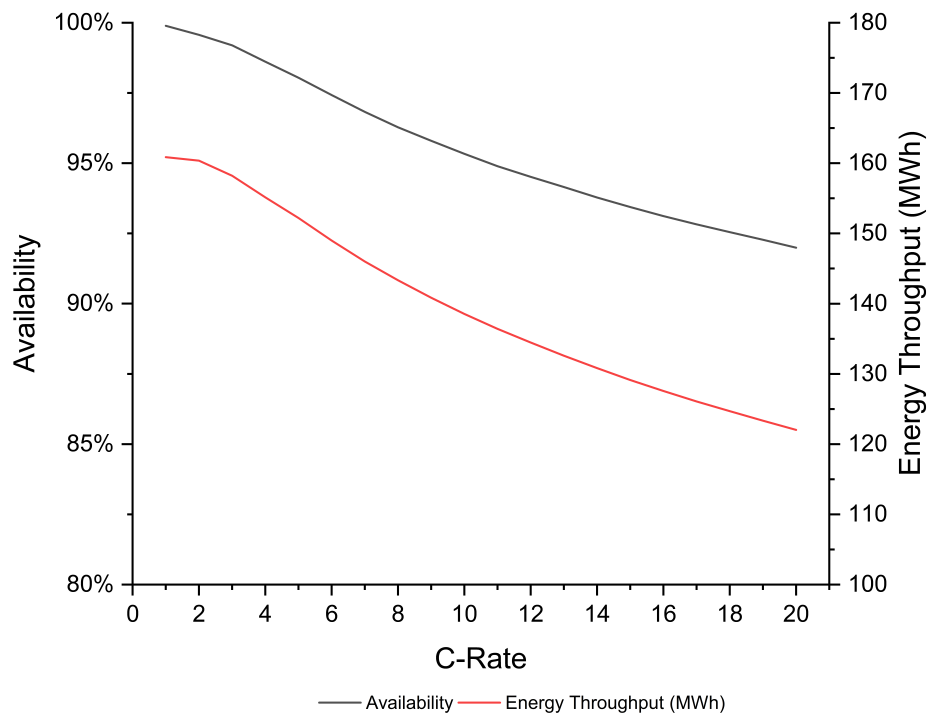


Figure 7.11: C-Rate sensitivity analysis when utilising the response envelope shown in Figure 7.10 with a 1MW/1MWh/1C FESS providing a 1MW service
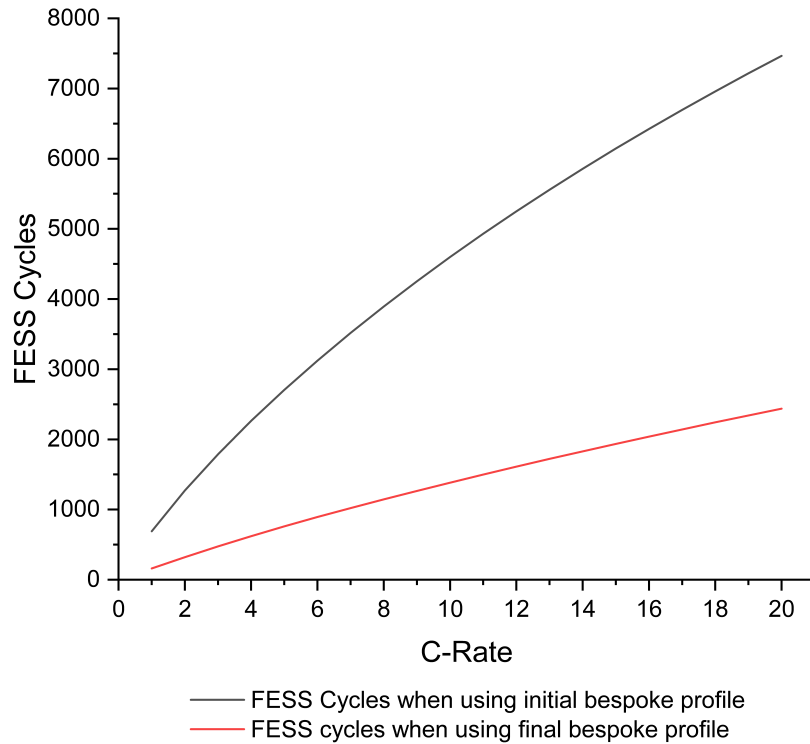
Figure 7.12: Cycles experienced by the FESS under the initial and final response envelope for varying C-Rates

would mean that all systems with a C-Rate of 9C and above would likely require replacement before the required 25-year lifespan was achieved (4,254 cycles per year for 25 years would result in 106,350 cycles experienced for a 9C system). Of course, it is important to note that many manufacturers quote the cycle life for FESSs as unlimited, in which case this would cease to be an issue.

Looking at the final bespoke profile, however, all of the C-Rates studied would comfortably fall below even this lower limit, with the maximum value of 2,439 cycles per year resulting in just 60,975 cycles. It is clear that at this level of cycling more traditional ESSs such as Li-ion BESSs would not be able to deliver the same service as they are most often quoted with a maximum cycle life of 10,000.

## 7.4.3 Higher C-Rate Analysis

A final study was conducted to optimise the response envelope for different FESS C-Rates. The key criteria was achieving the highest availability possible whilst attempting to match, or improve upon, the lowest energy throughput provided by an existing service (83.9MWh - DC). An example of how this was conducted for a 5C system is shown in Table 7.10 and Table 7.11. In Table 7.10, the cells are highlighted to show the highest average availability in green, trending downwards to the lowest availability in red. In Table 7.11, the green cells are highlighted as

Table 7.10: Excerpt of Average Availability based knee-point optimisation for a 5C system

| Average Availability for 5C System | | $f_{-K}$ | | | |
|---|---|---|---|---|---|
| | | 50.18 | 50.19 | 50.2 | 50.21 |
| $f_K$ (Hz) | 49.81 | 98.57% | 97.66% | 96.77% | 95.98% |
| | 49.8 | 99.24% | 98.51% | 97.66% | 96.83% |
| | 49.79 | 99.21% | 99.25% | 98.50% | 97.69% |
| | 49.78 | 98.63% | 99.34% | 99.21% | 98.47% |
| | 49.77 | 98.01% | 98.81% | 99.47% | 99.18% |

Table 7.11: Excerpt of Energy Throughput (MWh) based knee point optimisation of a 5C system

| Energy Throughput for 5C System | | $f_{-K}$ (Hz) | | | |
|---|---|---|---|---|---|
| | | 50.18 | 50.19 | 50.2 | 50.21 |
| $f_K$ (Hz) | 49.81 | 93.55 | 88.33 | 83.50 | 79.17 |
| | 49.8 | 92.44 | 87.92 | 83.36 | 79.14 |
| | 49.79 | 89.65 | 87.30 | 83.20 | 79.11 |
| | 49.78 | 85.67 | 85.20 | 82.67 | 78.90 |
| | 49.77 | 81.85 | 81.66 | 81.17 | 78.57 |

achieving a higher overall energy throughput than the equivalent DM service whilst the cells highlighted in red fall short of achieving this. The investigations conducted for the other C-Rates are contained in the Appendix as Tables A1 to A6.

This analysis showed that whilst the average availability can be increased further, the energy throughput would then be decreased further. The combinations where the energy throughput falls below the desired level are discounted, with the highest availability from the remaining combinations taken as the best option. This optimisation balances the two to provide the most suitable overall service for each C-Rate. It should be noted however that if energy throughput was removed as a constraint then further increases in average availability could be achieved, albeit with the system providing less energy to and from the grid. For instance, in Table 7.10 and Table 7.11, a higher average availability could be achieved using the combination of 49.77/50.2Hz but would result in a loss of 4.03MWh of energy throughput across the year, for just a 0.13% increase in average availability.

The results of the study for a 5C, 10C, 15C and 20C system are shown in Table 7.12, with the 1C results determined previously included for reference.

These results show that for different C-Rates slight variations on the high and low knee points are required to extract the best combination of average availability and energy throughput. By tailoring the knee points to the C-Rate being considered, a 20C system was able to achieve a 95% availability, albeit with a slightly lower energy throughput than desired. The outcome of this study shows that with a small

Table 7.12: Results of C-Rate based optimisation of the response envelope knee points including average availability for each configuration when performing DC High/Low

| C-Rate | Low Knee Point (Hz) | High Knee Point (Hz) | Availability | Energy (MWh) | DC Availability |
|---|---|---|---|---|---|
| 1 | 49.87 | 50.12 | 99.89% | 143.88 | 99.18% |
| 5 | 49.78 | 50.19 | 99.34% | 85.20 | 92.22% |
| 10 | 49.79 | 50.18 | 97.80% | 85.63 | 88.04% |
| 15 | 49.80 | 50.17 | 95.93% | 85.68 | 85.44% |
| 20 | 49.78 | 50.18 | 95.00% | 76.05 | 83.40% |

amount of versatility in response envelope, much higher C-Rate systems can provide standalone frequency response services.

The key conclusion to be drawn from Table 7.12 is when comparing the average availability achieved under the bespoke profile with the availability achieved when performing the combined DC high and low service. Whilst there is a minimal improvement at the 1C configuration, it is in the more commonly found higher C-Rates that the true breakthrough of this research is realised. For a 20C FESS, the average availability that it can provide whilst running 24/7 is 11.60% higher for the bespoke profile jumping from 83.40% to 95%. Across all of the higher C-Rate systems studied, the FESS can now provide a much more reliable and worthwhile service all whilst delivering levels of energy throughput either in excess of or very close to that provided by a 1C system delivering DC High/Low (as previously noted in Table 7.5).

The response envelope developed in this section is a significant improvement over existing envelopes in terms of the ability for FESSs to provide a consistently high level of availability and energy throughput. However, it is possible that are alternative envelopes that would present further improvements over the one presented here. An area of further research on this work could implement a multi-objective GA with energy throughput and availability as objectives with the various set points as variables in order to fully explore the parameter space and potentially provide further improvements.

## 7.4.4 Economic Case Study

For the economic analysis, the following assumptions have been made to ensure the study falls in line with real-world conditions and maintains consistency with the other studies in this thesis;

- It is assumed that the payment mechanism will be identical to that already utilised by DFR. Payment will be made on a sliding scale, with full payment

at availability above 95%. This is a reasonable assumption as it is unlikely that a bespoke payment mechanism for this service would be worthwhile.

- The availability payment will be calculated in the same way (as a value of £/MW/hr).

- The average clearing price for availability payments will be within the same range as found in both historic DFR bids and recent bids from the new suite of services. For DFR this has been set throughout the thesis as £11.67/MW/hr, whilst the average clearing price over the past 12 months for DC, DM and DR is £15.58/MW/hr.

- Discount rate is set as 8% with the TCC of the FESS set to £780/kW. The discount rate has been set to a higher value to represent a slightly higher risk level of the investment. These values have been set to enable the impact of changing availability payment levels to be realised in the results, and represent a typical FESS system being installed to provide the service.

- Each FESS system uses the optimum settings for the response envelope outlined previously in Table 7.12

The main objective of this section is to analyse the required level of availability payment that would result in a typical FESS system achieving a positive NPV under current economic conditions. Using the same approach as the previous section, the systems studied will consist of a 1MW FESS with varying C-Rates between 5C and 20C to reflect typical FESS systems. Figure 7.13

When considering these results it is important to contextualise them by comparing them with values produced in similar studies. In [250], which looks at a combined wind battery system providing frequency response, shows the system achieving an NPV of £7.865m with a discount rate of 8%. Values varying between £1-40m NPV are achieved in [251], which looks at the optimal placement of BESS within the UK to provide frequency response services. Finally, in [252], a BESS providing a frequency response service is able to achieve NPV in the region of €12.9-18.2m when operating in an isolated power system.

With the context understood, Figure 7.13 can now be analysed. It was detailed above that the availability price has historically averaged in the region of £10-15/MW/hr. With an increase in availability price, this impacts significantly on the NPV of the system. For a price of £10/MW/hr, the NPV ranges between £128,000 for a 5C system to -£45,000 for a 20C system. Whilst for a £15/MW/hr, the NPV ranges between £583,000 for a 5C system to £323,000 for a 20C system. These two availability prices line up with the common averages for existing services, giving
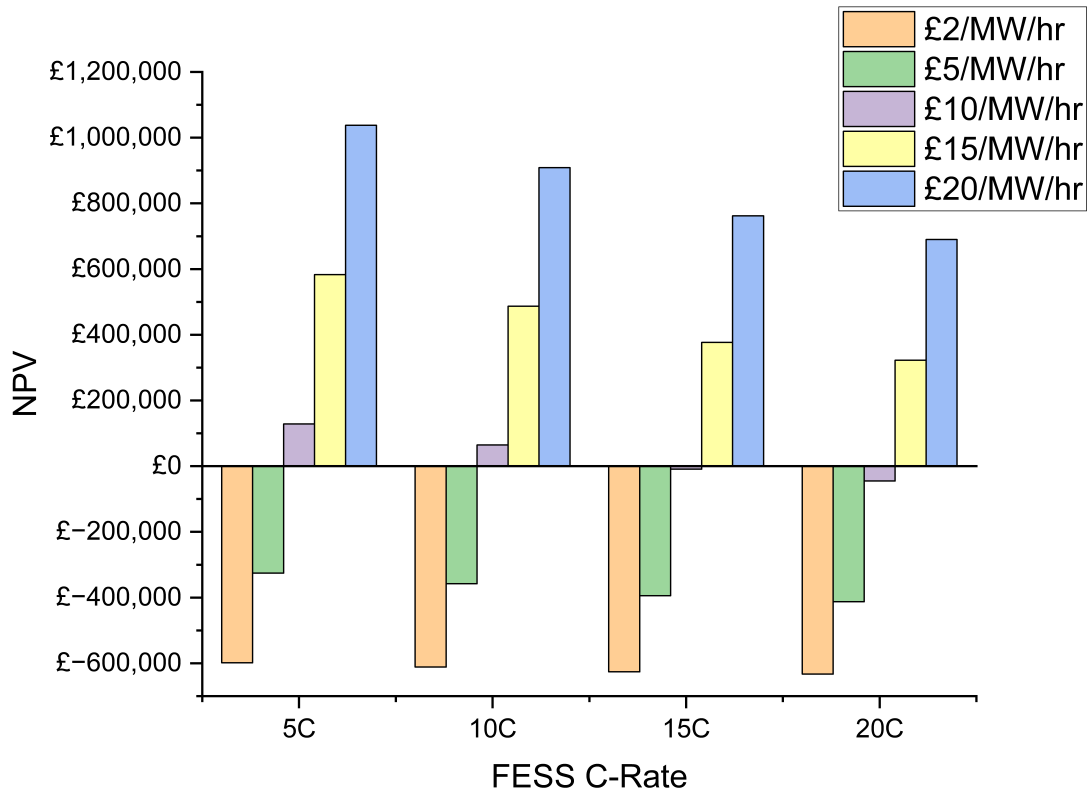
Figure 7.13: Economic Analysis of Bespoke Response Envelopes

the best indicator of how profitable a FESS could be under the bespoke response profiles. At the lowest availability price studied, the NPV of the system would be negative for all of the C-Rates studied.

The highlight of these results becomes apparent when they are compared to the values achieved in Chapter 5 Section 5.3.1. Taking the 5C system for example, this configuration had a negative NPV when operating under the DFR response profile as discussed previously. However, when the response envelope is specifically tailored to the FESS advantages, the NPV can become positive. This above all else emphasises the significant impact that such a service could have on the viability of allowing other ESS technologies to participate in the frequency response market.

## 7.4.5 Sensitivity Analysis

To further investigate the viability of FESSs for providing this bespoke service, a sensitivity analysis was then performed to determine the highest TCC at which the system could provide a positive NPV. To do this, the availability payment was set as £10/MW/hr in line with the lowest value from Figure 7.13 that produced a positive NPV for all C-Rates. This was done to represent a 'worst-case' scenario in terms of income, along with keeping the discount rate at 8%. The TCC is then varied
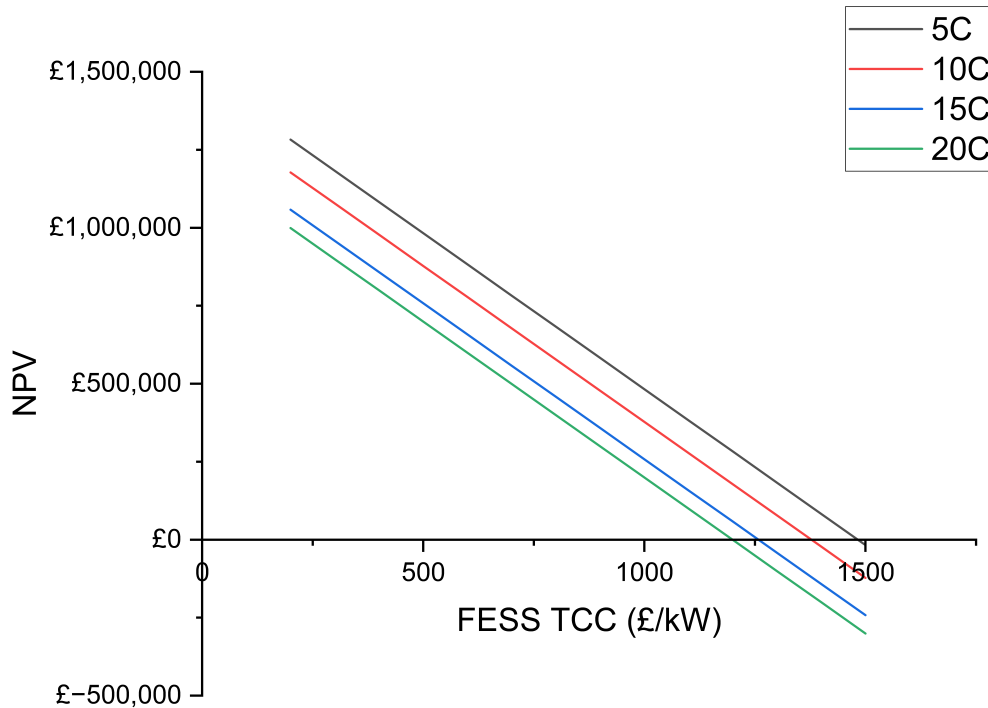
Figure 7.14: Sensitivity analysis on varying FESS TCC and C-Rate for bespoke response profile

between £200/kW and £1,500/kW and the results are shown in Figure 7.14

It can be seen that across a significant range of TCC values, all four different FESS configurations can provide a significantly positive NPV under these conditions. The highest threshold value is £1,482 for a 5C system providing a positive NPV, which means any system cheaper than this will produce in excess of 8% return on investment. The lowest threshold on the other hand is still a value of £1,119 for a 20C system. This leads to the conclusion that there is significant potential for a large range of FESS costs and configurations that can be deployed to provide positive economic results.

## 7.4.6   Discussion

In this study, a bespoke frequency response service has been designed and analysed. When considering a baseline 1MW/1MWh/1C system providing a 1MW service, a peak average availability of 99.89% can be achieved when operating the service 24/7 delivering the response envelope shown in Figure 7.10.

Subsequently, this response envelope has been investigated for different FESS C-Rates. It has been shown that different FESS C-Rates require slightly different

response profiles in order to extract maximum performance benefits. By using these small modifications to the response profile, a 20C FESS can achieve an average availability of 95%.

Finally, the economic implications were assessed showing significant positive NPV was available for a range of different FESS configurations and availability prices when using a FESS with a TCC of £780/kW. The NPV that was achievable under varying scenarios was shown to be competitive with values found in the literature for BESSs.

The research presented in this study has the potential to open up the frequency response market to a much wider range of energy storage technologies such as FESSs and Super-capacitors than has been previously suggested.

## 7.5   Chapter Conclusions

In this chapter, a novel and important insight into the future of frequency response services for energy-limited assets has been presented.

Firstly, the suitability for an energy-limited asset such as a FESS for the new suite of frequency response services was studied and discussed, concluding that the performance of a standalone FESS would not be able to provide the required levels of service to participate in this market without the use of hybridisation to increase the overall energy capacity. This provides clarity on the new set of frequency response services, showing that the intended goal of NGESO of widening the types of storage that will be able to participate in the frequency market has not been achieved for these services.

Whilst it is acknowledged that this study has been undertaken from a technology-derived perspective rather than that of NGESO, the service developed in this chapter represents an ability to guarantee a defined contribution of continuous frequency support, which could then be utilised in the higher level modelling performed by NGESO such as the overall inertia model and could form an important part of a wider suite of service profiles and can be used to inform frequency response service strategy going forward.

Following this a different approach was taken, considering how a frequency response service could be set up to enable a FESS to perform at the required level. Through an iterative design process, a response envelope suitable for delivery by energy-limited assets was developed. This represents a significant step in diversifying the storage technologies utilised in frequency response, as it shows that when consideration is given to the strengths of different technologies then they can compete with and even outperform the widely deployed existing ESS technologies.

The demonstration of the fast-acting very short-duration FESS providing a ro-

bust level of service is especially important when considering the 'System Needs and Product Strategy' report from 2017 which described an increasing need for fast-acting sources of frequency response [253].

To conclude the works, an economic study was also undertaken, showing that with competitive pricing and payment mechanisms, a FESS could definitively compete with and most likely outperform a BESS installation. This highlights the fact that a much broader range of ESS technologies can be used viably for frequency response services as long as the services are designed appropriately. The fact that this service could be carried out on a 24/7 basis also removes significant degrees of complexity from the procurement process, as it can be awarded on a fixed-term contract basis rather than going through daily bidding processes.

# Chapter 8

# Conclusions & Further Work

This thesis has presented an extensive investigation into the potential for FESSs to be deployed in various grid-scale applications and additionally how they can be utilised to extend the lifetime of Li-ion BESSs. This investigation has shown how to exploit the unique operational characteristics of FESSs to provide greater techno-economic value to both proposed and existing installations. It has provided a wide-ranging study that opens up new avenues for further research into FESSs and by extension, other very short-duration ESSs whilst providing novel tools and processes with which to perform this research. Additionally, it has provided insight for manufacturers to use the outcomes of this research and increase the deployment of FESSs across different applications.

The following sections detail an overview of the contributions of each chapter, followed by a discussion on the objectives set out at the beginning of this Thesis in Chapter 1. Finally, recommendations for future work are provided.

## 8.1 Chapter Contributions

### 8.1.1 Chapter 3

This chapter concentrated on the development of a new modelling and analytical framework for both FESSs and BESSs. Initially, the different methods of modelling energy storage systems were discussed and critiqued, with the conclusion being drawn that 'bucket' modelling was the most suitable approach for these systems. The novel model was then introduced with a step-by-step analysis of the different blocks used within the overall system along with explanations of the theory behind different subsystems such as degradation modelling and cycle counting. The rapid nature of the developed model was demonstrated by showing that across four different applications, a year could be simulated in no longer than 9.9 minutes.

Following this, a set of verification analyses were undertaken. Firstly, the opera-

tion of the BESS model was assessed by comparing the outputs with real-world data when subjected to different types of input. This showed that the model is highly accurate in replicating both standard step change load profiles and more complex frequency response profiles, resulting in RMSE in the range of 0.25%-2.78% depending on the data set being used.

The subsequent verification exercise looked at the degradation algorithm used within the model. Six different cycle profiles have been executed over 9 iterations on a set of DMEGC Li-Ion cells, producing experimental degradation results. These results have then been compared with the equivalent degradation simulated by the model, where it was shown that an overall RMSE of 0.43% has been achieved between the experimental and simulated results.

Finally, the analytical framework provided by the model was introduced, showing the novel range of different visualisation options available for monitoring ESS operation. This was followed by a discussion about how this information could be utilised to inform decisions regarding the sizing and control of hybrid systems.

## 8.1.2 Chapter 4

The work in this chapter highlighted the issue of export limitation on the Great Britain distribution network in the context of locally curtailed wind generation sites. In an initial literature review section, it was shown that this is a growing concern as the deployment and connection of DG increases. The lack of prior research in this area was also discussed, along with a review of literature that discusses similar issues at the national distribution level.

The first part of the chapter discussed a theoretical implementation of a FESS for the alleviation of export limitation issues and how it could be utilised to drive techno-economic benefit for a wind generation site. The results of this study showed that there is significant scope for FESSs to be deployed in this area but with a cautionary note that they must meet the correct sizing and cost criteria to be effective.

The TCC values at which a FESS could be effective on a theoretical level were discussed. Under the current economic conditions (an average TCC across literature studied of £780/kW) it is likely that only a 1C FESS would be viable for this application. If, however, the TCC of £500/kW could be achieved, a C-Rate of up to 10C for the FESS could be economically viable. At £200/kW, a FESS up to 20C could be implemented, this is however unlikely to be achievable in the near future but does indicate what may be possible with further advancements and cost reductions.

This analysis was then verified against a real-world case study. A techno-economic comparison between BESSs and FESSs for this application showed that

whilst a BESS can moderately outperform a FESS on a technical basis, once economic considerations are taken into account their effectiveness is dramatically reduced due to excessive cycle based degradation.

It was shown that for this real-world case study, the FESS can provide a positive techno-economic impact up to a high capital cost ceiling, whilst a BESS would be far more restricted by capital cost. For a 7.5kWh 8C FESS the highest TCC that can provide a positive economic impact at this site was determined to be £1500/kW, whilst for the BESS this threshold is £500/kW.

Overall, this chapter provided a first-of-its-kind study which can be utilised to effectively relieve a growing problem that is restricting the potential for distributed generation deployment and operation across Great Britain.

### 8.1.3 Chapter 5

The varied analysis in this chapter concentrated on exploring the potential for FESSs to be utilised in the field of frequency response services.

Initially, the chapter set out to explore the existing literature on frequency response provision by ESSs before concentrating on the ability for FESSs to be deployed for this application. It introduced a detailed overview of the DFR service historically offered by NGESO and the service characteristics.

An analysis was then conducted on the ability for FESSs to provide frequency response services as standalone units. This was done initially by modelling the operation of varying FESS configurations conducting a 24/7 DFR service. This analysis was conducted to investigate what specification of FESS would be required to provide the required level of technical performance. With a threshold requirement of 95% availability, the 2.5C system was the highest C-Rated FESS able to provide this service. As the C-Rate was increased beyond this, the technical performance dropped suggesting higher C-Rate FESSs are likely unsuited from a technical perspective.

Building upon the technical modelling, NPV calculations were carried out over a range of FESS configurations and economic parameters. This produced a detailed view of what TCC thresholds would result in positive economic impact for a range of different FESS configurations. For a 5C system, 44.4% of the scenarios studied resulted in a positive NPV, whilst for a 2.5C system this number rises to 51.4%.

Finally, an initial study on hybridisation was conducted, exploring how introducing varying sizes of BESS to the system impacted the technical and economic performance of the site. Specifically, this analysis was conducted on a 5C system, representing the most borderline case in which a standalone FESS could be economically viable. The outcome of this study showed that whilst there are some scenarios

in which the addition of a BESS can improve the performance of the site, there are also many scenarios where a BESS will have a negative impact.

Overall, the chapter provided a novel and extensive investigation into the ability for FESSs to provide frequency response services from an economic and technical standpoint.

### 8.1.4   Chapter 6

This chapter built upon the work conducted in Chapter 5 by further exploring the ability of FESSs to deliver frequency response services, this time from a hybrid perspective. Specifically, this chapter covered the enhancement of a BESS installation by introducing elements of FESS.

A baseline of a 1MW/1MWh/1C BESS providing a 1MW DFR service was introduced, along with 7 hybrid control strategies for the FESS/BESS hybrid. These novel control strategies represent a range of different options for controlling a hybrid system.

Following this, an overview of the modelling and data visualisation framework developed for this work was presented showing the options for analysing the operational characteristics of each system, such as time spent cycling at different C-Rates and SOC ranges.

The remaining two sections of the chapter were dedicated to two different methods of techno-economic assessment of the 7 hybrid control strategies, with the first section approaching this via the use of genetic algorithms, and the second section using an iterative approach. The peak NPVC achieved was £1,187,900 using CS-2 and a 91kWh 4C FESS. Overall, a positive NPVC could be achieved with C-Rates varying between 4C and 12C, as well as energy capacities between 28kWh and 1000kWh, showcasing the significant impact that a wide range of different FESS specifications can have.

Additionally, the NPVC that could be achieved across a range of different TCCs determined, showing how economically viable each combination of control strategy and FESS specification could be under different economic conditions. From this analysis, it was shown that a 50kWh 4C FESS operating under CS-5 could achieve a positive economic impact at the highest TCC of £5,105/kW.

### 8.1.5   Chapter 7

Finally, the possibility of designing a frequency response service specifically for delivery by very short duration energy storage such as FESSs was explored in this chapter.

The first part of this chapter focused on providing a first-of-its-kind analysis of the delivery of the new suite of frequency response services by FESSs, and what this means for the future outlook of FESSs being deployed for this application.

Overall, In terms of a standalone FESS, the only service that is likely to be able to be provided by a higher C-Rate system is Dynamic Containment. However, as was detailed within the chapter, the existing service parameters (specifically around minimum states of energy) mean that this is unlikely to be able to be implemented without changes to the way the service operates.

The final piece of work involved designing a service envelope that could be delivered by high C-Rate systems using an iterative design approach. Whilst this study produced a technology-derived response profile rather than one developed from a grid requirements standpoint, this service would still provide a valid contribution as part of a suite of other service profiles.

The results of this novel study showed that a FESS with a C-Rate of 20C could provide 95% availability using the designed service envelope operating on a 24/7 basis. This could provide an avenue for significantly increased deployment of varied ESSs and reduce the over-reliance of the system on a narrow band of technology types, mostly BESSs.

## 8.2 Objectives Review

Now that the main contributions of the thesis have been discussed, a review of the objectives set out at the beginning of this thesis can take place, focusing on whether the objectives have been met and the key contribution that has been provided.

**Objective 1** - *Develop a model that can rapidly and accurately simulate both Flywheel and Battery Energy Storage Systems that are also easily configurable to different applications.* - This objective was fully explored throughout the thesis. After the introduction of the models in Chapter 3 which highlighted the many advantages of utilising this model, the remaining chapters went on to implement the model in a range of different applications including wind generation, frequency response and HESS implementation. The BESS model was verified using both real-world data from the Willenhall ESS and lab based experimental data. Each chapter where the model was used presents the different parameters and modified blocks that are specific to the given applications. By fulfilling this objective, this thesis has contributed an advancement to the field of energy storage modelling, allowing rapid simulation of complex systems and applications.

**Objective 2** - *Explore the potential for Energy Storage Systems to provide sup-*

*port to DG sites that are export limited, exploring the techno-economic benefits of different types of ESS* - Within Chapter 4, this objective was explored in great depth both introducing and explaining the issue as well as providing a wide-ranging techno-economic analysis on the ability of both FESSs and BESSs to be deployed for this application. As part of meeting this objective, this thesis has unlocked a novel new avenue of ESS research and shown a promising suite of results to suggest future directions for the research.

**Objective 3** - *Produce a detailed exploration on the suitability of FESSs for the provision of traditional frequency response services, both as standalone and hybrid units.* - Throughout Chapters 5 and 6, multiple separate lines of investigation were explored in order to fulfil the requirements of this objective. Extensive exploration of FESSs for standalone frequency response service provision was undertaken, concluding that the majority of traditional FESS configurations would be unsuitable, and introducing elements of BESS to the installation had a minor but worthwhile impact. However, subsequent analysis of introducing FESSs to an existing BESS installation showed significant improvements from both technical and economic standpoints. From this analysis, this thesis has provided a wide-ranging suite of results that can increase the impact of existing BESS installations and provide a viable route to deployment for a diverse selection of FESS configurations.

**Objective 4** - *Explore the possibilities of designing frequency response services specifically for delivery by FESSs, and what technical and economic parameters would be required for this to be feasible.* - In a first-of-its-kind study, Chapter 7 presented a detailed analysis of this topic. It was shown that by designing a service that takes advantage of the specific characteristics of a FESS, a wide range of configurations would be able to both compete with and in some cases outperform BESSs. The contributions of this work have the potential to shape the way that frequency response services are designed and delivered, opening up new avenues for ESSs of varying technologies and storage durations and reducing the over-reliance on BESSs.

**Objective 5** - *Provide an expansive investigation into the required economic parameters that manufacturers need to meet in order to allow FESSs to be deployed as competitive energy storage units in different applications.* - Over the course of the work presented in this thesis, the economic considerations of the applications being discussed have been at the forefront of the philosophy. This objective has been comprehensively explored, with all studies presented in this thesis being given economic consideration. This work has shown how different FESS configurations can be viable for deployment across different applications and economic conditions,

giving an extensive and novel study that will allow FESSs to continue to progress as a key part of the ESS market.

## 8.3 Further Work

The work presented in this thesis represents an under-explored element of energy storage research and any further work should continue the themes of trying to diversify the ESS technologies being deployed for grid services.

One key element of further work that should be looked into is more practical work on the implementation of the concepts discussed in this thesis. Whilst the topology of hybrid ESSs was briefly discussed, there is significant potential in exploring how such systems can be operated on a technical level, and where improvements in efficiency and performance can be achieved through novel system architectures.

Another area that should be explored further is the impact of larger-scale deployment of technology-specific frequency response profiles on the stability of the grid as a whole, using grid-wide models and considering how aspects such as inertia can be affected by such services being implemented.

Additionally, a key area of future work is to verify the FESS model against a real-world example, if access to an existing installation can be obtained. This could involve tailoring the model to different types of FESS construction and identifying more stringent operational parameters.

Finally, it would be useful to consider similar sets of analysis on other very short duration ESSs such as supercapacitors, and how different combinations of ESSs can be hybridised to enable the disadvantages of individual systems to be negated.

# References

[1] S. Koohi-Fayegh and M. A. Rosen, "A review of energy storage types, applications and recent developments," *Journal of Energy Storage*, vol. 27, no. November 2019, p. 101047, 2020. [Online]. Available: https://doi.org/10.1016/j.est.2019.101047

[2] Battery University. (2019) BU-205: Types of Lithium-ion. [Online]. Available: https://batteryuniversity.com/article/bu-205-types-of-lithium-ion

[3] United Nations Framework Convention on Climate Change, "PARIS AGREEMENT - Conference of the Parties COP 21," United Nations, Tech. Rep. December, 2015. [Online]. Available: http://unfccc.int/resource/docs/2015/cop21/eng/l09r01.pdf

[4] UNFCCC, "COP 26 Glasgow Climate Pact Advance unedited version Decision," UNFCCC, Tech. Rep., 2021. [Online]. Available: https://unfccc.int/sites/default/files/resource/cop26{_}auv{_}2f{_}cover{_}decision.pdf

[5] Parliament of the United Kingdom, "Climate Change Act 2008," *HM Government*, pp. 1–103, 2008. [Online]. Available: http://www.legislation.gov.uk/ukpga/2008/27/pdfs/ukpga{_}20080027{_}en.pdf

[6] Vivid Economics, "Accelerated electrification and the GB electricity system - Report prepared for Committee on Climate Change," no. April, pp. 1–79, 2019. [Online]. Available: https://www.theccc.org.uk/wp-content/uploads/2019/05/CCC-Accelerated-Electrification-Vivid-Economics-Imperial-1.pdf

[7] National Grid ESO. (2021) FES 2021 Data Workbook V08. [Online]. Available: https://www.nationalgrideso.com/future-energy/future-energy-scenarios/fes-2021/documents

[8] BEIS. (2021) Digest of UK Energy Statistics (DUKES): electricity. [Online]. Available: https://www.gov.uk/government/statistics/electricity-chapter-5-digest-of-united-kingdom-energy-statistics-dukes

[9] S. Gordon, C. McGarry, and K. Bell, "The growth of distributed generation and associated challenges: A Great Britain case study," *IET Renewable Power Generation*, vol. 16, no. 9, pp. 1827–1840, 2022.

[10] National Grid ESO. (2021) Historic Frequency Data. [Online]. Available: https://www.nationalgrideso.com/balancing-services/ frequency-response-services/historic-frequency-data

[11] ——, "The Grid Code - UK," National Grid ESO, Tech. Rep. 5, 2017. [Online]. Available: https://www.nationalgrid.com/sites/default/files/ documents/8589935310-CompleteGridCode.pdf

[12] S. Homan and S. Brown, "An analysis of frequency events in Great Britain," *Energy Reports*, vol. 6, pp. 63–69, 2020. [Online]. Available: https://doi.org/10.1016/j.egyr.2020.02.028

[13] National Grid ESO. (2022) Frequency response services. [Online]. Available: https://www.nationalgrideso.com/industry-information/ balancing-services/frequency-response-services

[14] UK Parliament, "Low carbon network infrastructure inquiry," Tech. Rep., 2016. [Online]. Available: http://www.parliament.uk/business/committees/ committees-a-z/commons-select/energy-and-climate-change-committee/ inquiries/parliament-2015/low-carbon-network/

[15] Energy Solutions. (2022) DNO – Distribution Network Operators. [Online]. Available: https://www.energybrokers.co.uk/electricity/ dno-distribution-network-operators

[16] Enegry Networks Association, "Engineering Recommendation G100 Issue 1 Amendment 2 2018 Technical Requirements for Customer Export Limiting Schemes," Energy Networks Association, Tech. Rep. 1, 2018. [Online]. Available: www.energynetworks.org

[17] Western Power Distribution. (2022) Network Capacity Map. [Online]. Available: https://www.westernpower.co.uk/our-network/network-capacity-map/

[18] The Association for Decentralised Energy. (2022) Technical Guidance for Customer Export Limiting Schemes - Engineering Recommendation G100. [Online]. Available: https://www.theade.co.uk/news/market-news/ technical-guidance-for-customer-export-limiting-schemes-engineering-recomme

[19] International Energy Agency, "Innovation in batteries and electricity storage," no. September, p. 98, 2020. [Online]. Available: https://www.iea.org/reports/innovation-in-batteries-and-electricity-storage

[20] IEA, "Informing Energy Sector Transformations," 2017. [Online]. Available: www.iea.org/etp/tracking

[21] OXTO Energy. OXTO Energy. [Online]. Available: https://www.oxtoenergy.com/

[22] National Grid ESO, "Technical Report on the events of 9 August 2019," *Technical Report*, pp. 1–37, 2019.

[23] Battery University. (2021) BU-402: What Is C-rate? [Online]. Available: https://batteryuniversity.com/article/bu-402-what-is-c-rate

[24] National Grid ESO, "Britain's Electricity Explained : June 2022," Tech. Rep. June, 2022.

[25] Q. Ma, "Overview of energy storage technology based on distributed energy system," *IOP Conference Series: Earth and Environmental Science*, vol. 631, no. 1, 2021.

[26] Paul W. Parfomak, "Energy Storage for Power Grids and Electric Transportation," Tech. Rep., 2012.

[27] B. Bolund, H. Bernhoff, and M. Leijon, "Flywheel energy and power storage systems," *Renewable and Sustainable Energy Reviews*, vol. 11, no. 2, pp. 235–258, 2007.

[28] S. Choudhury, "Flywheel energy storage systems: A critical review on technologies, applications, and future prospects," *International Transactions on Electrical Energy Systems*, vol. 31, no. 9, pp. 1–26, 2021.

[29] Stornetic. Enwheel. [Online]. Available: https://www.stornetic.com/our-technology/enwheel

[30] Amber Kinetics. Amber Kinetics M32. [Online]. Available: https://www.amberkinetics.com/wp-content/uploads/2020/05/Amber-Kinetics-DataSheet.pdf

[31] S. Karrari, M. Noe, and J. Geisbuesch, "High-speed Flywheel Energy Storage System (FESS) for Voltage and Frequency Support in Low Voltage Distribution Networks," *2018 IEEE 3rd International Conference on Intelligent Energy*

*and Power Systems, IEPS 2018 - Proceedings*, vol. 2018-Janua, pp. 176–182, 2018.

[32] F. Nadeem, S. M. Hussain, P. K. Tiwari, A. K. Goswami, and T. S. Ustun, "Comparative review of energy storage systems, their roles, and impacts on future power systems," *IEEE Access*, vol. 7, no. December 2018, pp. 4555–4585, 2019.

[33] A. G. Olabi, T. Wilberforce, M. A. Abdelkareem, and M. Ramadan, "Critical review of flywheel energy storage system," *Energies*, vol. 14, no. 8, pp. 1–33, 2021.

[34] R. Peña-Alzola, R. Sebastián, J. Quesada, and A. Colmenar, "Review of flywheel based energy storage systems," *International Conference on Power Engineering, Energy and Electrical Drives*, no. May, 2011.

[35] M. E. Amiryar and K. R. Pullen, "A review of flywheel energy storage system technologies and their applications," *Applied Sciences*, vol. 7, no. 3, 2017.

[36] M. A. Awadallah and B. Venkatesh, "Energy storage in flywheels: An overview," *Canadian Journal of Electrical and Computer Engineering*, vol. 38, no. 2, pp. 183–193, 2015.

[37] I. Hadjipaschalis, A. Poullikkas, and V. Efthimiou, "Overview of current and future energy storage technologies for electric power applications," *Renewable and Sustainable Energy Reviews*, vol. 13, no. 6-7, pp. 1513–1522, 2009.

[38] L. A. Wong, V. K. Ramachandaramurthy, P. Taylor, J. B. Ekanayake, S. L. Walker, and S. Padmanaban, "Review on the optimal placement, sizing and control of an energy storage system in the distribution network," *Journal of Energy Storage*, vol. 21, no. December 2018, pp. 489–504, 2019. [Online]. Available: https://doi.org/10.1016/j.est.2018.12.015

[39] B. Zakeri and S. Syri, "Electrical energy storage systems: A comparative life cycle cost analysis," *Renewable and Sustainable Energy Reviews*, vol. 42, pp. 569–596, 2015. [Online]. Available: http://dx.doi.org/10.1016/j.rser.2014.10.011

[40] J. Liu, C. Hu, A. Kimber, and Z. Wang, "Uses, Cost-Benefit Analysis, and Markets of Energy Storage Systems for Electric Grid Applications," *Journal of Energy Storage*, vol. 32, no. June, p. 101731, 2020. [Online]. Available: https://doi.org/10.1016/j.est.2020.101731

[41] C. K. Das, O. Bass, G. Kothapalli, T. S. Mahmoud, and D. Habibi, "Overview of energy storage systems in distribution networks: Placement, sizing, operation, and power quality," *Renewable and Sustainable Energy Reviews*, vol. 91, no. November 2016, pp. 1205–1230, 2018. [Online]. Available: https://doi.org/10.1016/j.rser.2018.03.068

[42] M. Aneke and M. Wang, "Energy storage technologies and real life applications – A state of the art review," *Applied Energy*, vol. 179, pp. 350–377, 2016. [Online]. Available: http://dx.doi.org/10.1016/j.apenergy.2016.06.097

[43] Active Power. Flywheel Technology. [Online]. Available: https://www.activepower.com/en-GB/2813/flywheel-technology

[44] Adaptive Balancing Power. Product. [Online]. Available: https://www.adaptive-balancing.de/en/product/

[45] Beacon Power. Resources. [Online]. Available: https://beaconpower.com/resources/

[46] Energiestro. Technology. [Online]. Available: https://energiestro.net/technology/

[47] KineticCore. Meet KineticCore Solutions. [Online]. Available: https://www.kineticcore.com/

[48] Levisys. Our Technology. [Online]. Available: https://www.levisys.com/la-technologie?lang=en

[49] Revterra. Cost effective & long duration storage. [Online]. Available: https://www.revterra.io/

[50] Spinlectrix. The Revolution. [Online]. Available: https://www.spinlectrix.com/the-revolution

[51] Teraloop. Our Products. [Online]. Available: https://www.teraloop.org/products

[52] Vycon Energy. (2016) VYCON Direct Connect (VDC) Kinetic Energy Storage Systems. [Online]. Available: https://www.calnetix.com/sites/default/files/CA{_}VYCON{_}VDC{_}BROCHURE{_}ENGLISH{_}WEB{_}6{_}15{_}16.pdf

[53] I. Mexis and G. Todeschini, "Battery energy storage systems in the united kingdom: A review of current state-of-the-art and future applications," *Energies*, vol. 13, no. 14, 2020.

[54] H. Chen, T. N. Cong, W. Yang, C. Tan, Y. Li, and Y. Ding, "Progress in electrical energy storage system: A critical review," *Progress in Natural Science*, vol. 19, no. 3, pp. 291–312, 2009. [Online]. Available: http://dx.doi.org/10.1016/j.pnsc.2008.07.014

[55] M. A. Hannan, S. B. Wali, P. J. Ker, M. S. Rahman, M. Mansor, V. K. Ramachandaramurthy, K. M. Muttaqi, T. M. Mahlia, and Z. Y. Dong, "Battery energy-storage system: A review of technologies, optimization objectives, constraints, approaches, and outstanding issues," *Journal of Energy Storage*, vol. 42, no. August, p. 103023, 2021. [Online]. Available: https://doi.org/10.1016/j.est.2021.103023

[56] J. Wang, J. Purewal, P. Liu, J. Hicks-Garner, S. Soukazian, E. Sherman, A. Sorenson, L. Vu, H. Tataria, and M. W. Verbrugge, "Degradation of lithium ion batteries employing graphite negatives and nickel-cobalt-manganese oxide + spinel manganese oxide positives: Part 1, aging mechanisms and life estimation," *Journal of Power Sources*, vol. 269, pp. 937–948, 2014. [Online]. Available: http://dx.doi.org/10.1016/j.jpowsour.2014.07.030

[57] C. Liu, Y. Wang, and Z. Chen, "Degradation model and cycle life prediction for lithium-ion battery used in hybrid energy storage system," *Energy*, vol. 166, pp. 796–806, 2019.

[58] T. Feehally, A. J. Forsyth, R. Todd, M. P. Foster, D. Gladwin, D. A. Stone, and D. Strickland, "Battery energy storage systems for the electricity grid: UK research facilities," in *IET Conference Publications*, vol. 2016, no. CP684. Institution of Engineering and Technology, 2016.

[59] Department for Energy Security and Net Zero. (2023) Renewable Energy Planning Database: quarterly extract. [Online]. Available: https://www.gov.uk/government/publications/renewable-energy-planning-database-monthly-extract

[60] M. I. Daoud, A. M. Massoud, A. S. Abdel-Khalik, A. Elserougi, and S. Ahmed, "A Flywheel Energy Storage System for Fault Ride Through Support of Grid-Connected VSC HVDC-Based Offshore Wind Farms," *IEEE Transactions on Power Systems*, vol. 31, no. 3, pp. 1671–1680, 2016.

[61] L. Wang, J. Y. Yu, and Y. T. Chen, "Dynamic stability improvement of an integrated offshore wind and marine-current farm using a flywheel energy-storage system," *IET Renewable Power Generation*, vol. 5, no. 5, pp. 387–396, 2011.

[62] X. Wang, D. Yu, S. Le Blond, Z. Zhao, and P. Wilson, "A novel controller of a battery-supercapacitor hybrid energy storage system for domestic applications," *Energy and Buildings*, vol. 141, pp. 167–174, 2017.

[63] T. S. Babu, K. R. Vasudevan, V. K. Ramachandaramurthy, S. B. Sani, S. Chemud, and R. M. Lajim, "A Comprehensive Review of Hybrid Energy Storage Systems: Converter Topologies, Control Strategies and Future Prospects," *IEEE Access*, vol. 8, pp. 148 702–148 721, 2020.

[64] Energymonitor.ai. (2022) Inflation bites at the battery storage bonanza. [Online]. Available: https://www.energymonitor.ai/tech/energy-storage/inflation-bites-at-the-battery-storage-bonanza

[65] Clean Technica. (2022) More Utility Scale Battery Projects For The UK To Help With Wind Curtailment Issues. [Online]. Available: https://cleantechnica.com/2022/11/29/more-utility-scale-battery-projects-for-the-uk-to-help-with-wind-curtailment-issues/

[66] Saur Energy. (2023) TagEnergy Energises 50 MW Battery Storage Facility For UK. [Online]. Available: https://www.saurenergy.com/solar-energy-news/tagenergy-energises-50mw-battery-storage-facility-for-uk

[67] The Engineer, "Exagen submits plans for £350m grid-scale battery," 2023. [Online]. Available: https://www.theengineer.co.uk/content/news/exagen-submits-plans-for-350m-grid-scale-battery/#:~:text=The%20%C2%A3350m%20containerised%20battery,fluctuations%20in%20intermittent%20renewable%20energy.

[68] Smart Energy. (2023) RWE begins construction on 220MW frequency-stabilising battery system. [Online]. Available: https://www.smart-energy.com/storage/rwe-begins-construction-on-220mw-frequency-stabilising-battery-system/

[69] Solar Power Portal. (2022) Iberdrola switches on 25MWh battery system in Ireland. [Online]. Available: https://www.solarpowerportal.co.uk/iberdrola{_}switches{_}on{_}25mwh{_}battery{_}system{_}in{_}ireland/

[70] Smart Energy. (2023) UK gives green light for 'world's largest' battery project. [Online]. Available: https://www.smart-energy.com/storage/uk-gives-green-light-for-worlds-largest-battery-project/

[71] Teslarati. (2023) Tesla Megapack powers £75M BESS in Europe, the continent's largest. [Online]. Available: https://www.teslarati.com/tesla-megapack-bess-europe-pillswood-196-mwh/

[72] T. Kousksou, P. Bruel, A. Jamil, T. El Rhafiki, and Y. Zeraouli, "Energy storage: Applications and challenges," *Solar Energy Materials and Solar Cells*, vol. 120, no. PART A, pp. 59–80, 2014.

[73] International Energy Agency, "Technology Roadmap," IEA, Tech. Rep., 2014.

[74] M. Khalid and A. V. Savkin, "Minimization and control of battery energy storage for wind power smoothing: Aggregated, distributed and semi-distributed storage," *Renewable Energy*, vol. 64, pp. 105–112, 2014. [Online]. Available: http://dx.doi.org/10.1016/j.renene.2013.09.043

[75] B. Olateju, A. Kumar, and M. Secanell, "A techno-economic assessment of large scale wind-hydrogen production with energy storage in Western Canada," *International Journal of Hydrogen Energy*, vol. 41, no. 21, pp. 8755–8776, 2016. [Online]. Available: http://dx.doi.org/10.1016/j.ijhydene.2016.03.177

[76] J. Atherton, R. Sharma, and J. Salgado, "Techno-economic analysis of energy storage systems for application in wind farms," *Energy*, vol. 135, pp. 540–552, 2017. [Online]. Available: http://dx.doi.org/10.1016/j.energy.2017.06.151

[77] D. Q. Oliveira, O. R. Saavedra, K. Santos-Pereira, J. D. Pereira, D. S. Cosme, L. S. Veras, R. G. Bento, and V. B. Riboldi, "A critical review of energy storage technologies for microgrids," *Energy Systems*, no. 0123456789, 2021. [Online]. Available: https://doi.org/10.1007/s12667-021-00464-6

[78] A. Z. AL Shaqsi, K. Sopian, and A. Al-Hinai, "Review of energy storage services, applications, limitations, and benefits," *Energy Reports*, vol. 6, pp. 288–306, 2020. [Online]. Available: https://doi.org/10.1016/j.egyr.2020.07.028

[79] H. Alharbi and K. Bhattacharya, "Stochastic optimal planning of battery energy storage systems for isolated microgrids," *IEEE Transactions on Sustainable Energy*, vol. 9, no. 1, pp. 211–227, 2018.

[80] F. Meishner and D. U. Sauer, "Wayside energy recovery systems in DC urban railway grids," *eTransportation*, vol. 1, p. 100001, 2019. [Online]. Available: https://doi.org/10.1016/j.etran.2019.04.001

[81] J. Martins and J. Miles, "A techno-economic assessment of battery business models in the UK electricity market," *Energy Policy*, vol. 148, 2021.

[82] S. M. Salam and M. M. Rashid, "A new approach to analysis and simulation of flywheel energy storage system," in *8th International Conference on Mechatronics Engineering (ICOM 2022)*, vol. 2022, 2022, pp. 90–94.

[83] V. S. Diaz, D. A. Cantane, A. Q. O. Santos, and O. H. Ando Junior, "Comparative Analysis of Degradation Assessment of Battery Energy Storage Systems in PV Smoothing Application," *Energies*, vol. 14, no. 12, p. 3600, 2021.

[84] T. Mesbahi, P. Bartholomeus, N. Rizoug, R. Sadoun, F. Khenfri, and P. L. Moigne, "Advanced Model of Hybrid Energy Storage System Integrating Lithium-Ion Battery and Supercapacitor for Electric Vehicle Applications," *IEEE Transactions on Industrial Electronics*, vol. 68, no. 5, pp. 3962–3972, 2021.

[85] H. Meng, M. Wang, O. Olumayegun, X. Luo, and X. Liu, "Process design, operation and economic evaluation of compressed air energy storage (CAES) for wind power through modelling and simulation," *Renewable Energy*, vol. 136, pp. 923–936, 2019. [Online]. Available: https://doi.org/10.1016/j.renene.2019.01.043

[86] Y. Yang, S. Bremner, C. Menictas, and M. Kay, "Modelling and optimal energy management for battery energy storage systems in renewable energy systems: A review," *Renewable and Sustainable Energy Reviews*, vol. 167, no. June, p. 112671, 2022. [Online]. Available: https://doi.org/10.1016/j.rser.2022.112671

[87] M. Moncecchi, C. Brivio, S. Mandelli, and M. Merlo, "Battery energy storage systems in microgrids: Modeling and design criteria," *Energies*, vol. 13, no. 8, pp. 1–18, 2020.

[88] M. Shen and Q. Gao, "A review on battery management system from the modeling efforts to its multiapplication and integration," *International Journal of Energy Research*, vol. 43, no. 10, pp. 5042–5075, 2019.

[89] T. Simpkins and C. O. Donnell, "Optimizing Battery Sizing and Dispatching To Maximize Economic Return," *Battcon Stationary Battery Conference*, no. May, pp. 1–14, 2017. [Online]. Available: www.battcon.com

[90] J. M. Reniers, G. Mulder, S. Ober-Blöbaum, and D. A. Howey, "Improving optimal control of grid-connected lithium-ion batteries through more accurate battery and degradation modelling," *Journal of Power Sources*, vol. 379, no. December 2017, pp. 91–102, 2018. [Online]. Available: https://doi.org/10.1016/j.jpowsour.2018.01.004

[91] L. K. Gan, J. Reniers, and D. Howey, "A hybrid vanadium redox/lithium-ion energy storage system for off-grid renewable power," *2017 IEEE Energy Conversion Congress and Exposition, ECCE 2017*, vol. 2017-Janua, no. section II, pp. 1016–1023, 2017.

[92] C. Jankowiak, A. Zacharopoulos, C. Brandoni, P. Keatley, P. MacArtain, and N. Hewitt, "The role of domestic integrated battery energy storage systems for electricity network performance enhancement," *Energies*, vol. 12, no. 20, pp. 1–27, 2019.

[93] R. H. G. Tan and G. K. Tinakaran, "Development of battery energy storage system model in MATLAB/Simulink," *International Journal of Smart Grid and Clean Energy*, no. 1, pp. 180–188, 2020.

[94] S. Ould Amrouche, D. Rekioua, T. Rekioua, and S. Bacha, "Overview of energy storage in renewable energy systems," *International Journal of Hydrogen Energy*, vol. 41, no. 45, pp. 20 914–20 927, 2016.

[95] A. Jaafar, B. Sareni, X. Roboam, and M. Thiounn-Guermeur, "Sizing and Energy Management of a Hybrid Locomotive Based on Flywheel and Accumulators," *2010 IEEE Vehicle Power and Propulsion Conference, VPPC 2010*, vol. 58, no. 8, pp. 3947–3958, 2010.

[96] R. Arghandeh, M. Pipattanasomporn, and S. Rahman, "Flywheel energy storage systems for ride-through applications in a facility microgrid," *IEEE Transactions on Smart Grid*, vol. 3, no. 4, pp. 1955–1962, 2012.

[97] L. Shen, Q. Cheng, Y. Cheng, L. Wei, and Y. Wang, "Hierarchical control of DC micro-grid for photovoltaic EV charging station based on flywheel and battery energy storage system," *Electric Power Systems Research*, vol. 179, no. November 2018, p. 106079, 2020. [Online]. Available: https://doi.org/10.1016/j.epsr.2019.106079

[98] R. Sebastián and R. Peña Alzola, "Flywheel energy storage systems: Review and simulation for an isolated wind power system," *Renewable and Sustainable Energy Reviews*, vol. 16, no. 9, pp. 6803–6813, 2012.

[99] S. N. Motapon, E. Lachance, L.-A. Dessaint, and K. Al-Haddad, "A Generic Cycle Life Model for Lithium-Ion Batteries Based on Fatigue Theory and Equivalent Cycle Counting," *IEEE Open Journal of the Industrial Electronics Society*, vol. 1, no. August, pp. 207–217, 2020.

[100] D. Peralta, C. Canizares, and K. Bhattacharya, "Practical Modeling of Flywheel Energy Storage for Primary Frequency Control in Power Grids," *IEEE Power and Energy Society General Meeting*, vol. 2018-Augus, no. November 2017, pp. 1–5, 2018.

[101] J. Li, J. Bi, G. Yan, Y. Ge, and P. Jin, "Research on improving power quality of wind power system based on the flywheel energy storage system," *China International Conference on Electricity Distribution, CICED*, vol. 2016-Septe, no. Ciced, pp. 1–6, 2016.

[102] S. D. Sessa, A. Tortella, M. Andriollo, and R. Benato, "Li-ion battery-flywheel hybrid storage system: Countering battery aging during a grid frequency regulation service," *Applied Sciences (Switzerland)*, vol. 8, no. 11, pp. 1–15, 2018.

[103] J. M. Reniers, G. Mulder, S. Ober-Blöbaum, and D. A. Howey, "Improving optimal control of grid-connected lithium-ion batteries through more accurate battery and degradation modelling," *Journal of Power Sources*, vol. 379, no. January, pp. 91–102, 2018. [Online]. Available: https://doi.org/10.1016/j.jpowsour.2018.01.004

[104] F. Calero, C. A. Cañizares, and K. Bhattacharya, "Detailed and Average Battery Energy Storage Model Comparison," *Proceedings of 2019 IEEE PES Innovative Smart Grid Technologies Europe, ISGT-Europe 2019*, 2019.

[105] M. Berger, I. Kocar, E. Farantatos, and A. Haddadi, "Modeling of Li-ion battery energy storage systems (BESSs) for grid fault analysis," *Electric Power Systems Research*, vol. 196, 2021.

[106] K. S. El-Bidairi, H. D. Nguyen, T. S. Mahmoud, S. D. Jayasinghe, and J. M. Guerrero, "Optimal sizing of Battery Energy Storage Systems for dynamic frequency control in an islanded microgrid: A case study of Flinders Island, Australia," *Energy*, vol. 195, p. 117059, 2020. [Online]. Available: https://doi.org/10.1016/j.energy.2020.117059

[107] P. L. Camunas, J. Lopez Merino, A. P. Asensio, M. Garcia Plaza, and S. A. Gomez, "Analysis of methods to improve energy storage arbitrage benefit considering capacity degradation," *Proceedings of the IEEE International Conference on Industrial Technology*, vol. 2021-March, pp. 573–578, 2021.

[108] R. H. G. Tan and G. K. Tinakaran, "Development of battery energy storage system model in MATLAB/Simulink," *International Journal of Smart Grid and Clean Energy*, no. 1, pp. 180–188, 2020.

[109] A. J. Hutchinson and D. T. Gladwin, "Verification and analysis of a Battery Energy Storage System model," *Energy Reports*, vol. 8, pp. 41–47, 2022. [Online]. Available: https://doi.org/10.1016/j.egyr.2022.05.042

[110] S. Saberi Oskouee, S. Kamali, and T. Amraee, "Primary Frequency Support in Unit Commitment Using a Multi-Area Frequency Model with Flywheel Energy Storage," *IEEE Transactions on Power Systems*, vol. 36, no. 6, pp. 5105–5119, 2021.

[111] A. M. Aly, A. M. Kassem, K. Sayed, and I. Aboelhassan, "Design of Microgrid with Flywheel Energy Storage System Using HOMER Software for Case Study," *Proceedings of 2019 International Conference on Innovative Trends in Computer Engineering, ITCE 2019*, no. February, pp. 485–491, 2019.

[112] R. Sebastián and R. Peña-Alzola, "Flywheel energy storage and dump load to control the active power excess in a wind diesel power system," *Energies*, vol. 13, no. 8, 2020.

[113] A. Saleh, A. Awad, and W. Ghanem, "Modeling, Control, and Simulation of a New Topology of Flywheel Energy Storage Systems in Microgrids," *IEEE Access*, vol. 7, pp. 160 363–160 376, 2019.

[114] M. Khodaparastan and A. Mohamed, "Flywheel vs. Supercapacitor as wayside energy storage for electric rail transit systems," *Inventions*, vol. 4, no. 4, 2019.

[115] M. Nadour, A. Essadki, and T. Nasser, "Power Smoothing Control of DFIG Based Wind Turbine using Flywheel Energy Storage System," *2020 International Conference on Electrical and Information Technologies, ICEIT 2020*, pp. 0–6, 2020.

[116] C. Strunck and C. Rehtanz, "Development of a dynamic Combined Heat and Power Plant and Flywheel Energy Storage System Model validated with Field Tests," *2021 IEEE Madrid PowerTech, PowerTech 2021 - Conference Proceedings*, 2021.

[117] H. A. Moghaddam, M. H. Saeedinia, S. Mohamadian, M. S. Mahdavi, and G. B. Gharehpetian, "Integrated Modeling of Power Network and Connected Flywheel Energy Storage System for Optimal Power and Energy Ratings of Flywheel," *IEEE Transactions on Energy Conversion*, vol. 36, no. 3, pp. 1589–1599, 2021.

[118] J. Li, W. Zou, Q. Yang, F. Yi, Y. Bai, Z. Wei, and H. He, "Size optimization and power allocation of a hybrid energy storage system for

frequency service," *International Journal of Electrical Power and Energy Systems*, vol. 141, no. February, p. 108165, 2022. [Online]. Available: https://doi.org/10.1016/j.ijepes.2022.108165

[119] L. Wei, M. Wu, M. Yan, S. Liu, Q. Cao, and H. Wang, "A Review on Electrothermal Modeling of Supercapacitors for Energy Storage Applications," *IEEE Journal of Emerging and Selected Topics in Power Electronics*, vol. 7, no. 3, pp. 1677–1690, 2019.

[120] L. H. Saw, H. M. Poon, W. T. Chong, C. T. Wang, M. C. Yew, M. K. Yew, and T. C. Ng, "Numerical modeling of hybrid supercapacitor battery energy storage system for electric vehicles," *Energy Procedia*, vol. 158, pp. 2750–2755, 2019. [Online]. Available: https://doi.org/10.1016/j.egypro.2019.02.033

[121] I. N. Jiya, N. Gurusinghe, and R. Gouws, "Electrical circuit modelling of double layer capacitors for power electronics and energy storage applications: A review," *Electronics (Switzerland)*, vol. 7, no. 11, 2018.

[122] M. Krpan, I. Kuzle, A. Radovanovic, and J. V. Milanovic, "Modelling of Supercapacitor Banks for Power System Dynamics Studies," *IEEE Transactions on Power Systems*, vol. 36, no. 5, pp. 3987–3996, 2021.

[123] M. Şahin, "Modelling of Supercapacitors Based on Simplified Equivalent Circuit," *CPSS Transactions on Power Electronics and Applications*, vol. 6, no. 1, pp. 31–39, 2021.

[124] C. Li, D. Wang, D. Liu, J. Wu, Y. Li, C. Mao, and J. Wang, "Mathematical modelling of large-scale compressed air energy storage systems," *ICAC 2019 - 2019 25th IEEE International Conference on Automation and Computing*, no. September, pp. 5–7, 2019.

[125] S. Chen, A. Arabkoohsar, T. Zhu, and M. P. Nielsen, "Development of a micro-compressed air energy storage system model based on experiments," *Energy*, vol. 197, p. 117152, 2020. [Online]. Available: https://doi.org/10.1016/j.energy.2020.117152

[126] H. Jin, P. Liu, and Z. Li, "Dynamic modeling and design of a hybrid compressed air energy storage and wind turbine system for wind power fluctuation reduction," *Computers and Chemical Engineering*, vol. 122, pp. 59–65, 2019. [Online]. Available: https://doi.org/10.1016/j.compchemeng.2018.05.023

[127] I. Calero, C. A. Cañizares, and K. Bhattacharya, "Compressed Air Energy Storage System Modeling for Power System Studies," *IEEE Transactions on Power Systems*, vol. 34, no. 5, pp. 3359–3371, 2019.

[128] S. Kharel and B. Shabani, "Hydrogen as a long-term large-scale energy storage solution to support renewables," *Energies*, vol. 11, no. 10, 2018.

[129] Z. Abdin and W. Mérida, "Hybrid energy systems for off-grid power supply and hydrogen production based on renewable energy: A techno-economic analysis," *Energy Conversion and Management*, vol. 196, no. January, pp. 1068–1079, 2019. [Online]. Available: https://doi.org/10.1016/j.enconman.2019.06.068

[130] D. N. Luta and A. K. Raji, "Optimal sizing of hybrid fuel cell-supercapacitor storage system for off-grid renewable applications," *Energy*, vol. 166, pp. 530–540, 2019. [Online]. Available: https://doi.org/10.1016/j.energy.2018.10.070

[131] M. A. V. Rad, R. Ghasempour, P. Rahdan, S. Mousavi, and M. Arastounia, "Techno-economic analysis of a hybrid power system based on the cost-effective hydrogen production method for rural electrification, a case study in Iran," *Energy*, vol. 190, p. 116421, 2020. [Online]. Available: https://doi.org/10.1016/j.energy.2019.116421

[132] P. Gabrielli, A. Poluzzi, G. J. Kramer, C. Spiers, M. Mazzotti, and M. Gazzani, "Seasonal energy storage for zero-emissions multi-energy systems via underground hydrogen storage," *Renewable and Sustainable Energy Reviews*, vol. 121, p. 109629, 2020. [Online]. Available: https://doi.org/10.1016/j.rser.2019.109629

[133] M. Möller, D. Kucevic, N. Collath, A. Parlikar, P. Dotzauer, B. Tepe, S. Englberger, A. Jossen, and H. Hesse, "SimSES: A holistic simulation framework for modeling and analyzing stationary energy storage systems," *Journal of Energy Storage*, vol. 49, no. February, p. 103743, 2022. [Online]. Available: https://doi.org/10.1016/j.est.2021.103743

[134] C. Kupper, B. Weißhar, S. Rißmann, and W. G. Bessler, "End-of-Life Prediction of a Lithium-Ion Battery Cell Based on Mechanistic Aging Models of the Graphite Electrode," *Journal of The Electrochemical Society*, vol. 165, no. 14, pp. A3468–A3480, 2018.

[135] T. F. Fuller, M. Doyle, and J. Newman, "Simulation and Optimization of the Dual Lithium Ion Insertion Cell," *Journal of The Electrochemical Society*, vol. 141, no. 1, pp. 1–10, 1994.

[136] A. Jokar, B. Rajabloo, M. Désilets, and M. Lacroix, "Review of simplified Pseudo-two-Dimensional models of lithium-ion batteries," *Journal of Power Sources*, vol. 327, pp. 44–55, 2016. [Online]. Available: http://dx.doi.org/10.1016/j.jpowsour.2016.07.036

[137] Comsol, "Single Particle Model of a Lithium-Ion Battery Introduction," pp. 1–16, 2021. [Online]. Available: www.comsol.com/trademarks.

[138] W. He, N. Williard, M. Osterman, and M. Pecht, "Prognostics of lithium-ion batteries based on Dempster-Shafer theory and the Bayesian Monte Carlo method," *Journal of Power Sources*, vol. 196, no. 23, pp. 10 314–10 321, 2011. [Online]. Available: http://dx.doi.org/10.1016/j.jpowsour.2011.08.040

[139] J. M. Reniers, G. Mulder, and D. A. Howey, "Review and Performance Comparison of Mechanical-Chemical Degradation Models for Lithium-Ion Batteries," *Journal of The Electrochemical Society*, vol. 166, no. 14, pp. A3189–A3200, 2019.

[140] Z. Xue, Y. Zhang, C. Cheng, and G. Ma, "Remaining useful life prediction of lithium-ion batteries with adaptive unscented kalman filter and optimized support vector regression," *Neurocomputing*, vol. 376, pp. 95–102, 2020.

[141] M. Catelani, L. Ciani, R. Fantacci, G. Patrizi, and B. Picano, "Remaining Useful Life Estimation for Prognostics of Lithium-Ion Batteries Based on Recurrent Neural Network," *IEEE Transactions on Instrumentation and Measurement*, vol. 70, pp. 1–11, 2021.

[142] I. Laresgoiti, S. Käbitz, M. Ecker, and D. U. Sauer, "Modeling mechanical degradation in lithium ion batteries during cycling: Solid electrolyte interphase fracture," *Journal of Power Sources*, vol. 300, pp. 112–122, 2015.

[143] B. Xu, A. Oudalov, A. Ulbig, G. Andersson, and D. S. Kirschen, "Modeling of lithium-ion battery degradation for cell life assessment," *IEEE Transactions on Smart Grid*, vol. 9, no. 2, pp. 1131–1140, 2018.

[144] D. Wang, J. Coignard, T. Zeng, C. Zhang, and S. Saxena, "Quantifying electric vehicle battery degradation from driving vs. vehicle-to-grid services," *Journal of Power Sources*, vol. 332, pp. 193–203, 2016. [Online]. Available: http://dx.doi.org/10.1016/j.jpowsour.2016.09.116

[145] D. I. Stroe, V. Knap, M. Swierczynski, A. I. Stroe, and R. Teodorescu, "Operation of a grid-connected lithium-ion battery energy storage system for primary frequency regulation: A battery lifetime perspective," *IEEE Transactions on Industry Applications*, vol. 53, no. 1, pp. 430–438, 2017.

[146] D. I. Stroe, M. Swierczynski, A. I. Stroe, R. Laerke, P. C. Kjaer, and R. Teodorescu, "Degradation Behavior of Lithium-Ion Batteries Based on Lifetime Models and Field Measured Frequency Regulation Mission Profile," *IEEE Transactions on Industry Applications*, vol. 52, no. 6, pp. 5009–5018, 2016.

[147] D. I. Stroe, M. Swierczynski, A. I. Stan, R. Teodorescu, and S. J. Andreasen, "Accelerated lifetime testing methodology for lifetime estimation of lithium-ion batteries used in augmented wind power plants," *IEEE Transactions on Industry Applications*, vol. 50, no. 6, pp. 4006–4017, 2014.

[148] Y. Xing, E. W. Ma, K. L. Tsui, and M. Pecht, "An ensemble model for predicting the remaining useful performance of lithium-ion batteries," *Microelectronics Reliability*, vol. 53, no. 6, pp. 811–820, 2013. [Online]. Available: http://dx.doi.org/10.1016/j.microrel.2012.12.003

[149] B. Gundogdu and D. T. Gladwin, "A Fast Battery Cycle Counting Method for Grid-Tied Battery Energy Storage System Subjected to Microcycles," *iEECON 2018 - 6th International Electrical Engineering Congress*, 2018.

[150] L. R. GopiReddy, L. M. Tolbert, B. Ozpineci, and J. O. Pinto, "Rainflow Algorithm-Based Lifetime Estimation of Power Semiconductors in Utility Applications," *IEEE Transactions on Industry Applications*, vol. 51, no. 4, pp. 3368–3375, 2015.

[151] A. Antonopoulos, S. Drarco, M. Hernes, and D. Peftitsis, "Challenges and strategies for a real-time implementation of a rainflow-counting algorithm for fatigue assessment of power modules," *Conference Proceedings - IEEE Applied Power Electronics Conference and Exposition - APEC*, vol. 2019-March, no. March, pp. 2708–2713, 2019.

[152] S. F. Schneider, P. Novak, and T. Kober, "Rechargeable batteries for simultaneous demand peak shaving and price arbitrage business," *IEEE Transactions on Sustainable Energy*, vol. 12, no. 1, pp. 148–157, 2021.

[153] S. You and C. N. Rasmussen, "Generic modelling framework for economic analysis of battery systems," in *IET Conference Publications*, vol. 2011, no. 579 CP, 2011, p. 122.

[154] S. Loew, A. Anand, and A. Szabo, "Economic model predictive control of li-ion battery cyclic aging via online rainflow-analysis," *Energy Storage*, vol. 3, no. 3, p. e228, 2021. [Online]. Available: https://onlinelibrary.wiley.com/doi/abs/10.1002/est2.228

[155] Siemens. Rainflow Counting. [Online]. Available: https://community.sw. siemens.com/s/article/rainflow-counting

[156] D. Jiang, "A Sequence Retainable Iterative Algorithm for Rainflow Cycle Counting," *SAE International Journal of Materials and Manufacturing*, vol. 7, no. 1, pp. 108–114, 2014.

[157] D. Shaw-Williams, C. Susilawati, and G. Walker, "Value of residential investment in photovoltaics and batteries in networks: A techno-economic analysis," *Energies*, vol. 11, no. 4, 2018.

[158] M. Bahloul and S. K. Khadem, "An analytical approach for techno-economic evaluation of hybrid energy storage system for grid services," *Journal of Energy Storage*, vol. 31, oct 2020.

[159] B. Lian, A. Sims, D. Yu, C. Wang, and R. W. Dunn, "Optimizing LiFePO4 Battery Energy Storage Systems for Frequency Response in the UK System," *IEEE Transactions on Sustainable Energy*, vol. 8, no. 1, pp. 385–394, 2017.

[160] S. Bhattacharjee and P. K. Nayak, "PV-pumped energy storage option for convalescing performance of hydroelectric station under declining precipitation trend," *Renewable Energy*, vol. 135, pp. 288–302, 2019. [Online]. Available: https://doi.org/10.1016/j.renene.2018.12.021

[161] D. Roch-Dupré, Á. J. López-López, R. R. Pecharromán, A. P. Cucala, and A. Fernández-Cardador, "Analysis of the demand charge in DC railway systems and reduction of its economic impact with Energy Storage Systems," *International Journal of Electrical Power and Energy Systems*, vol. 93, pp. 459–467, 2017.

[162] S. Yoomak and A. Ngaopitakkul, "Feasibility analysis of different energy storage systems for solar road lighting systems," *Conference Record - Industrial and Commercial Power Systems Technical Conference*, vol. 2019-May, 2019.

[163] Volstora. (2023) Financial Analysis of Energy Storage. [Online]. Available: https://volstora.com/financial-analysis-of-energy-storage/{#}:{~}

[164] Www.rateinflation.com. United Kingdom Inflation Rates: 1989 to 2021. [Online]. Available: https://www.rateinflation.com/inflation-rate/ uk-historical-inflation-rate/

[165] Trading Economics. (2023) United Kingdom Electricity Price. [Online]. Available: https://tradingeconomics.com/united-kingdom/electricity-price

[166] Bank of England. (2023) Official Bank Rate history. [Online]. Available: https://www.bankofengland.co.uk/boeapps/database/Bank-Rate.asp

[167] S. Schoenung, "Energy storage systems cost update: a study for the DOE energy storage systems Program," *Sandia National Laboratories, DE-AC04-94AL85000*, no. January, pp. 1–30, 2011. [Online]. Available: http://prod.sandia.gov/techlib/access-control.cgi/2011/112730.pdf

[168] S. Gill, G. W. Ault, and I. Kockar, "The optimal operation of energy storage in a wind power curtailment scheme," *IEEE Power and Energy Society General Meeting*, pp. 1–8, 2012.

[169] G. Carpinelli, G. Celli, S. Mocci, F. Mottola, F. Pilo, and D. Proto, "Optimal integration of distributed energy storage devices in smart grids," *IEEE Transactions on Smart Grid*, vol. 4, no. 2, pp. 985–995, 2013.

[170] D. Kroniger and R. Madlener, "Hydrogen storage for wind parks: A real options evaluation for an optimal investment in more flexibility," *Applied Energy*, vol. 136, pp. 931–946, 2014. [Online]. Available: http://dx.doi.org/10.1016/j.apenergy.2014.04.041

[171] J. Cho and A. N. Kleit, "Energy storage systems in energy and ancillary markets: A backwards induction approach," *Applied Energy*, vol. 147, pp. 176–183, 2015. [Online]. Available: http://dx.doi.org/10.1016/j.apenergy.2015.01.114

[172] A. Chen and P. K. Sen, "Deployment of battery energy storage system for energy arbitrage applications," *NAPS 2016 - 48th North American Power Symposium, Proceedings*, pp. 1–8, 2016.

[173] X. Yan, C. Gu, F. Li, and Q. Ai, "Cost-benefit Comparison of Different Techniques for Addressing Wind Curtailment," *Energy Procedia*, vol. 142, pp. 1759–1764, 2017. [Online]. Available: https://doi.org/10.1016/j.egypro.2017.12.560

[174] C. Diyoke, M. Aneke, M. Wang, and C. Wu, "Techno-economic analysis of wind power integrated with both compressed air energy storage (CAES) and biomass gasification energy storage (BGES) for power generation," *RSC Advances*, vol. 8, no. 39, pp. 22 004–22 022, 2018.

[175] V. Efthymiou, C. Yianni, and G. Georghiou, "Economic viability of battery energy storage for the provision of frequency regulation service," *Journal of Power of Technologies*, vol. 98, no. 5, p. 403, 2018.

[176] A. Pino, F. J. P. Lucena, and J. G. MacHo, "Economic Analysis for Solar Energy Integration in a Microbrewery," *SEST 2019 - 2nd International Conference on Smart Energy Systems and Technologies*, 2019.

[177] Y. Wang, R. Das, G. Putrus, and R. Kotter, "Economic evaluation of photovoltaic and energy storage technologies for future domestic energy systems – A case study of the UK," *Energy*, vol. 203, p. 117826, 2020. [Online]. Available: https://doi.org/10.1016/j.energy.2020.117826

[178] F. Fan, G. Zorzi, D. Campos-Gaona, G. Burt, O. Anaya-Lara, J. Nwobu, and A. Madariaga, "Sizing and coordination strategies of battery energy storage system co-located with wind farm: The uk perspective," *Energies*, vol. 14, no. 5, 2021.

[179] S. Cupples, A. Abtahi, and S. A. Raziei, "Modeling, Optimizing and Financial Analysis of Hybrid Renewable Energy Systems Coupled with Energy Storage," *2021 16th International Conference on Ecological Vehicles and Renewable Energies, EVER 2021*, pp. 1–7, 2021.

[180] M. Stecca, T. B. Soeiro, L. R. Elizondo, P. Bauer, and P. Palensky, "Lifetime Estimation of Grid-Connected Battery Storage and Power Electronics Inverter Providing Primary Frequency Regulation," *IEEE Open Journal of the Industrial Electronics Society*, vol. 2, no. March, pp. 240–251, 2021.

[181] X. Fan, W. Ji, L. Guo, Z. Gao, L. Chen, and J. Wang, "Thermo-economic analysis of the integrated system of thermal power plant and liquid air energy storage," *Journal of Energy Storage*, vol. 57, no. September 2022, p. 106233, 2023. [Online]. Available: https://doi.org/10.1016/j.est.2022.106233

[182] Y. Al-Wreikat, E. K. Attfield, and J. R. Sodré, "Model for payback time of using retired electric vehicle batteries in residential energy storage systems," *Energy*, vol. 259, no. August, 2022.

[183] K. Kosowski, M. Piwowarski, W. Włodarski, P. Ziemiański, and G. Pawlak, "Technical and economic analysis of energy storage in the compressed air technology with low capacity for the production plant," *Energy Conversion and Management*, vol. 282, no. February, 2023.

[184] T. S. Le, T. N. Nguyen, D. K. Bui, and T. D. Ngo, "Optimal sizing of renewable energy storage: A techno-economic analysis of hydrogen, battery and hybrid systems considering degradation and seasonal storage," *Applied Energy*, vol. 336, no. February, p. 120817, 2023. [Online]. Available: https://doi.org/10.1016/j.apenergy.2023.120817

[185] F. Anvari-Azar, D. Strickland, N. Filkin, and H. Townshend, "Net Present Value Analysis of a Hybrid Gas Engine Energy Storage System in the Balancing Mechanism," *Energies*, vol. 13, no. 15, 2020.

[186] O. Schmidt, S. Melchior, A. Hawkes, and I. Staffell, "Projecting the Future Levelized Cost of Electricity Storage Technologies," *Joule*, vol. 3, no. 1, pp. 81–100, 2019. [Online]. Available: https://doi.org/10.1016/j.joule.2018.12.008

[187] X. Ouyang and B. Lin, "Levelized cost of electricity (LCOE) of renewable energies and required subsidies in China," *Energy Policy*, vol. 70, pp. 64–73, 2014. [Online]. Available: http://dx.doi.org/10.1016/j.enpol.2014.03.030

[188] Medium.com. (2018) What is electrical frequency and why does it matter? [Online]. Available: https://medium.com/drax/what-is-electrical-frequency-and-why-does-it-matter-fb60ae883246

[189] A. Tomczewski, L. Kasprzyk, and Z. Nadolny, "Reduction of power production costs in a wind power plant–flywheel energy storage system arrangement," *Energies*, vol. 12, no. 10, 2019.

[190] P. Boonluk, A. Siritaratiwat, P. Fuangfoo, and S. Khunkitti, "Optimal siting and sizing of battery energy storage systems for distribution network of distribution system operators," *Batteries*, vol. 6, no. 4, pp. 1–16, 2020.

[191] S. Breban, "Genetic Algorithm Optimization of an Energy Storage System Design and Fuzzy Logic Supervision for Battery Electric Vehicles," *Intech*, vol. i, no. Optimization Algorithms- Methods and Applications compared, p. 13, 2016.

[192] C. Chen, X. Wang, and J. Xiao, "An energy allocation strategy for hybrid ship DC power system based on genetic algorithm," *IETE Journal of Research*, vol. 62, no. 3, pp. 301–306, 2016. [Online]. Available: http://dx.doi.org/10.1080/03772063.2015.1093966

[193] A. Trpovski, P. Banerjee, Y. Xu, and T. Hamacher, "A Hybrid Optimization Method for Distribution System Expansion Planning with Lithium-ion Battery Energy Storage Systems," *iSPEC 2020 - Proceedings: IEEE Sustainable Power and Energy Conference: Energy Transition and Energy Internet*, pp. 2015–2021, 2020.

[194] A. F. Crossland, D. Jones, and N. S. Wade, "Planning the location and rating of distributed energy storage in LV networks using a genetic algorithm with simulated annealing," *International Journal of Electrical*

*Power and Energy Systems*, vol. 59, pp. 103–110, 2014. [Online]. Available: http://dx.doi.org/10.1016/j.ijepes.2014.02.001

[195] A. Abdelkader, A. Rabeh, D. Mohamed Ali, and J. Mohamed, "Multi-objective genetic algorithm based sizing optimization of a stand-alone wind/PV power supply system with enhanced battery/supercapacitor hybrid energy storage," *Energy*, vol. 163, pp. 351–363, 2018. [Online]. Available: https://doi.org/10.1016/j.energy.2018.08.135

[196] A. Szultka, R. Malkowski, S. Czapp, and S. Szultka, "Impact of R/X ratio of distribution network on selection and control of energy storage units," *Proceedings of the International Conference on Information and Digital Technologies, IDT 2017*, pp. 359–364, 2017.

[197] S. Akhavan Shams and R. Ahmadi, "Dynamic optimization of solar-wind hybrid system connected to electrical battery or hydrogen as an energy storage system," *International Journal of Energy Research*, vol. 45, no. 7, pp. 10 630–10 654, 2021.

[198] H. Xia, H. Chen, Z. Yang, F. Lin, and B. Wang, "Optimal energy management, location and size for stationary energy storage system in a metro line based on genetic algorithm," *Energies*, vol. 8, no. 10, pp. 11 618–11 640, 2015.

[199] H. H. Eldeeb, A. T. Elsayed, C. R. Lashway, and O. Mohammed, "Hybrid Energy Storage Sizing and Power Splitting Optimization for Plug-In Electric Vehicles," *IEEE Transactions on Industry Applications*, vol. 55, no. 3, pp. 2252–2262, 2019.

[200] S. Jalali Kashani and E. Farjah, "Applying neural network and genetic algorithm for optimal placement of ultra-capacitors in metro systems," *2011 IEEE Electrical Power and Energy Conference, EPEC 2011*, pp. 35–40, 2011.

[201] S. B. Peterson, J. Apt, and J. F. Whitacre, "Lithium-ion battery cell degradation resulting from realistic vehicle and vehicle-to-grid utilization," *Journal of Power Sources*, vol. 195, no. 8, pp. 2385–2392, 2010.

[202] Z. Wang, D. T. Gladwin, M. J. Smith, and S. Haass, "Practical state estimation using Kalman filter methods for large-scale battery systems," *Applied Energy*, vol. 294, jul 2021.

[203] A. Kadri, H. Marzougui, A. Aouiti, and F. Bacha, "Energy management and control strategy for a DFIG wind turbine/fuel cell hybrid system with super capacitor storage system," *Energy*, vol. 192, p. 116518, 2020. [Online]. Available: https://doi.org/10.1016/j.energy.2019.116518

[204] K. Smith, A. Saxon, M. Keyser, B. Lundstrom, Z. Cao, and A. Roc, "Life prediction model for grid-connected Li-ion battery energy storage system," *Proceedings of the American Control Conference*, no. August, pp. 4062–4068, 2017.

[205] M. A. Hannan, D. N. How, M. S. Hossain Lipu, P. J. Ker, Z. Y. Dong, M. Mansur, and F. Blaabjerg, "SOC Estimation of Li-ion Batteries with Learning Rate-Optimized Deep Fully Convolutional Network," *IEEE Transactions on Power Electronics*, vol. 36, no. 7, pp. 7349–7353, 2021.

[206] M. Lange, "On the Uncertainty of Wind Power Predictions—Analysis of the Forecast Accuracy and Statistical Distribution of Errors," *Journal of Solar Energy Engineering*, vol. 127, no. 2, p. 177, 2005. [Online]. Available: http://solarenergyengineering.asmedigitalcollection.asme.org/article.aspx?articleid=1457258

[207] DMEGC, "INR18650-29E Test Report," Tech. Rep. [Online]. Available: https://www.dmegcbattery.com/wp-content/uploads/2021/05/INR18650-29E-data-sheet.pdf

[208] UK Government. (2019) Average wind speed and deviations from the long term mean. [Online]. Available: https://assets.publishing.service.gov.uk/government/uploads/system/uploads/attachment{_}data/file/828562/ET{_}7.2.xls

[209] M. Yoon and S. Jung, "An economic ESS design method based on wind system capacity factor for island power grid," *International Journal of Engineering & Technology*, vol. 7, no. 3.3, p. 368, 2018.

[210] J. G. Simpson and E. Loth, "Super-rated operational concept for increased wind turbine power with energy storage," *Energy Conversion and Management: X*, vol. 14, no. September 2021, p. 100194, 2022. [Online]. Available: https://doi.org/10.1016/j.ecmx.2022.100194

[211] R. P. Praveen and K. V. Chandra Mouli, "Performance enhancement of parabolic trough collector solar thermal power plants with thermal energy storage capability," *Ain Shams Engineering Journal*, vol. 13, no. 5, p. 101716, 2022. [Online]. Available: https://doi.org/10.1016/j.asej.2022.101716

[212] M. Andoni, V. Robu, W. G. Früh, and D. Flynn, "Game-theoretic modeling of curtailment rules and network investments with distributed generation," *Applied Energy*, vol. 201, pp. 174–187, 2017. [Online]. Available: http://dx.doi.org/10.1016/j.apenergy.2017.05.035

[213] M. Jenkins and I. Kockar, "Impact of p2p trading on distributed generation curtailment in constrained distribution networks," *Electric Power Systems Research*, vol. 189, p. 106666, 2020. [Online]. Available: https://www.sciencedirect.com/science/article/pii/S0378779620304697

[214] K. L. Anaya and M. G. Pollitt, "Going smarter in the connection of distributed generation," *Energy Policy*, vol. 105, pp. 608–617, 2017. [Online]. Available: https://www.sciencedirect.com/science/article/pii/S0301421517300460

[215] C. Marantes, "Low Carbon Networks Fund Full Submission - Flexible Plug and Play Low Carbon Networks," LCN Fund, Tech. Rep. 0, 2013.

[216] J. X. Johnson, R. De Kleine, and G. A. Keoleian, "Assessment of energy storage for transmission-constrained wind," *Applied Energy*, vol. 124, pp. 377–388, 2014. [Online]. Available: http://dx.doi.org/10.1016/j.apenergy.2014.03.006

[217] N. S. Rayit, J. I. Chowdhury, and N. Balta-Ozkan, "Techno-economic optimisation of battery storage for grid-level energy services using curtailed energy from wind," *Journal of Energy Storage*, vol. 39, 2021.

[218] Drax Power. Getting Britain ready for the next generation of energy projects. [Online]. Available: https://www.drax.com/power-generation/getting-britain-ready-for-the-next-generation-of-energy-projects/

[219] Z. Zhou and C. Wang, "Output power curtailment control of variable-speed variable-pitch wind turbine generators," *Asia-Pacific Power and Energy Engineering Conference, APPEEC*, vol. 2015-March, no. March, 2014.

[220] F. Díaz-González, A. Sumper, O. Gomis-Bellmunt, and F. D. Bianchi, "Energy management of flywheel-based energy storage device for wind power smoothing," *Applied Energy*, vol. 110, pp. 207–219, 2013.

[221] C. Abbey and G. Joos, "Supercapacitor energy storage for wind energy applications," *IEEE Transactions on Industry Applications*, vol. 43, no. 3, pp. 769–776, 2007.

[222] Department for Levelling Up Housing and Communities. (2022) Government to launch consultation on local support on onshore wind. [Online]. Available: https://www.gov.uk/government/news/government-to-launch-consultation-on-local-support-on-onshore-wind

[223] A. Allegretti and H. Horton. (2022) Sunak set to end ban on new onshore wind-farms. [Online]. Available: https://www.theguardian.com/environment/2022/dec/06/sunak-set-end-ban-new-onshore-windfarms-england-tory-rebellion

[224] Wind Technik Nord. (2013) Wind Technik Nord 250 kW Turbine. [Online]. Available: http://www.rm-energy.co.uk/wp-content/uploads/2013/04/RME{_}WTN250{_}brochure{_}final.pdf

[225] CarbonBrief. Analysis: Record-low price for UK offshore wind is four times cheaper than gas. [Online]. Available: https://www.carbonbrief.org/analysis-record-low-price-for-uk-offshore-wind-is-four-times-cheaper-than-gas/

[226] K. Hama, Y. Fujimoto, and Y. Hayashi, "Expected wind speed estimation considering spatio-temporal anisotropy for generating synthetic wind power profiles," *Energy Procedia*, vol. 155, pp. 309–319, 2018. [Online]. Available: https://doi.org/10.1016/j.egypro.2018.11.047

[227] C. R. Shapiro, C. Ji, and D. F. Gayme, "Real-time energy market arbitrage via aerodynamic energy storage in wind farms," *Proceedings of the American Control Conference*, vol. 2020-July, pp. 4830–4835, 2020.

[228] A. F. Zobaa, *Energy Storage*. Rijeka: IntechOpen, Jan 2013. [Online]. Available: https://doi.org/10.5772/2550

[229] H. S. de Boer, L. Grond, H. Moll, and R. Benders, "The application of power-to-gas, pumped hydro storage and compressed air energy storage in an electricity system at different wind power penetration levels," *Energy*, vol. 72, pp. 360–370, 2014. [Online]. Available: https://www.sciencedirect.com/science/article/pii/S0360544214006136

[230] J. Li, F. Yao, Q. Yang, Z. Wei, and H. He, "Variable Voltage Control of a Hybrid Energy Storage System for Firm Frequency Response in the UK," *IEEE Transactions on Industrial Electronics*, 2022.

[231] National Grid ESO. Firm frequency response (FFR). [Online]. Available: https://www.nationalgrideso.com/industry-information/balancing-services/frequency-response-services/firm-frequency-response-ffr?overview

[232] D. M. Greenwood, K. Y. Lim, C. Patsios, P. F. Lyons, Y. S. Lim, and P. C. Taylor, "Frequency response services designed for energy storage," *Applied Energy*, vol. 203, pp. 115–127, 2017.

[233] M. L. Lazarewicz and T. M. Ryan, "Integration of flywheel-based energy storage for frequency regulation in deregulated markets," *IEEE PES General Meeting, PES 2010*, pp. 4–9, 2010.

[234] D. I. Stroe, V. Knap, M. Swierczynski, A. I. Stroe, and R. Teodorescu, "Operation of a grid-connected lithium-ion battery energy storage system for primary frequency regulation: A battery lifetime perspective," *IEEE Transactions on Industry Applications*, vol. 53, no. 1, pp. 430–438, 2017.

[235] B. Gundogdu, D. Gladwin, and D. Stone, "Battery energy management strategies for UK firm frequency response services and energy arbitrage," *The Journal of Engineering*, vol. 2019, no. 17, pp. 4152–4157, 2019.

[236] B. Mantar Gundogdu, S. Nejad, D. T. Gladwin, M. P. Foster, and D. A. Stone, "A battery energy management strategy for U.K. enhanced frequency response and triad avoidance," *IEEE Transactions on Industrial Electronics*, vol. 65, no. 12, pp. 9509–9517, 2018.

[237] S. Karrari, M. Noe, and J. Geisbuesch, "High-speed Flywheel Energy Storage System (FESS) for Voltage and Frequency Support in Low Voltage Distribution Networks," *2018 IEEE 3rd International Conference on Intelligent Energy and Power Systems, IEPS 2018 - Proceedings*, vol. 2018-Janua, pp. 176–182, 2018.

[238] S. Karrari, G. De Carne, and M. Noe, "Model validation of a high-speed flywheel energy storage system using power hardware-in-the-loop testing," *Journal of Energy Storage*, vol. 43, no. September, p. 103177, 2021. [Online]. Available: https://doi.org/10.1016/j.est.2021.103177

[239] W. Liu, C. Delacourt, C. Forgez, and S. Pelissier, "Study of graphite/NCA Li-ion cell degradation during accelerated aging tests - Data analysis of the Sim-Stock project," *2011 IEEE Vehicle Power and Propulsion Conference, VPPC 2011*, pp. 9–14, 2011.

[240] M. Broussely, P. Biensan, F. Bonhomme, P. Blanchard, S. Herreyre, K. Nechev, and R. J. Staniewicz, "Main aging mechanisms in Li ion batteries," *Journal of Power Sources*, vol. 146, no. 1-2, pp. 90–96, 2005.

[241] A. J. Hutchinson and D. T. Gladwin, "Genetic Algorithm Optimisation of Hybrid Energy Storage System providing Dynamic Frequency Response," in *2022 IEEE International Symposium on Industrial Electronics*. IEEE, 2022.

[242] S. Homan and S. Brown, "The future of frequency response in Great Britain," *Energy Reports*, vol. 7, pp. 56–62, 2021. [Online]. Available: https://doi.org/10.1016/j.egyr.2021.02.055

[243] National Grid, "Product Roadmap for Frequency Response and Reserve," National Grid ESO, Tech. Rep. December, 2017. [Online]. Available: https://www.nationalgrideso.com/sites/eso/files/documents/ProductRoadmapforFrequencyResponseandReserve.pdf

[244] National Grid ESO, "Dynamic Containment Overview," National Grid ESO, Tech. Rep., 2020. [Online]. Available: https://www.nationalgrideso.com/document/165496/download

[245] ——. Dynamic Containment. [Online]. Available: https://www.nationalgrideso.com/balancing-services/frequency-response-services/dynamic-containment{#}:{~}:

[246] ——. (2022) Dynamic Moderation. [Online]. Available: https://www.nationalgrideso.com/industry-information/balancing-services/Frequency-Response-Services/Dynamic-Moderation

[247] ——. (2022) Dynamic Regulation. [Online]. Available: https://www.nationalgrideso.com/industry-information/balancing-services/Frequency-Response-Services/Dynamic-Regulation

[248] A. Abdulkarim and D. T. Gladwin, "A Sensitivity Analysis on Power to Energy Ratios for Energy Storage Systems providing both Dynamic Firm and Dynamic Containment Frequency Response Services in the UK," *IECON Proceedings (Industrial Electronics Conference)*, vol. 2021-Octob, 2021.

[249] L. Ochoa-Eguilegor, N. Goitia-Zabaleta, A. Gonzalez-Garrido, A. Saez-de Ibarra, H. Gaztanaga, and A. Hernandez, "Optimized Market Bidding of Energy Storage Systems for Dynamic Containment Service," in *2021 IEEE International Conference on Environment and Electrical Engineering*, 2021, pp. 1–6.

[250] F. Fan, G. Zorzi, D. Campos-gaona, and J. Nwobu, "Wind-Plus-Battery system optimisation for frequency response service : The UK perspective," *Electric Power Systems Research*, vol. 211, no. July, p. 108400, 2022. [Online]. Available: https://doi.org/10.1016/j.epsr.2022.108400

[251] P. Mercier, R. Cherkaoui, and A. Oudalov, "Optimizing a battery energy storage system for frequency control application in an isolated power system," *IEEE Transactions on Power Systems*, vol. 24, no. 3, pp. 1469–1477, 2009.

[252] W. Ou, R. Dunn, W. Kong, J. Yu, and Q. Li, "Optimal Allocation of Battery Energy Storage System in the UK Power System for the Frequency Regulation with High Wind Penetration," *2020 IEEE/IAS Industrial and Commercial Power System Asia, I and CPS Asia 2020*, pp. 1192–1197, 2020.

[253] NGH, "System needs and product strategy," National Grid ESO, Tech. Rep. June, 2017.

# Appendix

Table A1: Excerpt of Energy Throughput based knee-point optimisation for a 10C system

| 10C | | $P_{-K}$ (Hz) | | | |
|---|---|---|---|---|---|
| | | 50.17 | 50.18 | 50.19 | 50.2 |
| $P_K$ (Hz) | 49.82 | 94748 | 90501 | 86293 | 82278 |
| | 49.81 | 92896 | 89212 | 85465 | 81723 |
| | 49.8 | 90371 | 87796 | 84552 | 81108 |
| | 49.79 | 87149 | 85628 | 83365 | 80324 |
| | 49.78 | 83860 | 82908 | 81561 | 79290 |

Table A2: Excerpt of Energy Throughput based knee-point optimisation for a 15C system

| 15C | | $P_{-K}$ (Hz) | | | |
|---|---|---|---|---|---|
| | | 50.17 | 50.18 | 50.19 | 50.2 |
| $P_K$ (Hz) | 49.83 | 91750 | 88044 | 84285 | 80616 |
| | 49.82 | 89846 | 86718 | 83302 | 79913 |
| | 49.81 | 87925 | 85041 | 82167 | 79130 |
| | 49.8 | 85676 | 83388 | 80747 | 78128 |
| | 49.79 | 83256 | 81463 | 79318 | 76940 |

Table A3: Excerpt of Energy Throughput based knee-point optimisation for a 20C system

| 20C | | $P_{-K}$ (Hz) | | | |
|---|---|---|---|---|---|
| | | 50.16 | 50.17 | 50.18 | 50.19 |
| $P_K$ (Hz) | 49.82 | 88847 | 85946 | 83180 | 80282 |
| | 49.81 | 86313 | 83983 | 81460 | 78959 |
| | 49.8 | 83939 | 81880 | 79807 | 77484 |
| | 49.79 | 81503 | 79783 | 77901 | 75970 |
| | 49.78 | 78986 | 77620 | 76049 | 74334 |

Table A4: Excerpt of Average Availability based knee-point optimisation for a 10C system

| 10C | | $P_{-K}$ (Hz) | | | |
|---|---|---|---|---|---|
| | | 50.17 | 50.18 | 50.19 | 50.2 |
| $P_K$ (Hz) | 49.82 | 97.03% | 96.60% | 96.05% | 95.46% |
| | 49.81 | 97.45% | 97.18% | 96.75% | 96.20% |
| | 49.8 | 97.55% | 97.64% | 97.34% | 96.89% |
| | 49.79 | 97.33% | 97.80% | 97.80% | 97.47% |
| | 49.78 | 96.99% | 97.62% | 98.00% | 97.93% |

Table A5: Excerpt of Average Availability based knee-point optimisation for a 15C system

| 15C | | P<sub>-K</sub> (Hz) | | | |
|---|---|---|---|---|---|
| | | 50.17 | 50.18 | 50.19 | 50.2 |
| P<sub>K</sub> (Hz) | 49.83 | 95.09% | 94.85% | 94.47% | 94.02% |
| | 49.82 | 95.47% | 95.35% | 95.08% | 94.69% |
| | 49.81 | 95.76% | 95.73% | 95.57% | 95.29% |
| | 49.80 | 95.93% | 96.02% | 95.96% | 95.78% |
| | 49.79 | 95.95% | 96.20% | 96.25% | 96.15% |

Table A6: Excerpt of Average Availability based knee-point optimisation for a 20C system

| 20C | | P<sub>-K</sub> (Hz) | | | |
|---|---|---|---|---|---|
| | | 50.16 | 50.17 | 50.18 | 50.19 |
| P<sub>K</sub> (Hz) | 49.82 | 94.14% | 94.21% | 94.16% | 94.02% |
| | 49.81 | 94.32% | 94.48% | 94.48% | 94.43% |
| | 49.8 | 94.38% | 94.64% | 94.75% | 94.74% |
| | 49.79 | 94.41% | 94.71% | 94.91% | 95.00% |
| | 49.78 | 94.37% | 94.73% | 95.00% | 95.16% |

```matlab
function [FESSDischarge, FESSCharge] = fcn(FESSSOC,FESSAvailable,Request)

FSOCHighLimit = 98; % Set the high limit of the FESS SOC
FSOCLowLimit = 2; % Set the low limit of the FESS SOC
x = FESSAvailable*-1; % Placeholder for the maximum available charging
% power with FESS available being the maximum available discharging power

if(Request>=0) % Discharging Section
        if(FESSSOC>FSOCLowLimit && FESSAvailable>=Request)
        % if the FESS SOC is above the low limit, and the FESS has the
        % required power rating to fully handle the request, then
        % discharge the full requested power
        FESSCharge=0;
        FESSDischarge=Request;
        elseif(FESSSOC>FSOCLowLimit && FESSAvailable<Request)
        % if the FESS SOC is above the low limit, but the FESS does not
        % have the required power rating to fully handle the request, then
        % discharge as much power as possible
        FESSCharge=0;
        FESSDischarge=FESSAvailable;
        elseif(FESSSOC<=FSOCLowLimit)
        % if the FESS SOC falls below the low limit, no discharge is
        % allowed
        FESSCharge=0;
        FESSDischarge=0;
        else
        FESSCharge=0;
        FESSDischarge=0;
        end
    elseif(Request<0) % Charging Section
            if(FESSSOC<FSOCHighLimit && Request>=x)
            % if the FESS SOC is below the high limit, and the FESS has
            % the required power rating to fully handle the request, then
            % charge the full requested power
                FESSCharge=Request;
                FESSDischarge=0;
            elseif(FESSSOC<FSOCHighLimit && Request<x)
            % if the FESS SOC is below the high limit, and the FESS does
            % not have required power rating to fully handle the request,
            % then charge as much power as possible
                FESSCharge=FESSAvailable*-1;
                FESSDischarge=0;
            elseif(FESSSOC>=FSOCHighLimit)
            % if the FESS SOC rises above the high limit, no charge is
            % allowed
                FESSCharge=0;
                FESSDischarge=0;
            else
                FESSCharge=0;
                FESSDischarge=0;
            end
        else
                FESSCharge=0;
                FESSDischarge=0;
```

Figure A1: MATLAB function code for FESS DFR control

282
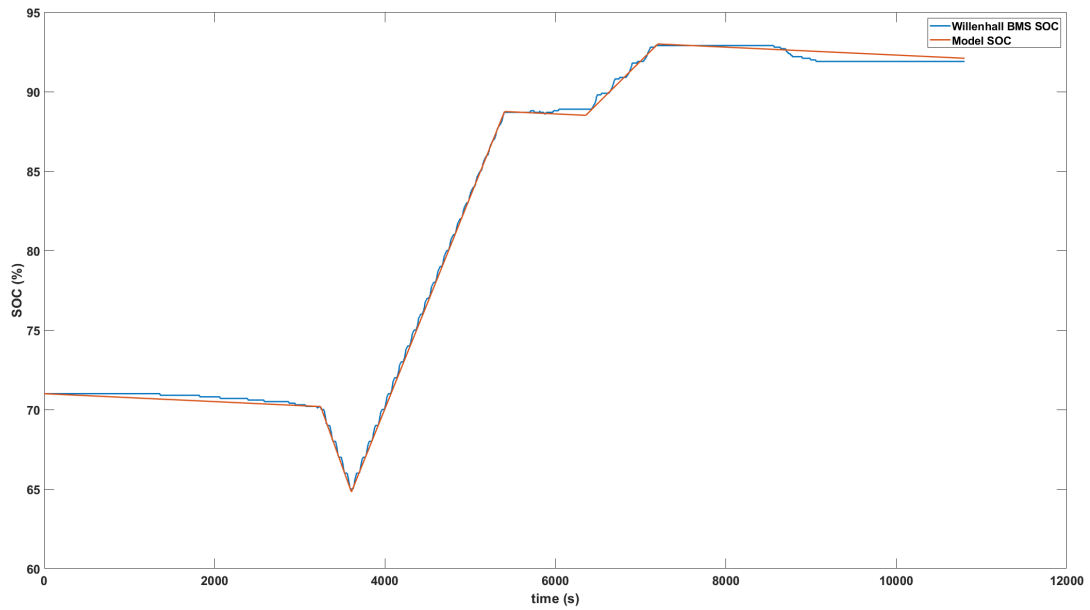
Figure A2: Verification 1 - BMS against Model
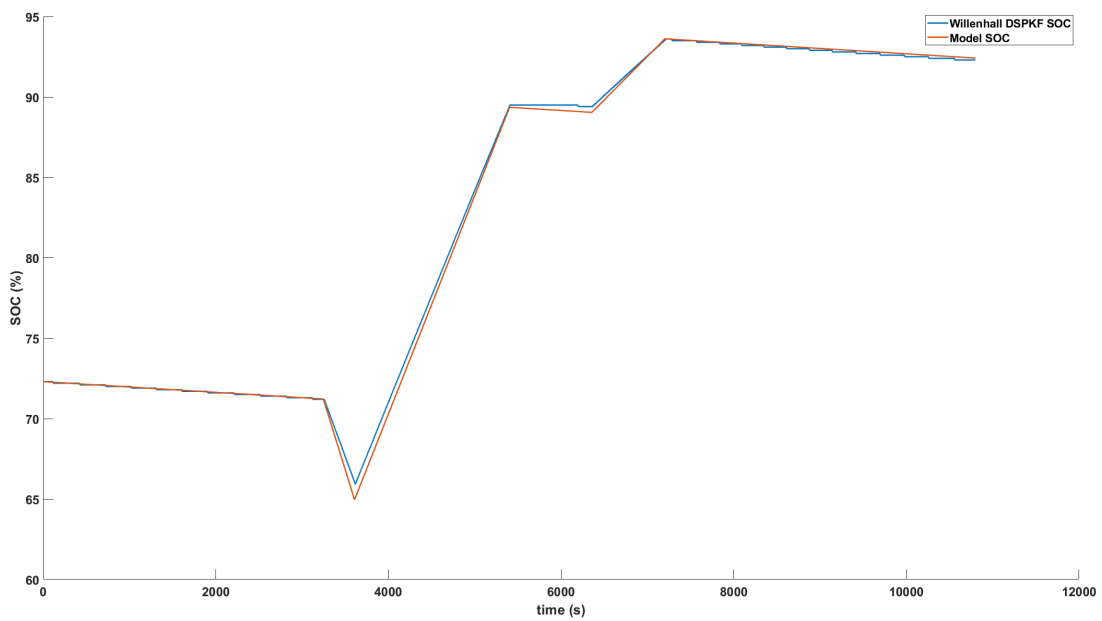


Figure A3: Verification 1 - DSPKF against Model
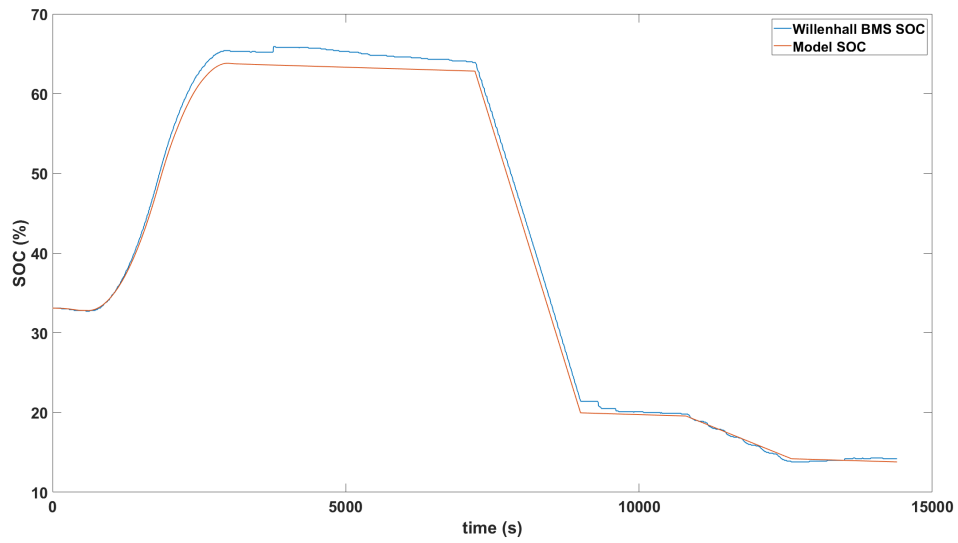
Figure A4: Verification 2 - BMS against Model
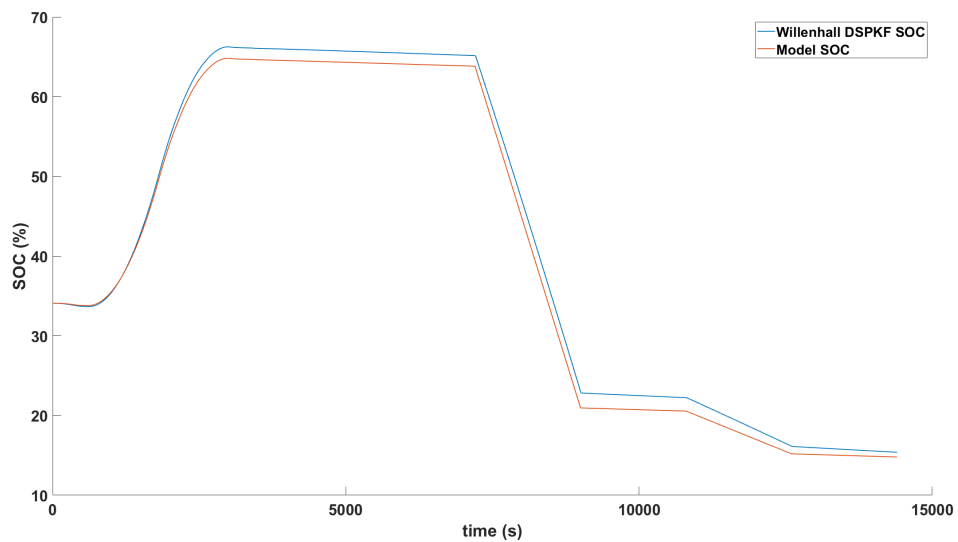


Figure A5: Verification 2 - DSPKF against Model
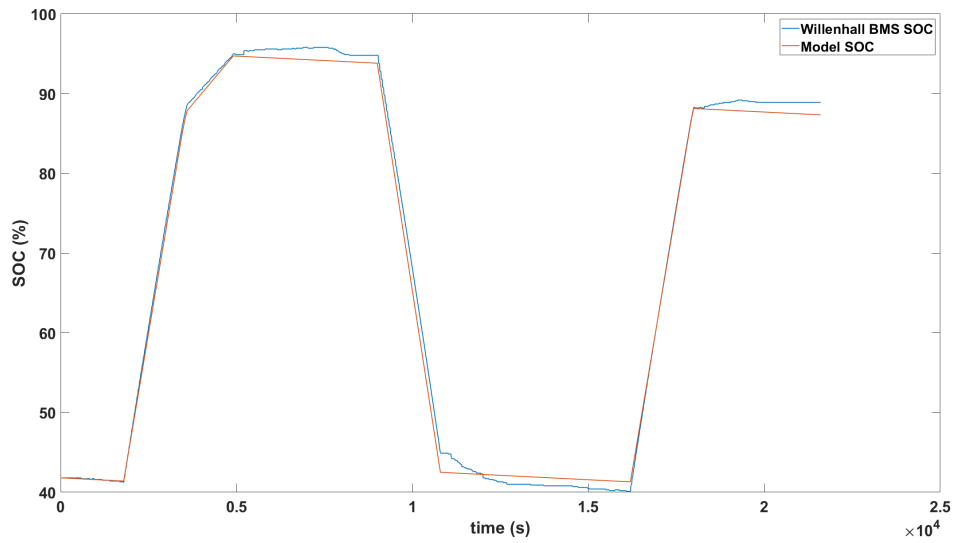
Figure A6: Verification 3 - BMS against Model
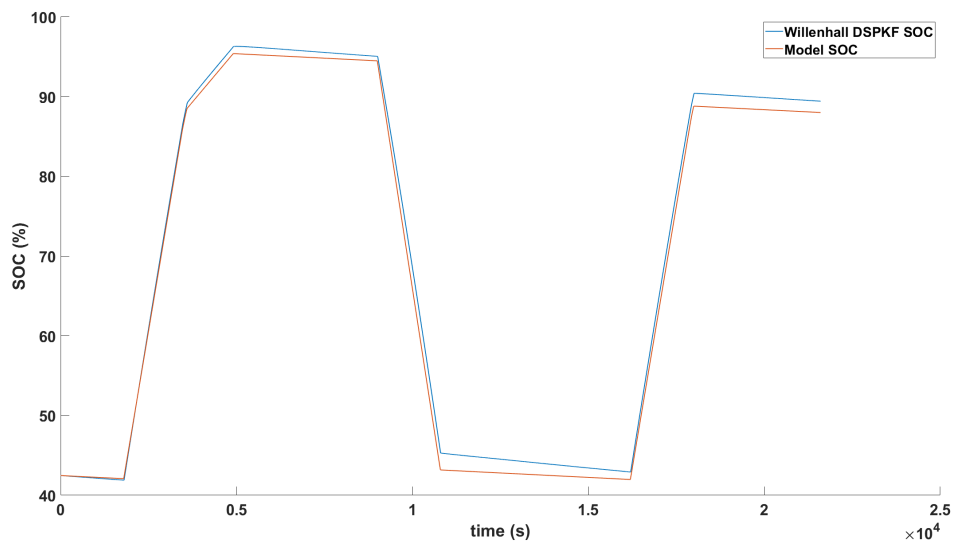


Figure A7: Verification 3 - DSPKF against Model
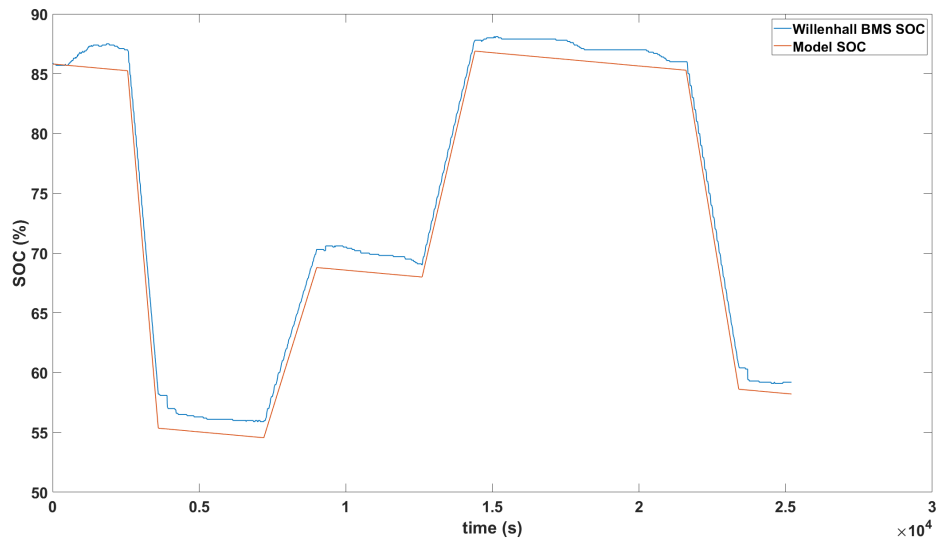
Figure A8: Verification 4 - BMS against Model
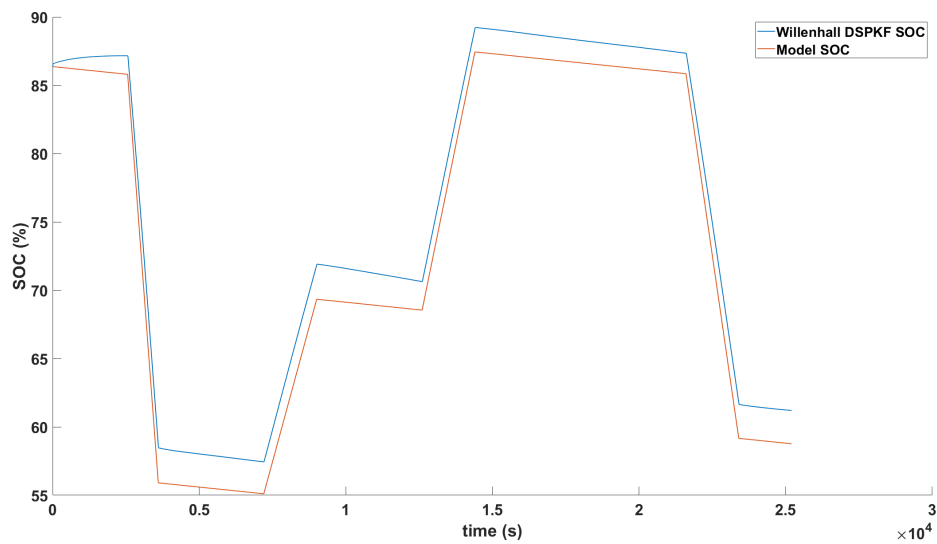


Figure A9: Verification 4 - DSPKF against Model
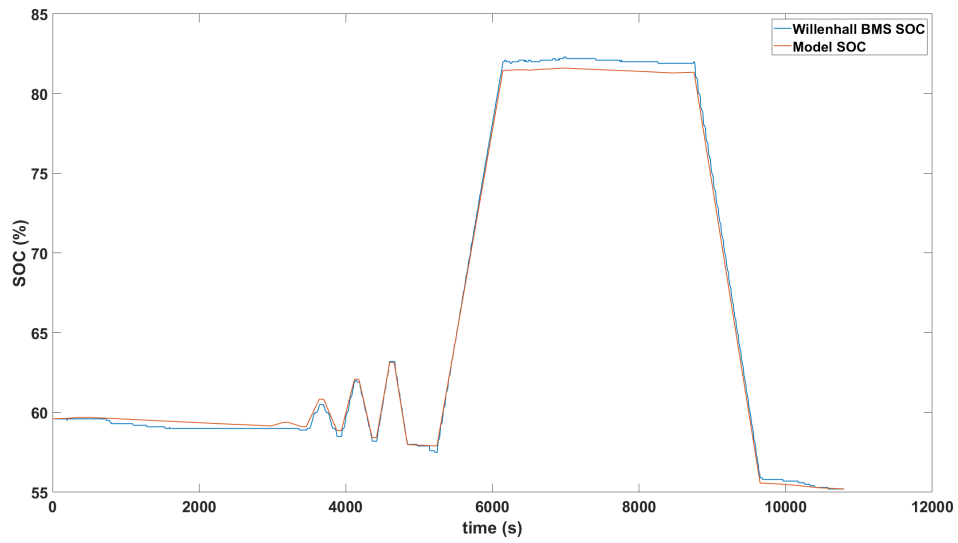
Figure A10: Verification 5 - BMS against Model
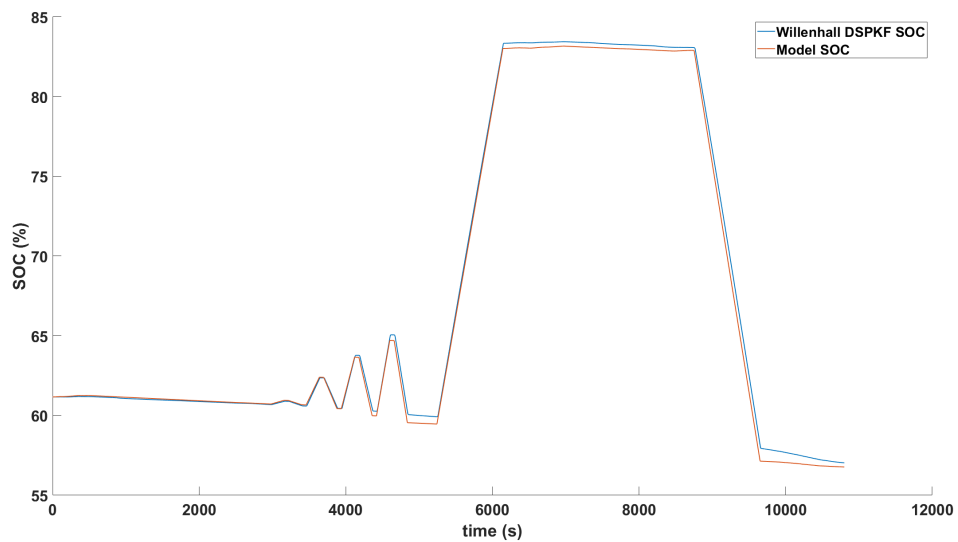


Figure A11: Verification 5 - DSPKF against Model

287
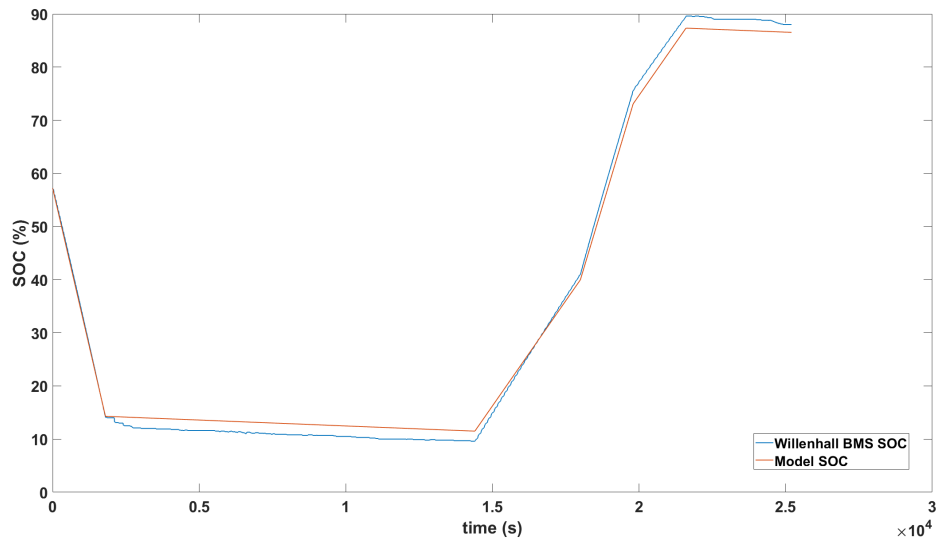
Figure A12: Verification 6 - BMS against Model
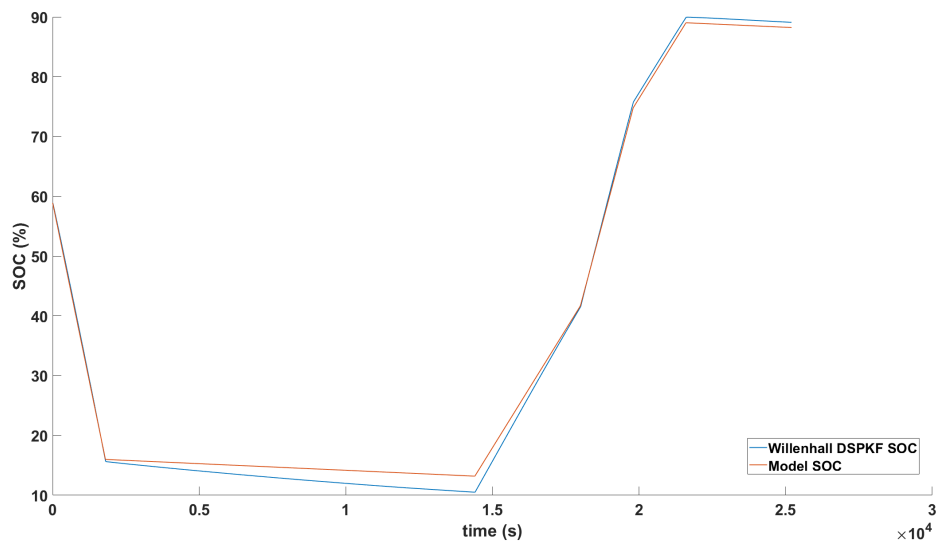


Figure A13: Verification 6 - DSPKF against Model
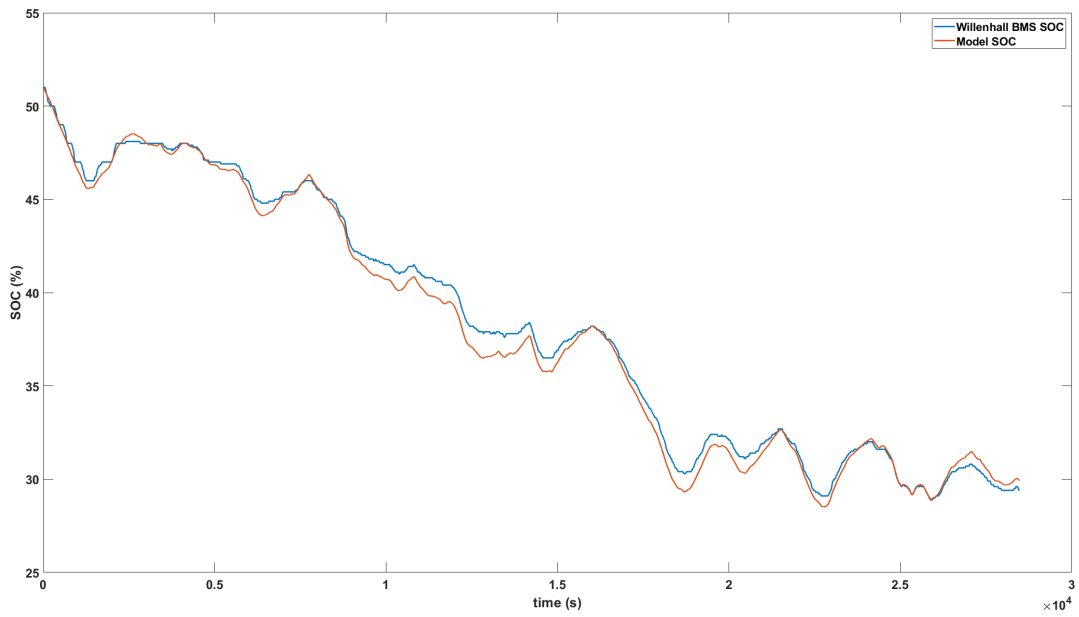
Figure A14: Verification 7 - BMS against Model
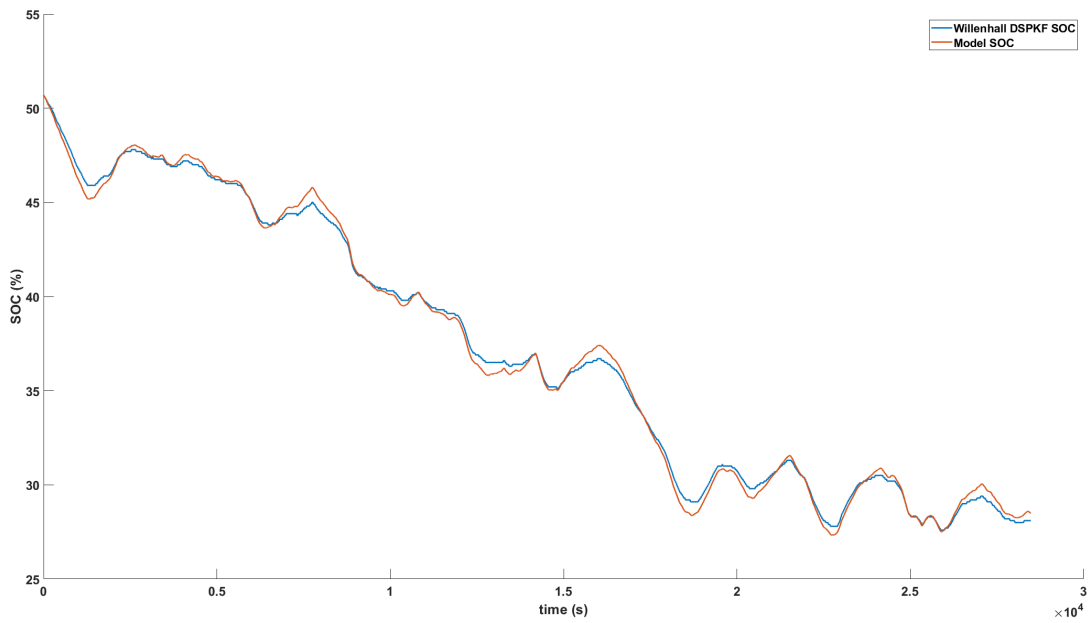


Figure A15: Verification 7 - DSPKF against Model
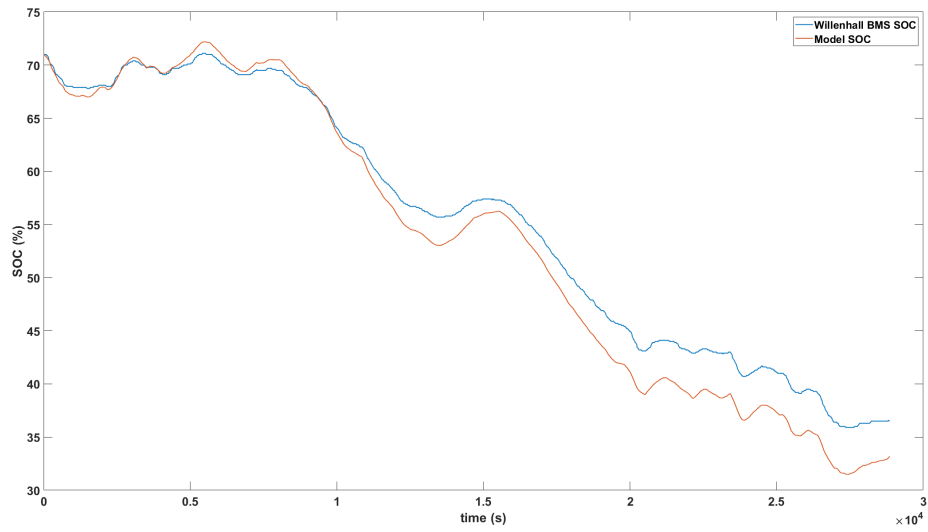
Figure A16: Verification 8 - BMS against Model
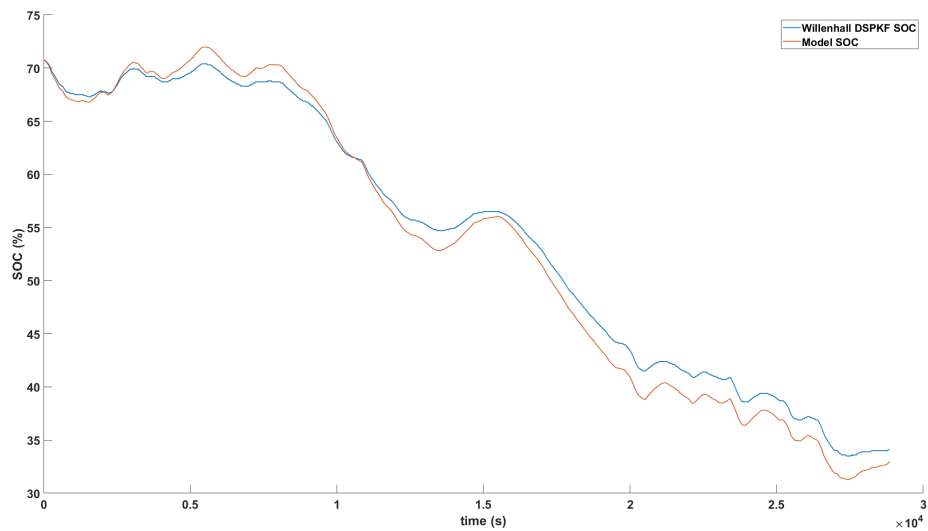


Figure A17: Verification 8 - DSPKF against Model
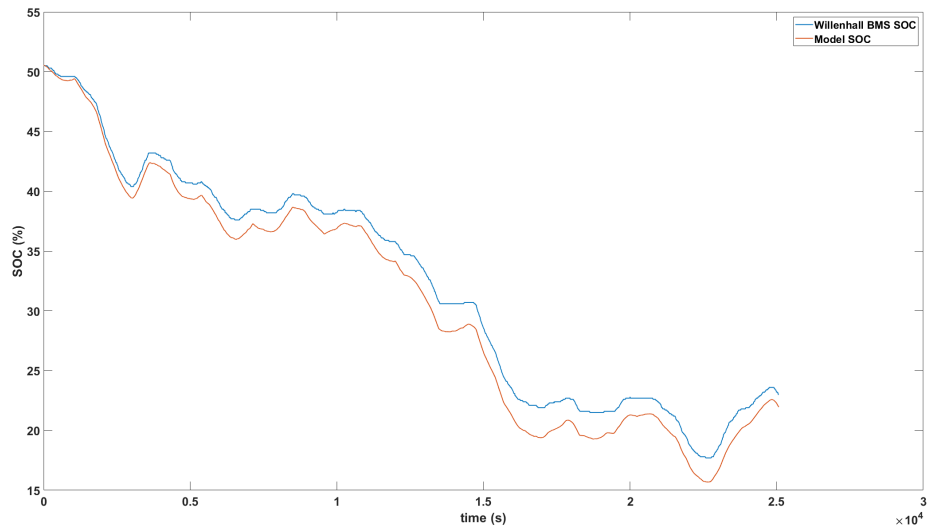
Figure A18: Verification 9 - BMS against Model
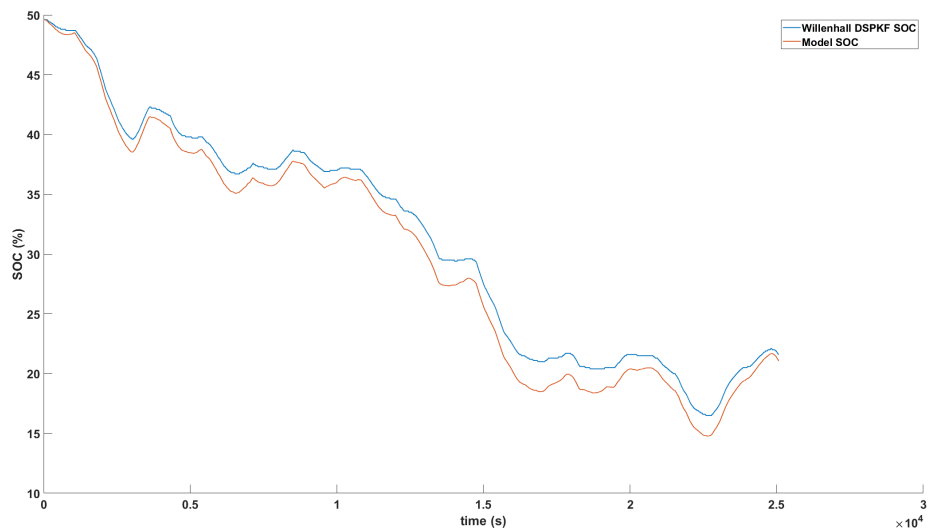


Figure A19: Verification 9 - DSPKF against Model
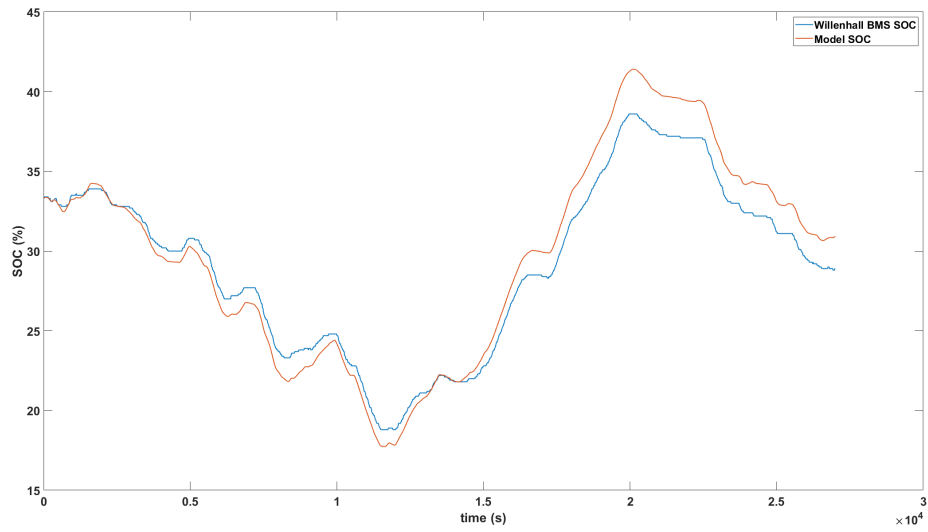
Figure A20: Verification 10 - BMS against Model
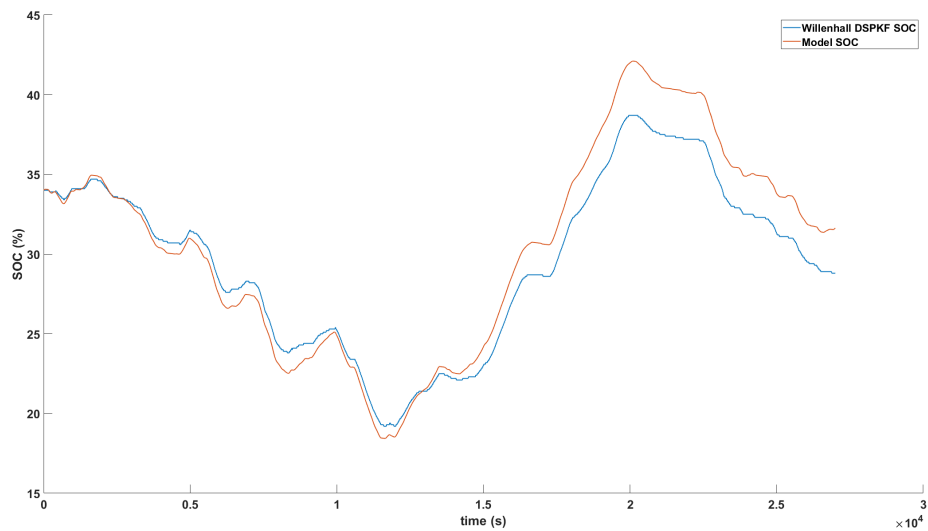


Figure A21: Verification 10 - DSPKF against Model
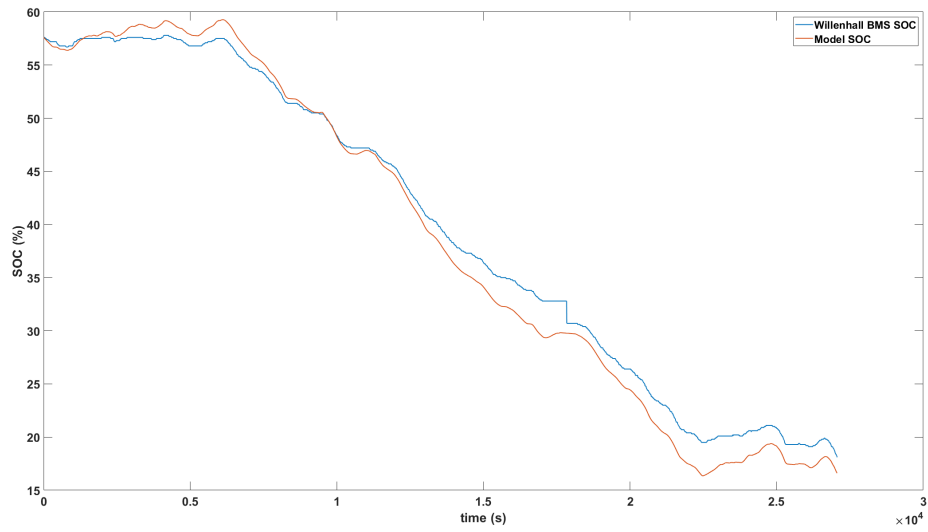
Figure A22: Verification 11 - BMS against Model
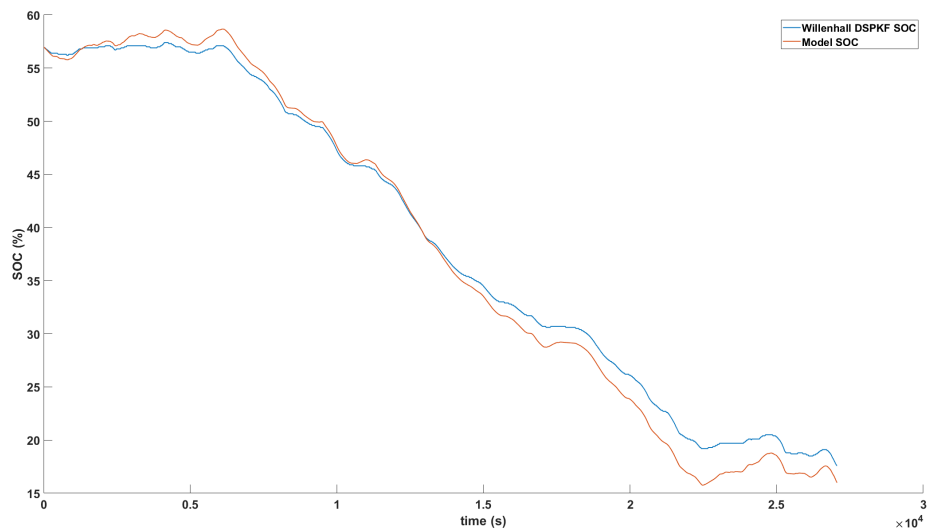


Figure A23: Verification 11 - DSPKF against Model
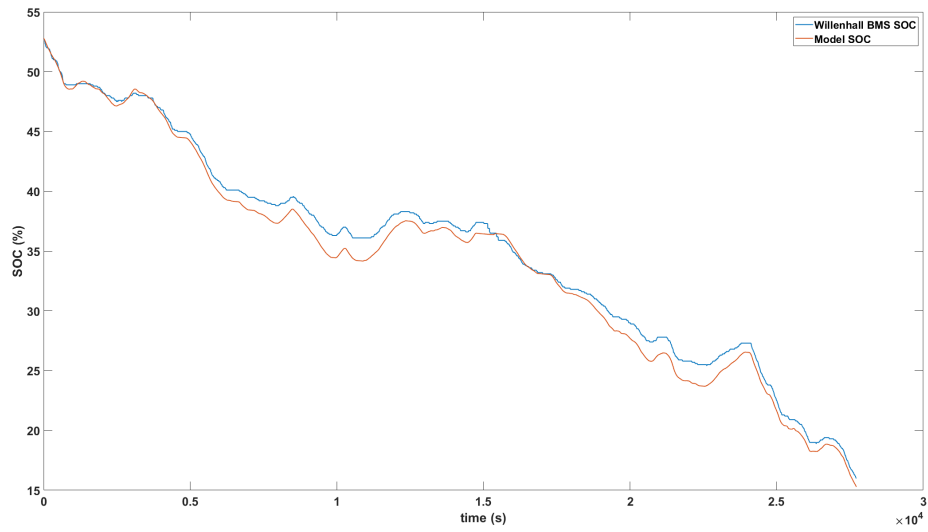
Figure A24: Verification 12 - BMS against Model
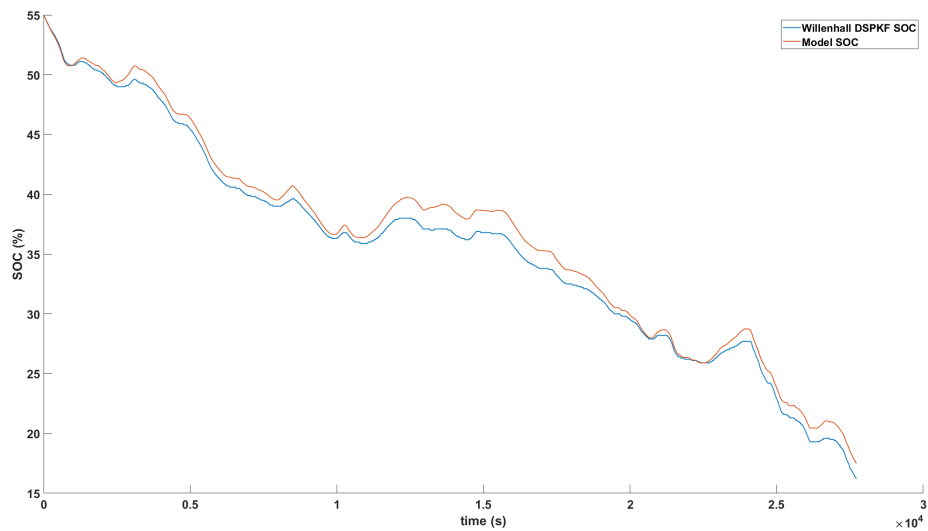


Figure A25: Verification 12 - DSPKF against Model
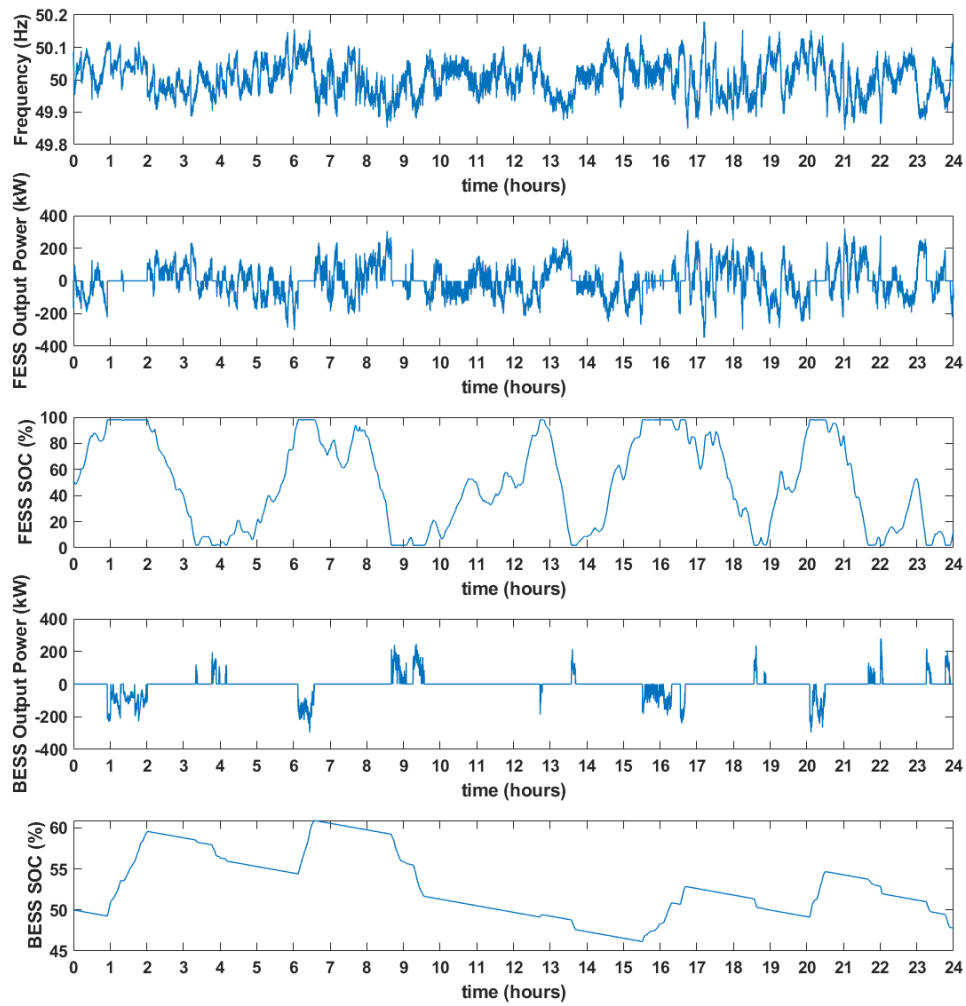
Figure A26: Simulation outputs when operating a 1MW 1C BESS with a 100kW 10C FESS under CS-2
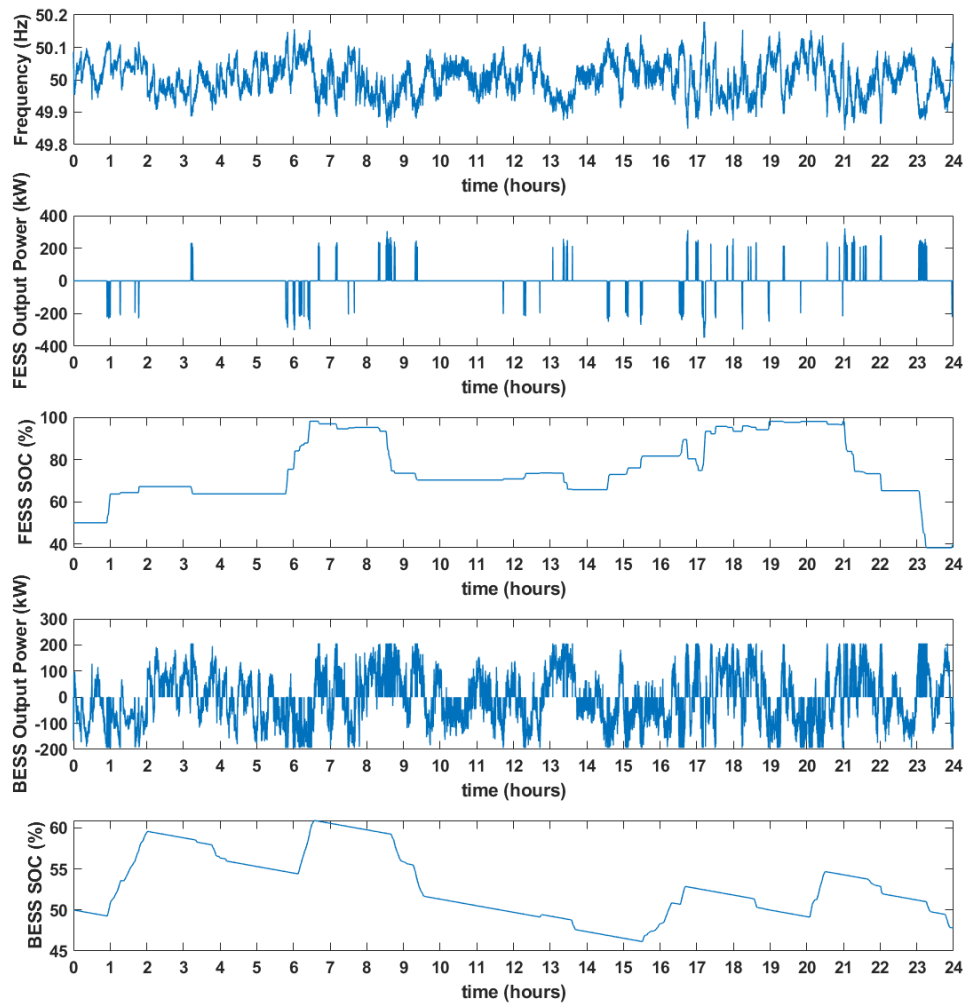
Figure A27: Simulation outputs when operating a 1MW 1C BESS with a 100kW 10C FESS under CS-3
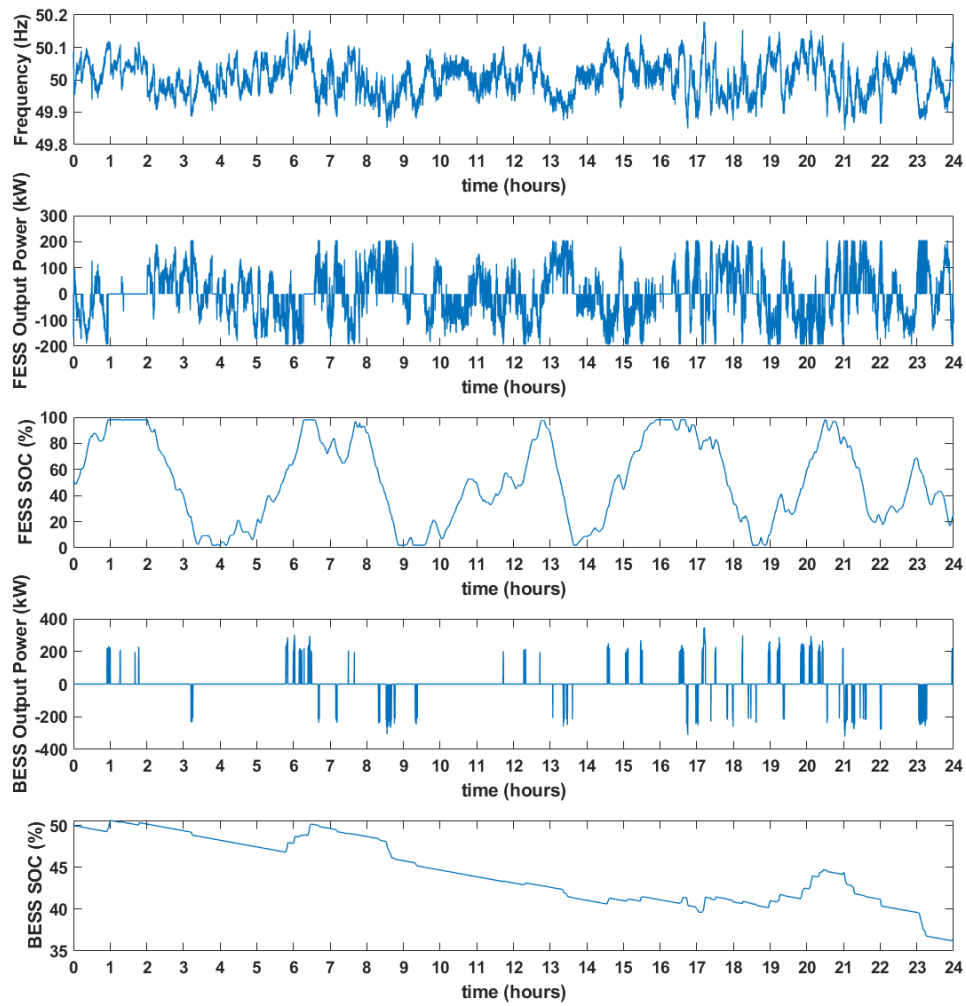
Figure A28: Simulation outputs when operating a 1MW 1C BESS with a 100kW 10C FESS under CS-4
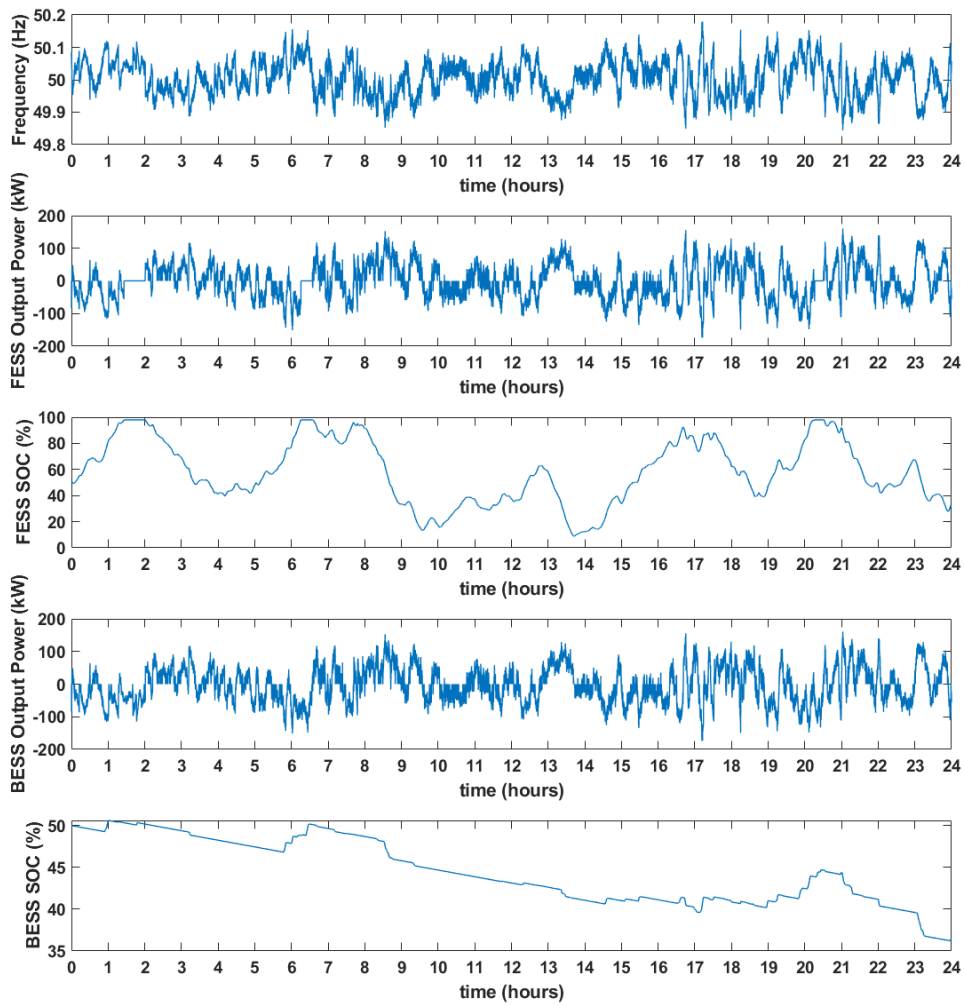
Figure A29: Simulation outputs when operating a 1MW 1C BESS with a 100kW 10C FESS under CS-5
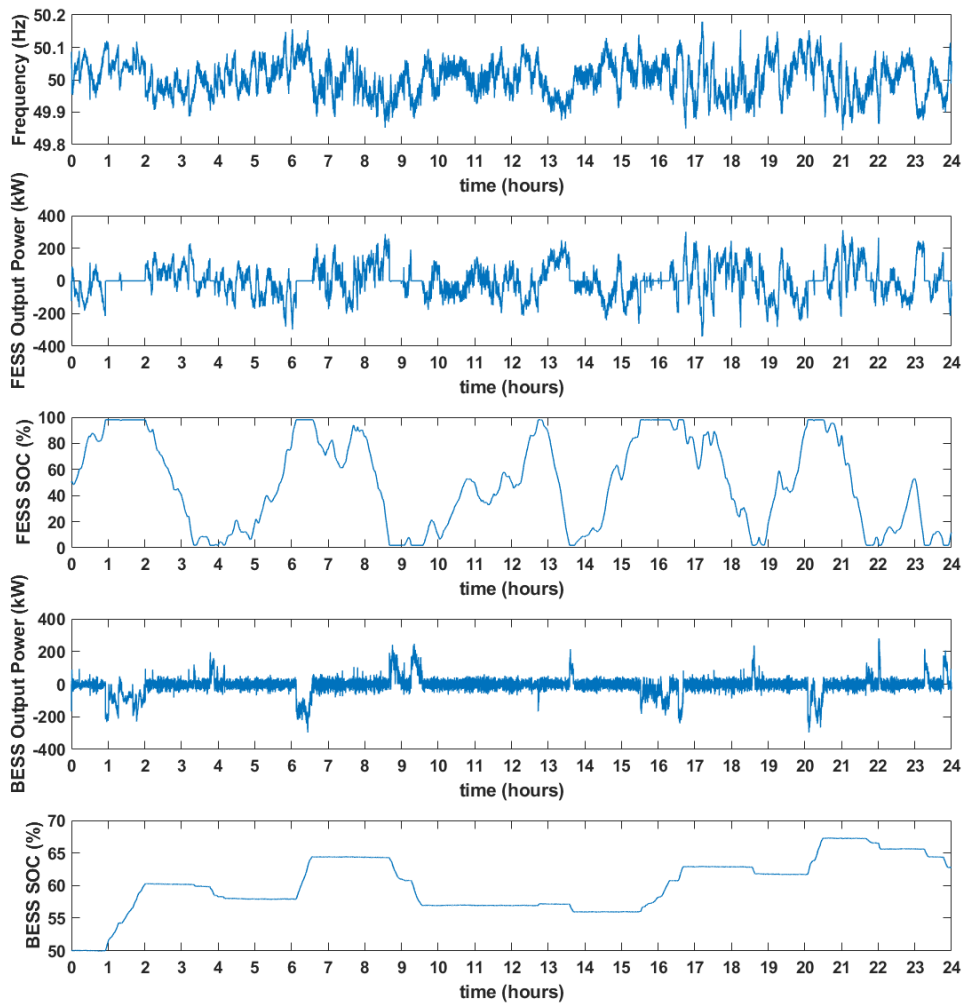
Figure A30: Simulation outputs when operating a 1MW 1C BESS with a 100kW 10C FESS under CS-6
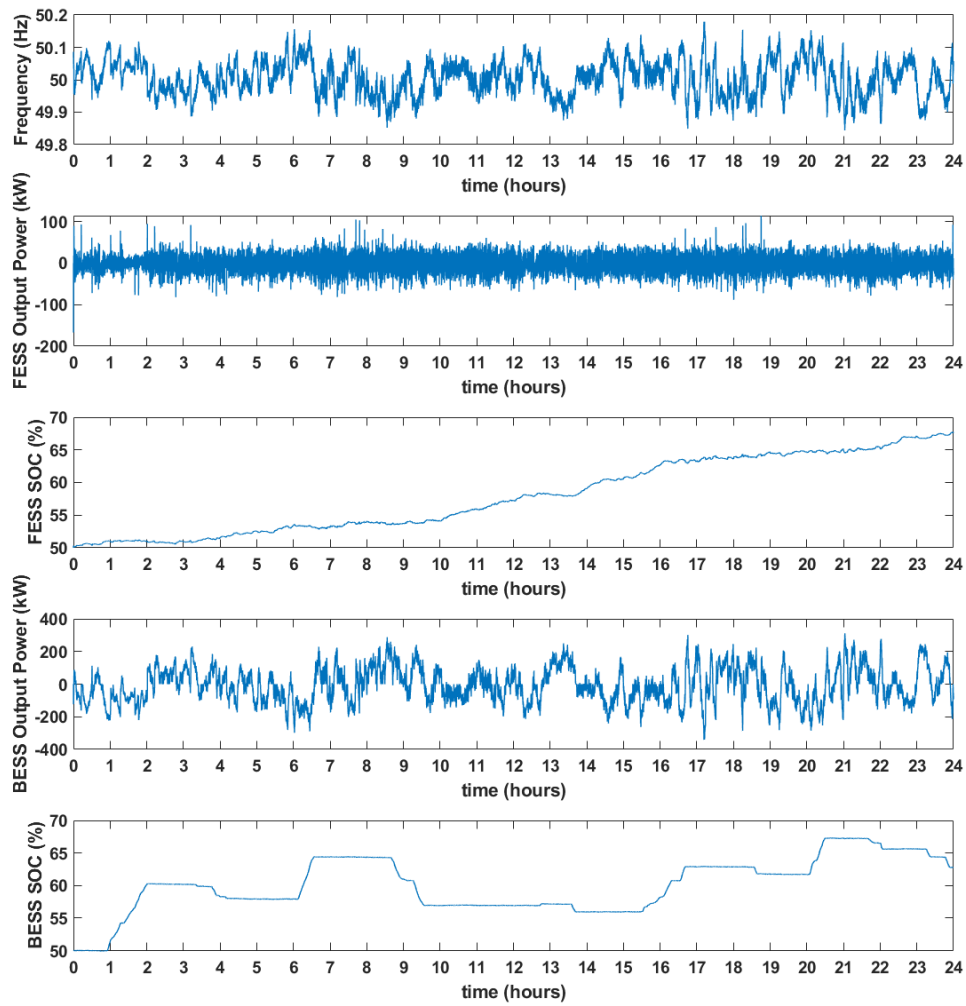
Figure A31: Simulation outputs when operating a 1MW 1C BESS with a 100kW 10C FESS under CS-7
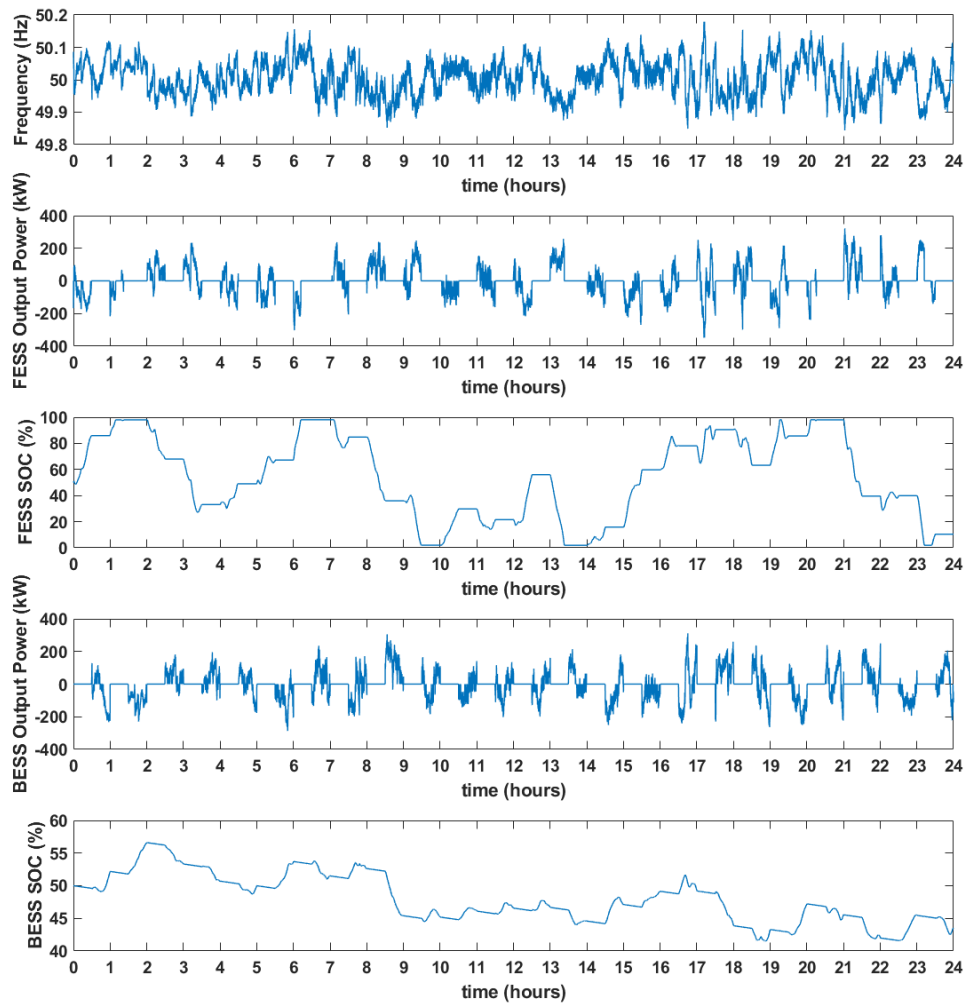
Figure A32: Simulation outputs when operating a 1MW 1C BESS with a 100kW 10C FESS under CS-8

```matlab
function Reward = NPVCalculator(NPV)

if(NPV<0)
    if(NPV>=-10000)
    Reward = 0.00009
    elseif(NPV>=-200000 && NPV<=-100000)
    Reward = 0.0001
    elseif(NPV>=-300000 && NPV<=-200000)
    Reward = 0.00015
    elseif(NPV>=-400000 && NPV<=-300000)
    Reward = 0.00020
    elseif(NPV>=-500000 && NPV<=-400000)
    Reward = 0.00025
    elseif(NPV>=-600000 && NPV<=-500000)
    Reward = 0.00030
    elseif(NPV>=-700000 && NPV<=-600000)
    Reward = 0.00035
    elseif(NPV>=-800000 && NPV<=-700000)
    Reward = 0.00040
    elseif(NPV>=-900000 && NPV<=-800000)
    Reward = 0.00045
    elseif(NPV>=-1000000 && NPV<=-900000)
    Reward = 0.00050
    elseif(NPV>=-1200000 && NPV<=-1000000)
    Reward = 0.00055
    elseif(NPV>=-1400000 && NPV<=-1200000)
    Reward = 0.00060
    elseif(NPV>=-1600000 && NPV<=-1400000)
    Reward = 0.00065
    elseif(NPV>=-1800000 && NPV<=-1600000)
    Reward = 0.00070
    else
        Reward = 0.00080;
    end
else
Reward = 1/(1+NPV)
end
```

Figure A33: MATLAB function for filtering negative NPV values in the GA
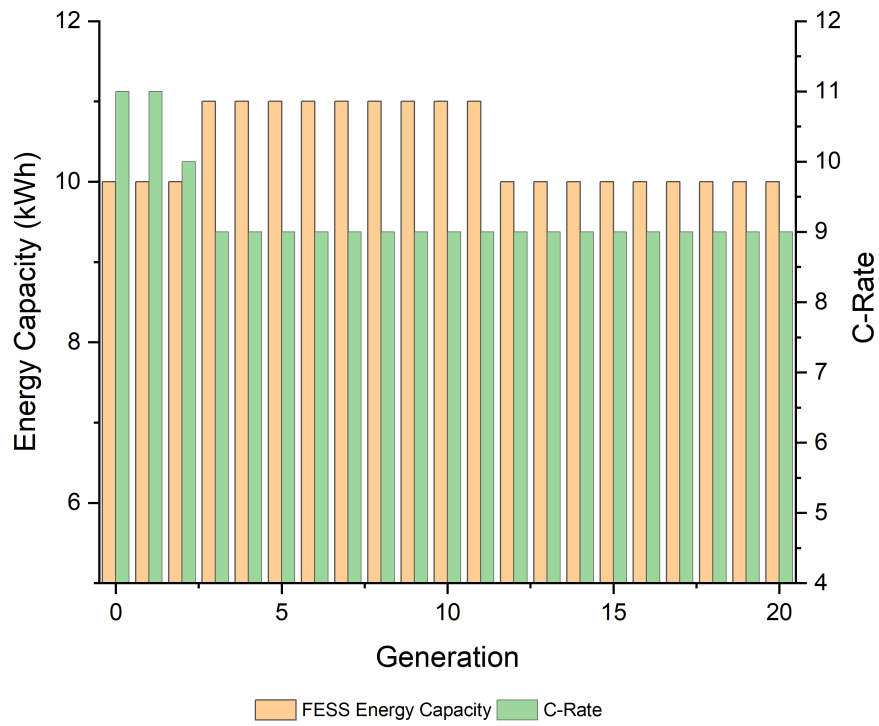
Figure A34: Best individuals per generation CS-7 , $t_{av} = 120$
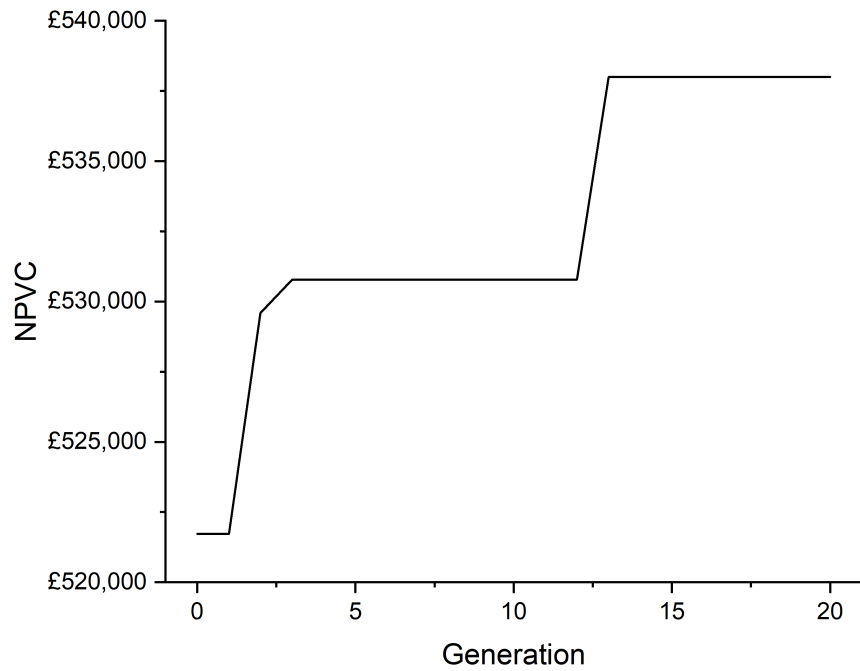


Figure A35: Maximum positive NPVC at each generation of the CS-7 GA , $t_{av} = 120$
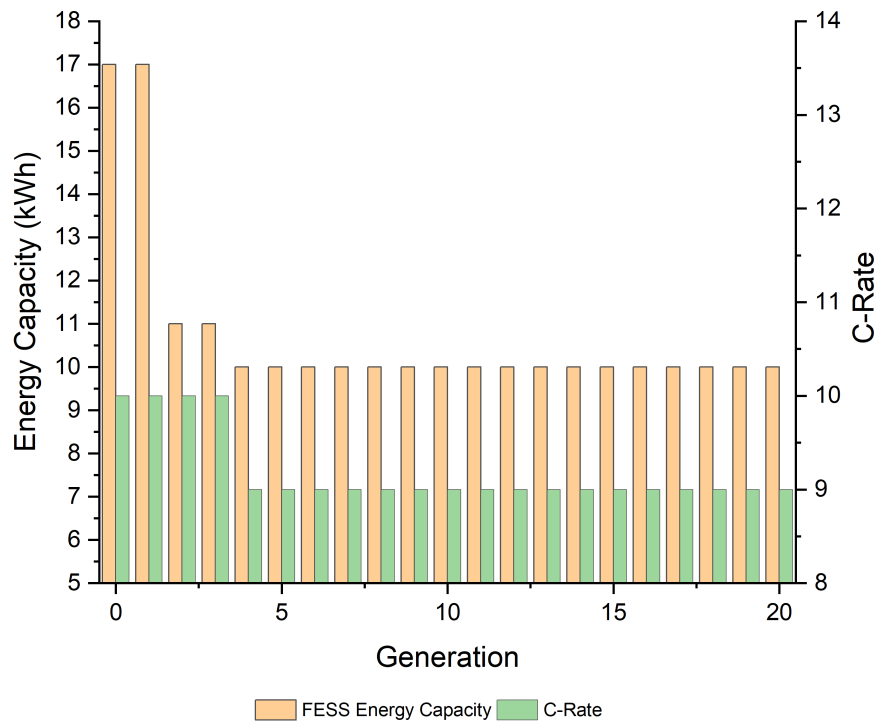
Figure A36: Best individuals per generation CS-7, $t_{\mathrm{av}} = 300$
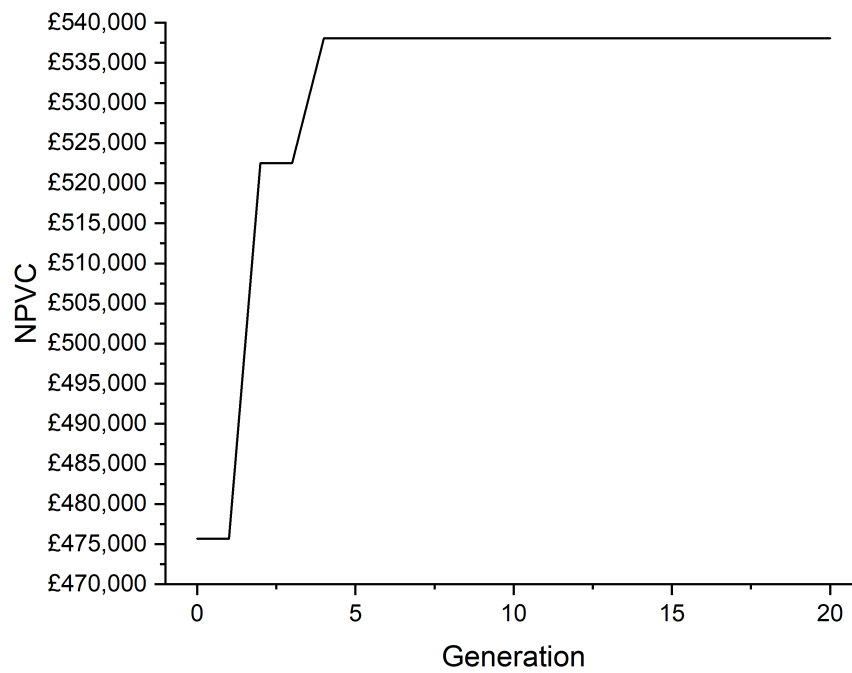


Figure A37: Maximum positive NPVC at each generation of the CS-7 GA, $t_{\mathrm{av}} = 300$